Elements of nuclear physics

Piotr Magierski, email: magiersk@if.pw.edu.pl, GF PW, pok. 226c
Program of the course can be found here: www.if.pw.edu.pl/~magiersk

Literature:

1) J-l. Basdevant, J. Rich, M. Spiro,
   Fundamentals in Nuclear Physics. From Nuclear Structure to Cosmology
2) W.N. Cottingham, D.A. Greenwood
   An introduction to Nuclear Physics, Cambridge Univ. Press
3) K. Heyde
   Basic Ideas and Concepts in Nuclear Physics, Inst. Of Phys. Publ.
4) B. Povh, K. Rith, C. Scholz, F. Zetsche
   Particles and Nuclei. An Introduction to the Physical Concepts
2) E. Skrzypczak, Z. Szefliński
   Wstęp do fizyki jądra atomowego i cząstek elementarnych, PWN
3) A. Strzałkowski
   Wstęp do fizyki jądra atomowego, PWN
4) K. Muchin
   Doświadczalna fizyka jądrowa, WNT

UNIA EUROPEJSKA
EUROPEJSKI
FUNDUSZ SPOŁECZNY

HUMAN CAPITAL
HUMAN – BEST INVESTMENT!

UNIA EUROPEJSKA
EUROPEJSKI
FUNDUSZ SPOŁECZNY

Nuclear Science: The Mission

Explain the origin, evolution, and structure of the baryonic matter of the universe - the matter that makes up stars, planets, and human life itself

Theory of Nuclei

Overarching goal:

To arrive at a comprehensive and unified microscopic description of all nuclei and low-energy reactions from the the basic interactions between the constituent protons and neutrons

- Self-bound, two-component quantum many-fermion system
- Complicated interaction based on QCD with at least two- and three-nucleon components
- We seek to describe the properties of finite and bulk nucleonic matter ranging from the deuteron to neutron stars and nuclear matter; including strange matter
- We want to be able to extrapolate to unknown regions

There is no "one size fits all" theory for nuclei, but all our theoretical approaches need to be linked. We are making great progress in this direction.

Building blocks of matter: **elementary particles.**

They can be divided into two families:

- fermions
-bosons

These two types of particles have very different properties. In general, fermions form an ordinary matter , whereas
bosons are responsible for fundamental interactions

- One has to remember however that sometimes people call elementary particles also particles which we know are complex entities like e.g. proton and neutron.
- This is due to historical reasons: In the 50's and 60's physicists detected many particles which seemed to be elementary. Although later it turned out that this is not true, still in a broad sense elementary particles are all subnuclear particles, i.e. particles which appear when colliding nuclei.
- All the elementary particles possess certain properties that allow to distinguish them from each other. They are:

  - **mass** (usually expressed in energy units: E=mc^2)
  - **electric charge** (in units of electronic charge)
  - **spin**, which is an internal angular momentum (in units of Planck's constant)

FERMIONS

matter constituents
spin = 1/2, 3/2, 5/2, ...

Leptons spin =1/2

Flavor	Mass GeV/c^2	Electric charge
ν_L lightest neutrino*	$(0-0.13)\times10^{-9}$	0
e electron	0.000511	–1
ν_M middle neutrino*	$(0.009-0.13)\times10^{-9}$	0
μ muon	0.106	–1
ν_H heaviest neutrino*	$(0.04-0.14)\times10^{-9}$	0
τ tau	1.777	–1

Quarks spin =1/2

Flavor	Approx. Mass GeV/c^2	Electric charge
u up	0.002	2/3
d down	0.005	–1/3
c charm	1.3	2/3
s strange	0.1	–1/3
t top	173	2/3
b bottom	4.2	–1/3

BOSONS

force carriers
spin = 0, 1, 2, …

Unified Electroweak spin = 1		
Name	Mass GeV/c^2	Electric charge
γ photon	0	0
W^-	80.39	–1
W^+ W bosons	80.39	+1
Z^0 Z boson	91.188	0

Strong (color) spin =1		
Name	Mass GeV/c^2	Electric charge
g gluon	0	0

Properties of the Interactions

The strengths of the interactions (forces) are shown relative to the strength of the electromagnetic force for two u quarks separated by the specified distances.

Property	Gravitational Interaction	Weak Interaction (Electroweak)	Electromagnetic Interaction (Electroweak)	Strong Interaction
Acts on:	Mass – Energy	Flavor	Electric Charge	Color Charge
Particles experiencing:	All	Quarks, Leptons	Electrically Charged	Quarks, Gluons
Particles mediating:	Graviton (not yet observed)	W^+ W^- Z^0	γ	Gluons
Strength at 10^{-18} m	10^{-41}	0.8	1	25
Strength at 3×10^{-17} m	10^{-41}	10^{-4}	1	60

Interactions among elementary particles are carried by bosons.

Bosons - particles with an integer spin (integer multiple of Planck's constant)
Fermions - particles with an half-integer spin

- Fundamental interactions:

All known phenomena in physics can be explained using the concept of interparticle interaction. These interactions are mediated by bosons. There are 4 types of interactions:

- electromagnetic
- weak
- strong
- gravitational

One of the goals of physics is to unify these interactions into one in the same way like electric and magnetic forces can be understood as manifestation of the unified electromagnetic field.

Elementary particles

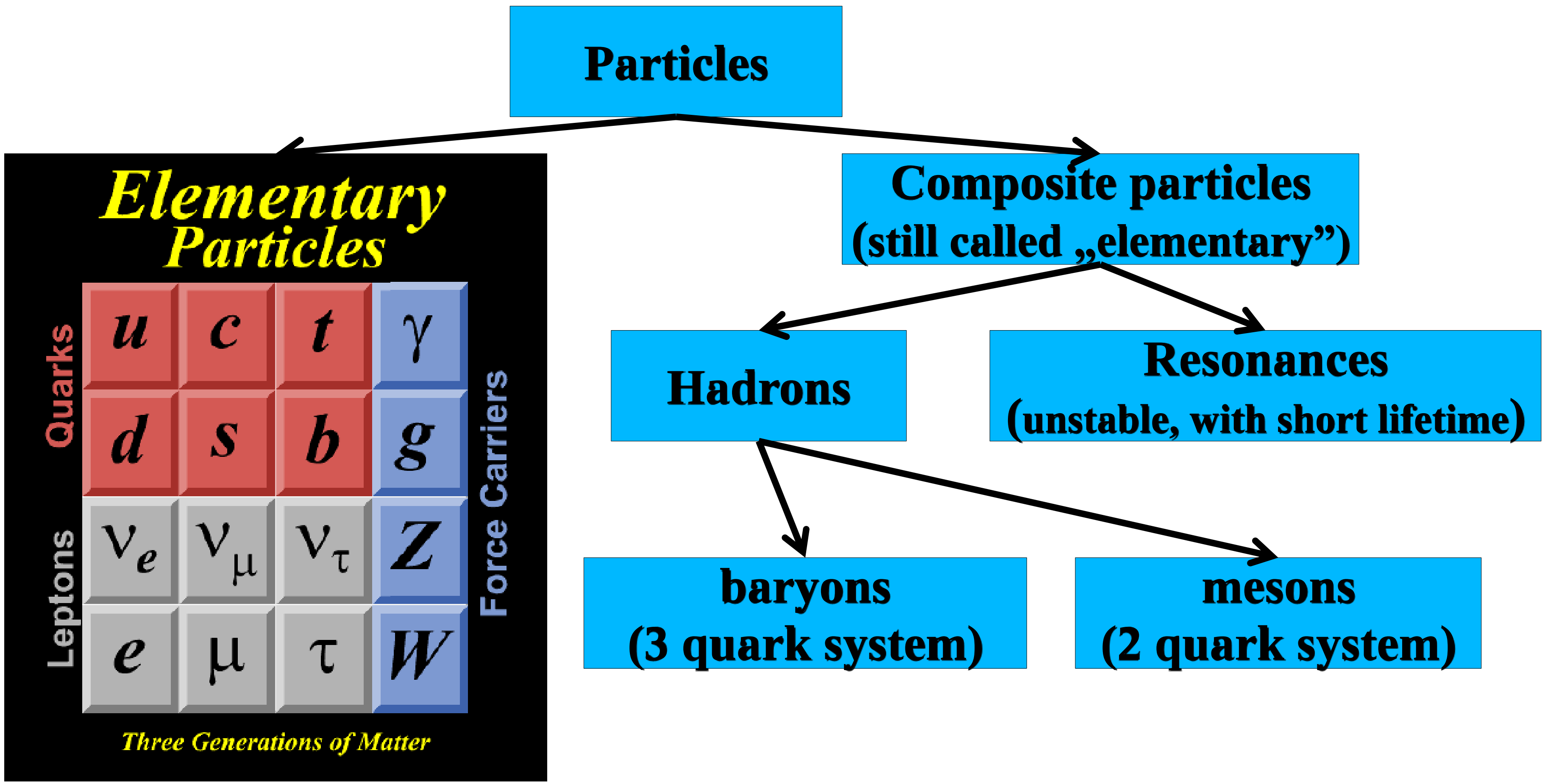

One of the interesting experimental observation is that each elementary particle has a partner of the same mass but an opposite charge.

They are called **antiparticles**.

For example positon is an antiparticle of electron, antiproton is an antiparticle of proton, etc.

Particle and antiparticle can annihilate producing radiation in the form of photons.

Antiparticles are rare on earth and has to be artificially created in accelerators.

This makes physicists speculate that maybe there is somewhere an antiworld which is made of antiparticles, where an ordinary matter is rare.

In theory such an antiworld in principle should be stable unless it would contact with a normal world.

Hadrons: strongly interacting particles

Baryons qqq and Antibaryons $\bar{q}\bar{q}\bar{q}$					
Symbol	Name	Quark content	Electric charge	Mass GeV/c^2	Spin
p	proton	uud	1	0.938	1/2
$\bar{p}$	anti-proton	$\bar{u}\bar{u}\bar{d}$	–1	0.938	1/2
n	neutron	udd	0	0.940	1/2
Λ	lambda	uds	0	1.116	1/2
Ω^-	omega	sss	–1	1.672	3/2

Mesons $q\bar{q}$ Mesons are bosonic hadrons. There are about 140 types of mesons.					
Symbol	Name	Quark content	Electric charge	Mass GeV/c^2	Spin
π^+	pion	$u\bar{d}$	+1	0.140	0
K^-	kaon	$s\bar{u}$	–1	0.494	0
ρ^+	rho	$u\bar{d}$	+1	0.770	1
B^0	B-zero	$d\bar{b}$	0	5.279	0
η_c	eta-c	$c\bar{c}$	0	2 .980	0

There are few hundreds of known hadrons

The most important hadrons (for us): **proton and neutron.**

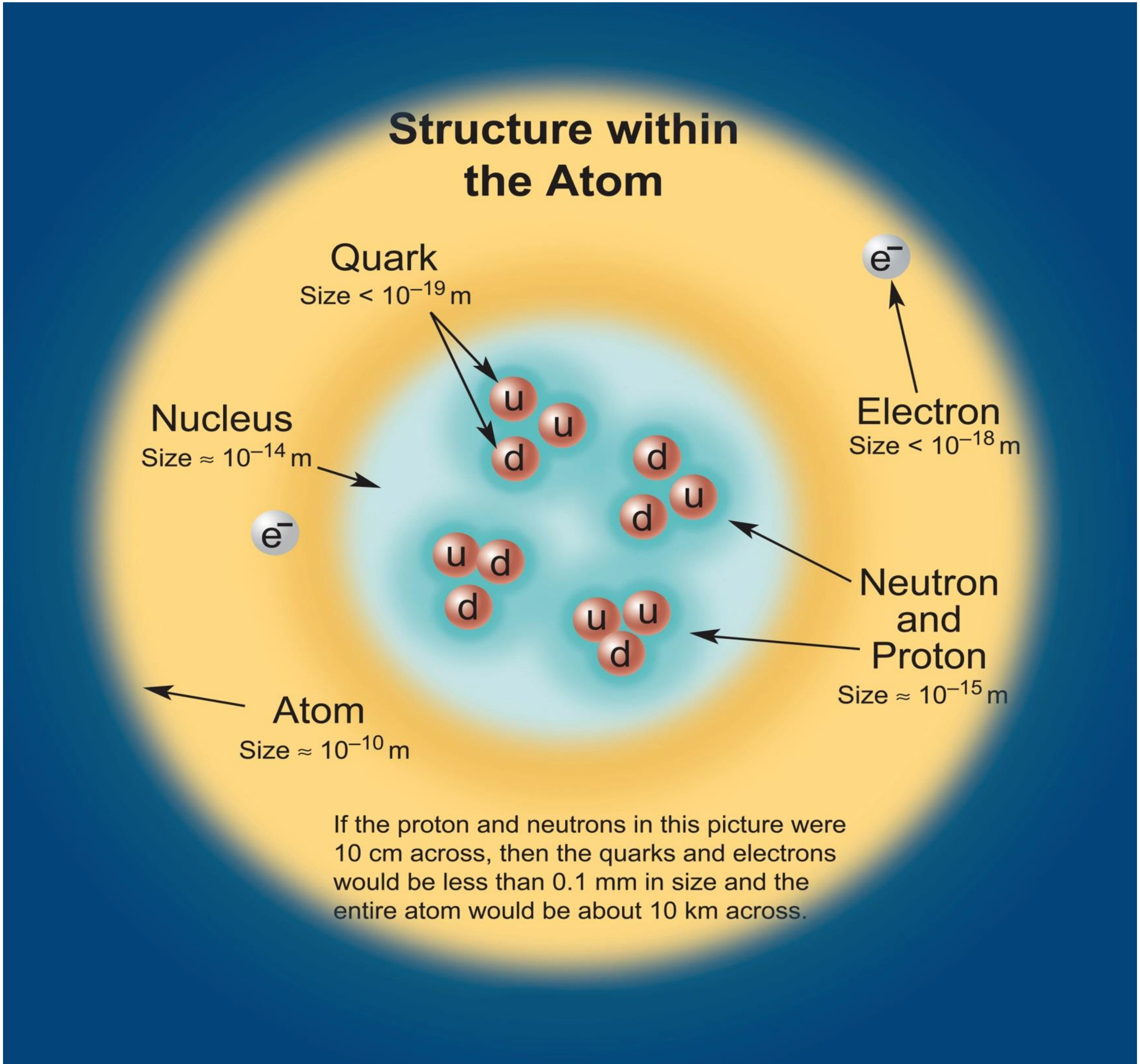
Structure within the Atom
Quark
Size < 10^{-19} m
u
u
d
e⁻
Electron
Size < 10^{-18} m
Nucleus
Size ≈ 10^{-14} m
d
u
d
e⁻
u
d
d
u
u
d
Neutron and Proton
Size ≈ 10^{-15} m
Atom
Size ≈ 10^{-10} m
If the proton and neutrons in this picture were 10 cm across, then the quarks and electrons would be less than 0.1 mm in size and the entire atom would be about 10 km across.

Quantum mechanics – language to describe the microscopic world

In classical physics, all things are either particles or waves.

Particles: atoms, electrons, cars, boats, houses, people…..

Waves: light, heat, water motion, radio signals, ….

Particles and waves are distinct objects, and things just don't have the properties of both.

However, if we look a little closer, these facts and interpretations start to blur…

We are led to conclude that ALL “things”, whether electrons or photons or automobiles or ...... are both particle and wave!

Which property we “measure” depends upon the type of measurement that is carried out.

Particles		Waves	
	$$E = \frac{p^2}{2m}$$	$$E = hf$$	
de Broglie wavelength	$$\lambda = \frac{h}{p} = \frac{h}{\sqrt{2mE}}$$	$$\lambda = \frac{c}{f} = \frac{hc}{E}$$	optical wavelength
	$$k = \frac{2\pi}{\lambda} = \frac{\sqrt{2mE}}{\hbar}$$	$$k = \frac{2\pi}{\lambda} = \frac{E}{\hbar c}$$	

While we use similar notation for particles and for true waves, various quantities are defined differently. Do not make the mistake of using *optical* definitions for *particles*.

Schroedinger equation (1926):

$$i\hbar\frac{\partial\psi(\mathbf{r},t)}{\partial t} = -\frac{\hbar^2}{2m}\nabla^2\psi(\mathbf{r},t) + V(\mathbf{r},t)\psi(\mathbf{r},t).$$

Describes the evolution of the wave function associated with the particle of mass ***m*** moving in a potential ***V(r,t)*** *(* Force ***F=-grad(V)*** *)*

Definition of $\Psi(r,t)$

- The probability $P(\boldsymbol{r},t)dV$ to find a particle associated with the wavefunction $\Psi(\boldsymbol{r},t)$ within a small volume dV around a point in space with coordinate $\boldsymbol{r}$ at some instant t is

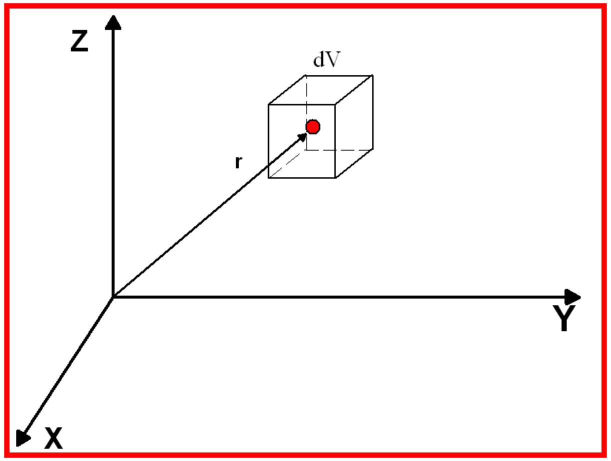

$$P(\mathbf{r},t)dV = |\Psi(\mathbf{r},t)|^2 dV$$

  - $P(\boldsymbol{r},t)$ is the probability density

- For one-dimensional case

$$P(x,t)dV = |\Psi(x,t)|^2 dx$$

$$\text{Here } |\Psi(\boldsymbol{r},t)|^2 = \Psi^*(\boldsymbol{r},t)\Psi(\boldsymbol{r},t)$$

Quantum Mechanics

- The methods of Quantum Mechanics consist in finding the wavefunction associated with a particle or a system

- Once we know this wavefunction we know “everything” about the system!

The Uncertainty Principle

An experiment cannot simultaneously determine a component of the momentum of a particle (e.g., p_x) and the exact value of the corresponding coordinate, x.

The best one can do is

$$\boxed{(\Delta p_x)(\Delta x) \geq \frac{\hbar}{2}}$$

Uncertainty principle between energy and time:

$$\boxed{(\Delta E)(\Delta t) \geq \frac{\hbar}{2}}$$

It implies eg. that one cannot measure precisely the energy of unstable particle

Finite Potential Well
Discrete energies of quantum states obtained from Schroedinger equation.
Graphical Results for Probability Density, $|\psi(x)|^2$

- The probability densities for the lowest three states are shown
- The functions are smooth at the boundaries
- Outside the box, the probability of finding the particle decreases exponentially, but it is not zero!

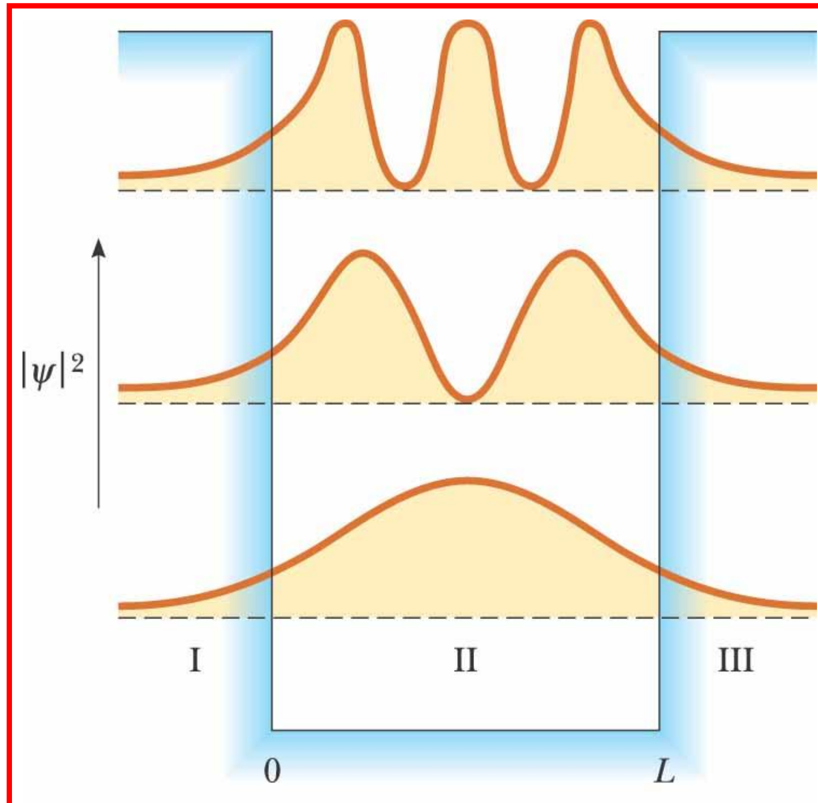

Pauli principle:

In many-particle system two identical fermions cannot occupy the same quantum state.

Quantum state can be described by a set of so-called **quantum numbers:**

<u>Examples:</u>

1) Quantum state of an electron in an atom can be described by:

- **the principal quantum number (associated with energy),**
- **orbital quantum number (associated with angular momentum),**
- **magnetic quantum number (associated with a projection of angular momentum on a given axis)**
- **spin quantum number (associated with a projection of spin on a given axis)**

2) Also a position in space can be regarded as a quantum state, where 4 quantum numbers can be associated with positions: x,y,z and spin.

Some history

- **1868** Mendeleev's periodic classification of the elements.
- **1895** Discovery of X-rays by Roentgen.
- **1896** Discovery of radioactivity by Becquerel.
- **1897** Identification of the electron by J.J. Thomson.
- **1898** Separation of the elements polonium and radium by Pierre and Marie Curie.
- **1908** Measurement of the charge +2 of the α particle by Geiger and Rutherford.
- **1911** Discovery of the nucleus by Rutherford; "planetary" model of the atom.
- **1913** Theory of atomic spectra by Niels Bohr.
- **1914** Measurement of the mass of the α particle by Robinson and Rutherford.
- **1924–1928** Quantum theory (de Broglie, Schrödinger, Heisenberg, Born, Dirac).
- **1928** Theory of barrier penetration by quantum tunneling, application to α radioactivity, by Gamow, Gurney and Condon.
- **1929–1932** First nuclear reactions with the electrostatic accelerator of Cockcroft and Walton and the cyclotron of Lawrence.
- **1930–1933** Neutrino proposed by Pauli and named by Fermi in his theory of beta decay.
- **1932** Identification of the neutron by Chadwick.
- **1934** Discovery of artificial radioactivity by F. and I. Joliot-Curie.
- **1934** Discovery of neutron capture by Fermi.
- **1935** Liquid-drop model and compound-nucleus model of N. Bohr.
- **1935** Semi-empirical mass formula of Bethe and Weizsäcker.
- **1938** Discovery of fission by Hahn and Strassman.
- **1939** Theoretical interpretation of fission by Meitner, Bohr and Wheeler.

- **1938** Bethe and Weizsäcker propose that stellar energy comes from thermonuclear fusion reactions.
- **1946** Gamow develops the theory of cosmological nucleosynthesis.
- **1953** Salpeter discovers the fundamental solar fusion reaction of two protons into deuteron.
- **1957** Theory of stellar nucleosynthesis by Burbidge, Burbidge, Fowler and Hoyle.
- **1960**– Detection of solar neutrinos
- **1987** Detection of neutrinos and γ-rays from the supernova SN1987a.

Mass number
(proton and neutron number)

Atomic number
(proton number)

Element

$$^{A}_{Z}X_{N}$$

Neutron number
N=A-Z

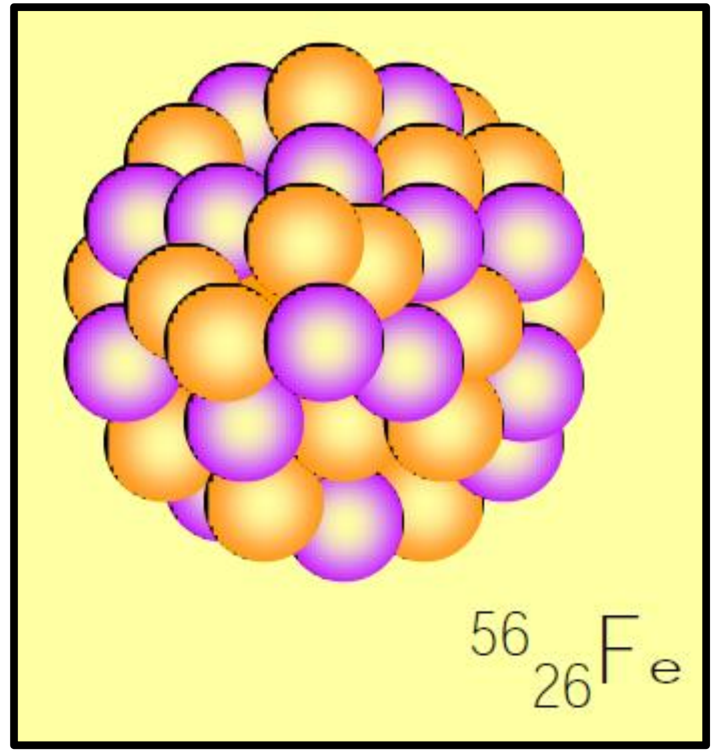

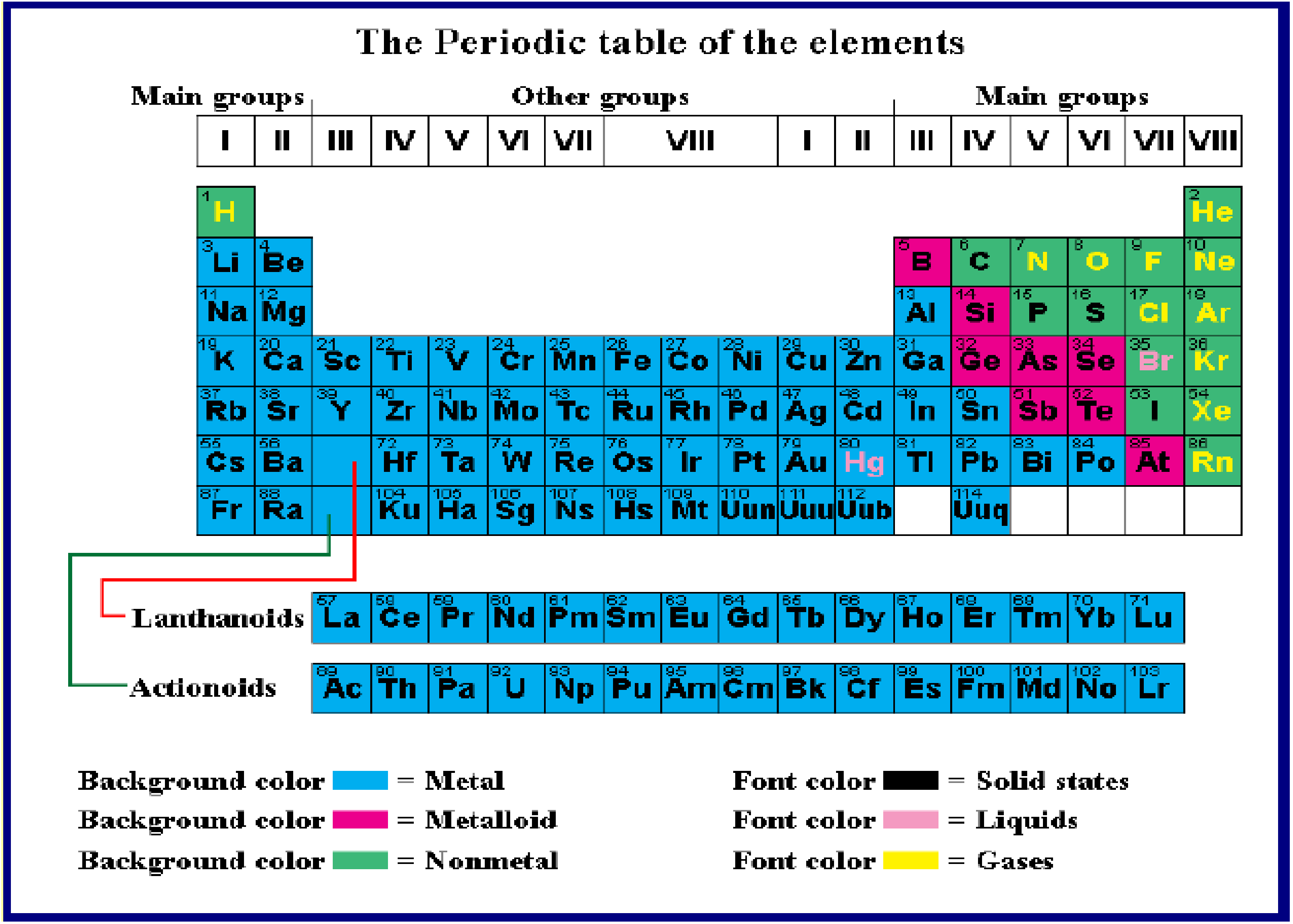

Neutron number may vary for each element.

Isotopes – nuclei of the same element possessing different number of neutrons

Isotones – nuclei with the same number of neutrons

Isobars – nuclei with the same mass number

Nuclear constituents:

Depends on the energy scale we are interested in:

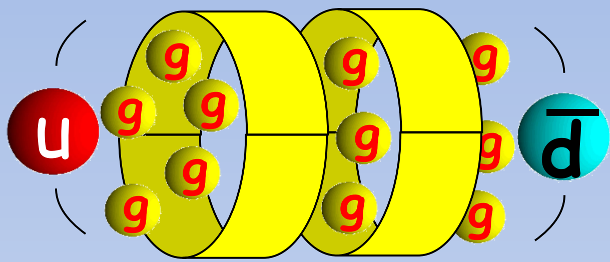

Quarks and gluons
QCD energy scale: 1000MeV

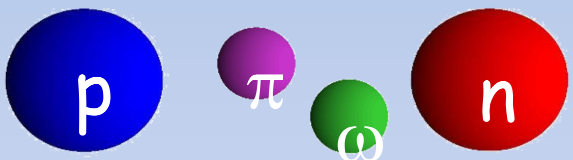

Baryons and mesons
Energy scale: 100MeV

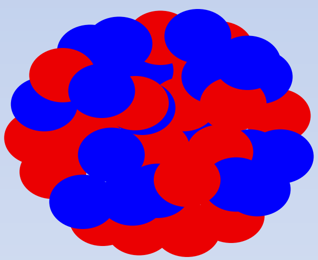

Nucleons
Energy scale: 10MeV

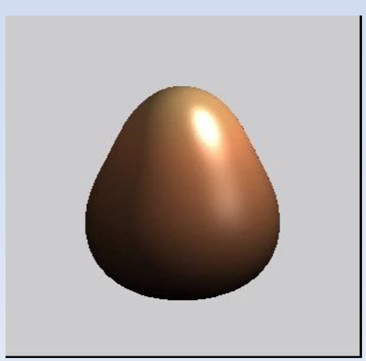

Collective degrees of freedom: 0.1-1MeV

For energies lower than 100 MeV nucleus consists of protons and neutrons (nucleons)

Masses of protons and neutrons:

$$m_{\mathrm{n}}c^2 = 939.56\,\mathrm{MeV} \qquad m_{\mathrm{p}}c^2 = 938.27\,\mathrm{MeV} \quad ,$$

i.e. a mass difference of order one part per thousand

$$(m_{\mathrm{n}} - m_{\mathrm{p}})c^2 \ = \ 1.29\,\mathrm{MeV} \ .$$

Compare to the electron mass which is 0.511 MeV only

Due to the presence of spin nucleons possess a magnetic moment (nucleons behave like small magnets)

$$\mu_{\mathrm{p}} = 2.792\,847\,386\,(63)\,\mu_{\mathrm{N}} \qquad \mu_{\mathrm{n}} = -1.913\,042\,75\,(45)\,\mu_{\mathrm{N}}\ ,$$

where the *nuclear magneton* is

$$\mu_{\mathrm{N}} = \frac{e\hbar}{2m_{\mathrm{p}}} = 3.152\,451\,66\,(28)\ \times 10^{-14}\mathrm{MeV\,T^{-1}}\ .$$

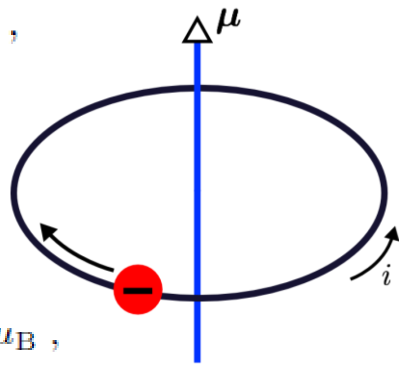

Compare to the electron magnetic moment:

$$\mu_{\mathrm{e}} = 1.001\,159\,652\,193\,(40)\,\mu_{\mathrm{B}}\ ,$$

where the *Bohr magneton* is

$$\mu_{\mathrm{B}} = \frac{q\hbar}{2m_{\mathrm{e}}} = 5.788\,382\,63\,(52)\ \times 10^{-11}\mathrm{MeV\,T^{-1}}\ .$$

Nuclear chart

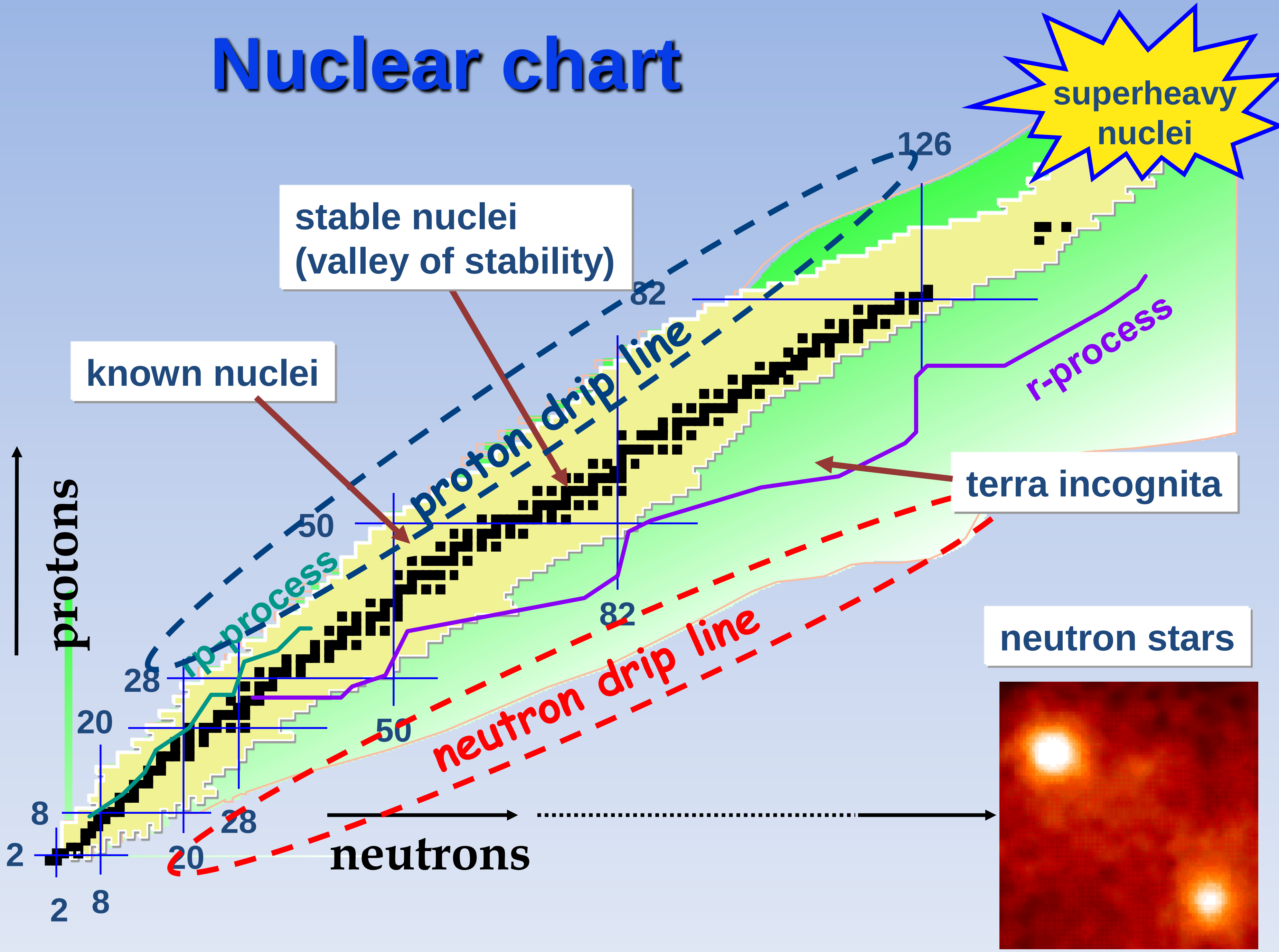

http://www.nndc.bnl.gov/

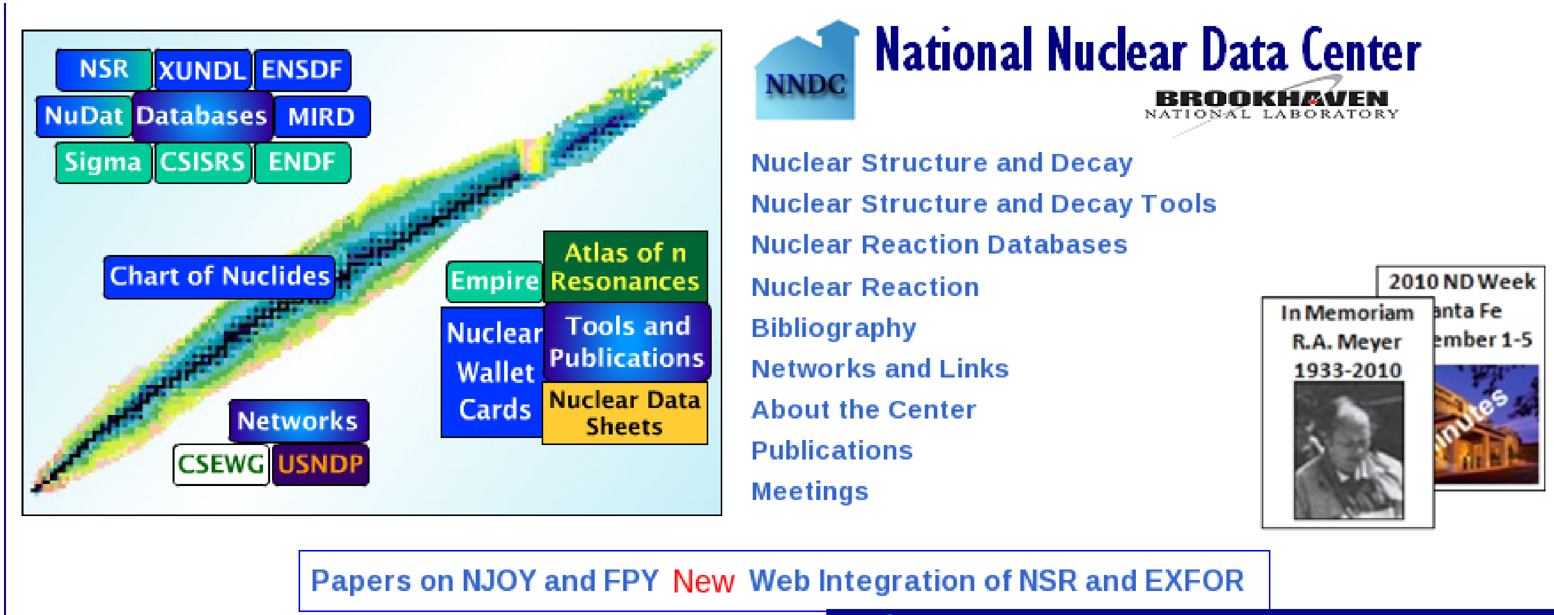

Various experimental and theoretical data concerning nuclei can be found on this web page.
In particular: binding energy, decay channels, half-lives, excitation spectrum, etc.

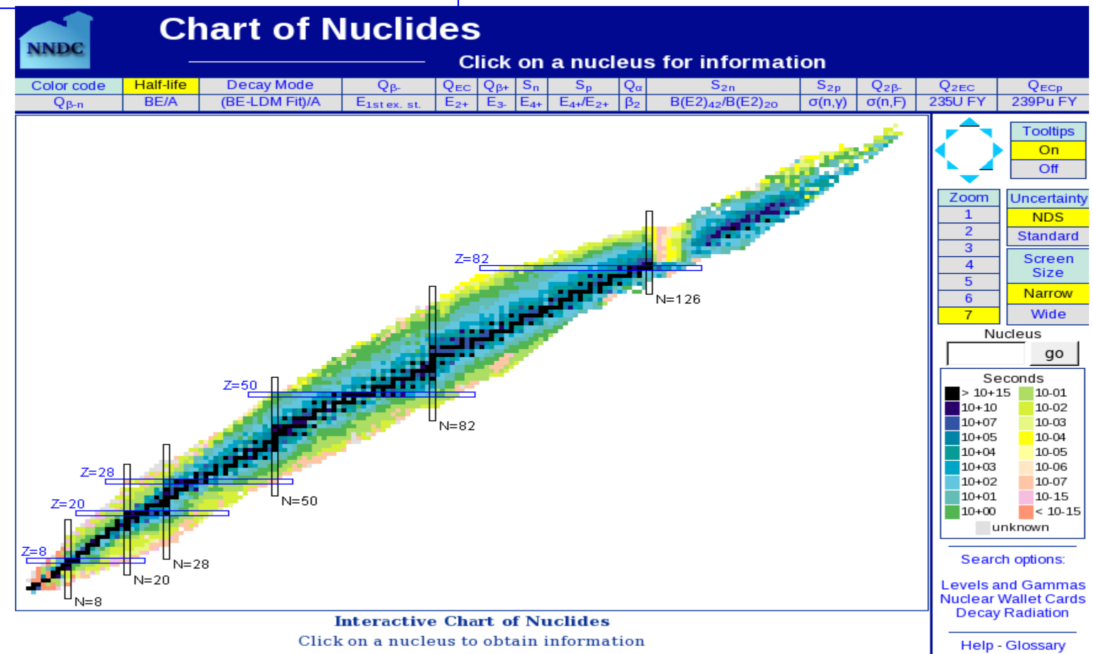

Nuclear sizes

Radius of a spherical nucleus: $\boxed{R = r_0 A^{1/3}}$

r_0=1.2 fm

Density distribution of nucleons inside a nucleus

One can parametrize the density distribution:

$$\boxed{\rho(r) = \frac{\rho_0}{1 + e^{(r-R)/a}}}$$

Where $\rho_0 \approx 0.15 - 0.16 \frac{n}{fm^3}$

$a \approx 0.5\, fm$

Approximately constant inside

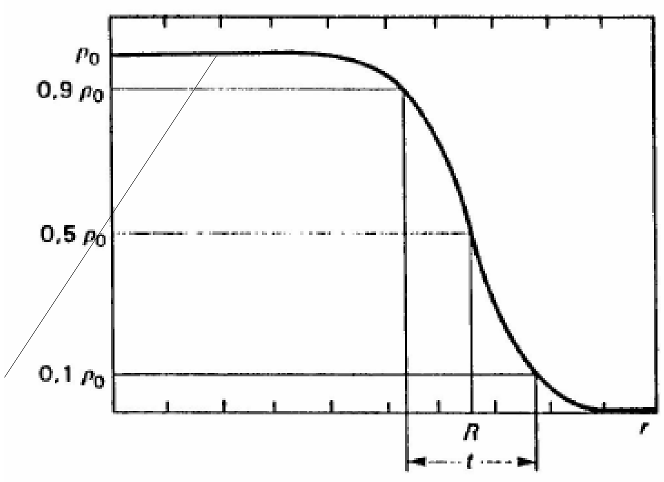

Mass density inside nucleus:

$$\rho_N \approx \frac{1,67 \cdot 10^{-24}\,\mathrm{g}}{\frac{4}{3}\pi(1,2\,\mathrm{fm})^3} \approx 2,3 \cdot 10^{14}\,\mathrm{g/cm^3} \approx 230\,\mathrm{mln\ ton/cm^3}$$

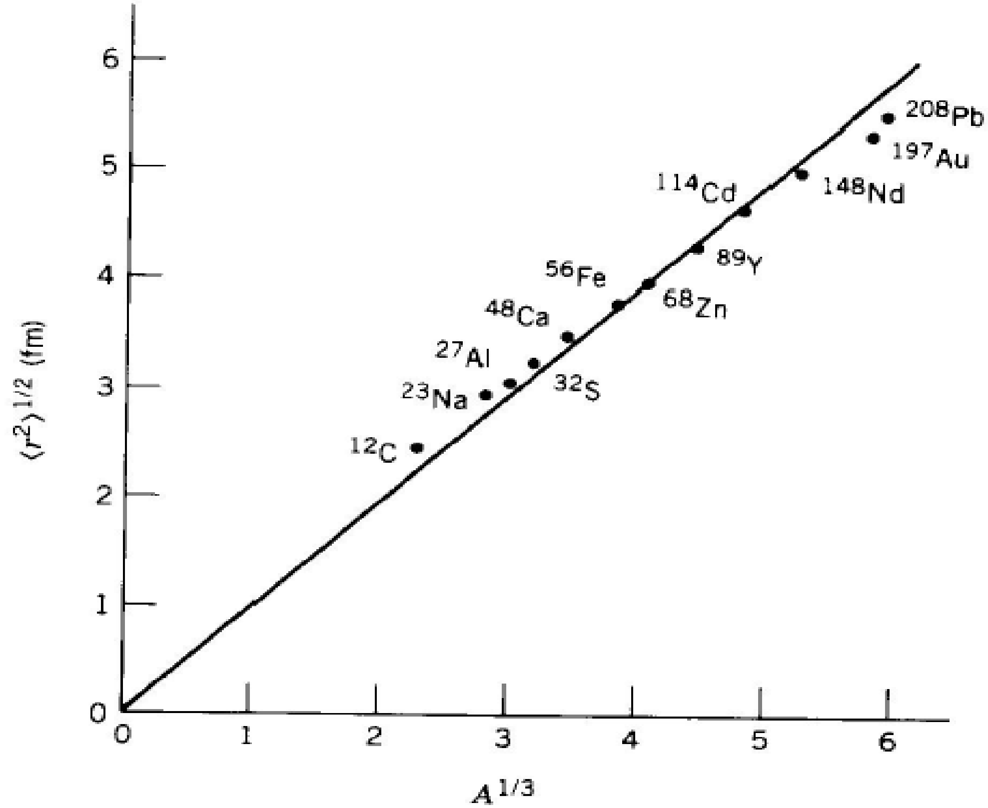

Figure 3.5 The rms nuclear radius determined from electron scattering experiments. The slope of the straight line gives $R_0 = 1.23$ fm. (The line is not a true fit to the data points, but is forced to go through the origin to satisfy the equation $R = R_0 A^{1/3}$.) The error bars are typically smaller than the size of the points (± 0.01 fm). More complete listings of data and references can be found in the review of C. W. de Jager et al., *Atomic Data and Nuclear Data Tables* **14**, 479 (1974).

$$(r_{\rm rms})^2 = \frac{\int \mathrm{d}^3\boldsymbol{r}\, r^2 \rho(\boldsymbol{r})}{\int \mathrm{d}^3\boldsymbol{r}\, \rho(\boldsymbol{r})} \,.$$

To extract the density distribution
inside a nucleus we scatter electrons
which interact with protons and
measure so-called charge density
distribution. We assume that
the distribution of neutrons is similar.

However it may not be true for nuclei
with large N/Z ratio.

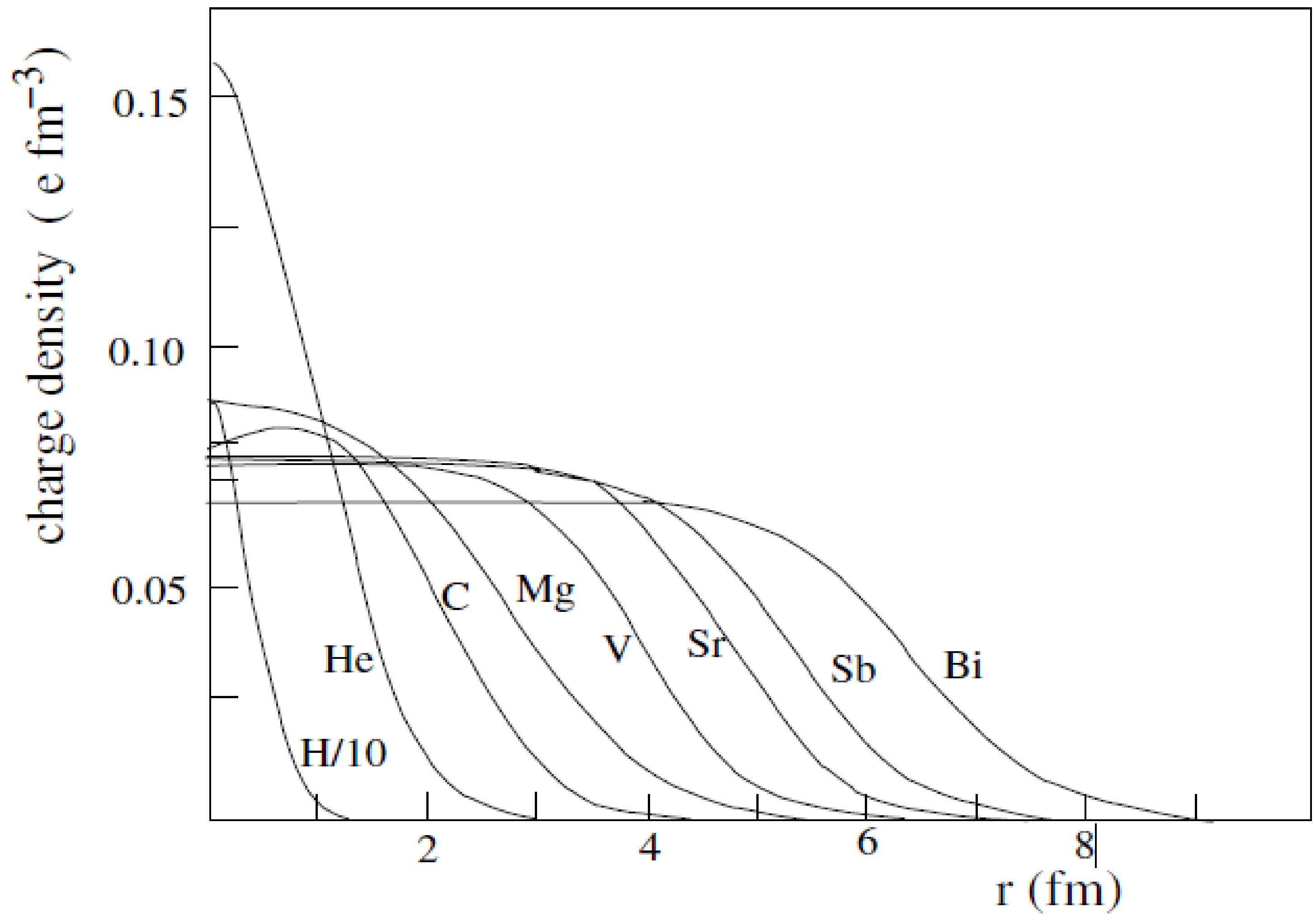

Fig. 1.1. Experimental charge density (e fm^{-3}) as a function of r(fm) as determined in elastic electron–nucleus scattering [8]. Light nuclei have charge distributions that are peaked at $r = 0$ while heavy nuclei have flat distributions that fall to zero over a distance of ~ 2 fm.

Table 1.1. Radii of selected nuclei as determined by electron–nucleus scattering [8]. The size of a nucleus is characterized by $r_{\rm rms}$ (1.11) or by the radius R of the uniform sphere that would give the same $r_{\rm rms}$. For heavy nuclei, the latter is given approximately by (1.9) as indicated in the fourth column. Note the abnormally large radius of ^{2}H.

nucleus	$r_{\rm rms}$ (fm)	R (fm)	$R/A^{1/3}$ (fm)	nucleus	$r_{\rm rms}$ (fm)	R (fm)	$R/A^{1/3}$ (fm)
^{1}H	0.77	1.0	1.0	^{16}O	2.64	3.41	1.35
^{2}H	2.11	2.73	2.16	^{24}Mg	2.98	3.84	1.33
^{4}He	1.61	2.08	1.31	^{40}Ca	3.52	4.54	1.32
^{6}Li	2.20	2.8	1.56	^{122}Sb	4.63	5.97	1.20
^{7}Li	2.20	2.8	1.49	^{181}Ta	5.50	7.10	1.25
^{9}Be	2.2	2.84	1.37	^{209}Bi	5.52	7.13	1.20
^{12}C	2.37	3.04	1.33				

Some nuclei violate this simple picture of density distribution

Halo nuclei: nuclei with weakly bound neutrons

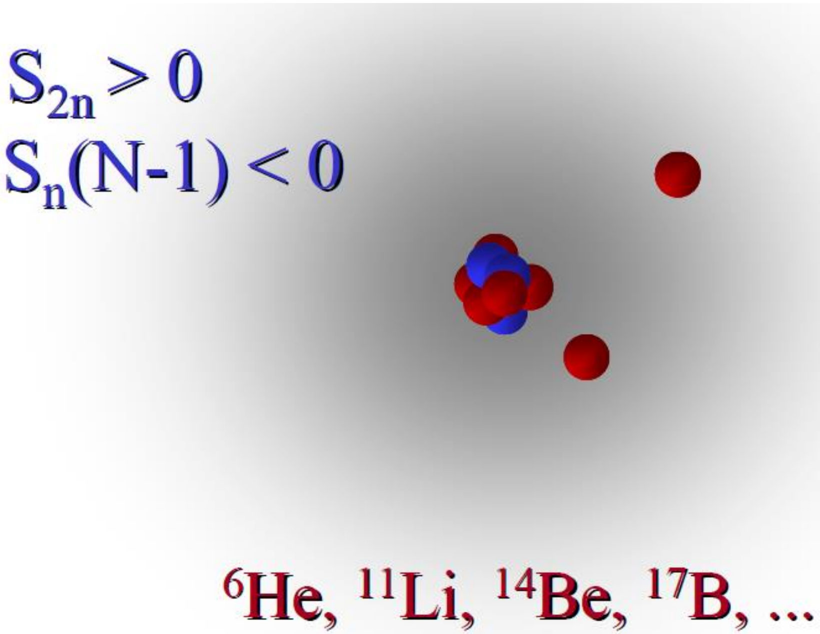

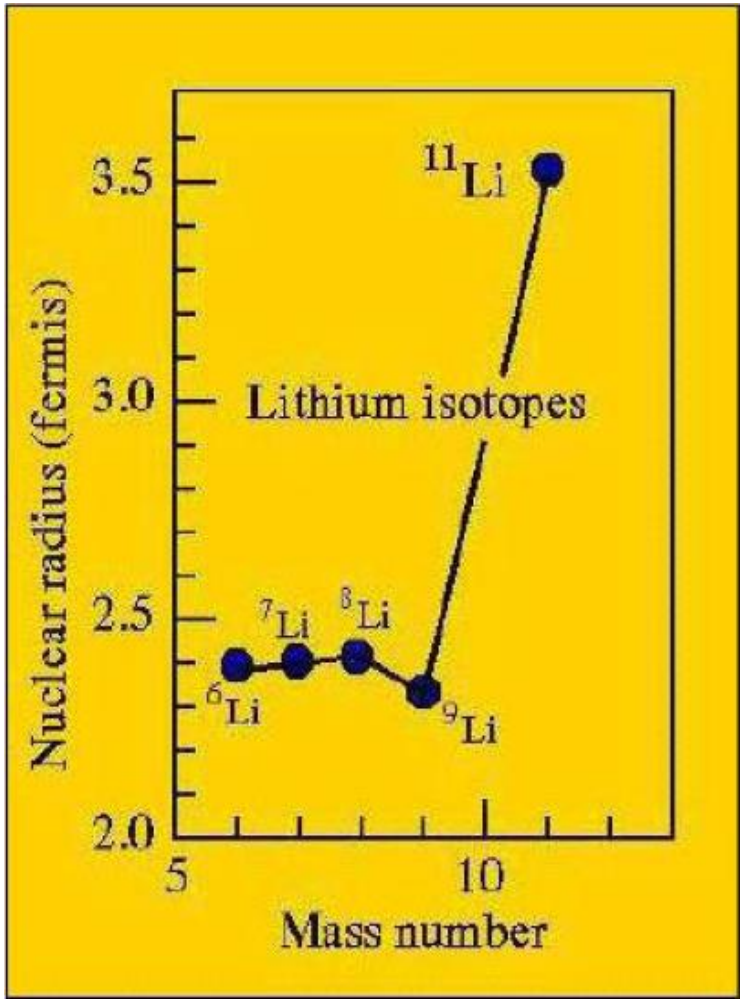

Nuclei can be deformed

Ground-state – the quantum state with the lowest energy

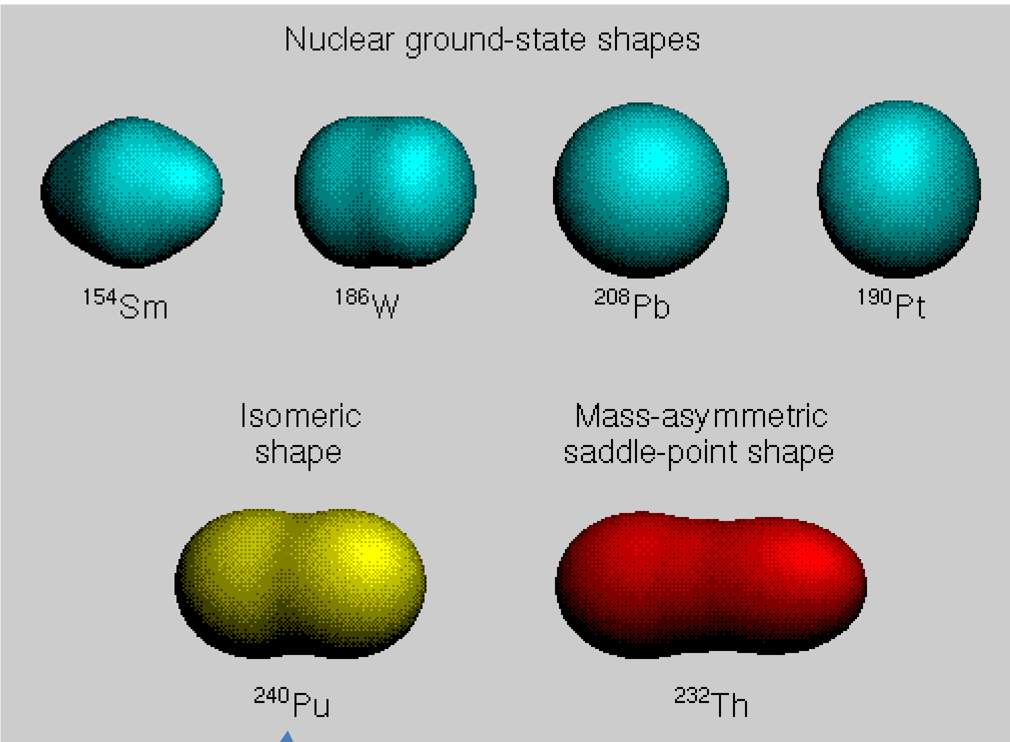

Nuclei can rotate and fast rotation can affect shape of a nucleus:

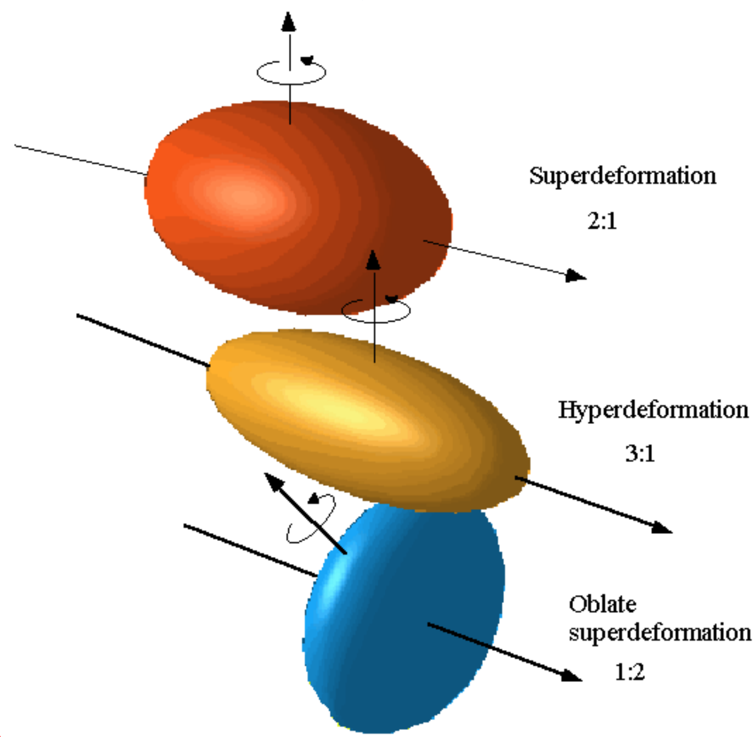

Some nuclei can exist in a long-lived excited state which has a different deformation than in the ground state – it is called an **isomeric state**

Binding energy of a nucleus

$$B(A,Z) = Nm_{\mathrm{n}}c^2 + Zm_{\mathrm{p}}c^2 - m(A,Z)c^2$$

Note that mass of a nucleus is smaller than the sum of masses of nucleons.
This is the so-called the **mass defect.**

It tells us that part of nucleon masses is used to keep the nucleus bound
(according to the Einstein formula: $E = mc^2$)

Binding energy can be easily measured experimentally and gives us one of the most
Important information about nuclei.

Typical value of B/A is of the order of 8 MeV

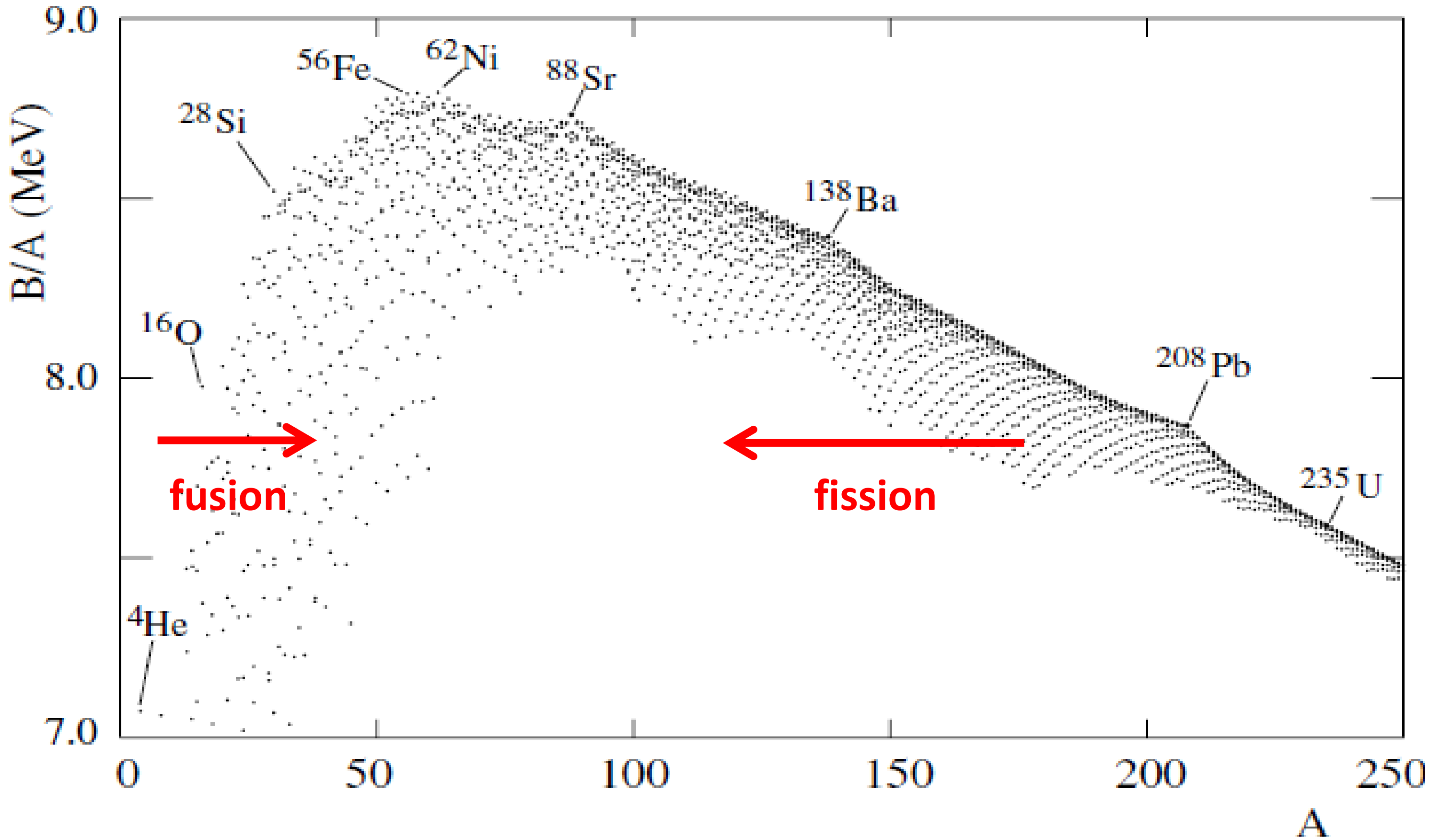

Fig. 1.2. Binding energy per nucleon, $B(A,Z)/A$, as a function of A. The upper panel is a zoom of the low-A region. The filled circles correspond to nuclei that are not β-radioactive (generally the lightest nuclei for a given A). The unfilled circles are unstable (radioactive) nuclei that generally β-decay to the lightest nuclei for a given A.

There are two ways of getting the energy from nuclear reaction:

- either by a synthesis of light nuclei
- or by fissioning of heavy nuclei

Some nuclei are more strongly bound than neighbors

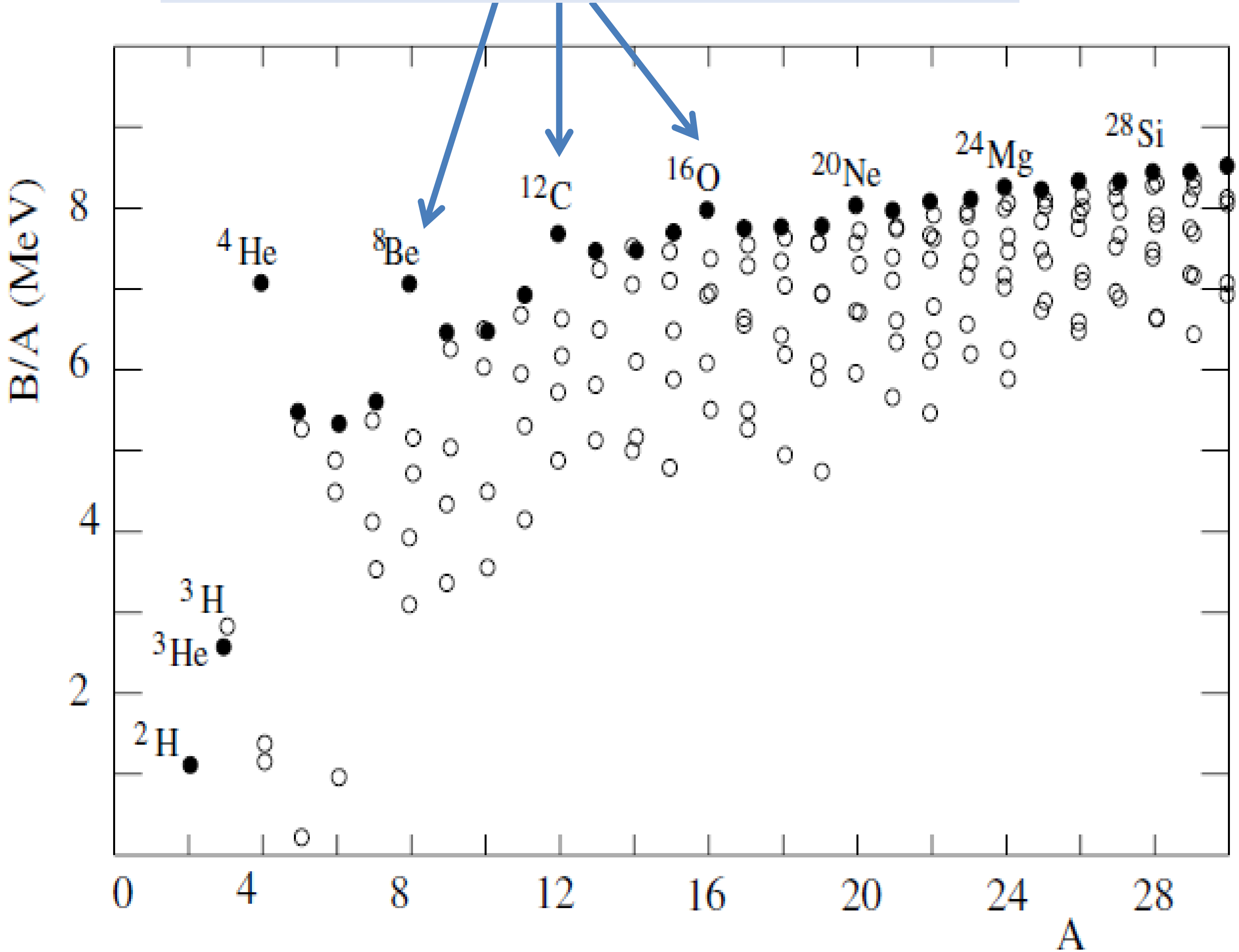

Some features related to binding energy behavior:

- B/A is approximately constant for a wide range of nuclei:
  7.7 MeV < B/A < 8.8 MeV for 12<A<225

- One could expect that B/A should be proportional to A if binding comes from interactions between two nucleons (since there are A(A-1)/2 pairs). The fact that B/A is approximately constant indicates that forces between nucleons are of short range. Hence there is only the interaction between nearest neighbors in nuclei – **saturation property of nuclear forces** (of course except Coulomb interaction which is long range)

- Numbers of protons and neutron for which nuclei are more strongly bound than nuclei in the vicinity are called:

- Numbers of protons and neutron for which nuclei are more strongly bound than nuclei in the vicinity are called:

MAGIC NUMBERS

Magic numbers: 2, 8, 20, 28, 50, 82, 126
Examples of doubly magic nuclei (both proton and neutron numbers are magic) : 4He, 20Ca, 56Ni, 132Sn, 208Pb

- The most strongly bound nucleus is **56Fe**

Separation energy

Neutron separation energy

$$S_n = m_n c^2 + m(Z, A-1)c^2 - m(Z, A) = B(Z, A) - B(Z, A-1)$$

$$S_p = m_p c^2 + m(Z-1, A-1)c^2 - m(Z, A) = B(Z, A) - B(Z-1, A-1)$$

Proton separation energy

Separation energy:
Energy required to separate either proton or neutron from a nucleus.

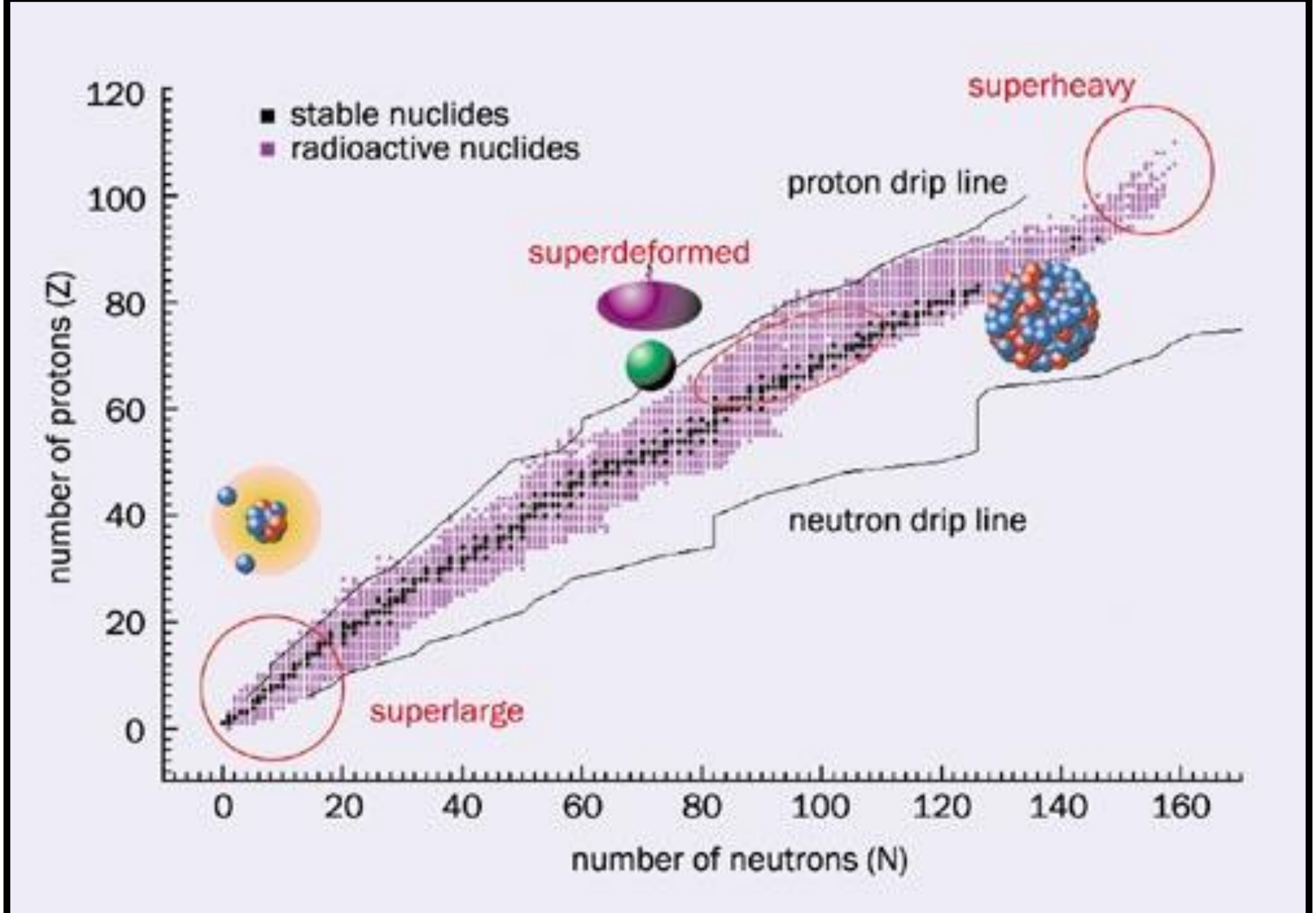

Proton drip line: $S_p \approx 0$

Neutron drip line: $S_n \approx 0$

Beyond the proton (neutron) drip line the proton (neutron) separation Energy becomes negative indicating that such nuclei can spontaneously emit protons (neutrons) from the ground state.

Negative separation energy does not tell us however how fast a nucleus will get rid of nucleons. Some nuclei (in particular beyond proton drip lines) can still have fairly large lifetime.

Note that so far we considered nuclei in their ground states only!
If a nucleus is excited it can still emit particles even in the case when the separation energy in positive providing the excitation energy is large enough, i.e. if the following inequalities hold:

$$S_n - E^* < 0$$ **- Possible to emit neutrons**

$$S_p - E^* < 0$$ **- Possible to emit protons**

where E* is an excitation energy.

Nuclear excited states

Nucleus can be excited in various ways. Some of them have simple interpretations:
e.g. rotations, vibration

If excitation energy is not too large then excited nucleus decays by emitting gamma radiation.

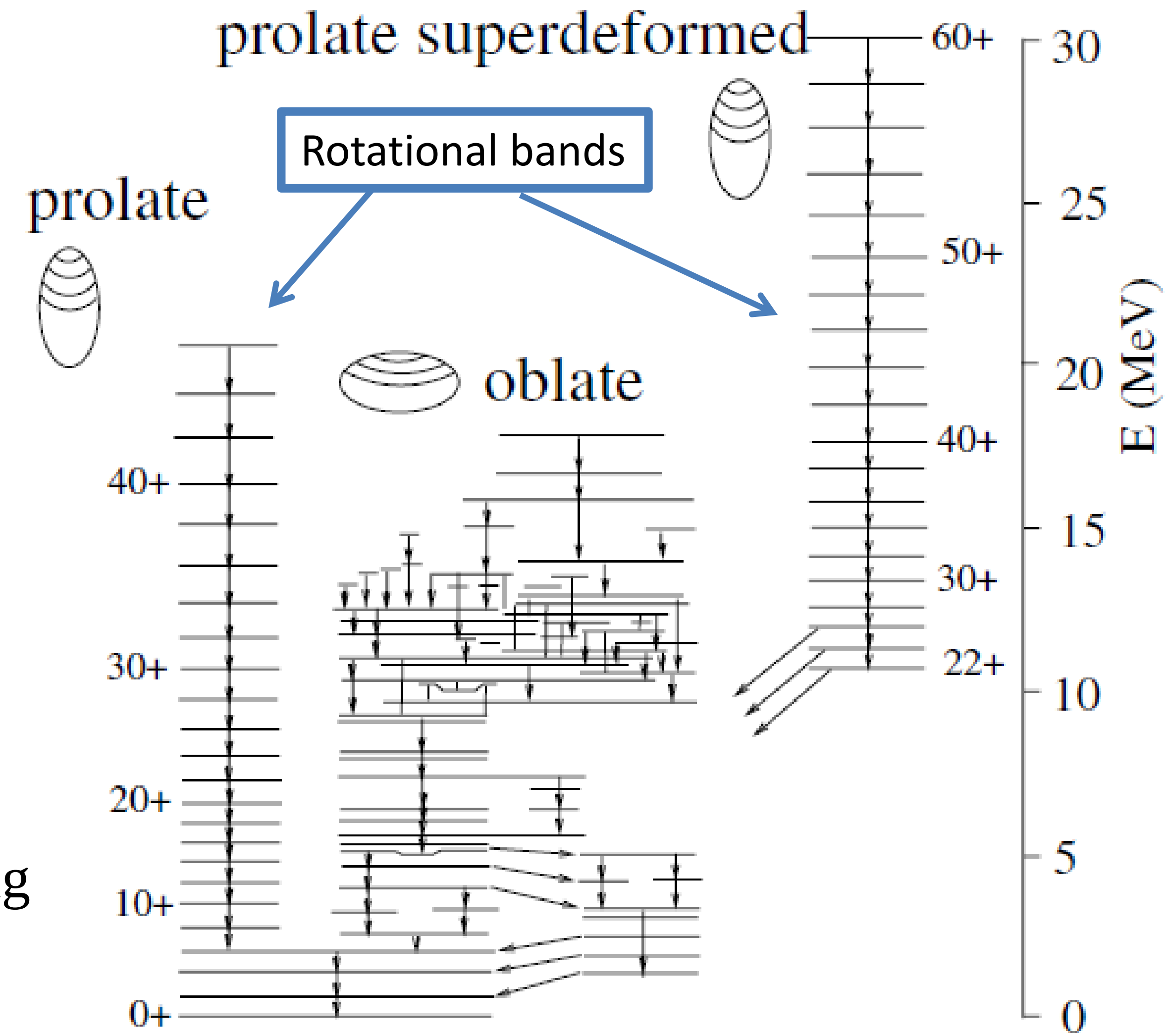

Excited states of ^{152}Dy

Exctited states – notation

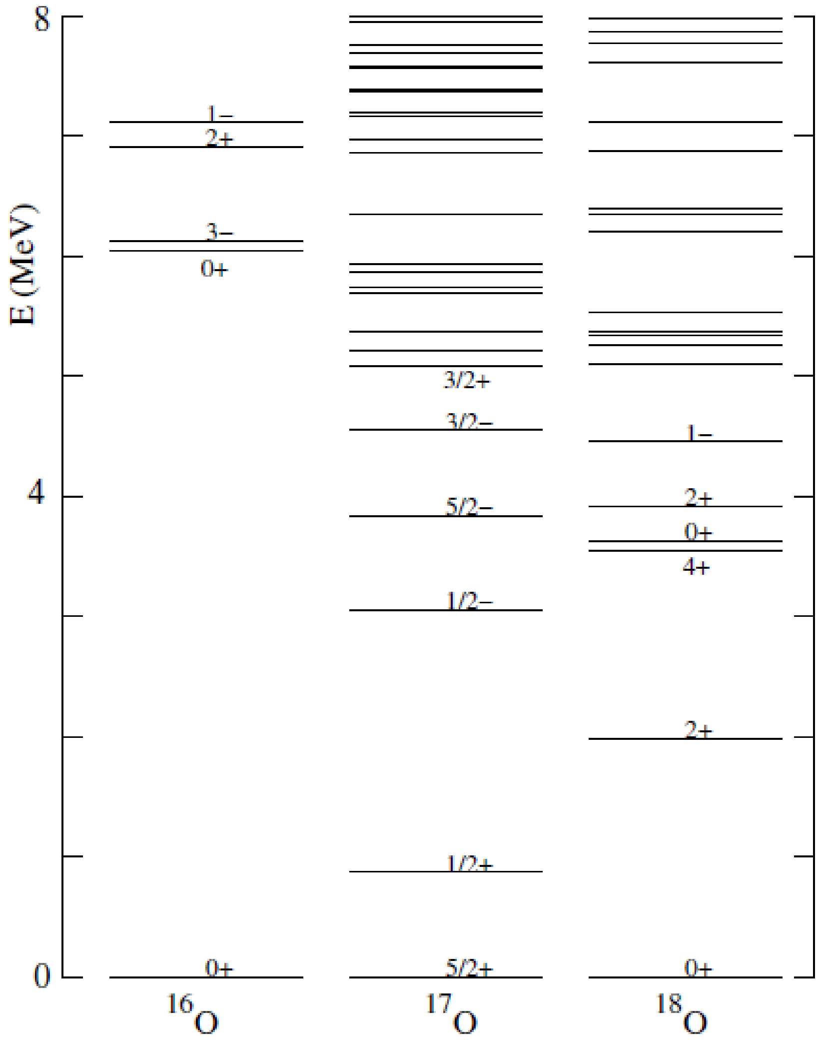

$$J^P \equiv \text{spin}^{\text{parity}}$$

Parity

Total angular momentum (total nuclear spin)

$$\vec{J} = \sum_i (\vec{L}_i + \vec{s}_i)$$

Orbital angular momentum

Spin

Parity is an internal symmetry of wave function with respect to spatial inversion (x,y,z)-> (-x,-y,-z). Parity is either **positive or negative** and it is **conserved** in processes involving **strong and electromagnetic interactions .**

Typical energy of gamma radiation emitted by nuclei: 10 keV – 1 MeV

$$E = \hbar\omega \; ; \quad \omega = ck = \frac{2\pi c}{\lambda}$$

$$E = \frac{2\pi\hbar c}{\lambda}; \quad \hbar c \approx 197 MeV \cdot fm$$

$$\lambda \approx \frac{2\pi \cdot 197}{(0.01-1)} fm = (1237.79 - 123779)\, fm \approx 0.001 - 0.1 nm$$

Visible light: $400nm < \lambda < 700nm$

Energy of gamma photon (light quantum) is about 1000 to 100000 times more energetic than quantum of visible light quantum.

Gamma detectors:

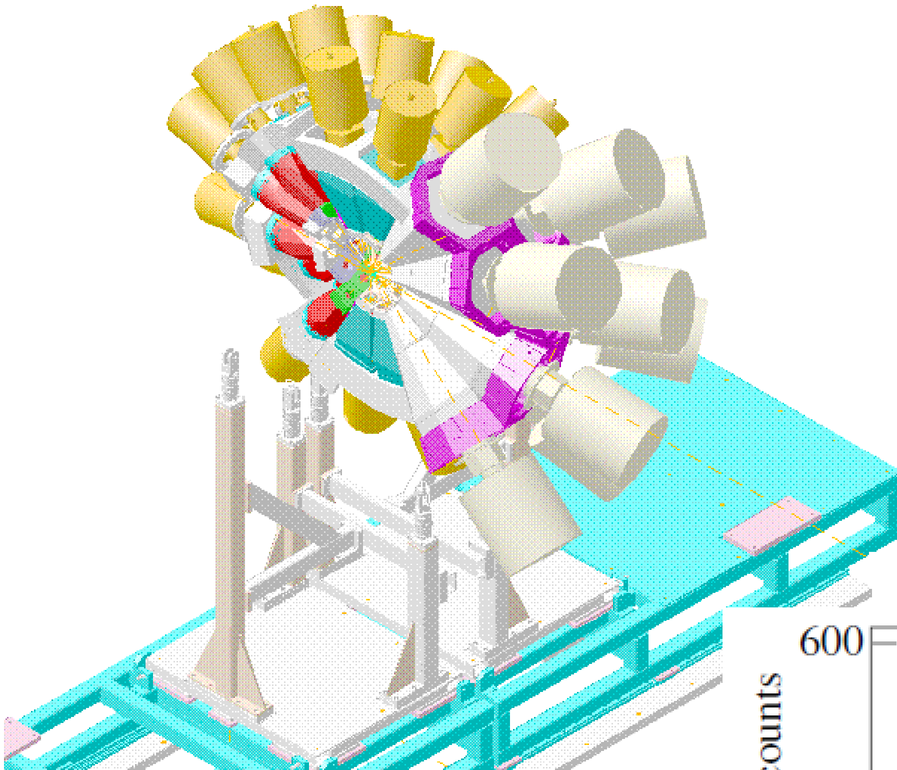

$$E(J) = \frac{J^2}{2I}$$

$$E_\gamma(J) = E(J+2) - E(J) = \frac{2J+1}{2I}$$

Gamma spectrum from rotational band

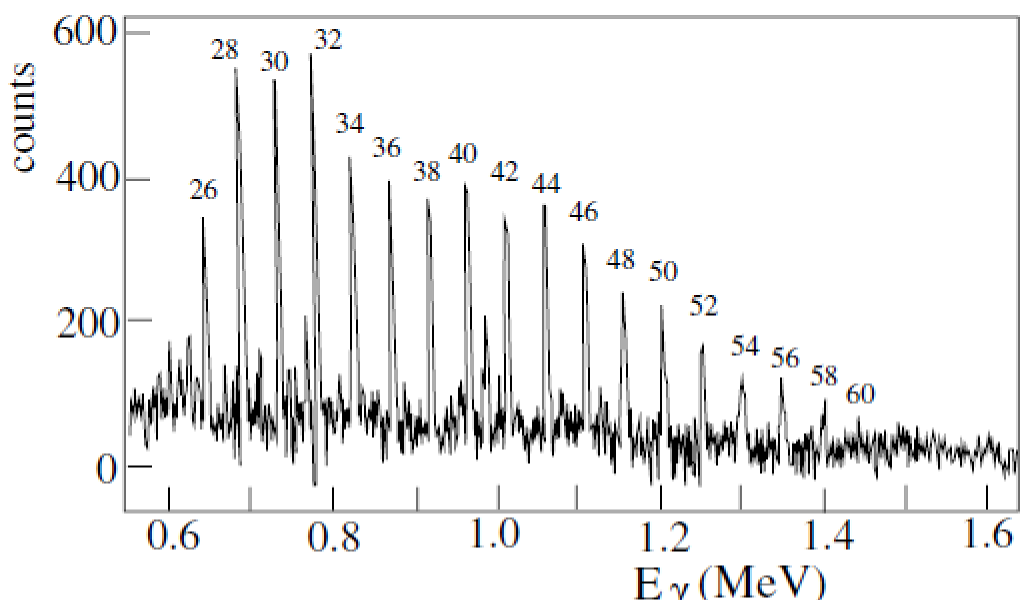

Mass spectrometer

$$qE = qvB \quad \Rightarrow \quad v = E/B$$

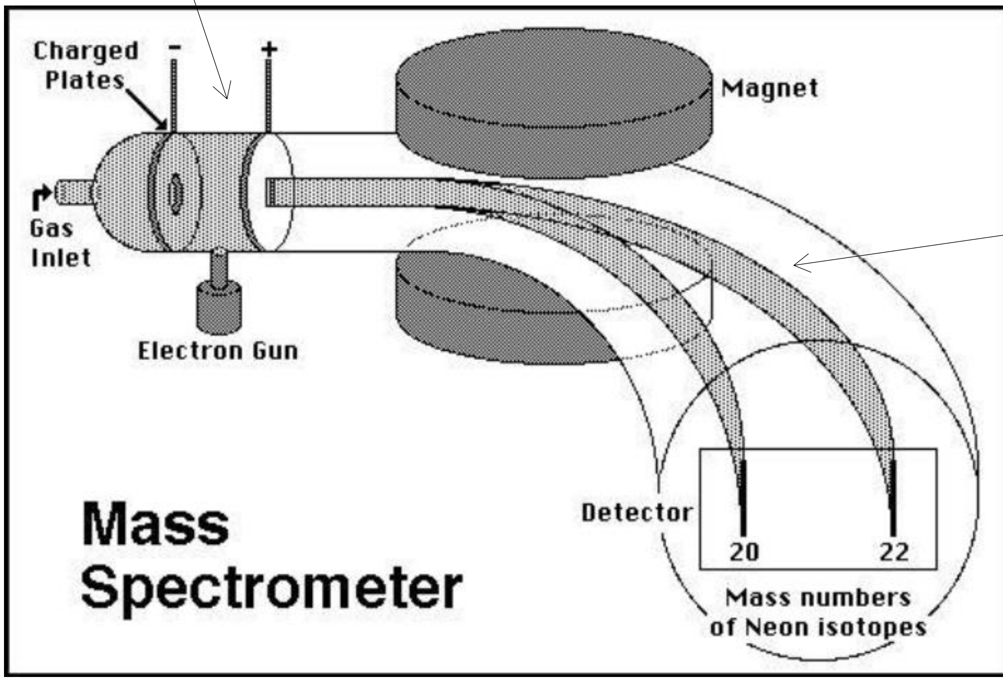

$$m\frac{v^2}{r} = qvB \quad \Rightarrow \quad r = mv/qB$$

$$m = qrB^2/E$$

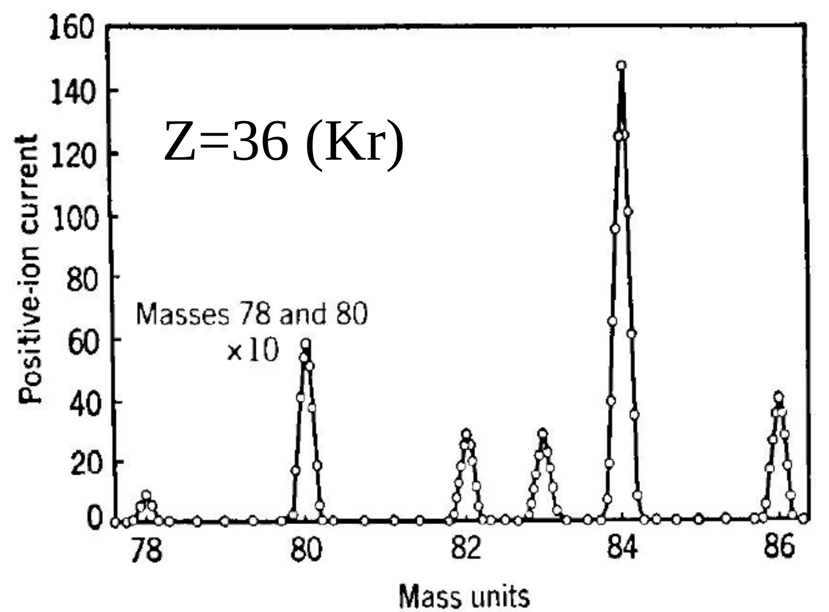

Cross section

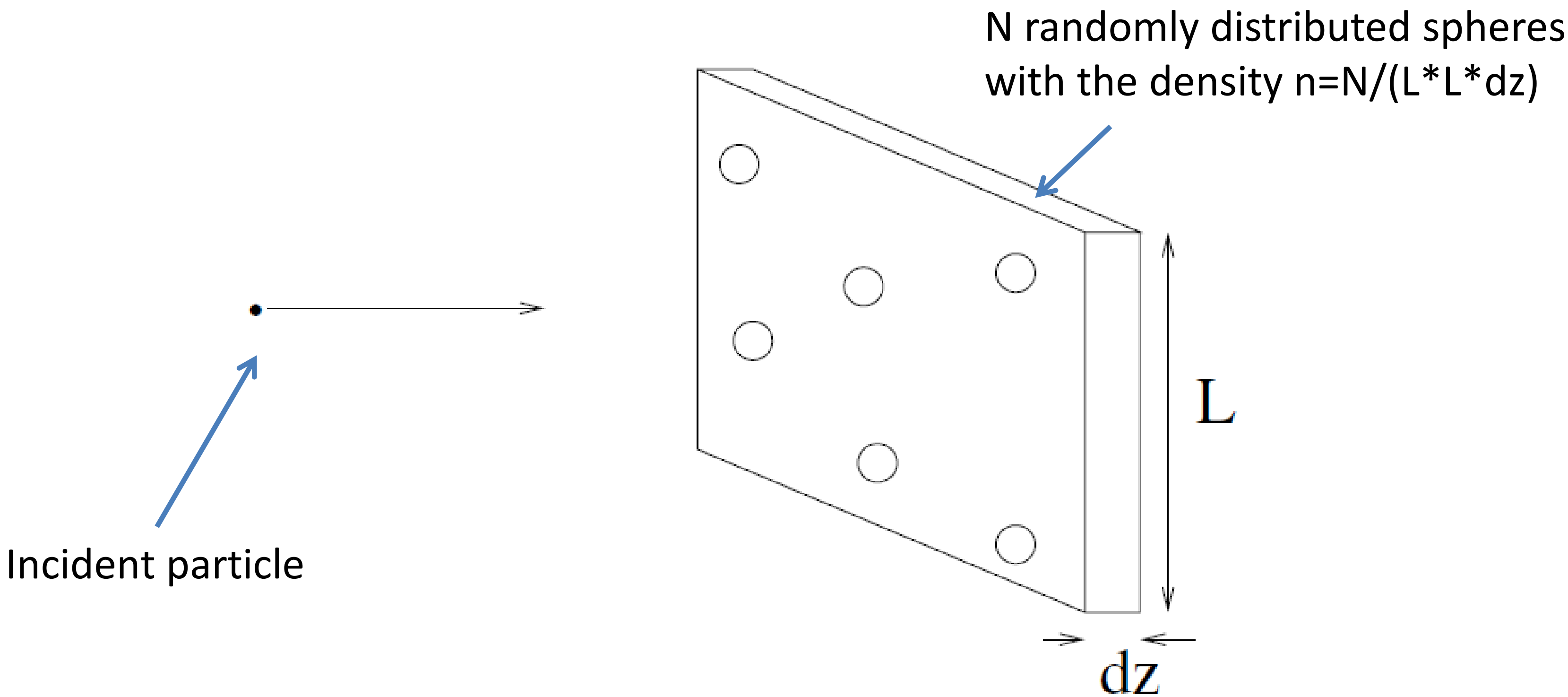

Fig. 3.1. A small particle incident on a slice of matter containing $N = 6$ target spheres of radius R. If the point of impact on the slice is random, the probability $\mathrm{d}P$ of it hitting a target particle is $\mathrm{d}P = N\pi R^2/L^2 = \sigma n \mathrm{d}z$ where the number density of scatterers is $n = N/(L^2 \mathrm{d}z)$ and the cross section per sphere is $\sigma = \pi R^2$.

Probability of an incident particle for hitting a sphere of a radius R reads:

$$\mathrm{d}P = \frac{N\pi R^2}{L^2} = \sigma n \mathrm{d}z \qquad \sigma = \pi R^2 .$$

Cross section: tells us what is the area of an obstacle as „seen" by the incident particle.

More precisely: σ

$$\boxed{\sigma = \frac{\text{Number of deflected particles per unit of time}}{\text{Number of incident particle per unit of time per unit area}}}$$

Cross section is the quantity which is relatively easy to measure experimentally

Generalization:

Suppose we are intersted in a certain reaction type which can be triggered by an incident particle. In such a case we ask for a probability that an incident particle will induce this particular reaction:

$$\mathrm{d}P_{\mathrm{r}} = \sigma_{\mathrm{r}}\, n\, \mathrm{d}z \; .$$

where σ_r is the cross section for this particular reaction.

In the case when contains several types of objects that can interact with an incident particles then the total probability of interactions read:

$$\mathrm{d}P = \sum_i n_i \sigma_i$$

where n_i is the density of objects of type „i”
and σ_i is the cross section for the reaction of incident particle with an object of type „i”

Units: $1\,\mathrm{b} = 100\,\mathrm{fm}^2 = 10^{-28}\,\mathrm{m}^2\,.$

Cross section for a particular process/reaction can be (and usually is) a function of energy of incident particles.

Cross section and mean free path

Suppose we bombard a target having a density n with an incident particles with flux $F(0)$
Flux = number of particles per unit of time per unit area.

Then

$$\mathrm{d}F = -F\sigma n \mathrm{d}z$$

equivalent to the differential equation

$$\frac{\mathrm{d}F}{\mathrm{d}z} = -\frac{F}{l},$$

where the "mean free path" l is

$$l = \frac{1}{n\sigma}.$$

Clearly:

$$F(z) = F(0)\mathrm{e}^{-z/l}.$$

$F(z)$ is the flux of incident particles in the target at the depth z

Mean free path described the average path of a particle in a medium between collisions, or before reaction occurs.

$$l = \langle x \rangle = \frac{\int_0^\infty x e^{-n\sigma x} dx}{\int_0^\infty e^{-n\sigma x} dx} = \frac{1}{n\sigma}$$

If the material contains different types of objects i of number density and cross-section n_i and σ_i, then (3.6) implies that the mean free path is given by

$$l^{-1} = \sum_i n_i \sigma_i \, . \tag{3.28}$$

The mean lifetime of a particle in the beam is the mean free path divided by the beam velocity v

$$\tau = \frac{l}{v} = \frac{1}{n_{\mathrm{T}} \sigma_{\mathrm{tot}} v} \, . \tag{3.29}$$

The inverse of the mean lifetime is the "reaction rate"

$$\lambda = n \sigma_{\mathrm{tot}} v \, .$$

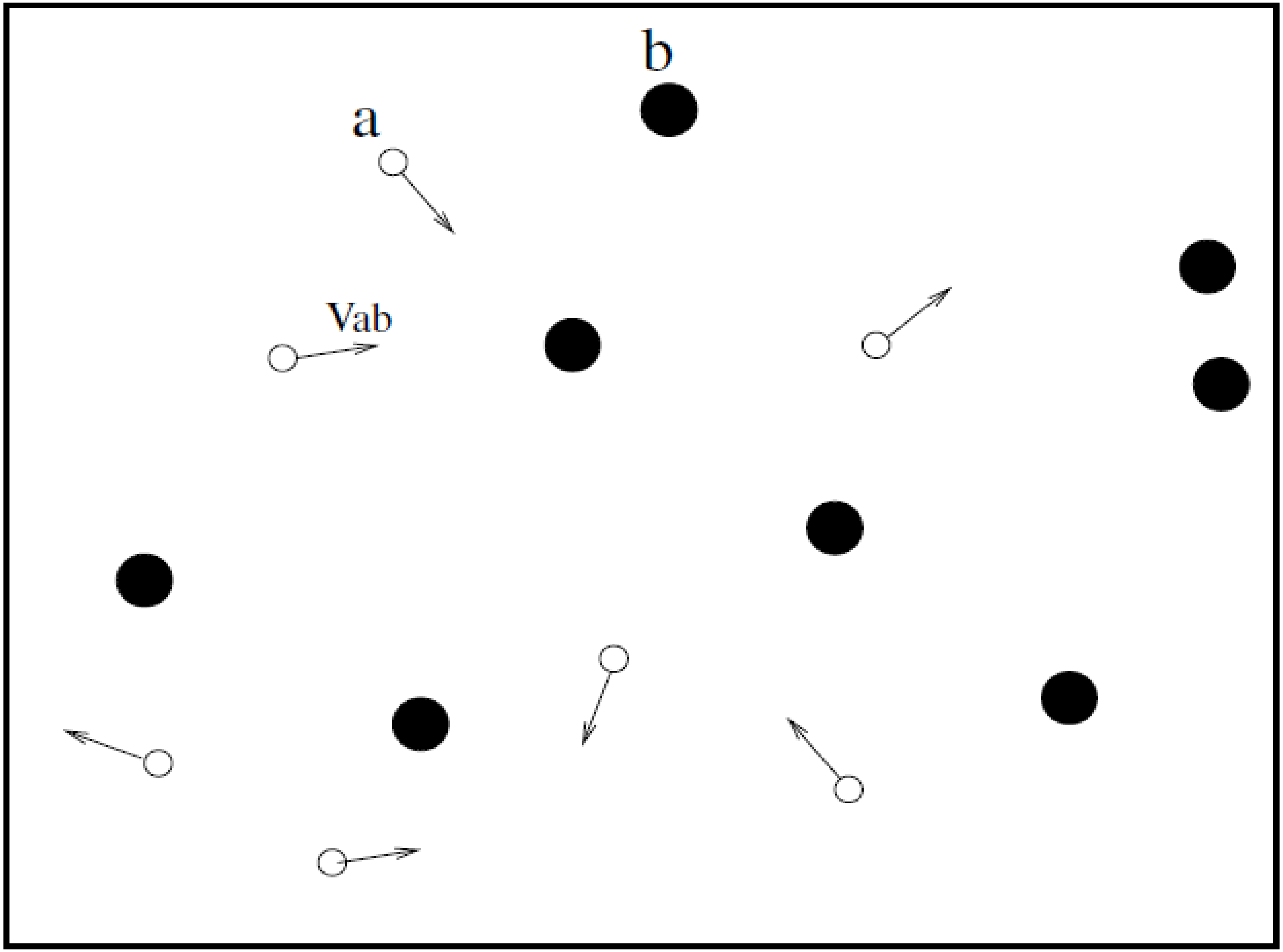

Fig. 3.3. A box containing two types of particles, a and b. The a particles move in random directions with velocity v_{ab} and can interact with the b particles (at rest) to form particles c and d with cross-section $\sigma_{ab\to cd}$. The time rate of change of the number density of particles a is determined by the Boltzmann equation (3.31).

Question:

What will be the density of particles „a” after time t providing that $\sigma_{ab \to cd}$ is the cross section for the reaction:

a+b -> c+d

$$\frac{dn_a}{dt} = -\frac{n_a}{\tau} = -n_a n_b \sigma_{ab \to cd} v_{ab} \;,$$

$$n_a(t) = n_a(0)\exp(-t/\tau)$$

In order to solve these eq. we actually implicitly averaged the value of $\sigma_{ab \to cd} v_{ab}$ over all particles.

In the case when inverse reaction: c+d->a+b is possible we will get more general form:

$$\frac{\mathrm{d}n_a}{\mathrm{d}t} = -n_a n_b \sigma_{ab\to cd} v_{ab} + n_c n_d \sigma_{cd\to ab} v_{cd} .$$

Note: there is a hidden temperature dependence in the above equations coming from the fact that average velocity of particles depends on *temperature.*

Differential cross section

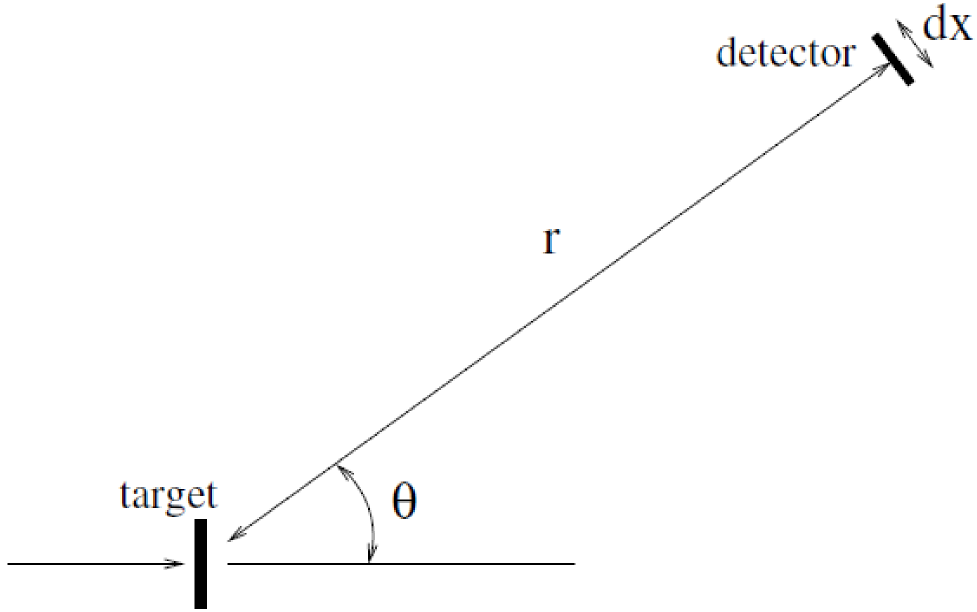

Fig. 3.2. A particle incident on a thin slice of matter containing n scatterers per unit volume of cross-section σ. A detector of area $\mathrm{d}x^2$ is placed a distance r from the target and oriented perpendicular to r. If an elastic scatter results in a random scattering angle, the probability to detect the particle is $\mathrm{d}P = n\mathrm{d}z\sigma(\mathrm{d}x^2/4\pi r^2) = n\mathrm{d}z(\sigma/4\pi)\mathrm{d}\Omega$, where $\mathrm{d}\Omega = x^2/r^2$ is the solid angle covered by the detector.

$$dP = \frac{d\sigma}{d\Omega} ndz d\Omega \quad ; \qquad d\Omega = \sin\theta d\theta d\varphi$$

Probability that a deflected particle will scatter to a certain direction specified by two angles:

$$\sigma = \int d\Omega \frac{d\sigma}{d\Omega} = \int_0^{2\pi} d\varphi \int_0^{\pi} \sin\theta d\theta \frac{d\sigma}{d\Omega}$$

$$\frac{d\sigma}{d\Omega}(\theta,\varphi)$$ - Differential cross section

<u>Types of scattering:</u>

- **elastic:** **kinetic energy is conserved**
- **inelastic:** **part of the kinetic energy of colliding particles is tranformed into internal excitations or reactions.**

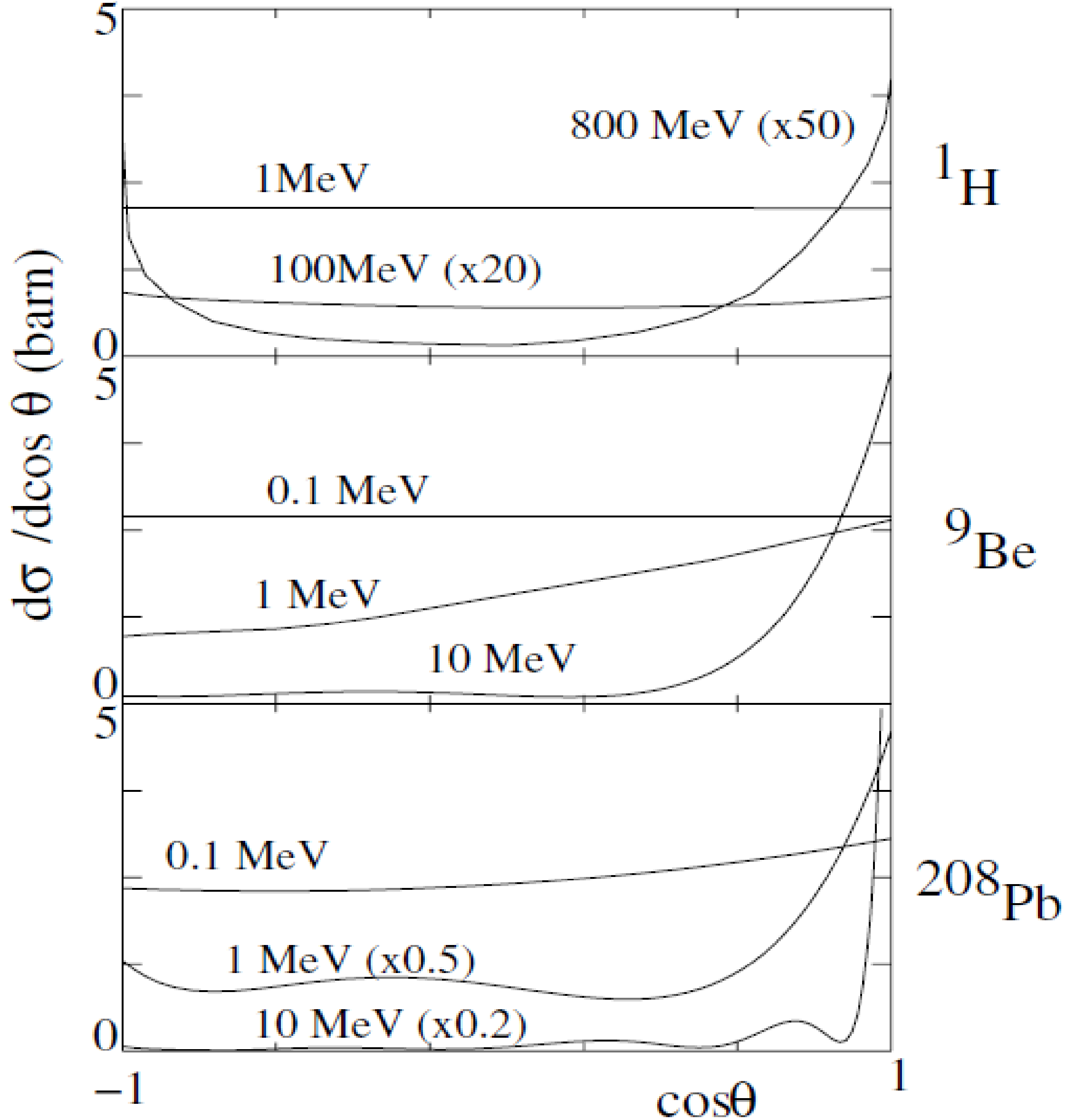

Fig. 3.6. The differential cross-section, $\mathrm{d}\sigma/\mathrm{d}\cos\theta = 2\pi\mathrm{d}\sigma/\mathrm{d}\Omega$, for elastic scattering of neutrons on ^{1}H, ^{9}Be and ^{208}Pb at incident neutron energies as indicated [30]. At low incident momenta, $p < \hbar/R_{\text{nucleus}}$, the scattering is isotropic whereas for high momenta, the angular distribution resembles that of diffraction from a disk of radius R. Neutron scattering on ^{1}H at high-energy also has a peak in the backward directions coming from the exchange of charged pions (Fig. 1.13).

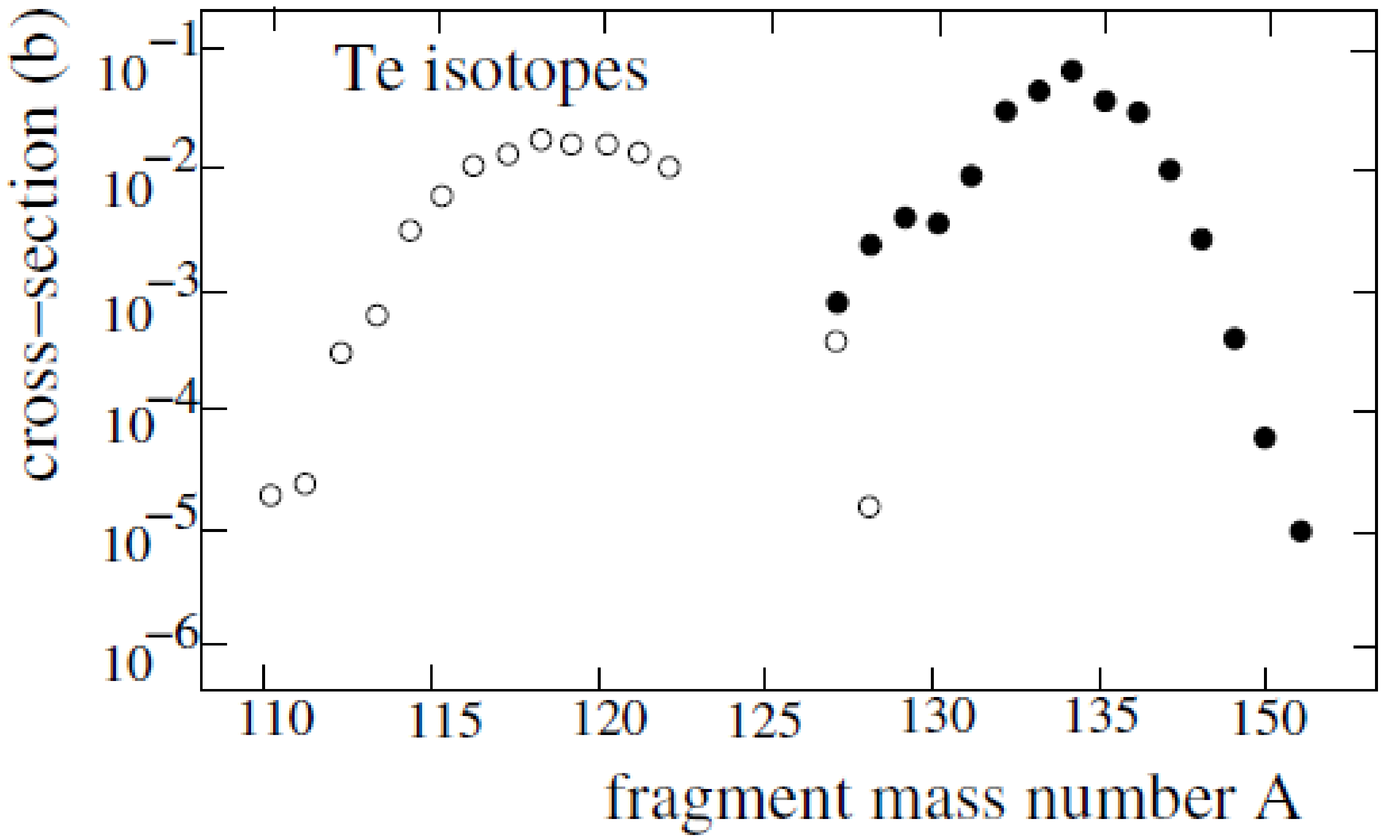

Fig. 3.7. The production of tellurium isotopes in the fragmentation of ^{129}Xe (790 MeV/nucleon) on a ^{27}Al target (open circles) and the collision-induced fission of ^{238}U (750 MeV/nucleon) on a Pb target (filled circles) [31]. Fragmentation leads to proton-rich isotopes while fission leads to neutron-rich isotopes.

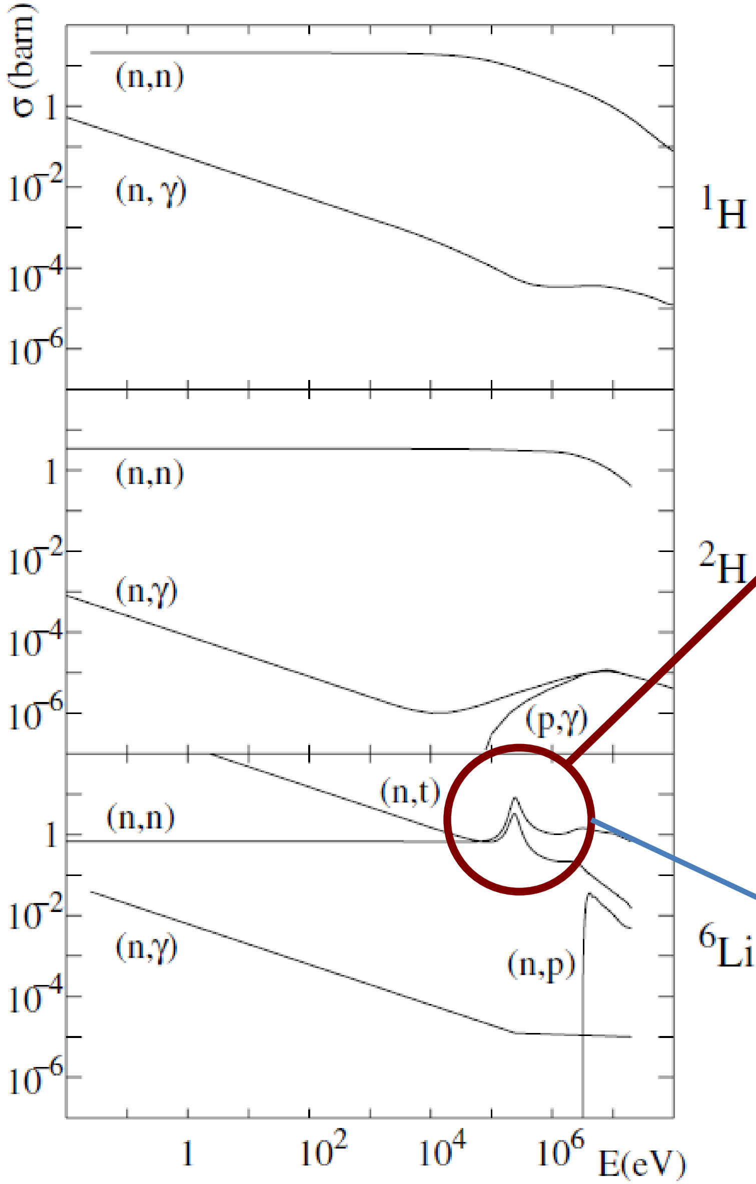

Fig. 3.4. Examples of reaction cross-sections on ^{1}H, ^{2}H, and ^{6}Li [30]. Neutron elastic scattering, (n,n), has a relatively gentle energy dependence while the exothermic reactions, (n, γ) and ^{6}Li(n, t)^{4}He (t=tritium=^{3}H), have a $1/v$ dependence at low energy. The exothermic (p, γ) reaction is suppressed at low energy because of the Coulomb barrier. The reaction ^{6}Li(n, p)^{6}Be has an energy threshold. The fourth excited state of ^{7}Li (Fig. 3.5) appears as a prominent resonance in n^{6}Li elastic scattering and in ^{6}Li(n, t)^{4}He.

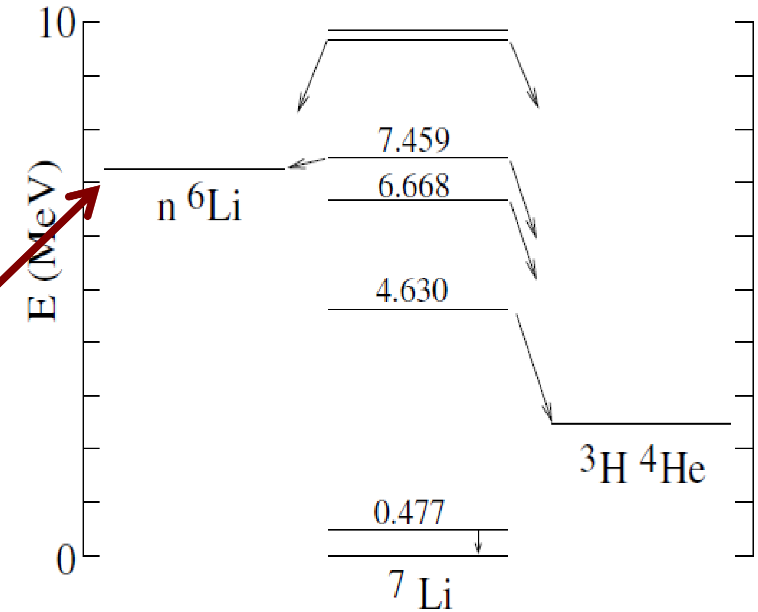

Fig. 3.5. The energy levels of ^{7}Li and two dissociated states n $-^6$Li and ^{3}H $-$ ^{4}He. The first excited state of ^{6}Li decays to the ground state via photon emission while the higher excited states decay to ^{3}H$-$^{4}He. The fourth and higher excited states can also decay to n $-^6$ Li. The fourth excited state (7.459 MeV) appears prominently as a resonance in n^{6}Li elastic scattering and in the exothermic (n,t) reaction n^{6}Li $\to$ ^{3}H^{4}He. The resonance is seen at $E_n \sim 200$ keV in Fig. 3.4.

$$\sigma \sim \frac{A}{(E - E_0)^2 + (\Gamma/2)^2}$$

Energy

Width

$$\boxed{\tau = \hbar / \Gamma}$$

- Lifetime of a resonance

Simplified mechanism of resonance scattering in the case of a particle in a potential

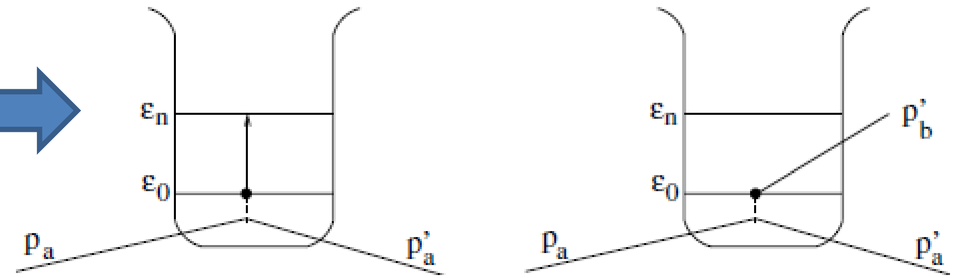

Fig. 3.18. Scattering of particle *a* on particle *b* in a bound state. Particle *b* can be left in bound state (left) or ejected from the potential (right).

Resonanse

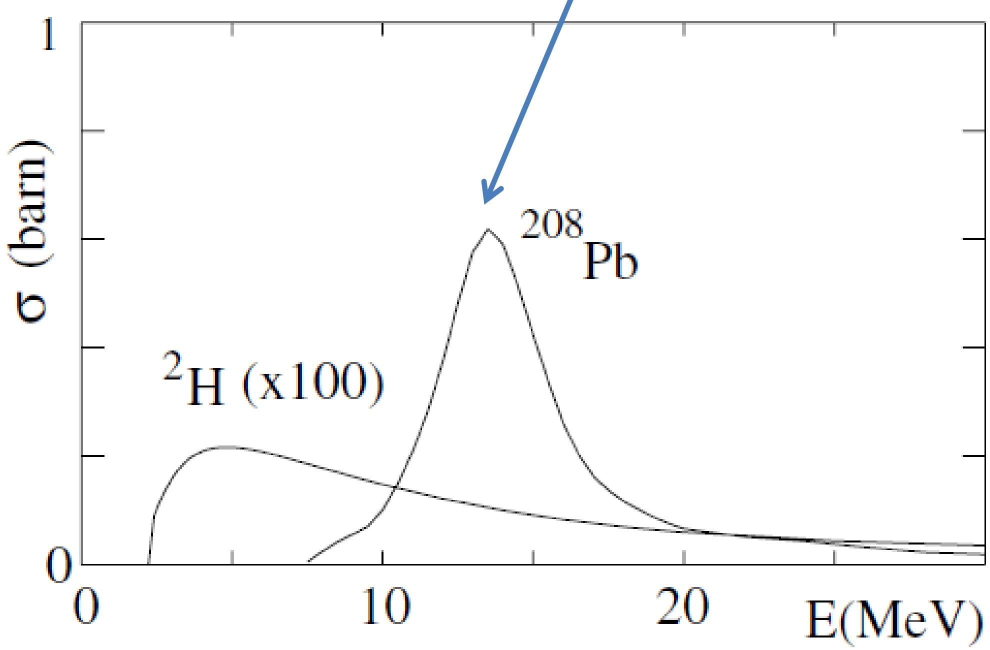

Fig. 3.8. The cross-sections for photo-dissociation of ^{2}H and of ^{208}Pb [30]. The cross-section of Pb exhibits a *giant resonance* typical of heavy nuclei.

The total $p\gamma$ cross section

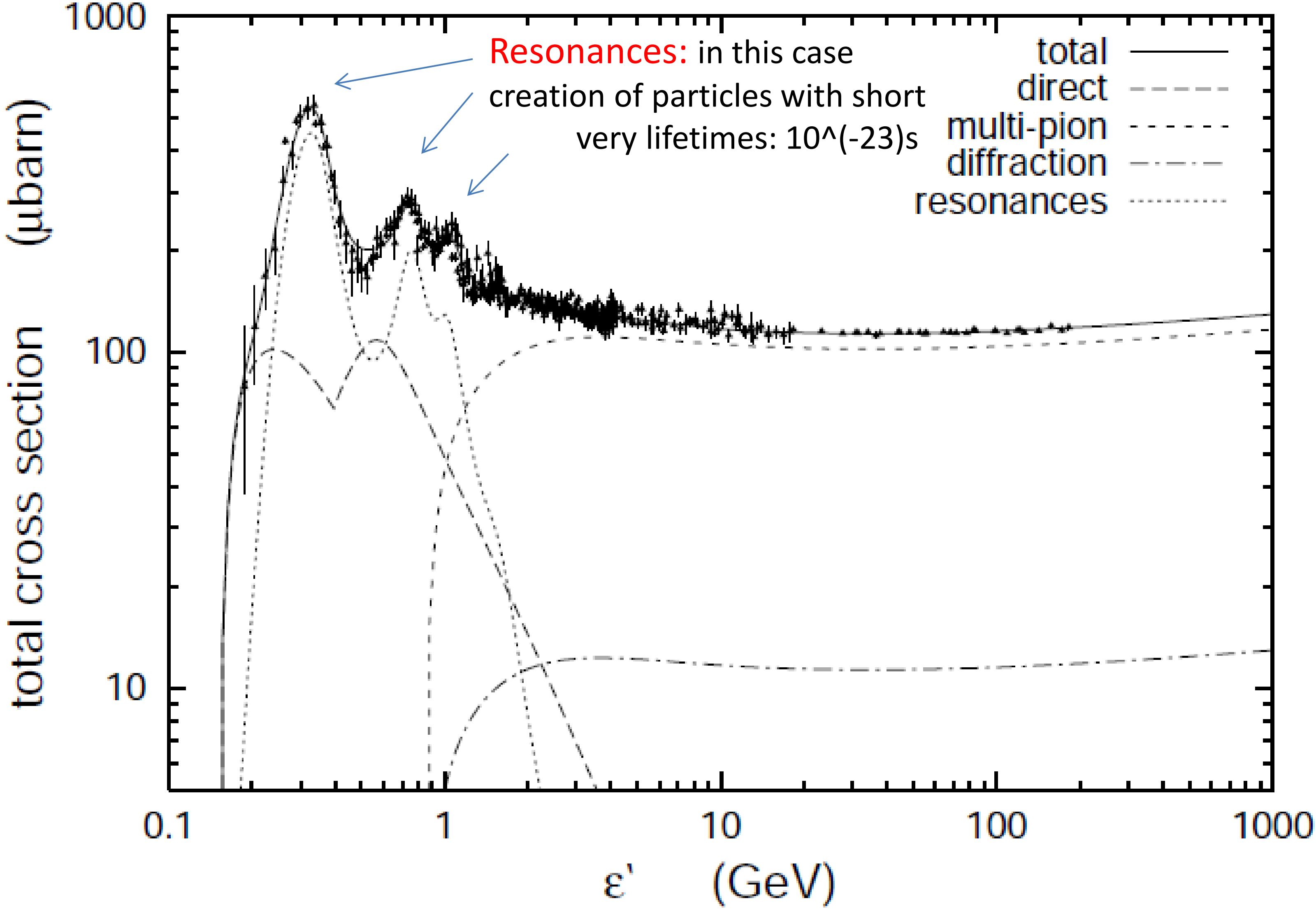

Baldini, A., Flaminio, V., Moorhead, W. G., & Morrison, D. R. O. 1988, in Landold-Börnstein, New Ser., Vol. I/12b,

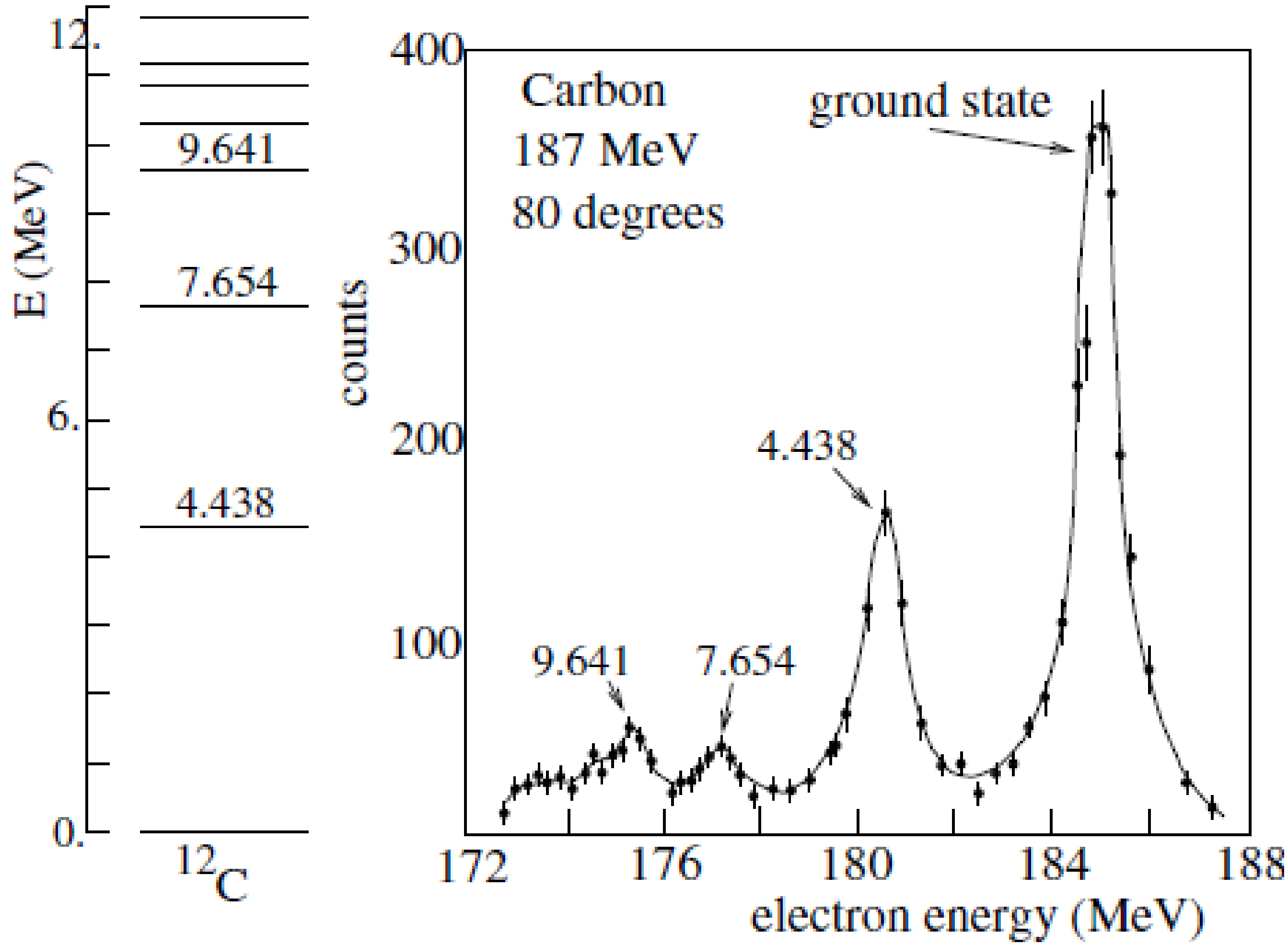

Fig. 3.21. The spectrum of excited states of ^{12}C (left) and the final-state energy spectrum of 187 MeV electrons scattering at 80 deg on ^{12}C (right). The peak at 185 MeV corresponds to elastic scattering. (2 MeV is taken by the recoiling nucleus.) The other peaks correspond to inelastic scattering leaving the ^{12}C nucleus in an excited state. The three lowest excitations are clearly visible.

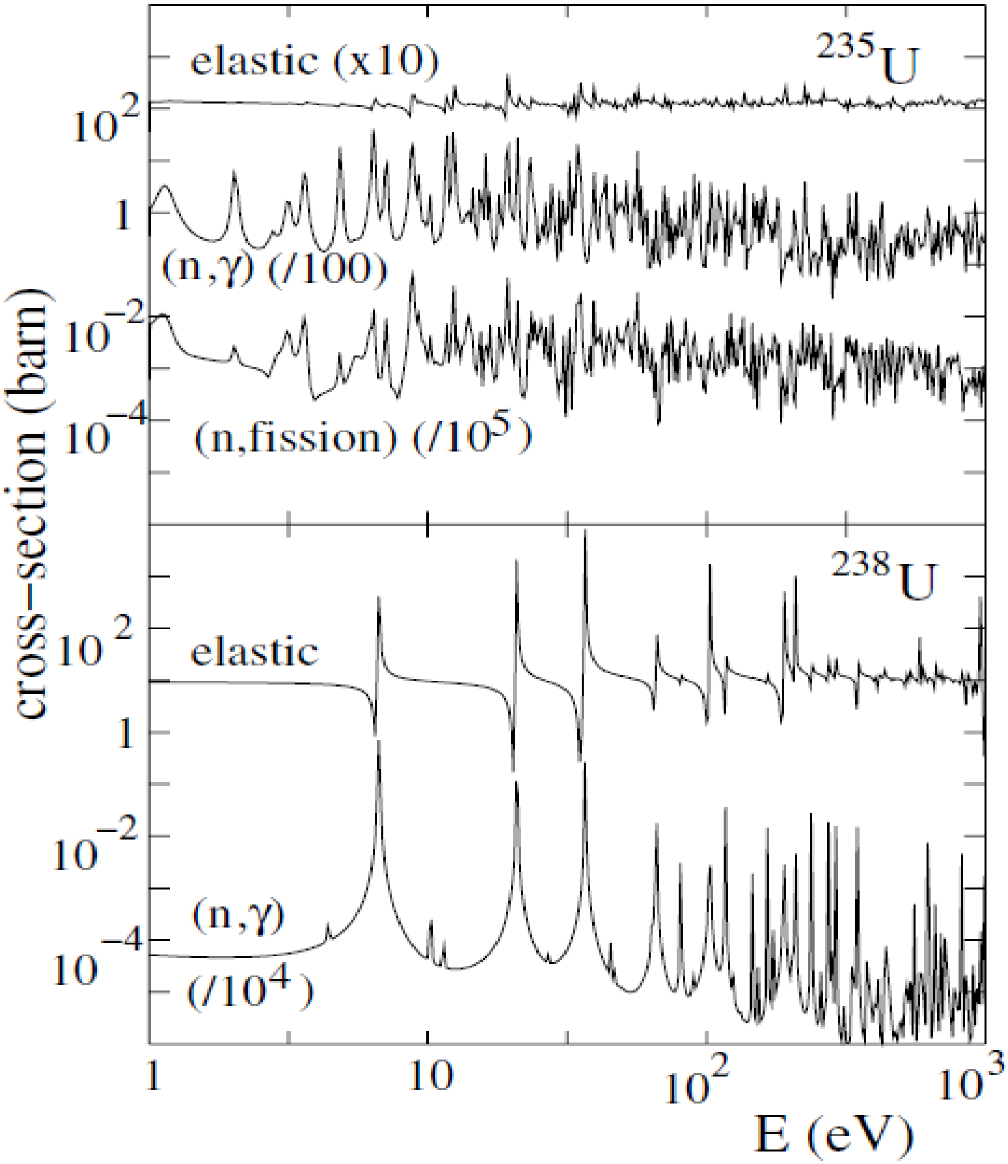

Fig. 3.26. The elastic and inelastic neutron cross-sections on ^{235}U (top) and ^{238}U (bottom). The peaks correspond to excited states of ^{236}U and ^{239}U. The excited states can contribute to the elastic cross-sections by decaying through neutron emission. They contribute to the (n, γ) cross-section by decaying by photon emission to the ground states of ^{236}U and ^{239}U. In the case of ^{236}U the states can also decay by fission so they contribute to the neutron-induced fission cross-section on ^{235}U.

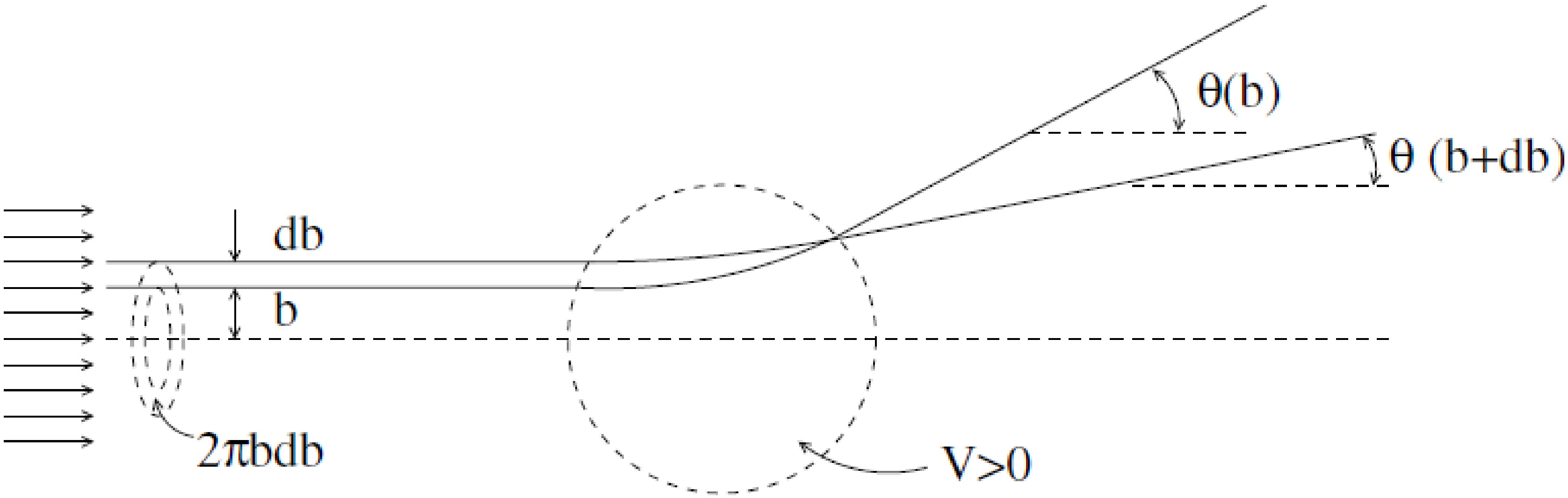

b - impact parametr

Example: **Rutherford scattering**

Elastic scattering of charged particles: Z1*e, Z2*e

$$\frac{d\sigma}{d\Omega} = \left(\frac{Z_1 Z_2 e^2}{16\pi\epsilon_0 E_k}\right)^2 \frac{1}{\sin^4\theta/2} \,.$$

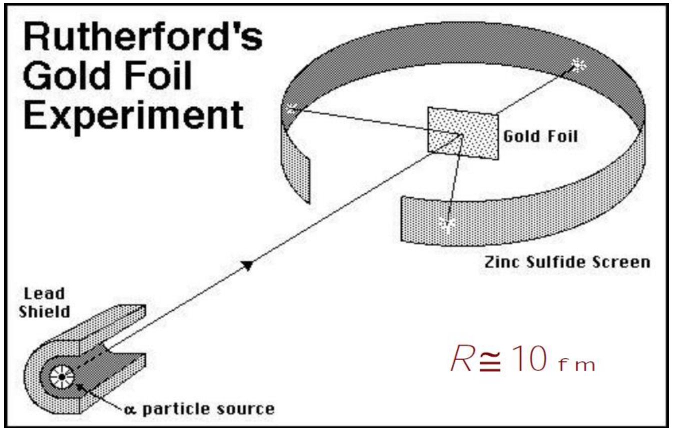

Note that total cross section is divergent!

Due to an infinite range of Coulomb potential: 1/r

Nuclear interaction

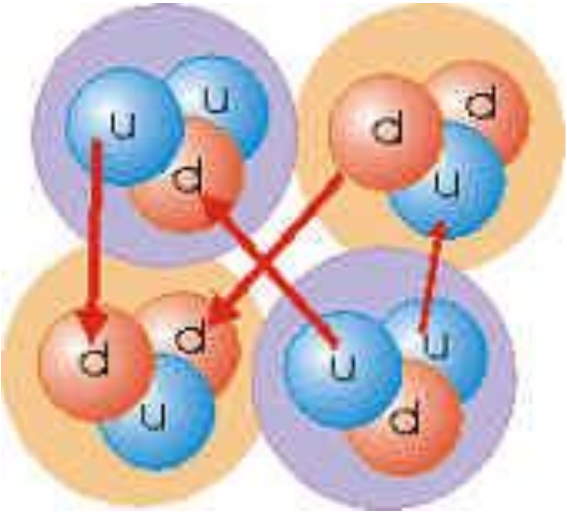

Nuclear interaction between nucleons
(protons and neutrons) comes from more fundamental
Interaction between quarks.

In principle it should be possible to derive this interaction
from quark-quark interaction, but unfortunately
the quark-quark interaction is extremely complex and
even though that it looks like there is a good theory
describing quarks and gluons, the so-called

Quantum Chromodynamics (QCD),

it is difficult to solve it even using supercomputers.

The situation is somewhat analogous to the case of molecular interaction, which originates from electromagnetic interaction between electrons and nuclei.

The Nuclear Many-Body Problem

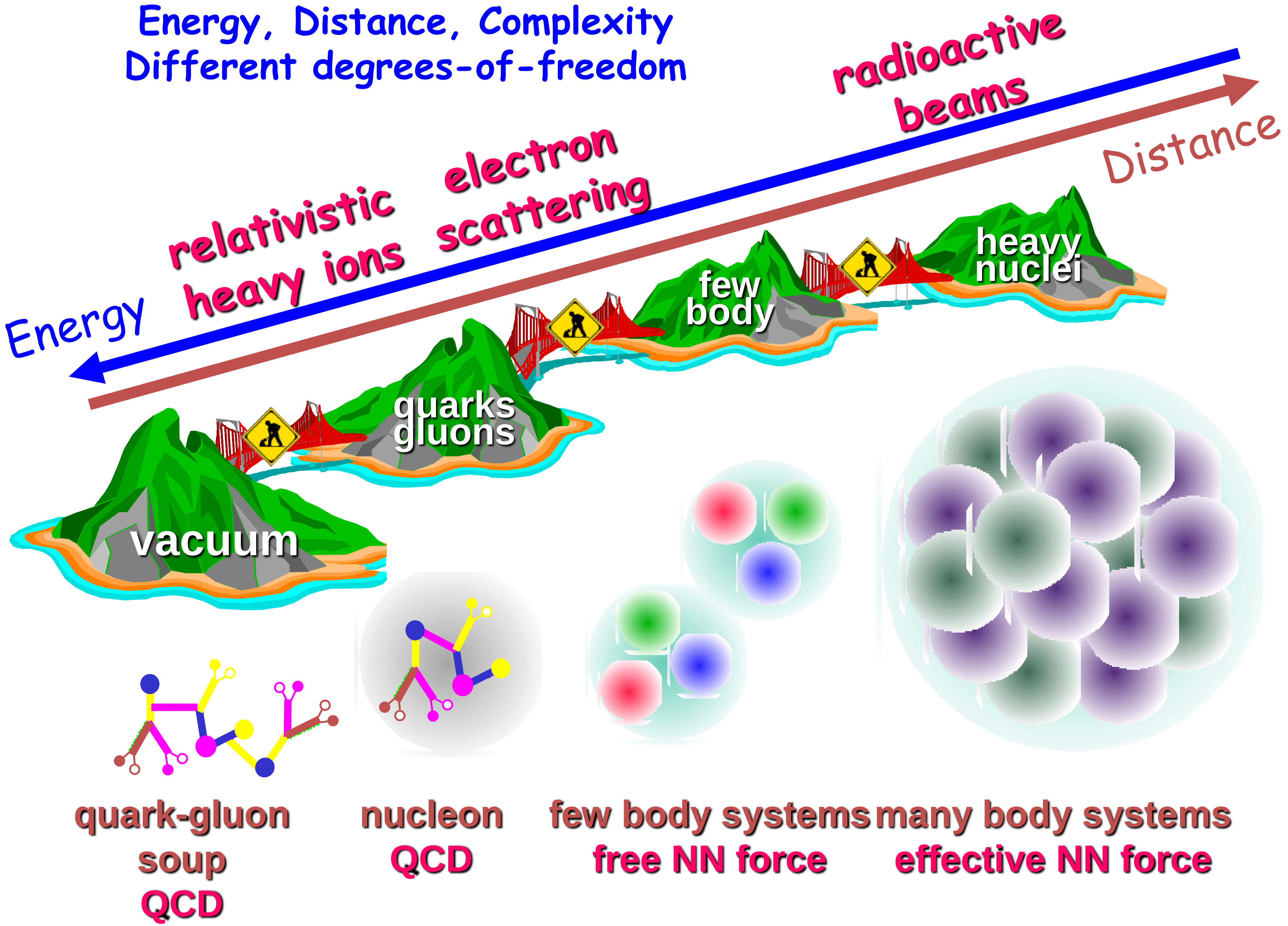

Features of NN interaction

- Attractive at long distances
- Repulsive at short distances
- Short range
- Charge independent (the same for protons and neutrons)
- Depend on the spin orientation of nucleons
- Depends on relative orientation of nucleon spin and angular momentum (spin-orbit interaction)
- Noncentral (partly resembles the interaction between electric dipoles)
- Contain also 3-body term

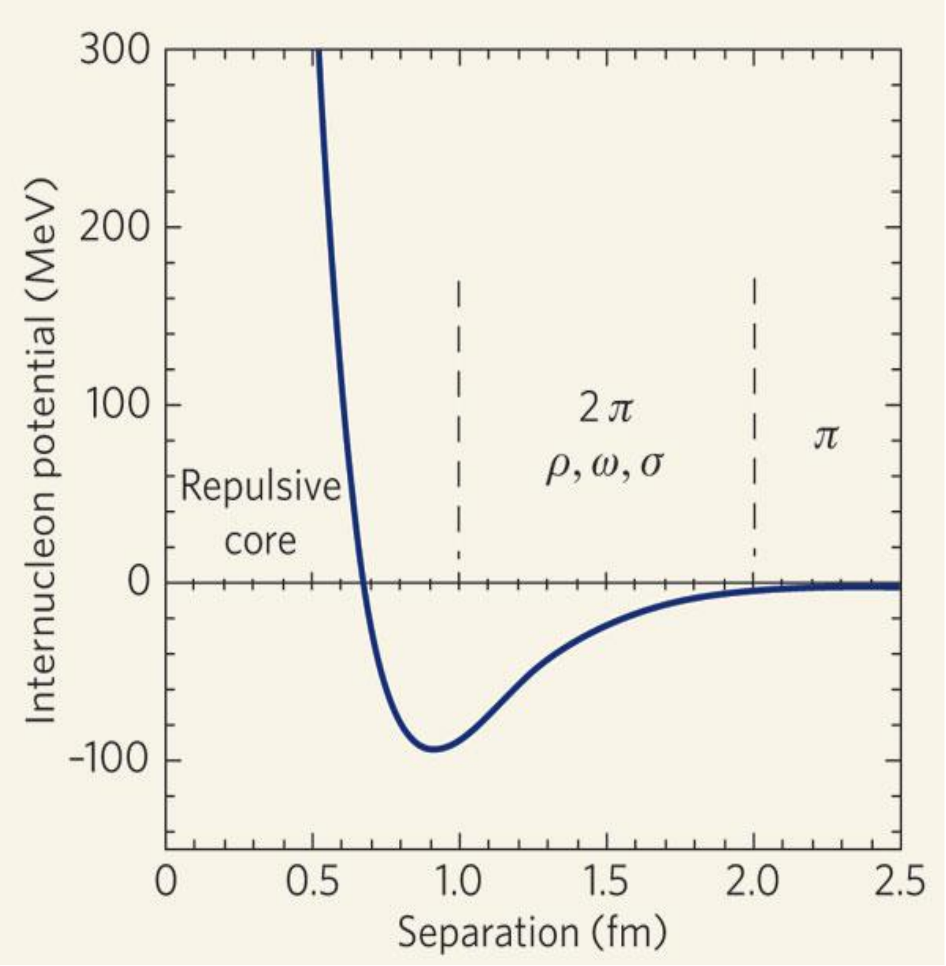

First attempt to nuclear interaction: Yukawa theory

Yukawa potential (1930)
(good at large distances)

$$\boxed{V(r) = g\frac{\hbar c}{r}\exp(-r/r_0) \quad .}$$

$$r_0 = \frac{\hbar}{m_\pi c} \approx 1.4\, fm$$

$m_\pi \simeq 140 MeV$ Masa mezonu Pi

$g \approx 15.5$ Stała sprzężenia w oddziaływaniu nukleon-pion

<u>Meson theory of strong interaction: Yukawa</u>

Based on assumption that nucleon-nucleon interaction is due to exchange of mesons. For example: pions are responsible for long range part of nuclear interaction.

<u>Problem I</u>: short range part of N-N interaction requires theory with many mesons (many coupling constants needed):

<u>Problem II:</u> coupling constants were not small, so perturbation theory failed $\pi, \rho, \omega, \ldots$

Nuclear interaction should fulfill several constraints associated with comservation laws:

1. Momentum conservation,
2. Total angular momentum conservation,
3. Galilean invariance: interaction cannot depend on the frame of reference,
4. Parity conservation.

These constraints have to be fulfill by any realistic nucleon-nucleon potential:

$$V(\vec{r}_1 - \vec{r}_2, \vec{p}_1 - \vec{p}_2, \vec{L}_1, \vec{L}_2, \vec{s}_1, \vec{s}_2, \vec{\tau}_1, \vec{\tau}_2) + V_{3body}$$

$\vec{s}_i$ - Spin of i-th nucleon

$\vec{\tau}_i$ - Isospin of i-th nucleon

Angular momentum in quantum mechanics

1. In quantum mechanics angular momentum is quantized i.e. can take only discrete values.
2. We can not determine accurately all 3 components of angular momentum (Heisenberg uncertainty principle). We know only the length (the absolute value) and projection on a specified axis, which can take value: $-J\hbar, (-J+1)\hbar, \ldots, J\hbar$

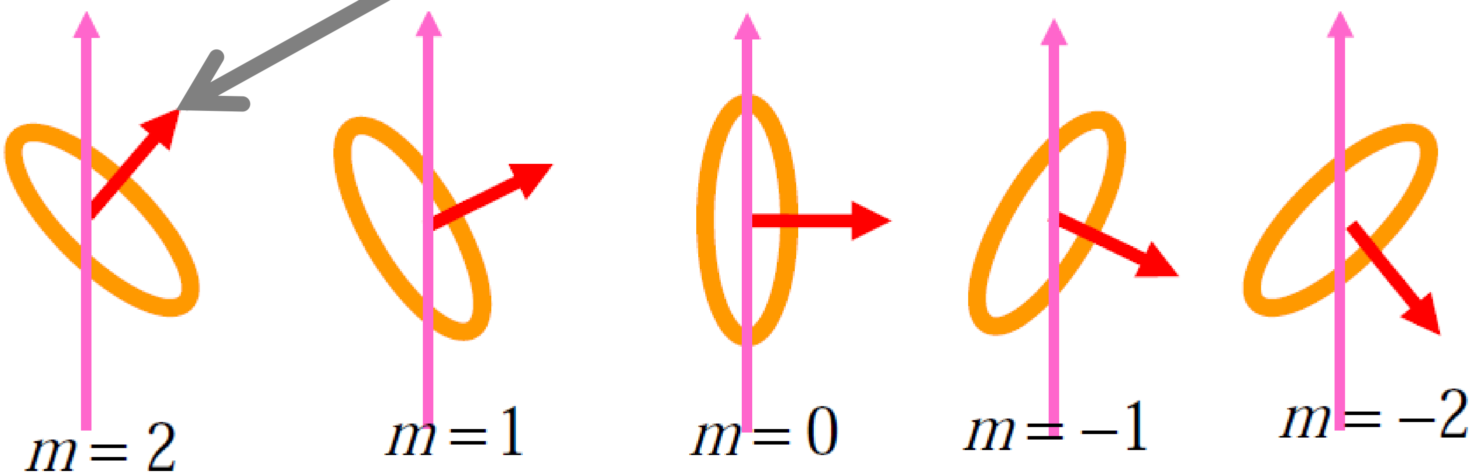

$$\vec{J} = \sum_i (\vec{L}_i + \vec{s}_i)$$

Orbital angular momentum

Spin

Spin

Neutron and proton spin is half of the Planck's constant. It implies that there are only two values of projection possible:

$$|\uparrow\rangle$$

$$|\downarrow\rangle$$

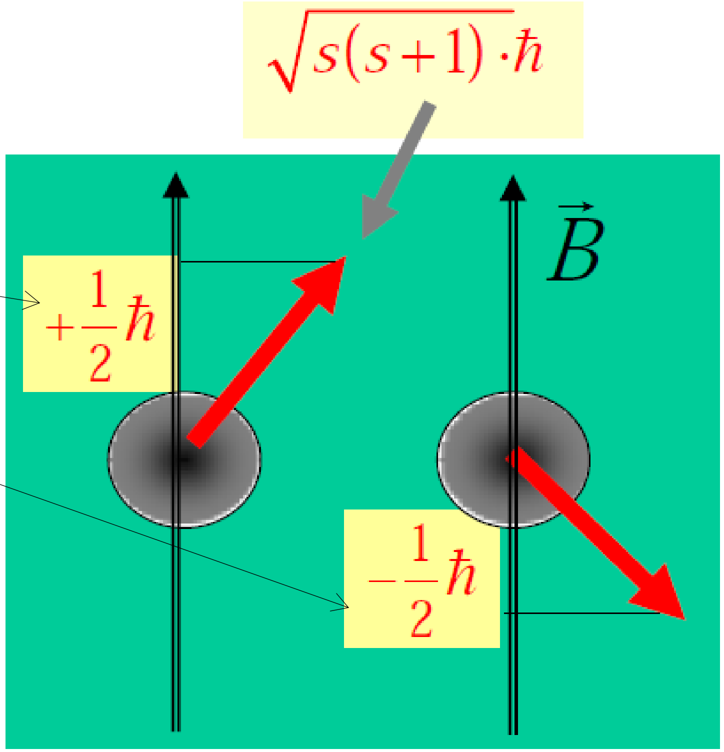

Hence both proton and neutron can appear in two spin states: spin-up and spin-down

Example: two protons or two neutrons can form in total 4 spin states:

$$(|\uparrow\rangle, |\downarrow\rangle) \otimes (|\uparrow\rangle, |\downarrow\rangle)$$

$$\boxed{|\uparrow\downarrow\rangle - |\downarrow\uparrow\rangle \ : J = 0, J_z = 0}$$

„Singlet state ”

$$\boxed{\left\{ \begin{array}{ll} |\uparrow\uparrow\rangle & : J = 1, J_z = 1 \\ |\uparrow\downarrow\rangle + |\downarrow\uparrow\rangle & : J = 1, J_z = 0 \\ |\downarrow\downarrow\rangle & : J = 1, J_z = -1 \end{array} \right.}$$

„Triplet state”

Conclusion:

For even (odd) number of fermions the total angular momentum is always integer (noninteger) multiple of Planck's constant

Isospin

Since neutron and proton have similar masses and are indistinguishable by the nuclear interaction we can treat them as **two states** of a particle called: **nucleon.**
Following the analogy with spin, we introduce the isospin of the absolute value 1/2, with two projections: -1/2 and +1/2

In general the total isospin T can produce (2T+1) different projections:
-T, -T+1, ..., T-1, T

Analogously to spin states, the two-nucleon state can appear as a singlet or triplet state **T=0 lub T=1**:

$$|T=1,T_3\rangle : \begin{cases} |T=1,T_3=1\rangle = |\mathrm{pp}\rangle \\ |T=1,T_3=0\rangle = (|\mathrm{pn}\rangle + |\mathrm{np}\rangle)/\sqrt{2} \\ |T=1,T_3=-1\rangle = |\mathrm{nn}\rangle \end{cases}$$

„isospin triplet”

$$|T=0,T_3=0\rangle : \quad |0,\ 0\rangle \ = \ (|\mathrm{pn}\rangle - |\mathrm{np}\rangle)/\sqrt{2} \quad .$$

„isospin singlet”

Deutron ground state

These states are unbound

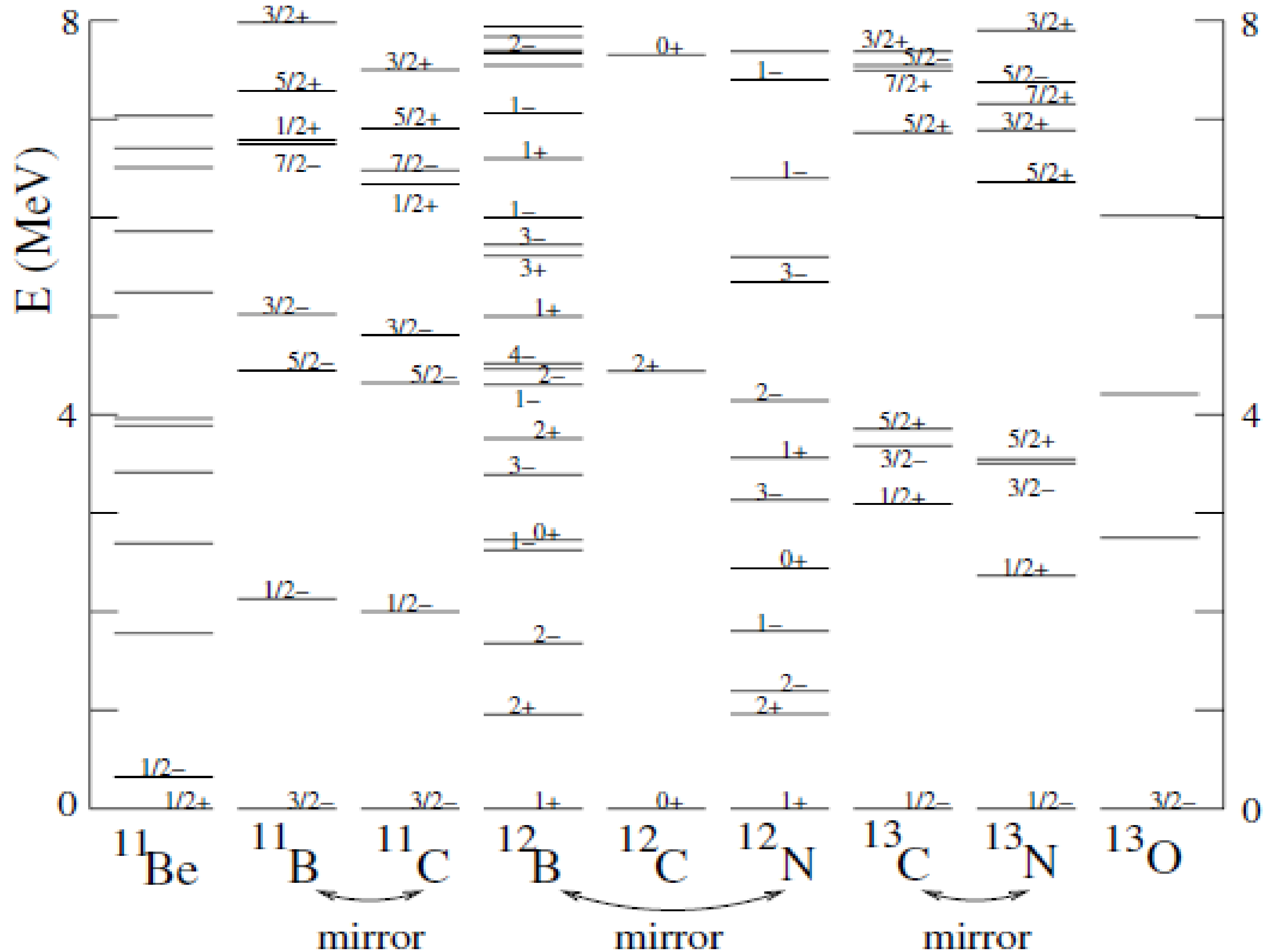

Fig. 1.16. Spectra of the low-lying levels for nuclei with $A = 11$, 12, and 13. The pairs of nuclei with N and Z interchanged (mirror nuclei) have remarkably similar spectra

Various components of the nucleon-nucleon interaction:

- Short range spatial interaction:
- Spin dependence of the interaction
- Tensor (non-central) interaction:

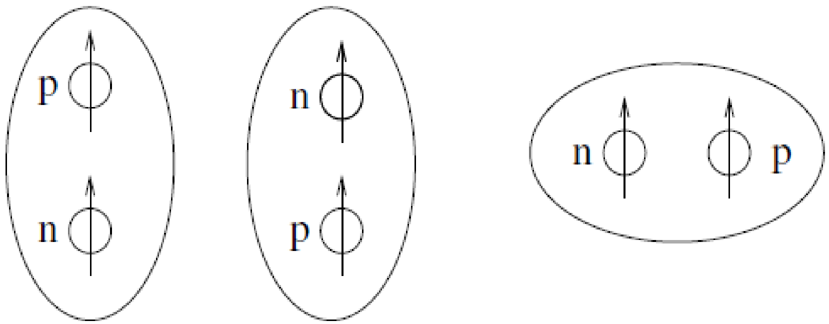

Fig. 1.11. The tensor potential for the $s = 1$ state (1.59) makes the configuration on the right ($\sigma \cdot r = 0$) have a different potential energy than the two configurations on the left ($\sigma \cdot r \neq 0$). This results in the permanent quadrupole moment of the deuteron.

- Spin-orbit interaction: interaction depends on the relative orientation of the spin vector and orbital angular momentum vector of particles.

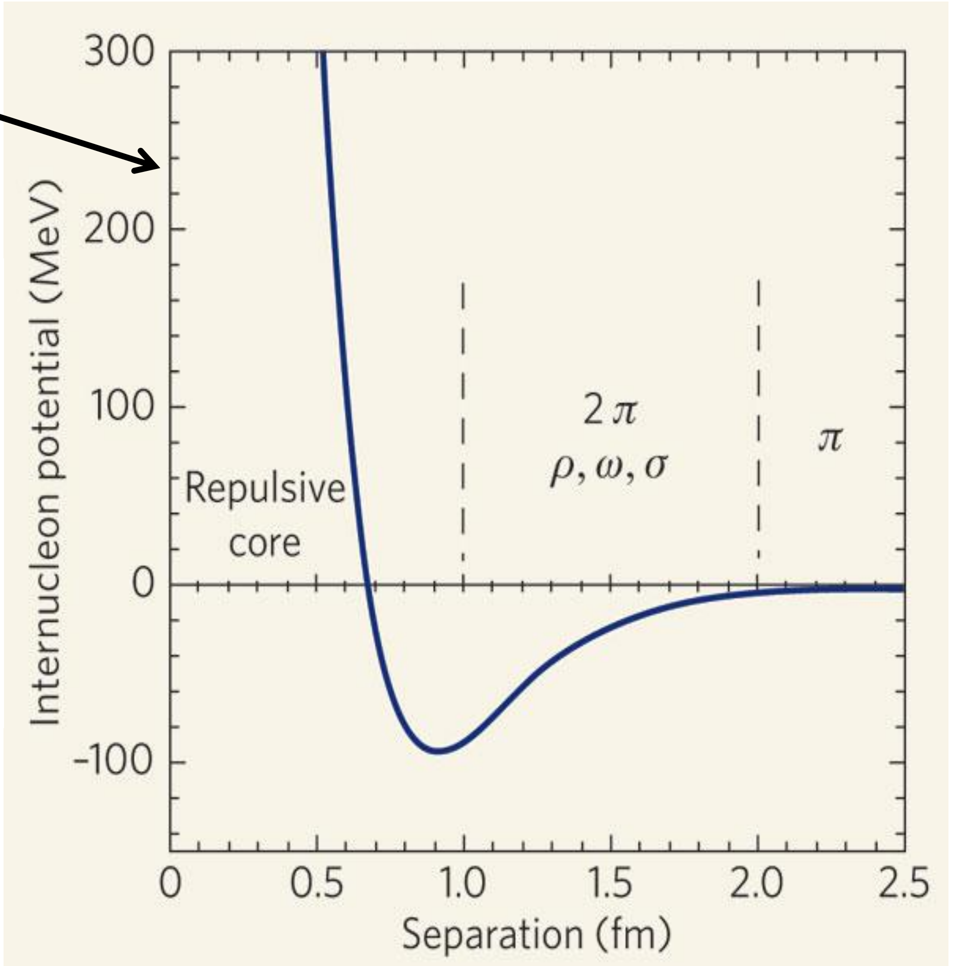

Besides in atomic nucleus there is a Coulomb repulsion between protons and weak interaction.

Nucleon-nucleon (N-N) interaction is an effective interaction

N-N force can be determined (except for the three-body term) from the proton-proton and proton-neutron scattering experiments.

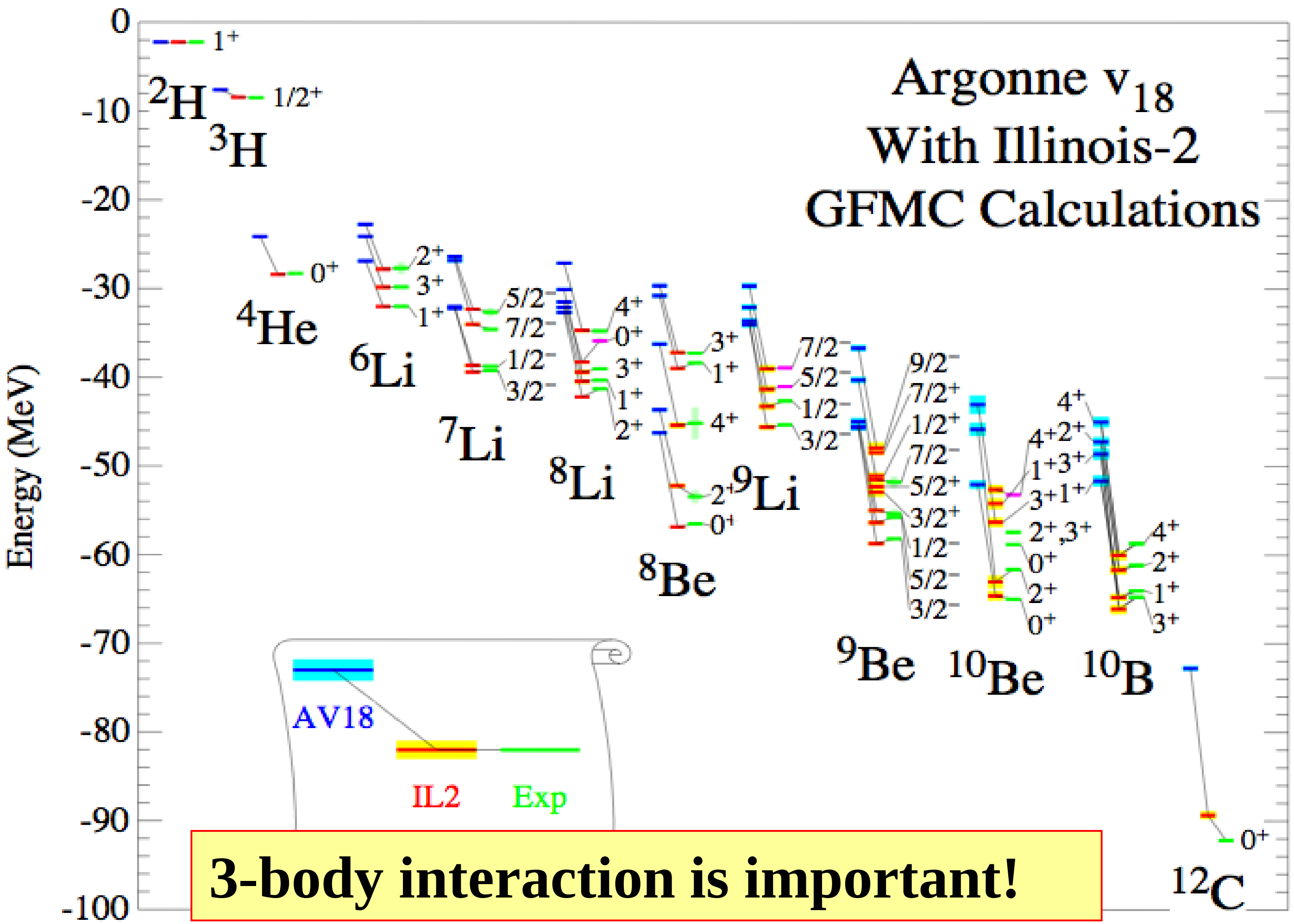

3-body interaction is important!

Results of solving Schroedinger eq. with N-N potential.

Blue – only two-body terms included.
Red – two-body and three-body terms.
Green – experiment.

Configuration Interaction

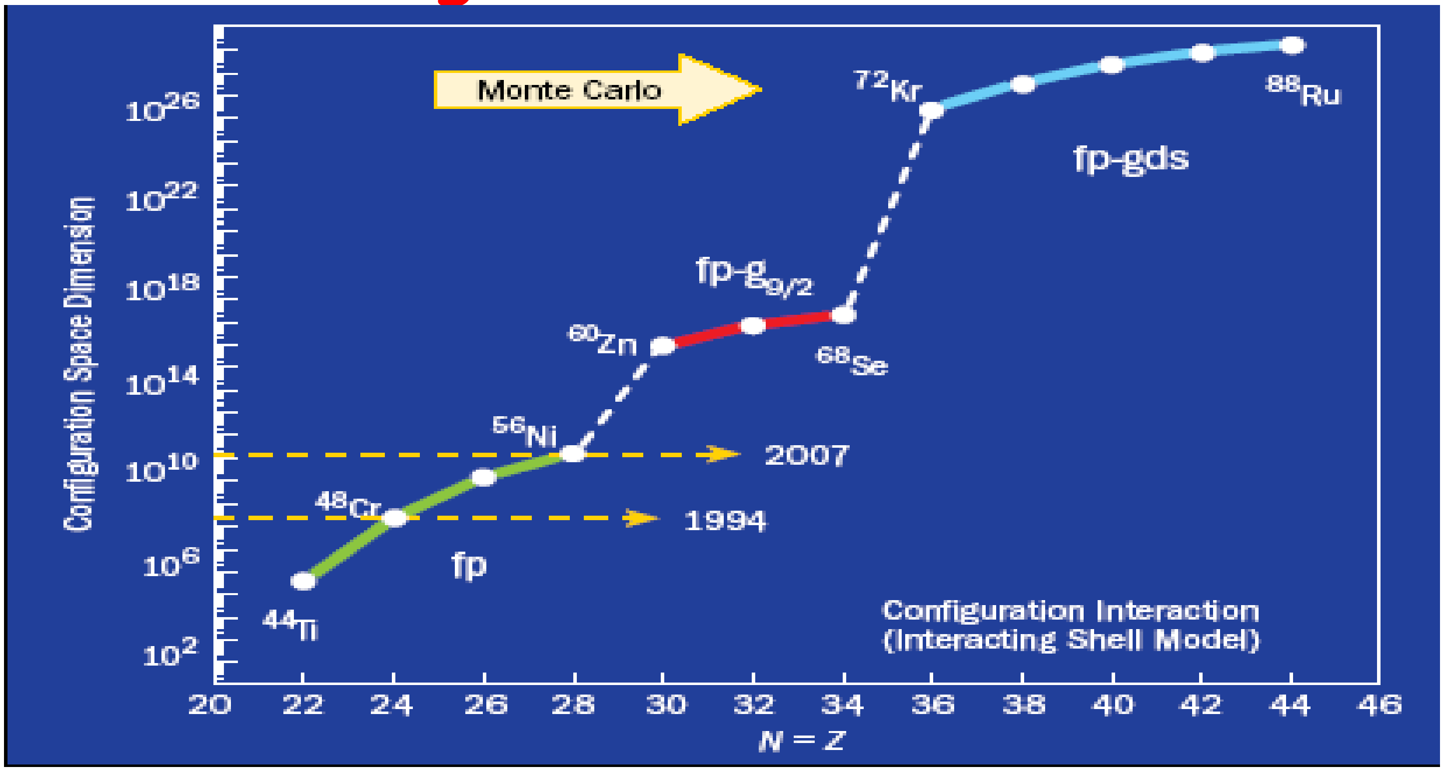

Figure 6. *Configuration space dimension of the interacting shell model for fp-shell nuclei.*

One valence shell CI works great,
but... 10^{24} is not an option!!!

Smarter solutions are needed

- Monte Carlo Shell Model
- Density Matrix Renormalization Group
- Factorization schemes

The simplest nontrivial nucleus: deuteron

- proton + neutron (proton-proton and neutron-neutron systems are unbound)
- It exists only in the ground state. Excited states are unbound. It has a relatively small binding energy: 2.225MeV
- It has the total angular momentum equal to one Planck's constant (it implies that nucleon-nucleon force should be spin dependent).
- Charge distribution is slightly nonspherical (it implies the presence of tensor component of the nucleon-nucleon force)

Nuclear Models

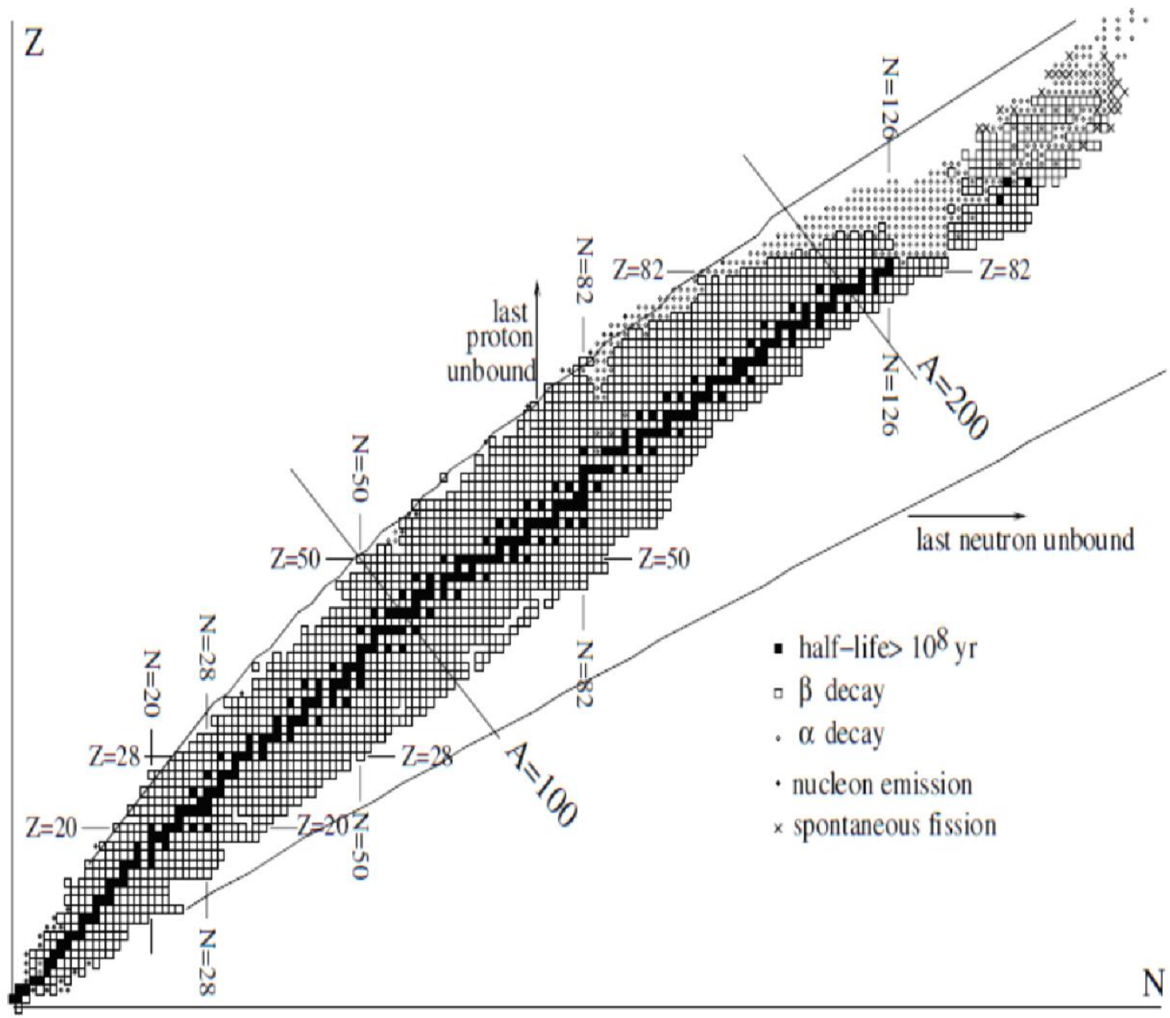

Fig. 2.1. The nuclei. The black squares are long-lived nuclei present on Earth. Combinations of (N, Z) that lie outside the lines marked "last proton/neutron unbound" are predicted to be unbound by the semi-empirical mass formula (2.13). Most other nuclei β-decay or α-decay to long-lived nuclei.

Liquid Drop Model

$$B(A,Z) = a_v A - a_s A^{2/3} - a_c \frac{Z^2}{A^{1/3}} - a_a \frac{(N-Z)^2}{A} + \delta(A)\,. \quad (2.13)$$

The coefficients a_i are chosen so as to give a good approximation to the observed binding energies. A good combination is the following:

$$a_v = 15.753 \text{ MeV}$$

$$a_s = 17.804 \text{ MeV}$$

$$a_c = 0.7103 \text{ MeV}$$

$$a_a = 23.69 \text{ MeV}$$

and

$$\delta(A) = \begin{cases} 33.6A^{-3/4} & \text{if } N \text{ and } Z \text{ are even} \\ -33.6A^{-3/4} & \text{if } N \text{and } Z \text{ are odd} \\ 0 & \text{si } A = N + Z \text{ is odd} \end{cases} \quad .$$

$$B(A,Z) = a_{\mathrm{v}}A - a_{\mathrm{s}}A^{2/3} - a_{\mathrm{c}}\frac{Z^2}{A^{1/3}} - a_{\mathrm{a}}\frac{(N-Z)^2}{A} + \delta(A)\,.$$

- The first term is a *volume* term which reflects the nearest-neighbor interactions, and which by itself would lead to a constant binding energy per nucleon $B/A \sim 16$ MeV.
- The term a_{s}, which lowers the binding energy, is a *surface* term. Internal nucleons feel isotropic interactions whereas nucleons near the surface of the nucleus feel forces coming only from the inside. Therefore this is a *surface tension* term, proportional to the area $4\pi R^2 \sim A^{2/3}$.
- The term a_{c} is the *Coulomb repulsion* term of protons, proportional to Q^2/R, i.e. $\sim Z^2/A^{1/3}$. This term is calculable. It is smaller than the nuclear terms for small values of Z. It favors a neutron excess over protons.
- Conversely, the *asymmetry* term a_{a} favors symmetry between protons and neutrons (isospin). In the absence of electric forces, $Z = N$ is energetically favorable.
- Finally, the term $\delta(A)$ is a quantum *pairing* term.

Valley of stability from liquid drop model

$$\frac{\partial B}{\partial Z} = 0 \Rightarrow Z(A) = \frac{A}{2 + a_{\mathrm{c}} A^{2/3}/2a_{\mathrm{a}}} \sim \frac{A/2}{1 + 0.0075\ A^{2/3}}\,.$$

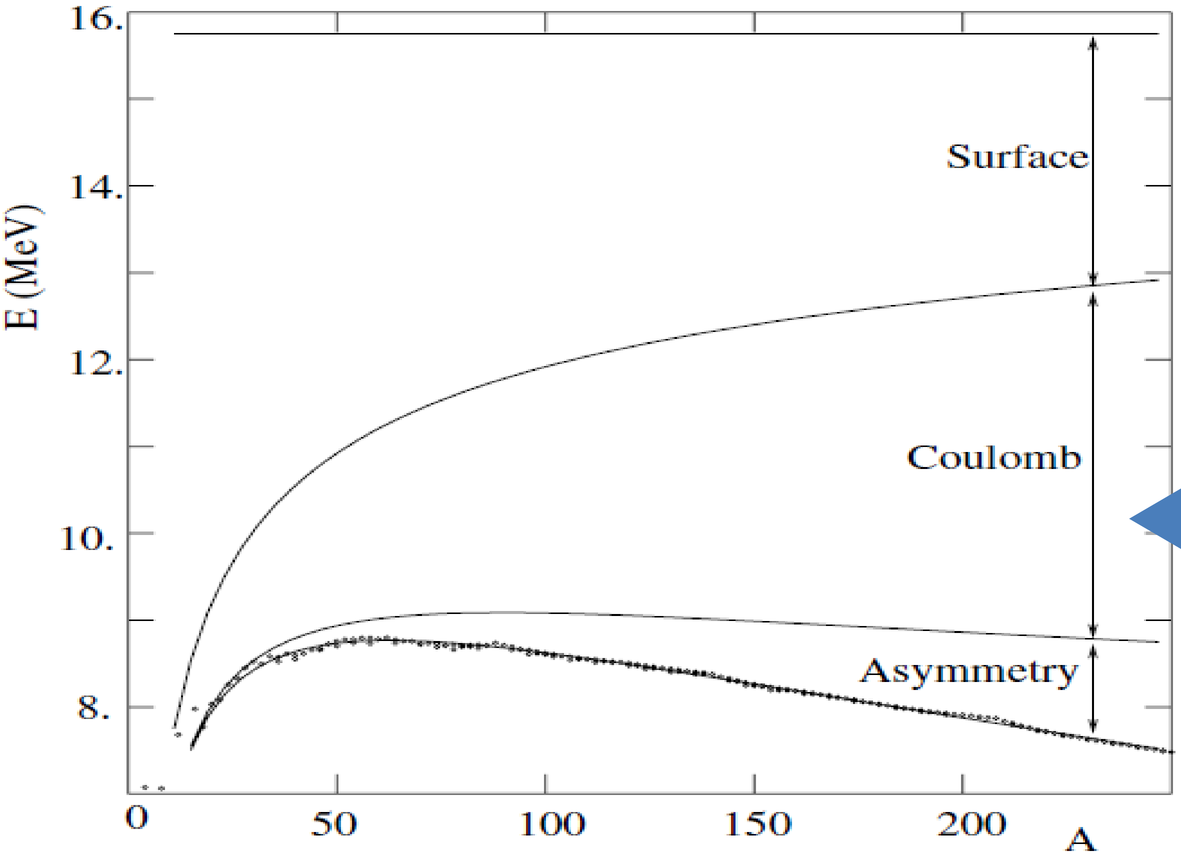

Fig. 2.5. The observed binding energies as a function of A and the predictions of the mass formula (2.13). For each value of A, the most bound value of Z is used corresponding to $Z = A/2$ for light nuclei but $Z < A/2$ for heavy nuclei. Only even–odd combinations of A and Z are considered where the pairing term of the mass formula vanishes. Contributions to the binding energy per nucleon of the various terms in the mass formula are shown.

Contributions to the LD formula coming from various terms as a function of nucleon number

Stability with respect to the nucleon emission

$$B(Z+1,N) - B(Z,N) > 0\,, \quad B(Z,N+1) - B(Z,N) > 0\,, \tag{2.16}$$

or equivalently

$$\frac{\partial B(Z,N)}{\partial Z} > 0\,, \qquad \frac{\partial B(Z,N)}{\partial N} > 0\,. \tag{2.17}$$

Stability with respect to alpha emission

$$B(Z,N) > B(Z-2, N-2) + B_\alpha$$

B_α - This value has to be taken from experiment because LD formula underestimates binding energy of alpha particle.

Note that we can also estimate kinetic energy of emitted alpha particle:

$$Q_\alpha = B(Z,N) - B(Z-2, N-2) - B_\alpha$$

Finding possible decay channels of atomic nucleus

$$(Z,N) \rightarrow (Z_1,N_1) + (Z_2,N_2)$$

This reaction is possible if the following condition is fulfilled:

$$B(Z,N) < B(Z_1,N_1) + B(Z_2,N_2)$$

A nucleus can have in principle several decay channels. The probability of decaying into a specific channel depends on both the energetics (above) as well as the details of a nuclear structure.

Beta decay from the LD formula

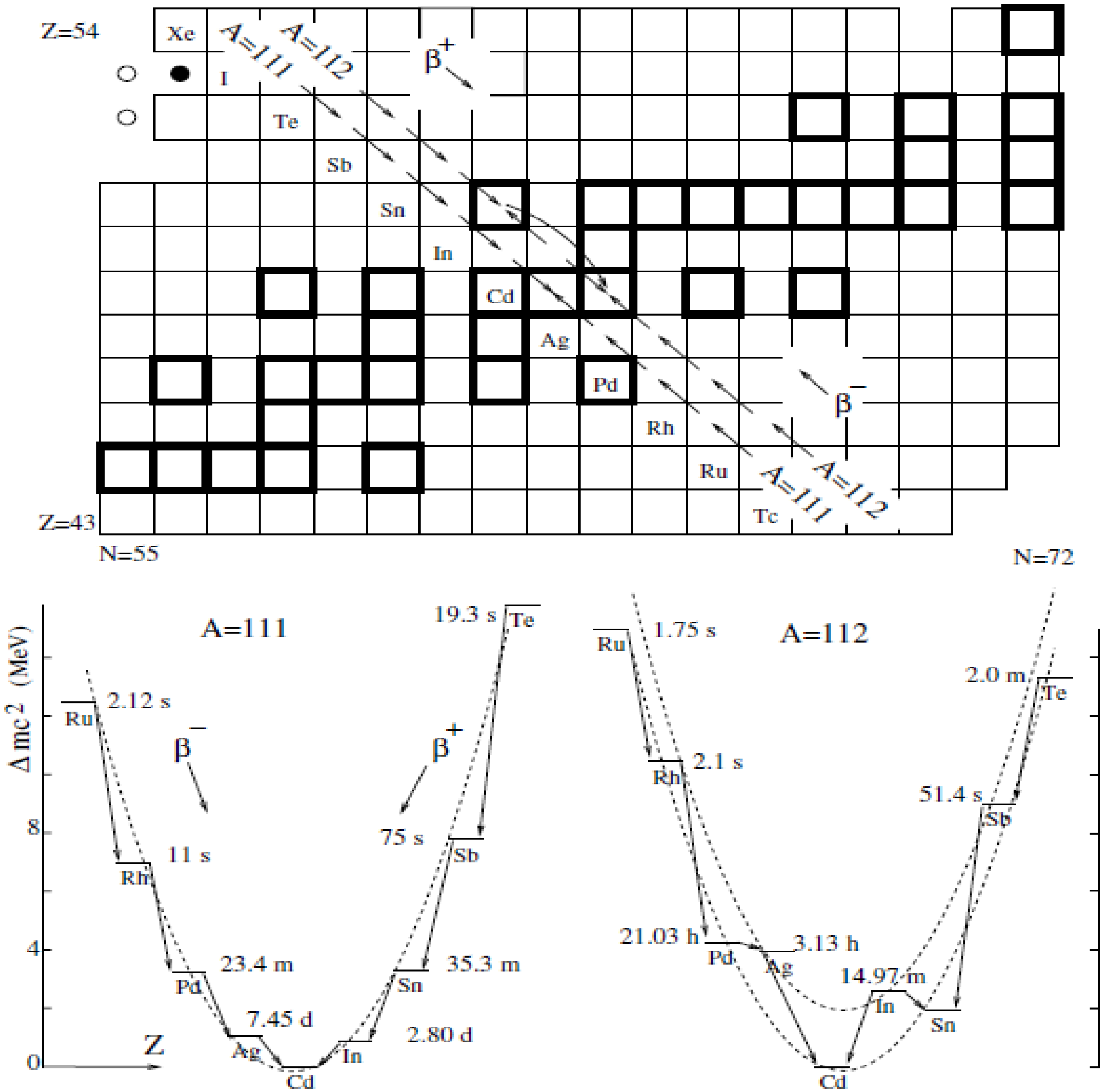

Fig. 2.6. The systematics of β-instability. The top panel shows a zoom of Fig. 2.1 with the β-stable nuclei shown with the heavy outlines. Nuclei with an excess of neutrons (below the β-stable nuclei) decay by β^- emission. Nuclei with an excess of protons (above the β-stable nuclei) decay by β^+ emission or electron capture. The bottom panel shows the atomic masses as a function of Z for $A = 111$ and $A = 112$. The quantity plotted is the difference between $m(Z)$ and the mass of the lightest isobar. The dashed lines show the predictions of the mass formula (2.13) after being offset so as to pass through the lowest mass isobars. Note that for even-A, there can be two β-stable isobars, e.g. ^{112}Sn and ^{112}Cd. The former decays by 2β-decay to the latter. The intermediate nucleus ^{112}In can decay to both.

Note that for even A one has two parabolas shifted by the value of pairing term.

Fermi gas model

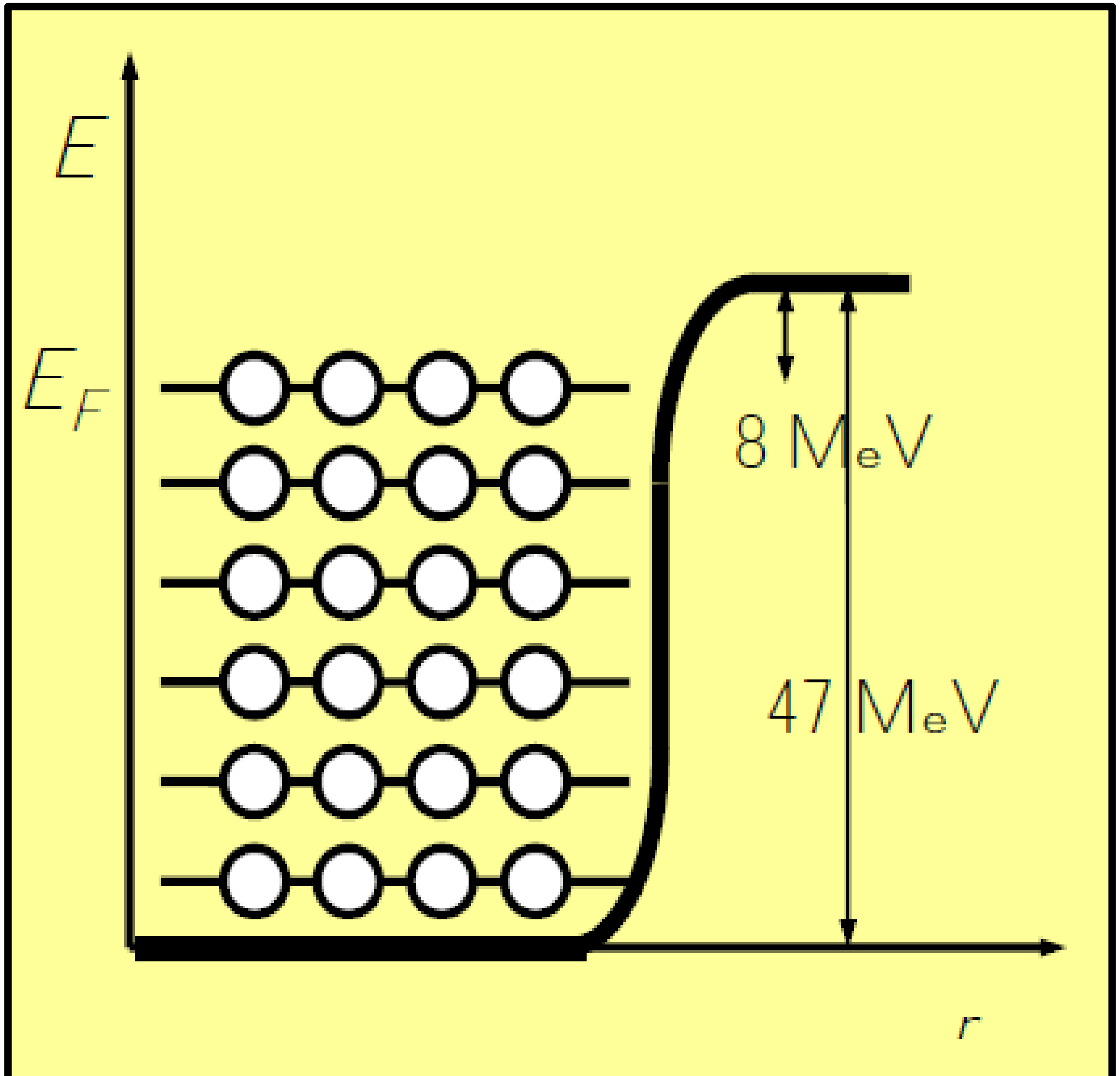

We assume that nucleons move independently of each other in a certain volume V corresponding to the volume of a nucleus.

This counterintuitive assumption can be justified taking into account **Pauli principle** which says that two nucleons cannot appear in the same state.

as a consequence in a nucleus nucleons occupy states up to the highest one (corresponding to The highest energy – **Fermi energy**).
nucleons in turn hardly interact because there is no space to scatter in particular for those with low energy

The Fermi model is based on the fact that a spin 1/2 particle confined to a volume V can only occupy a discrete number of states. In the momentum interval $\mathrm{d}^3\boldsymbol{p}$, the number of states is

$$\mathrm{d}\mathcal{N} = (2s+1)\frac{V\,\mathrm{d}^3\boldsymbol{p}}{(2\pi\hbar)^3} \quad , \tag{2.18}$$

with $s = 1/2$. This number will be derived below for a cubic container but it is, in fact, generally true. It corresponds to a density in *phase space* of 2 states per $2\pi\hbar^3$ of phase-space volume.

We now place $\mathcal{N}$ particles in the volume. In the ground state, the particles fill up the lowest single-particle levels, i.e. those up to a maximum momentum called the *Fermi momentum*, p_{F}, corresponding to a maximum energy $\varepsilon_{\mathrm{F}} = p_{\mathrm{F}}^2/2m$. The Fermi momentum is determined by

$$\mathcal{N} \;=\; \sum_{p<p_{\mathrm{F}}} \mathrm{d}\mathcal{N} \;=\; \frac{V\,p_{\mathrm{F}}^3}{3\pi^2\hbar^3} \quad . \tag{2.19}$$

This determines the Fermi energy

$$\varepsilon_{\mathrm{F}} \;=\; \frac{p_{\mathrm{F}}^2}{2m} \;=\; \frac{\hbar^2}{2m}(3\pi^2 n)^{2/3} \tag{2.20}$$

where n is the number density $n = \mathcal{N}/V$. The total (*kinetic*) energy $\mathcal{E}$ of the system is

$$\mathcal{E} \;=\; \sum_{p<p_{\mathrm{F}}} \frac{p^2}{2m} \;=\; \frac{3}{5}\mathcal{N}\varepsilon_{\mathrm{F}} \quad . \tag{2.21}$$

In a system of $A = Z + N$ nucleons, the densities of neutrons and protons are respectively $n_0(N/A)$ and $n_0(Z/A)$ where $n_0 \sim 0.15\,\mathrm{fm}^{-3}$ is the nucleon density. The total kinetic energy is then

$$\mathcal{E} = \mathcal{E}_Z + \mathcal{E}_N = 3/5 \left[Z \frac{\hbar^2}{2m} (3\pi^2 \frac{Z n_0}{A})^{2/3} + N \frac{\hbar^2}{2m} (3\pi^2 \frac{N n_0}{A})^{2/3} \right] . \quad (2.22)$$

In the approximation $Z \sim N \sim A/2$, this value of the nuclear density corresponds to a Fermi energy for protons and neutrons of

$$\varepsilon_{\mathrm{F}} = 35 \text{ MeV} \quad , \quad (2.23)$$

which corresponds to a momentum and a wave number

$$p_{\mathrm{F}} = 265 \mathrm{MeV}/c \, , \qquad k_{\mathrm{F}} = p_{\mathrm{F}}/\hbar = 1.33\,\mathrm{fm}^{-1} \quad . \quad (2.24)$$

2.3.2 The asymmetry energy

Consider now the system of the two Fermi gases, with N neutrons and Z protons inside the same sphere of radius R. The total energy of the two gases (2.22) is

$$E = \frac{3}{5}\varepsilon_{\mathrm{F}}\left(N(\frac{2N}{A})^{2/3} + Z(\frac{2Z}{A})^{2/3}\right) \quad , \tag{2.34}$$

where we neglect the surface energy. Expanding this expression in the neutron excess $\Delta = N - Z$, we obtain, to first order in Δ/A,

$$E = \frac{3}{5}\varepsilon_{\mathrm{F}} + \frac{\varepsilon_{\mathrm{F}}}{3}\frac{(N-Z)^2}{A} + \ldots \, . \tag{2.35}$$

This is precisely the form of the asymmetry energy in the Bethe–Weizsäcker formula. However, the numerical value of the coefficient $a_{\mathrm{a}} \sim 12$ MeV is half of the empirical value. This defect comes from the fact that the Fermi model is too simple and does not contain enough details about the nuclear interaction.

Shell Model

Problems with the Liquid Drop Model

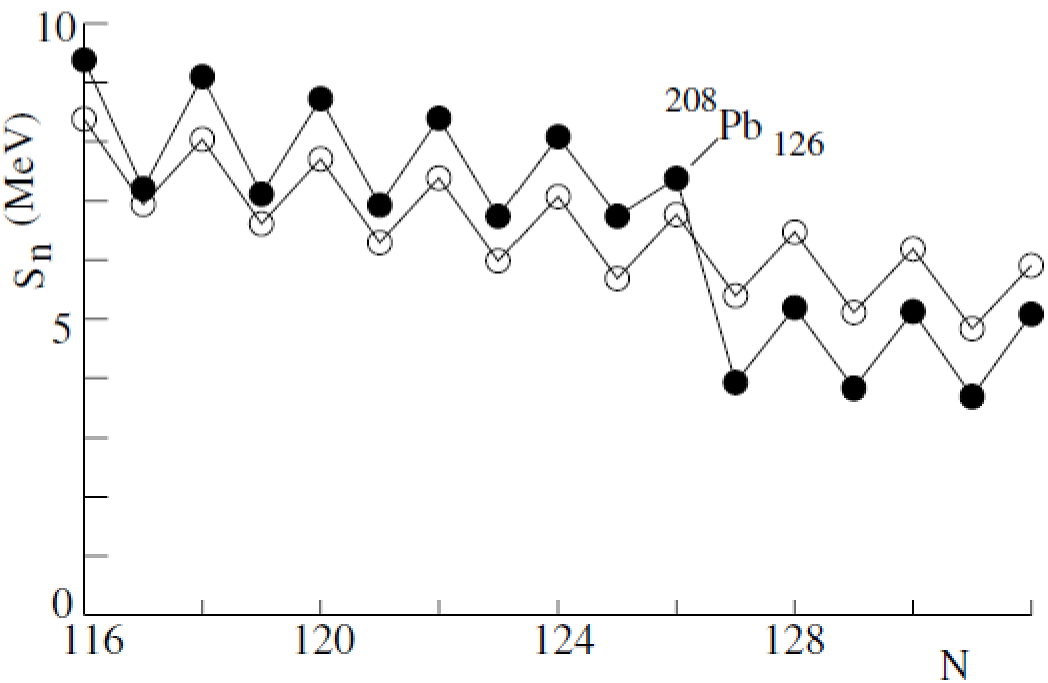

Fig. 2.7. The neutron separation energy in lead isotopes as a function of N. The filled dots show the measured values and the open dots show the predictions of the Bethe–Weizsäcker formula.

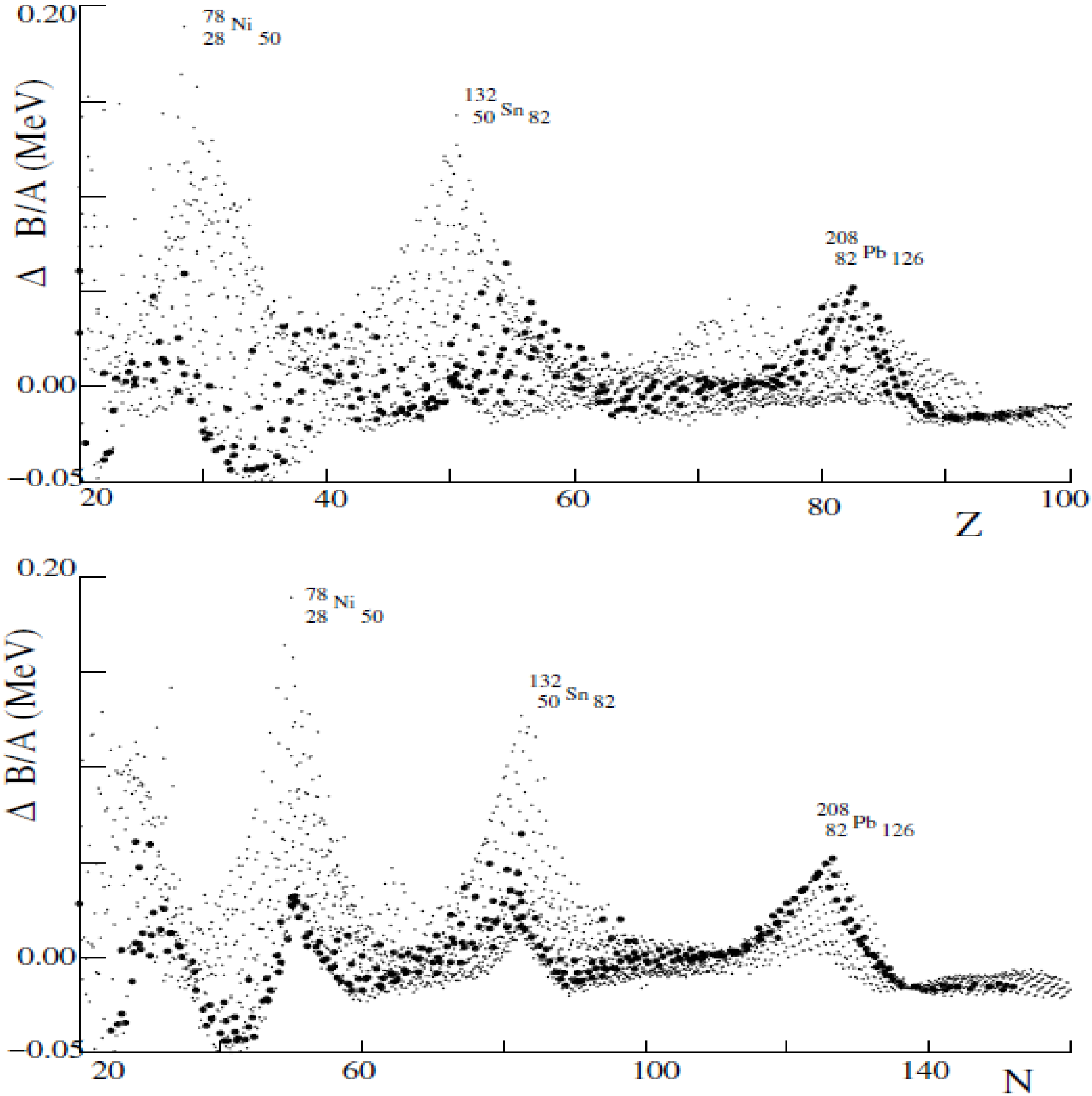

Fig. 2.8. Difference in MeV between the measured value of B/A and the value calculated with the empirical mass formula as a function of the number of protons Z (top) and of the number of neutrons N (bottom). The large dots are for β-stable nuclei. One can see maxima for the magic numbers $Z, N = 20$, 28, 50, 82, and 126. The largest excesses are for the doubly magic nuclides as indicated.

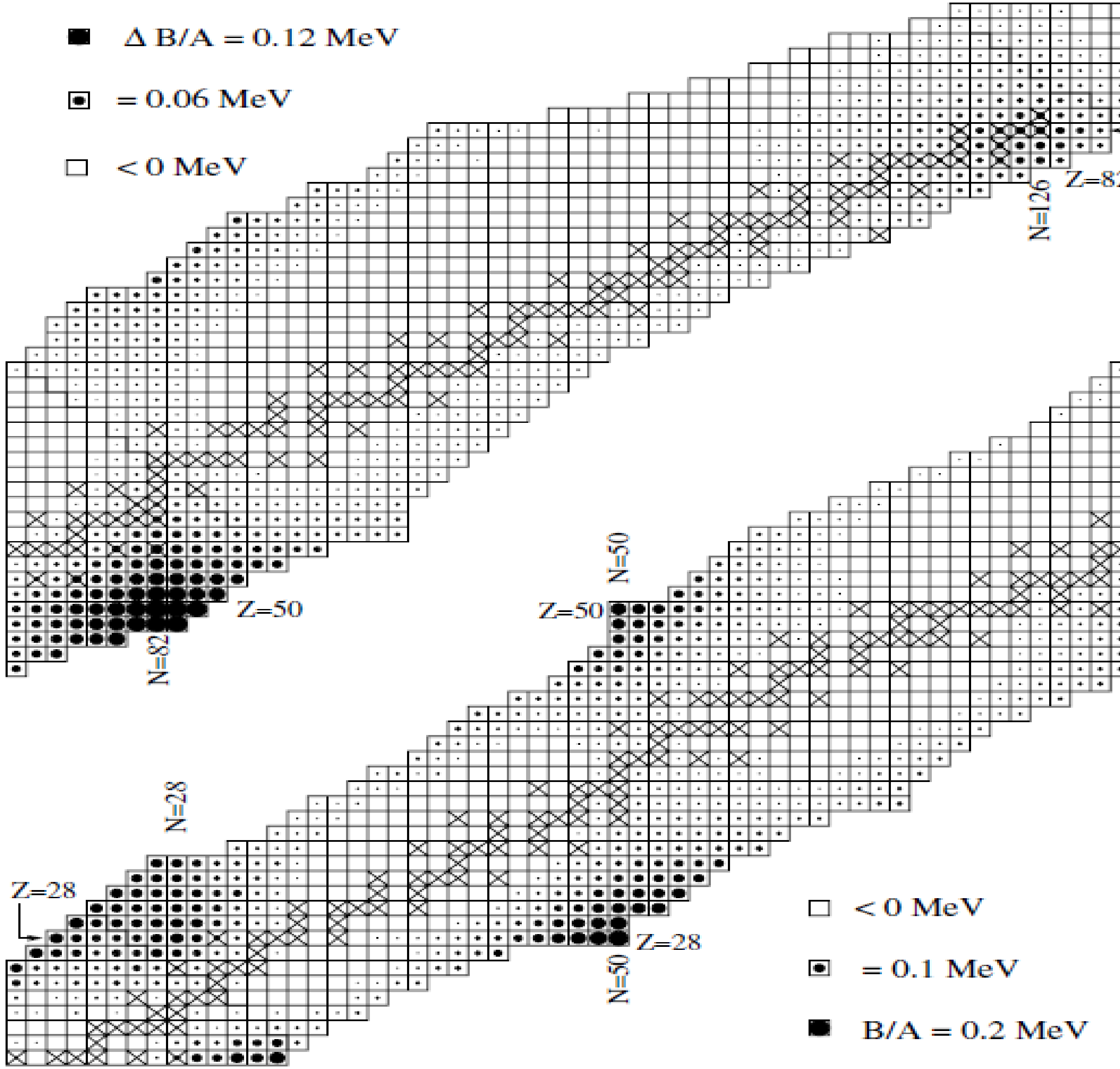

Fig. 2.9. Difference between the measured value of B/A and the value calculated with the mass formula as a function of N and Z. The size of the black dot increases with the difference. One can see the hills corresponding to the values of the magic numbers 28,50,82 and 126. Crosses mark β-stable nuclei.

There exist numbers of nucleons for which the nucleus have enhanced stability: **magic numbers**

$$2 \quad 8 \quad 20 \quad 28 \quad 50 \quad 82 \quad 126\,.$$

There is a similarity between this effect and the existence of so called noble gases in chemistry.

We know that noble gases appear due to the existence of shells which are occupied by electrons in atoms.
If a given shell is fully occupied (according to Pauli principle) then such an atom is chemically very stable (hardly reacts with anything).

The mean nuclear potential

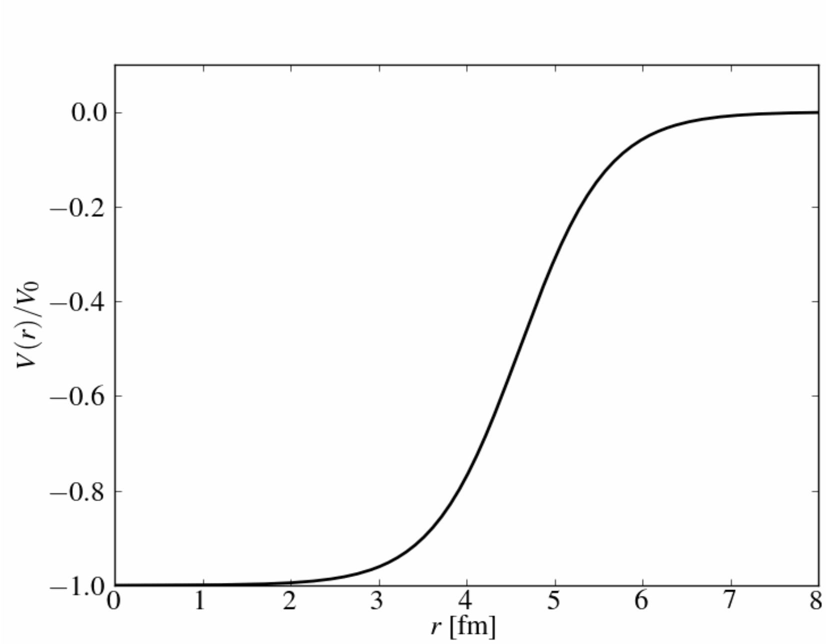

The shape of nuclear potential reflects the density distribution of nucleons inside a nucleus.

For protons we have additional Coulomb potential:

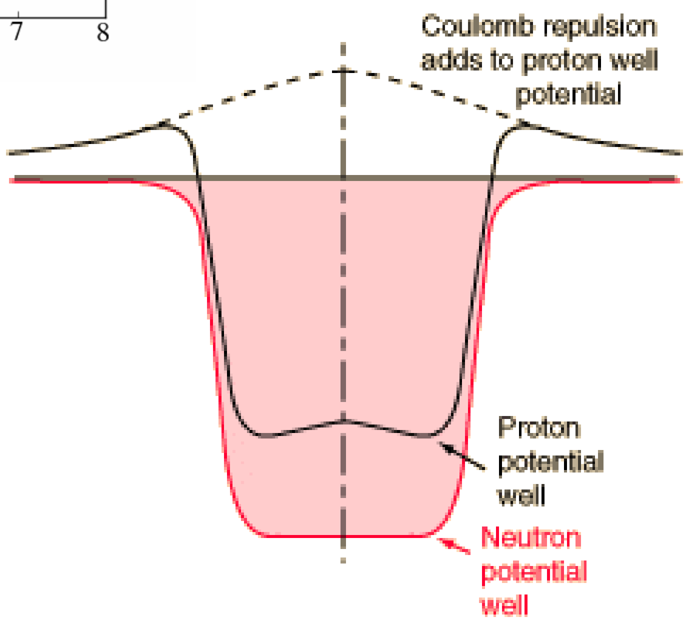

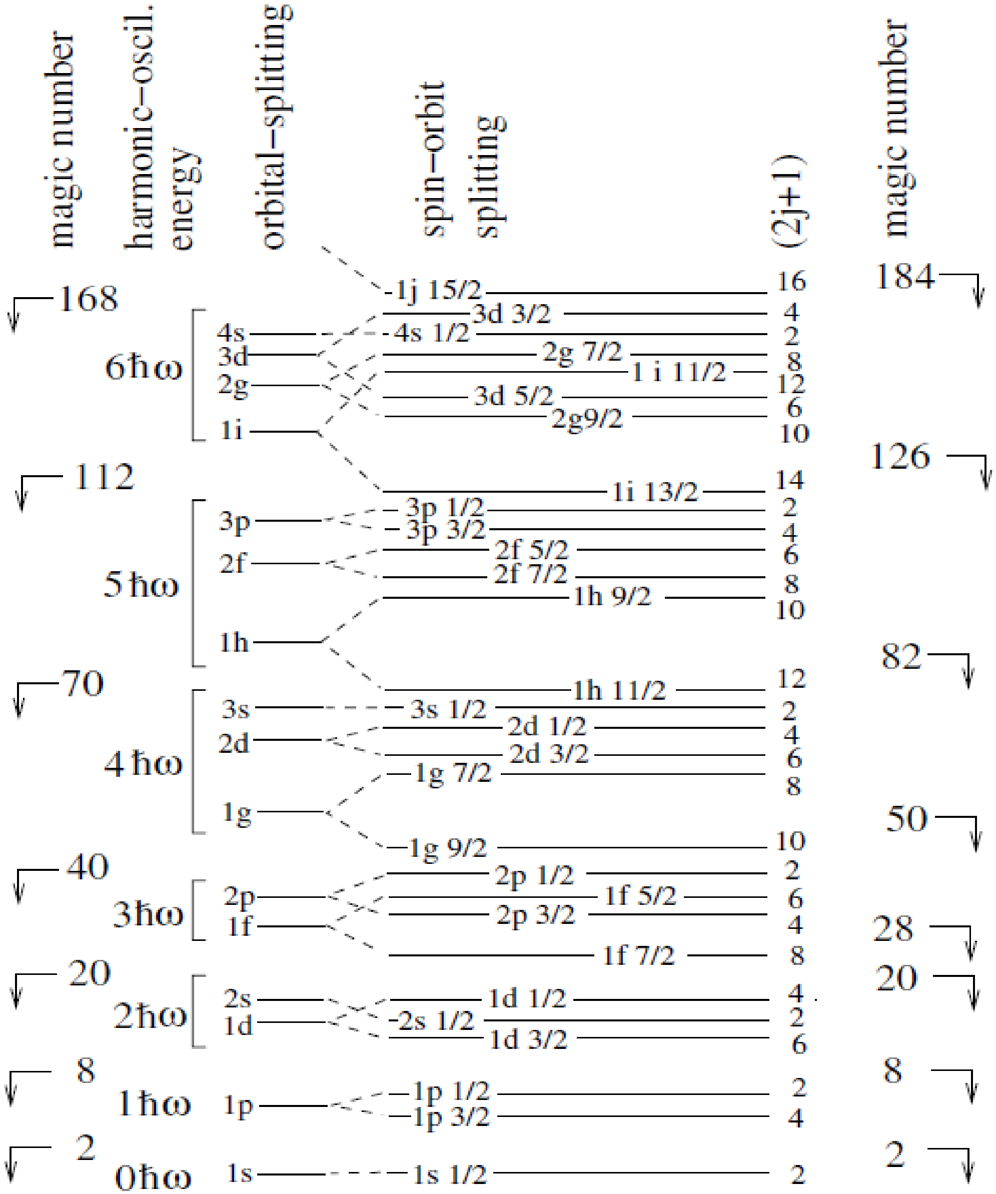

Fig. 2.10. Nucleon orbitals in a model with a spin-orbit interaction. The two left-most columns show the magic numbers and energies for a pure harmonic potential. The splitting of different values of the orbital angular momentum l can be arranged by modifying the central potential. Finally, the spin-orbit coupling splits the levels so that they depend on the relative orientation of the spin and orbital angular momentum. The number of nucleons per level $(2j+1)$ and the resulting magic numbers are shown on the right.

Notation:
s, p, d, f, g, h, i, j, k,…
denote orbital angular momentum:
0, 1, 2, 3, 4, 5, 6, 7, 8, … respectively

The half integer number denotes the value total angular momentum: orbital angular momentum + spin.

Remember that on each state corresponding to the total angular momentum j one can place (2j+1) neutrons or protons.

The spin-orbit term in the potential is crucial to obtain the magic numbers

Shell model adds to the smooth liquid drop behavior an oscillating part related to the ordering of single particle levels:

$$E = E_{LD} + E_{shell}$$

E_{shell} - Can be extracted from the structure of single particle levels in the mean field potential.

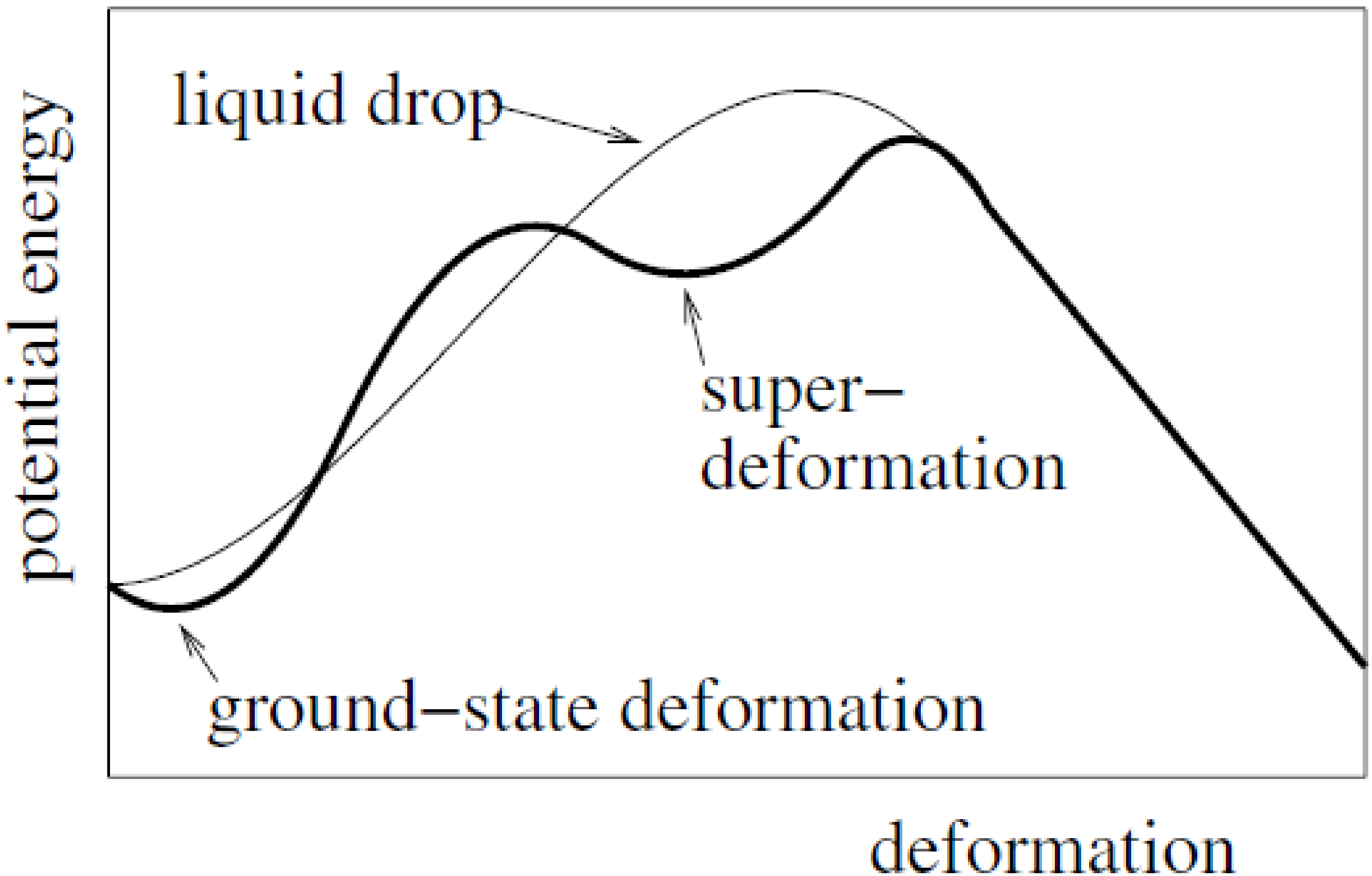

Fig. 2.11. Nuclear energies as a function of deformation. The liquid-drop model predicts that the energy has a local minimum for vanishing deformation because this minimizes the surface energy term. (As discussed in Chap. 6, in high-Z nuclei the energy eventually decreases for large deformations because of Coulomb repulsion, leading to spontaneous fission of the nucleus.) As explained in the text, the shell structure leads to a deformation of the ground state for nuclei with unfilled shells. Super-deformed local minima may also exist.

Magic and semimagic nuclei have:

- a binding energy greater than that predicted by the semi-empirical mass formula,
- a large number of stable isotopes or isotones,
- a large natural abundances,
- a large energy separation from the first excited state,
- a small neutron capture cross-section (magic-N only).

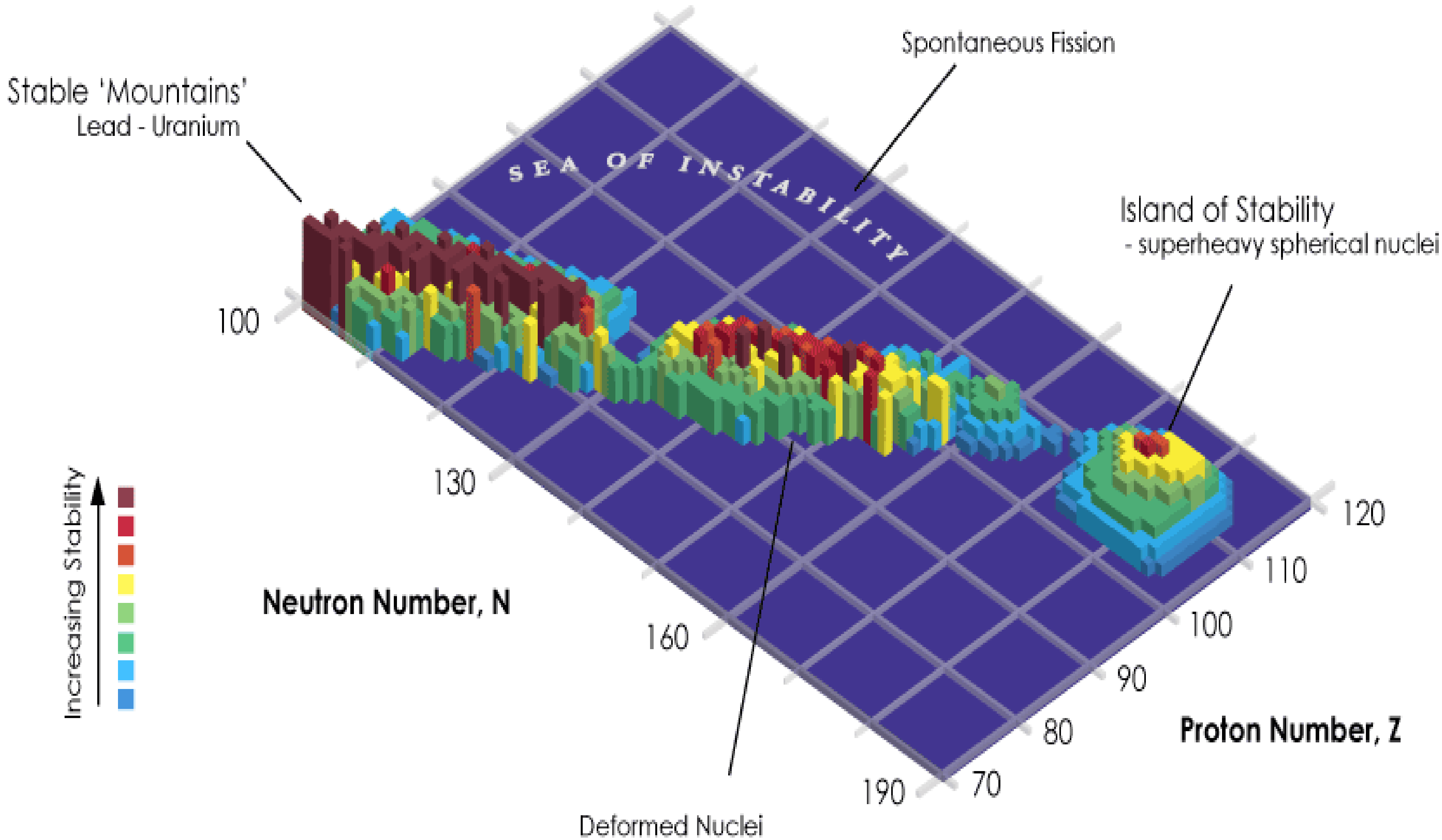
Stable 'Mountains'
Lead - Uranium
SEA OF INSTABILITY
Spontaneous Fission
Island of Stability
- superheavy spherical nuclei
100
130
160
190
Neutron Number, N
120
110
100
90
80
70
Proton Number, Z
Increasing Stability
Deformed Nuclei

4.1 Decay rates, generalities

4.1.1 Natural width, branching ratios

Decay rates and mean lifetimes can be defined by the same considerations as lead us to the definition of cross-sections in Chap. 3. An unstable particle has a probability $\mathrm{d}P$ to decay in a time interval $\mathrm{d}t$ that is proportional to $\mathrm{d}t$:

$$\mathrm{d}P = \frac{\mathrm{d}t}{\tau}\,, \tag{4.1}$$

where τ clearly has dimensions of time and is called the "mean lifetime" of the particle. This law governs the time dependence of the number $N(t)$ of an unstable state surviving after a time t:

$$N(t+\mathrm{d}t) - N(t) = -N(t)\mathrm{d}P \Rightarrow \frac{\mathrm{d}N}{\mathrm{d}t} = -\frac{N(t)}{\tau}\,, \tag{4.2}$$

which has the solution

$$N(t) \;=\; N(t=0)\mathrm{e}^{-t/\tau}\;. \tag{4.3}$$

The mean survival time is τ, justifying its name.

The inverse of the mean lifetime is the "decay rate"

$$\lambda \;=\; \frac{1}{\tau}\;. \tag{4.4}$$

We saw in Sect. 3.5 that an unstable particle (or more precisely an unstable quantum state) has a rest energy uncertainty or "width" of

$$\Gamma \;=\; \hbar\lambda \;=\; \frac{\hbar}{\tau} \;=\; \frac{6.58\;\times\;10^{-22}\,\mathrm{MeV\ sec}}{\tau}\;. \tag{4.5}$$

It is often the case that an unstable state has more than one "decay channel," each channel k having its own "branching ratio" B_k. For example the fourth excited state of ^{7}Li has

$$B_{n^6\mathrm{Li}} = 0.72 \qquad B_{^3\mathrm{H}^4\mathrm{He}} = 0.28 \qquad B_{\gamma^7\mathrm{Li}} \sim 0.0 \,, \tag{4.6}$$

where the third mode is the unlikely radiative decay to the ground state. In general we have

$$\sum_k B_k = 1 \,, \tag{4.7}$$

the sum of the "partial decay rates," $\lambda_k = B_k \lambda$

$$\sum_k \lambda_k = \lambda \,, \tag{4.8}$$

and the sum of the "partial widths," $\Gamma_k = B_k \Gamma$

$$\sum_k \Gamma_k = \Gamma \,. \tag{4.9}$$

Decay lifetimes span an interval from 10^(-22) sec. to 10^(21) years

$$^{7}\mathrm{Li}\,(7.459\,\mathrm{MeV}) \rightarrow \mathrm{n}\,^{6}\mathrm{Li},\;\; ^{3}\mathrm{H}\,^{4}\mathrm{He} \qquad \tau = 6 \times 10^{-21}\ \mathrm{sec}$$

to 10^{21} yr

$$^{76}\mathrm{Ge} \rightarrow\ ^{76}\mathrm{Se}\,2\mathrm{e}^{-}\,2\bar{\nu}_{\mathrm{e}} \qquad t_{1/2} = 1.6 \times 10^{21}\ \mathrm{yr}$$

- $\tau > 10^8$ yr (mostly α- and 2β-decay). The nuclei are still present on Earth (whose nuclei were formed about 5×10^9 year ago) and can be chemically and isotopically isolated in macroscopic quantities and their decays detected. The lifetime can then by determined from (4.3) and knowledge of the quantity N in the sample. An illustration of this technique is shown in Fig. 4.1.
- 10 min $< \tau <$ 10^8 yr (mostly α- and β-decay). The nuclei are no longer present on Earth in significant quantities and must be produced in nuclear reactions, either artificially or naturally (cosmic rays and natural radioactivity sequences). The lifetimes are long enough for chemical and (with more difficulty) isotopic purification. The decays can then be observed and (4.3) applied to derive τ. The case of ^{170}Tm is illustrated in Fig. 4.2. If the observation time is comparable to τ, knowledge of $N(t=0)$ is not necessary because τ can be derived from the time variation of the counting rate.
- 10^{-10}s $< \tau < 10^3$s (mostly β-, γ- and α-decay). While chemical and isotopic purification is not possible for such short lifetimes, particles produced in nuclear reactions can be slowed down and stopped in a small amount of material (Sect. 5.3). Decays can be counted and (4.3) applied to derive τ. Examples are shown in Figs. 2.18 and 2.19. The case of the first excited state of ^{170}Yb produced in the β-decay of ^{170}Tm is illustrated in Fig. 4.2.
- 10^{-15}s $< \tau < 10^{-10}$s. (mostly γ-decay). The time interval between production and decay is too short to be measured by standard timing techniques but a variety of ingenious techniques have been devised that apply to this range that covers most of the radiative nuclear decays. One technique uses the fact that the time for a particle to slow down in a material after having been produced in a nuclear reaction can be reliably calculated (Sect. 5.3). For particles with 10^{-15}s $< \tau < 10^{-10}$s, the disposition of material can be chosen so that some particles decay "in flight" and some after coming to rest. For the former, the energies of the decay particles are Doppler shifted and can be distinguished from those due to decays at rest. Measurement of the proportion of the two types and knowledge of the slowing-down time allows one to derive τ. The technique is illustrated in Fig. 4.3.

Another indirect technique for radiative transitions is the *Coulomb excitation* method. The cross-section for the production of an excited state in collisions with a charged particle is measured. As mentioned in Sect. 3.4.2, the cross-section involves the same matrix element between ground- and excited-nuclear states as that involved in the decay of the excited- to ground-state. In fact, the incident charged particle can be considered to be a source of virtual photons that can induce the transition. Knowledge of the cross-section allows one to deduce the radiative lifetime of the state.

- $\tau < 10^{-12}$s i.e. $\Gamma > 6 \times 10^{-10}$ MeV. (mostly γ-decay and dissociation). In this range where direct timing is impossible, the width of the state can be measured and (4.5) applied to derive τ. An example is shown in Fig. 3.4 where the energy dependence of the neutron cross-section on ^{6}Li can be used to derive the widths of excited states. In this example, the state is very wide because it decays by breakup to n^{6}Li or ^{3}H^{4}He. Widths of states that decay radiatively can only be measured with special techniques. An example is the use of the Mössbauer effect, as illustrated in Fig. 4.4.

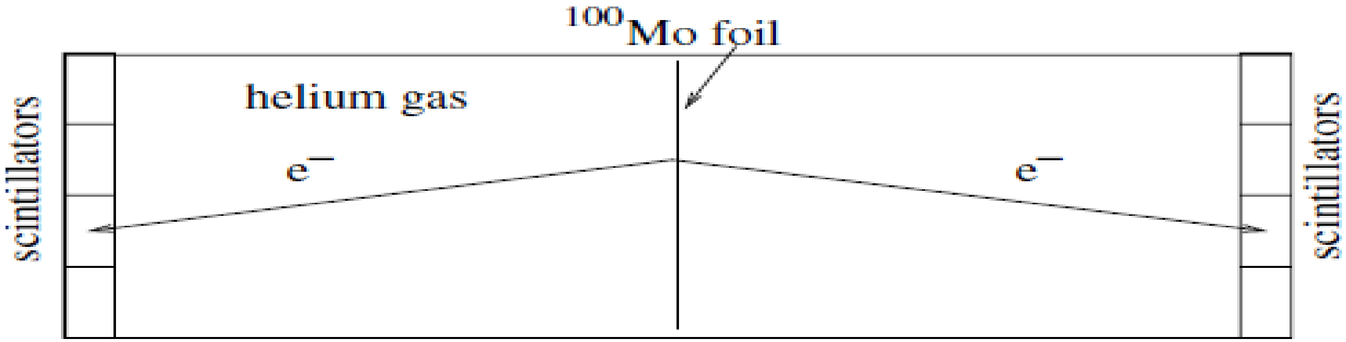

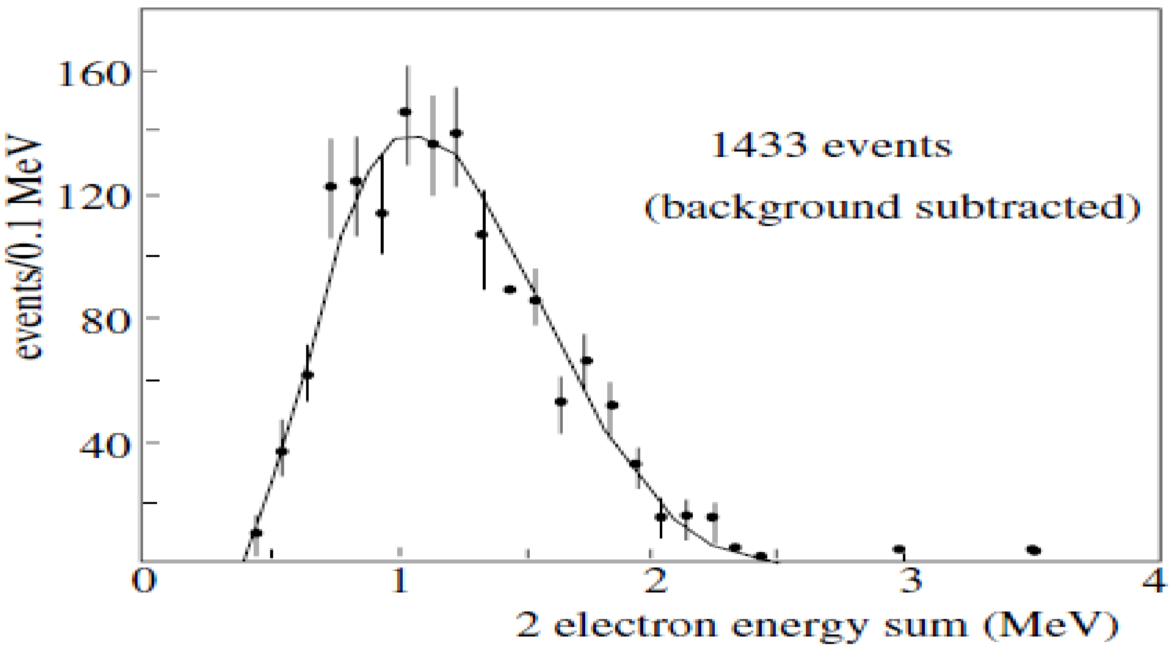

Fig. 4.1. The measurement of the double-β decay of ^{100}Mo $\to$ ^{100}Ru $2e^- 2\bar{\nu}_e$ [36]. The upper figure shows a simplified version of the experiment The source is a 40μm thick foil consisting of 172 g of isotopically enriched ^{100}Mo (98.4% compared to the natural abundance of 9.6%). After a decay, the daughter nucleus stays in the foil but the decay electrons leave the foil (Exercise 4.2) and traverse a volume containing helium gas. The gas is instrumented with high voltage wires that sense the ionization trail left by the passing electrons so as to determine the e^- trajectories. The electrons then stop in plastic scintillators which generate light in proportion to the electron kinetic energy. The bottom figure show the summed kinetic energy of electron pairs measured in this manner. A total of 1433 events were observed over a period of 6140 h, corresponding to a half-life of ^{100}Mo of $(0.95 \pm 0.11) \times 10^{19}$yr.

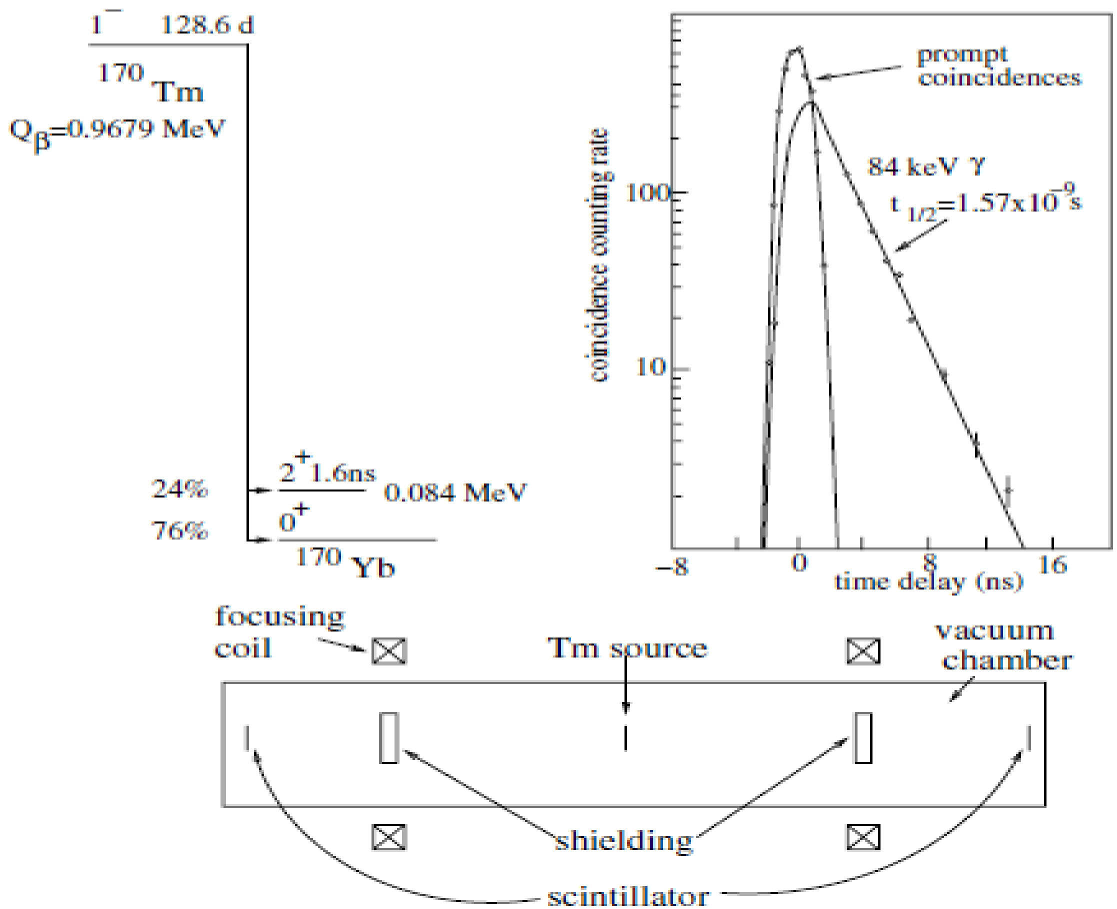

Fig. 4.2. Observation of the decay of ^{170}Tm and measurement of the lifetime of the first excited state of ^{170}Yb [37]. The radioactive isotope ^{170}Tm ($t_{1/2} = 128.6$day) is produced by irradiating a thin foil of stable ^{169}Tm with reactor neutrons. ^{170}Tm is produced through radiative neutron capture, $^{169}\mathrm{Tm}(\mathrm{n},\gamma)^{170}\mathrm{Tm}$. After irradiation, the foil is placed at a focus of a double-armed magnetic spectrometer. The decay $^{170}\mathrm{Tm} \rightarrow {}^{170}\mathrm{Yb}\, e^- \bar{\nu}_e$ proceeds as indicated in the diagram with a 76% branching ratio to the ground state of ^{170}Yb and with at 24% branching ratio to the 84 keV first excited state. The excited state subsequently decays either through γ-emission or by internal conversion where the γ-ray ejects an atomic electron of the Yb. Electrons emerging from the foil are momentum-selected by the magnetic field and focused onto two scintillators. Events with counts in both scintillators are due to a β-electron in one scintillator and to an internal conversion electron in the other. The distribution of time-delay between one count and the other is shown and indicates that the exited state has a lifetime of ~ 1.57 ns.

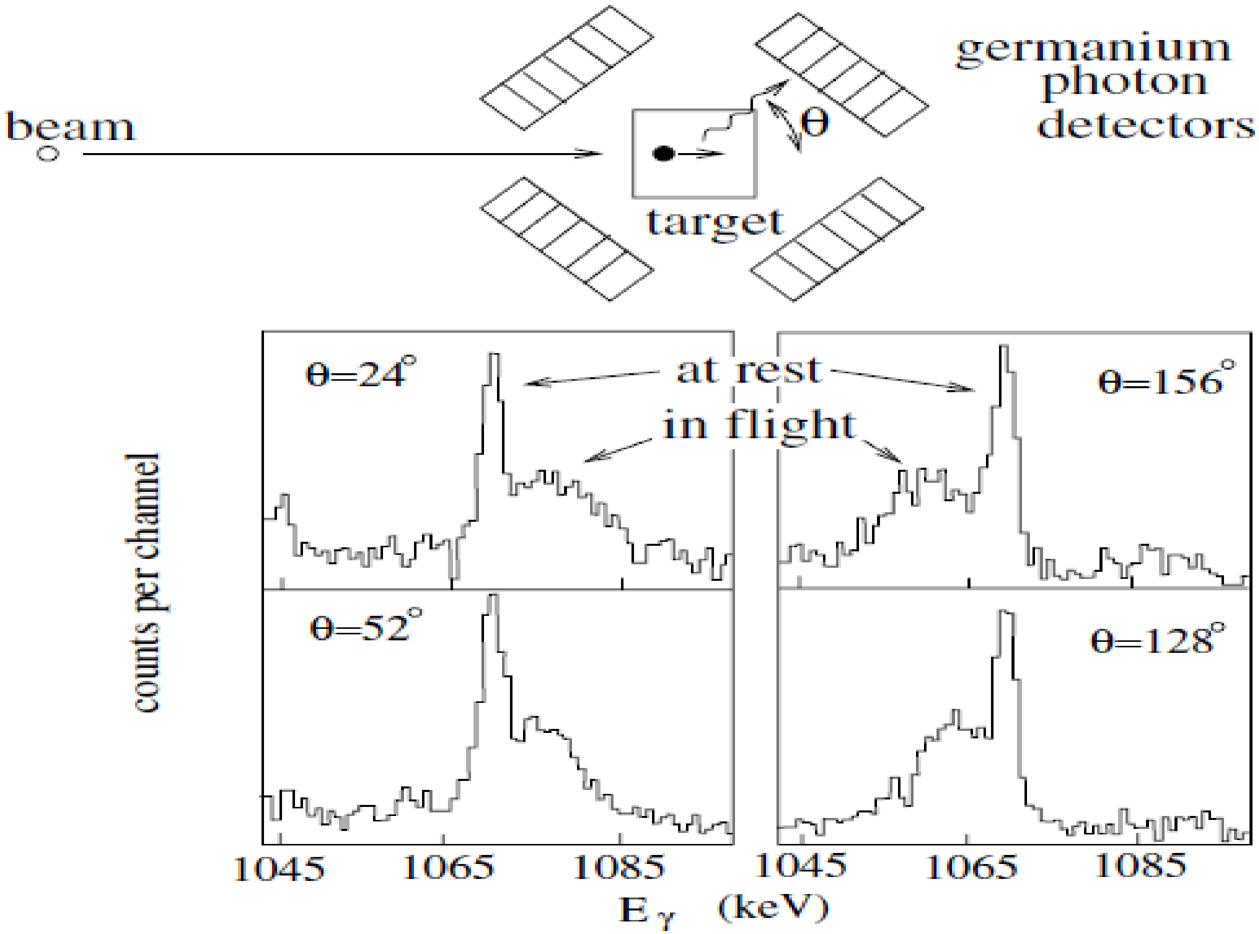

Fig. 4.3. Measurement of radiative-decay lifetimes by the "Doppler-shift attenuation method" [38]. The top figure is a simplified version of the apparatus used to measure the lifetimes of excited states of ^{74}Br. A beam of 70 MeV ^{19}F ions impinges upon a ^{58}Ni target, producing a variety of nuclei in a variety of excited states. The target is sufficiently thick that the produced nuclei stop in the target. Depending on the lifetime of the produced excited state, the state may decay before stopping ("in-flight" decays) or at rest. The target is surrounded by germanium-diode detectors (the Euroball array) that measure the energy of the photons. The bottom figure shows the energy distribution of photons corresponding to the 1068 keV line of ^{74}Br for four germanium diodes at different angles with respect to the beam direction. Each distribution has two components, a narrow peak corresponding to decays at rest and a broad tail corresponding to Doppler-shifted in-flight decays. Note that decays with $\theta > 90$ deg ($\theta > 90$ deg) have Doppler shifts that are positive (negative). Roughly half the decays are in-flight and half at-rest. Knowledge of the time necessary to stop a Br ion in the target allowed one to deduce a lifetime of 0.25 ps for the state that decays by emission of the 1068 keV gamma (Exercise 4.4).

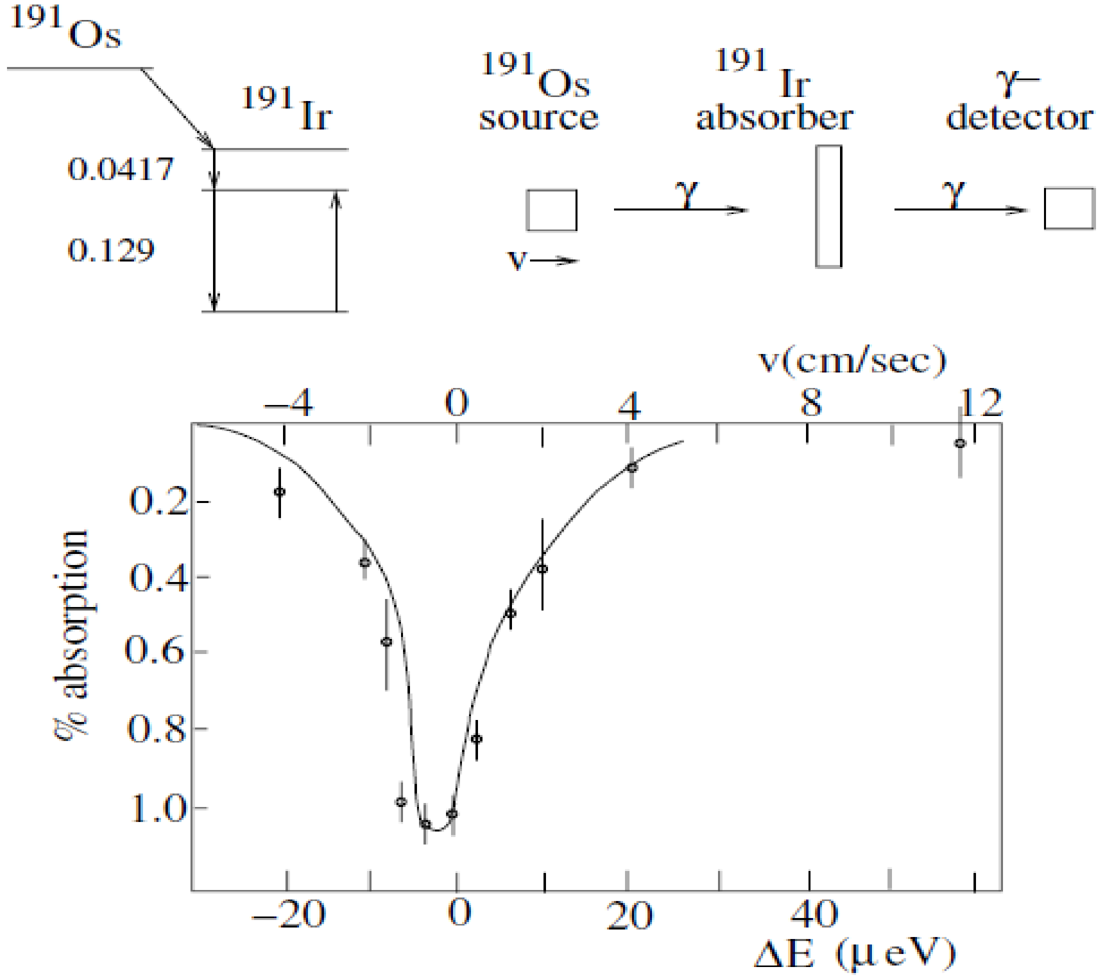

Fig. 4.4. Measurement of the width of the first excited state of ^{191}Ir through Mössbauer spectroscopy [39]. The excited state is produced by the β-decay of ^{191}Os. De-excitation photons can be absorbed by the inverse transition in a ^{191}Ir absorber. This resonant absorption can be prevented by moving the absorber with respect to the source with velocity v so that the photons are Doppler shifted out of the resonance. Scanning in energy then amounts to scanning in velocity with $\Delta E_\gamma/E_\gamma = v/c$. It should be noted that photons from the decay of *free* ^{191}Ir have insufficient energy to excite ^{191}Ir because nuclear recoil takes some of the energy (4.42). Resonant absorption is possible with $v = 0$ only if the ^{191}Ir nuclei is "locked" at a crystal lattice site so the crystal as a whole recoils. The nuclear kinetic energy $p^2/2m_A$ in (4.42) is modified by replacing the mass of the nucleus with the mass of the crystal. The photon then takes all the energy and has sufficient energy to excite the original state. This "Mössbauer effect" is not present for photons with $E > 200\,\text{keV}$ because nuclear recoil is sufficient to excite phonon modes in the crystal which take some of the energy and momentum.

Radiative decay

$$\boxed{{}^{A}_{Z}X^{*} \rightarrow {}^{A}_{Z}X + \gamma}$$

<= gamma decay

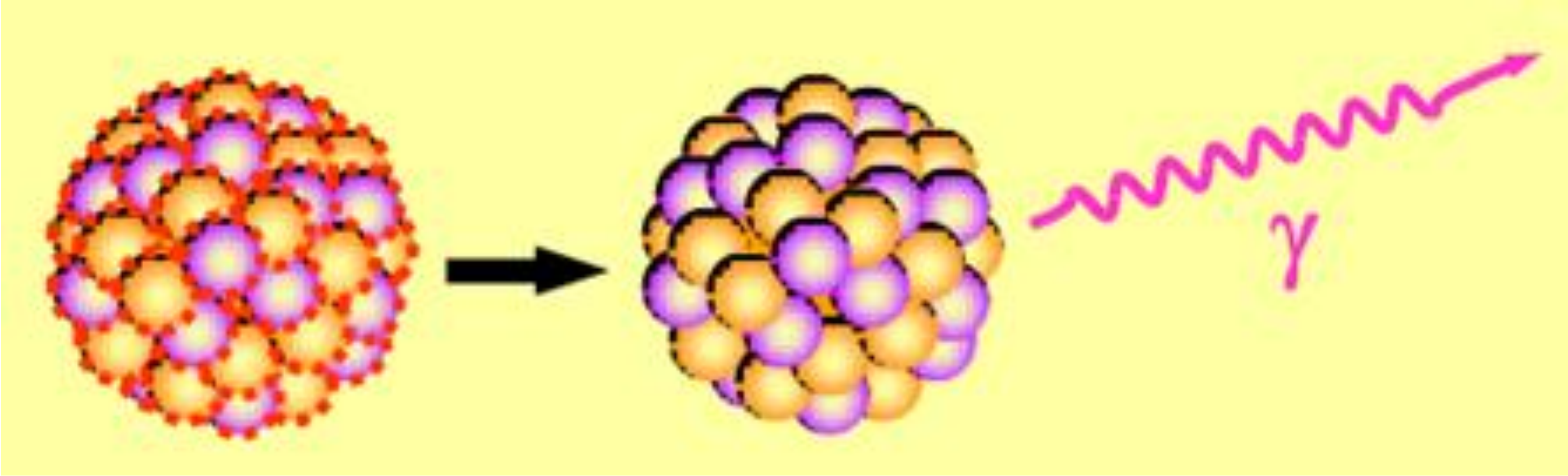

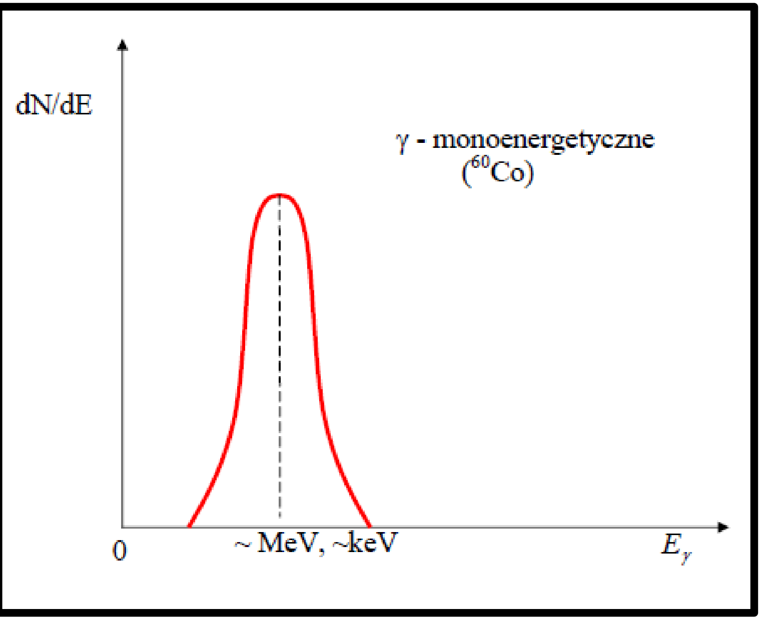

Discrete spectrum of radiation

$$\hbar\omega = E_i - E_f$$

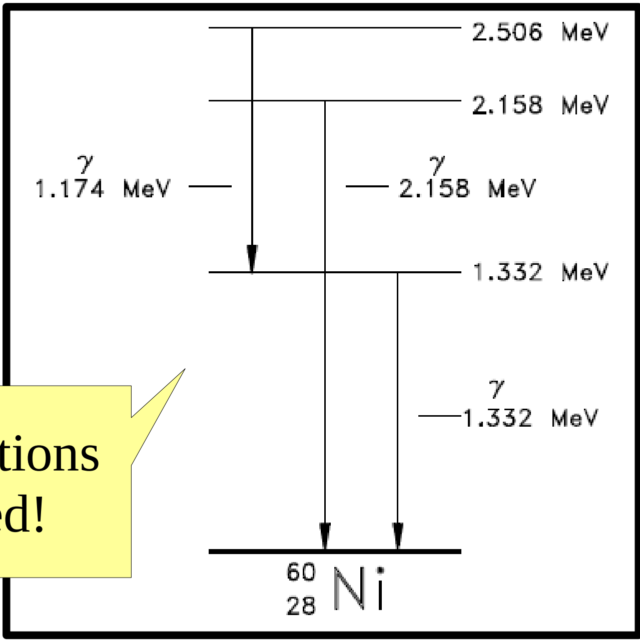

Not all transitions are allowed!

For nuclear transitions, $\langle r \rangle \sim A^{1/3} 10^{-15}$ m so

$$\lambda(\mathrm{E1}) \sim \hbar^{-1} \alpha E_\gamma^3 \left(\frac{A^{1/3}\mathrm{fm}}{\hbar c} \right)^2 . \tag{4.51}$$

For $E_\gamma \sim$ MeV, this gives rates of the order of 10^{15} to $10^{17}\mathrm{s}^{-1}$, i.e. lifetimes of the order of 10^{-17} to 10^{-15}s. The corresponding width, $\Gamma = \hbar/\tau \sim 10\,\mathrm{eV}$ is much less than the photon energy.

Just as higher classical multi-poles are less efficient radiators than classical electric dipoles, the quantum radiative rates decrease with increasing pole number:

$$\frac{\lambda(\mathrm{E}l)}{\lambda(\mathrm{E}1)} \sim \left(\frac{E_\gamma R}{\hbar c}\right)^{2l} \sim \left(\frac{E_\gamma(\mathrm{MeV})A^{1/3}}{200}\right)^{2l} , \tag{4.57}$$

i.e. about 2 orders of magnitude per pole.

Magnetic l-pole radiation is weaker than the corresponding electric l-pole radiation because fields generated by oscillating currents are smaller than fields generated by oscillating charges by a factor v/c where v is the velocity of the radiating charge. The uncertainty principle suggests that the velocity of nucleons in nuclei is of order $\hbar/(Rm_\mathrm{p})$ so we expect

$$B(\mathrm{M}l) \sim \left(\frac{\hbar c}{m_\mathrm{p}c^2 R}\right)^2 B(\mathrm{E}l) = \left(\frac{1}{5A^{1/3}}\right)^2 B(\mathrm{E}l) . \tag{4.58}$$

This implies that Ml transitions have rates between those of El and E$(l+1)$ transitions.

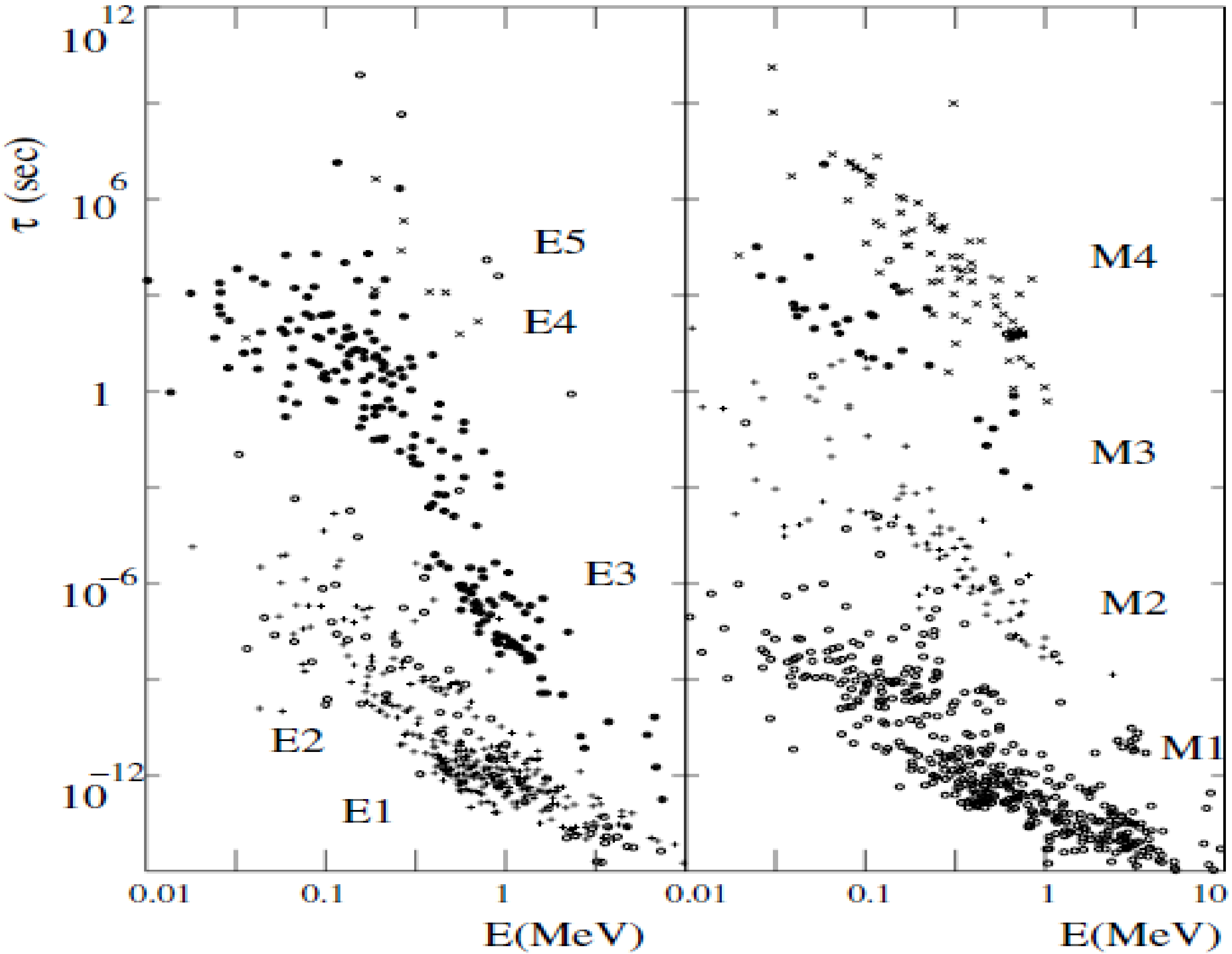

Fig. 4.5. Lifetimes of excited nuclear states as a function of E_γ for various electric and magnetic multipoles.. The various multipoles separate relatively well except for the E1 (open circles) and E2 (crosses) transitions that have similar lifetimes. (For clarity, only 10% of the available E1 and E2 transitions appear in the plot.) The surprising strength of the E2 transitions is because they are generally due to collective quadrupole motions of several nucleons, whereas E1 transitions can often be viewed as single nucleon transitions.

Table 4.1. Selection rules for radiative transitions

type	symbol	angular momentum change $\|\Delta J\| \leq$	parity change
electric dipole	E1	1	yes
magnetic dipole	M1	1	no
electric quadrupole	E2	2	no
magnetic quadrupole	M2	2	yes
electric octopole	E3	3	yes
magnetic octopole	M3	3	no
electric 16-pole	E4	4	no
magnetic 16-pole	M4	4	yes

Internal conversion

$$ {}^{A}_{Z}X^{*} + e^{-}_{\mathrm{pow.at.}} \rightarrow {}^{A}_{Z}X + e^{-} $$

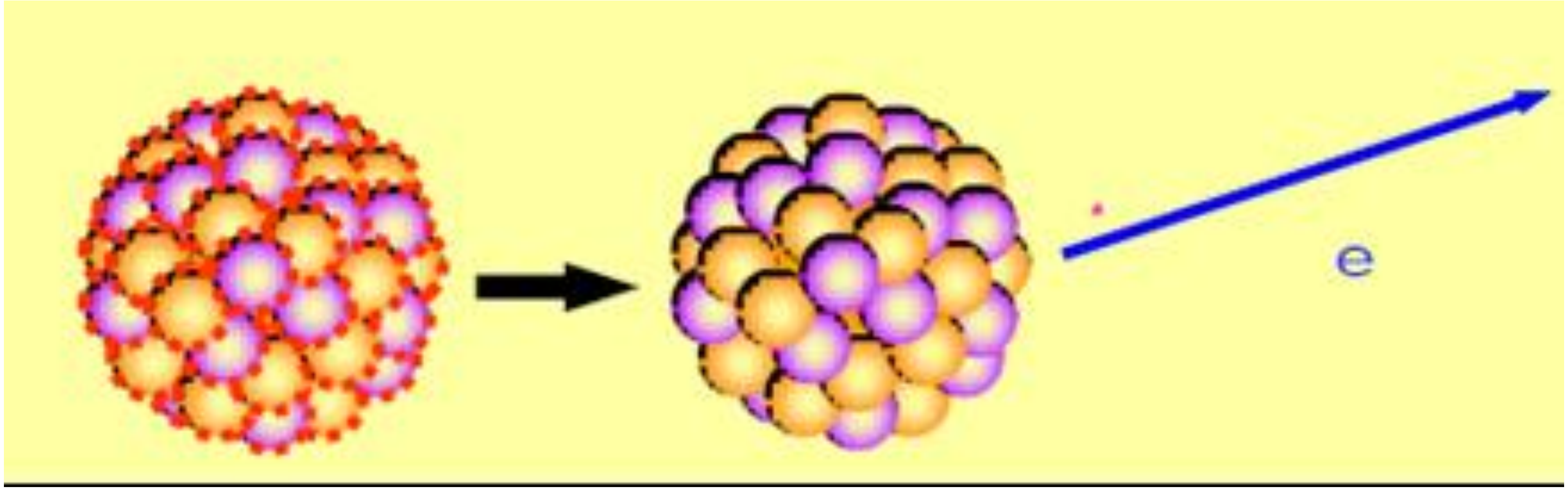

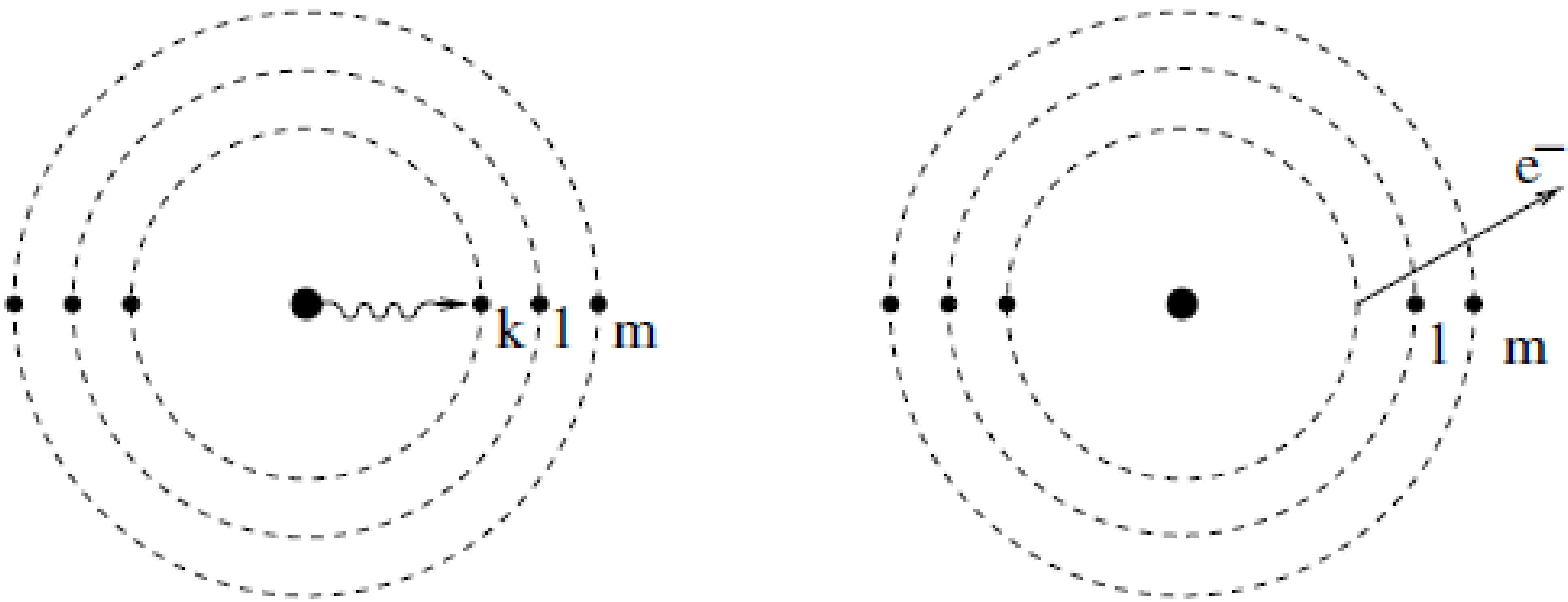

Fig. 4.6. An excited nucleus can transfer its energy to an atomic electron which is subsequently ejected from the atom. The process is called "internal conversion." The ejected electron can come from any of the atomic orbitals. In the figure, an electron from the deepest orbital is ejected, so-called K-conversion. Ejection of electrons in higher orbitals (L-, M- … conversion) are generally less probable.

The amplitude for internal conversion is proportional to the same nuclear matrix element responsible for radiative decay. The factor of proportionality depends on the multipolarity of the transition. An approximate expression for the probability for K-conversion compared to that for γ-emission is

$$\alpha_K \sim Z^3\alpha^4 \frac{l}{l+1}\left(\frac{2m_e c^2}{E_\gamma}\right)^{l+5/2} . \tag{4.61}$$

This formula applies in the limit $\alpha_K \ll 1$ and only if the atomic-electron binding energy is negligible compared to E_γ. It implies that internal conversion dominates over γ-emission for low-energy transitions:

$$E_\gamma < (Z^3\alpha^4)^{1/(l+5/2)} m_e c^2 . \tag{4.62}$$

Since we always have $Z^3\alpha^4 < 1$ this means that internal conversions is negligible for $E_\gamma > m_e c^2$. For E1 transitions, internal conversion is almost always small but for large l it becomes increasingly dominant for $E_\gamma < m_e c^2$. In all circumstances, numerical values α_K can be derived. These estimates are sufficiently accurate that the multipolarity of a transition can usually be determined if the conversion factor is measured. This is an important element in the assignment of spins and parities to nuclear states .

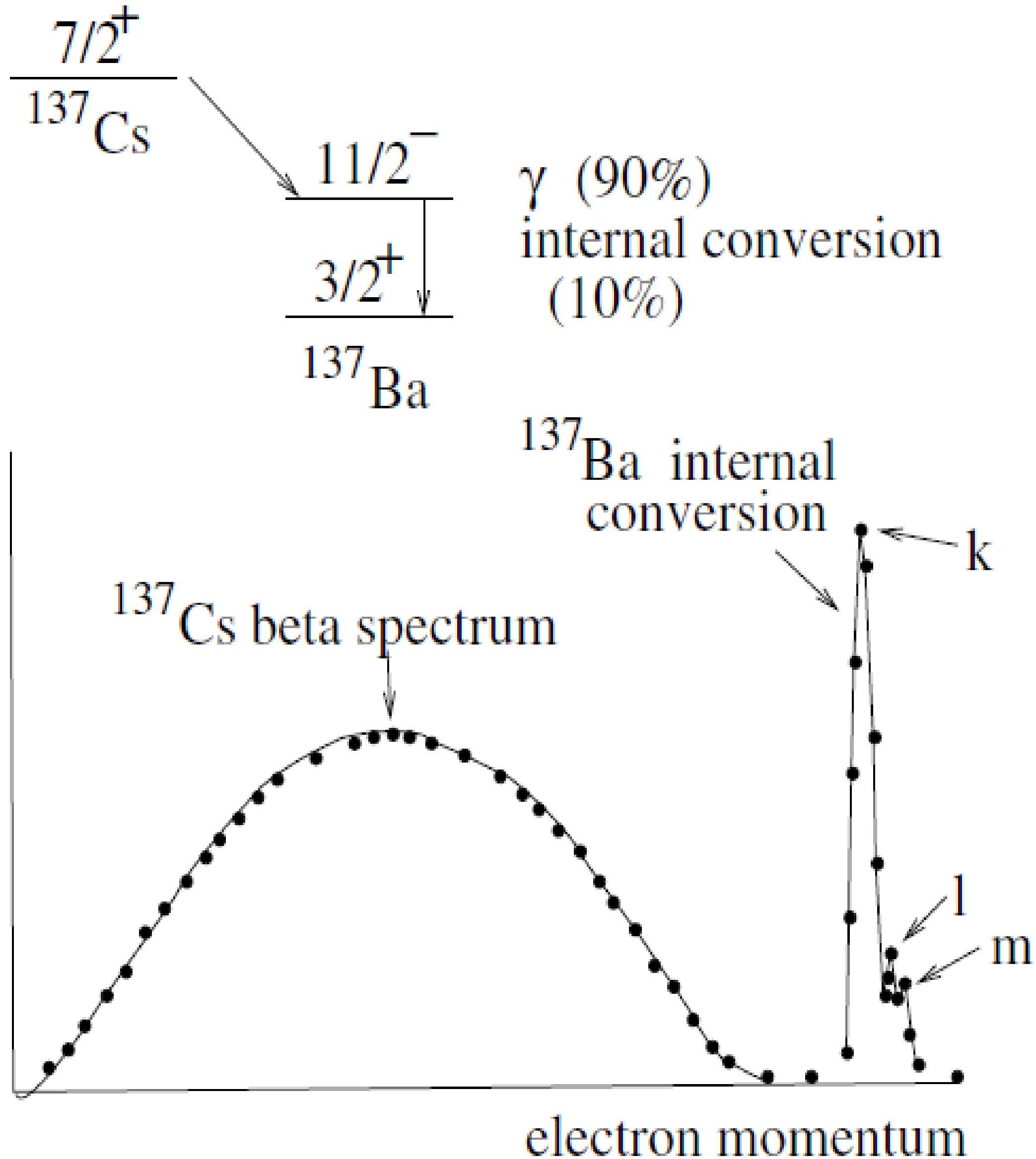

Fig. 4.7. The β-spectrum of ^{137}Cs and the internal conversion lines from the decay of the first excited state of ^{137}Ba [40]. Captures from the *K*, *L and M* orbitals are seen.

$$\boxed{{}^{A}_{Z}X \rightarrow {}^{A}_{Z\pm 1}Y + e^{\pm} + \begin{matrix} \nu_e \\ \tilde{\nu}_e \end{matrix}}$$

$$\boxed{{}^{0}_{-1}e^{-} + {}^{A}_{Z}X \rightarrow {}^{A}_{Z-1}Y + \nu_e}$$

2.5 β-instability

As already emphasized, nuclei with a non-optimal neutron-to-proton ratio can decay in A-conserving β-decays. As illustrated in Fig. 2.6, nuclei with an excess of neutrons will β^- decay:

$$(A, Z) \rightarrow (A, Z+1)\, e^- \,\bar{\nu}_e \tag{2.41}$$

which is the nuclear equivalent of the more fundamental particle reaction

$$n \rightarrow p + e^- + \bar{\nu}_e \; . \tag{2.42}$$

Nuclei with an excess of protons will either β^+ decay

$$(A, Z) \rightarrow (A, Z-1)\, e^+ \bar{\nu}_e \tag{2.43}$$

or, if surrounded by atomic electrons, decay by electron capture

$$e^- \,(\mathrm{A}, \mathrm{Z}) \rightarrow (\mathrm{A}, \mathrm{Z}-1)\, \bar{\nu}_e \quad . \tag{2.44}$$

These two reactions are the nuclear equivalents of the particle reactions

$$e^- \, p \;\rightarrow\; n\, \nu_e \qquad\qquad p \rightarrow n\, e^+ \nu_e \; . \tag{2.45}$$

In order to conserve energy-momentum, proton β^+-decay is only possible in nuclei.

The energy release in β^--decay is given by

$$\begin{aligned} Q_{\beta^-} &= m(A, Z) - m(A, Z+1) - m_e \\ &= (B(A, Z+1) - B(A, Z)) + (m_n - m_p - m_e) \end{aligned} \tag{2.46}$$

while that in β^+-decay is

$$\begin{aligned} Q_{\beta^+} &= m(A, Z) - m(A, Z-1) - m_e \\ &= (B(A, Z-1) - B(A, Z)) - (m_n - m_p - m_e) \; . \end{aligned} \tag{2.47}$$

The energy release in electron capture is larger than that in β^+-decay

$$Q_{ec} = Q_{\beta^+} + 2m_e \tag{2.48}$$

so electron capture is the only decay mode available for neighboring nuclei separated by less than m_e in mass.

The energy released in β-decay can be estimated from the semi-empirical mass formula. For moderately heavy nuclei we can ignore the Coulomb term and the estimate is

$$Q_\beta \sim \frac{8a_a}{A}|Z - A/2| \sim \frac{100\,\text{MeV}}{A} \ . \tag{2.49}$$

For nuclei that can decay by both electron capture and β^+-decay, the ratio between the two rates is given by

$$\frac{\lambda_{\mathrm{ec}}}{\lambda_{\beta^+}} \sim (Z\alpha)^3 \frac{Q_{\mathrm{ec}}^2 (m_{\mathrm{e}}c^2)^3}{(Q_{\mathrm{ec}} - 2m_{\mathrm{e}}c^2)^5} \qquad Q_{\mathrm{ec}} > 2m_{\mathrm{e}}c^2 \, . \tag{2.52}$$

Beta decay from the LD formula

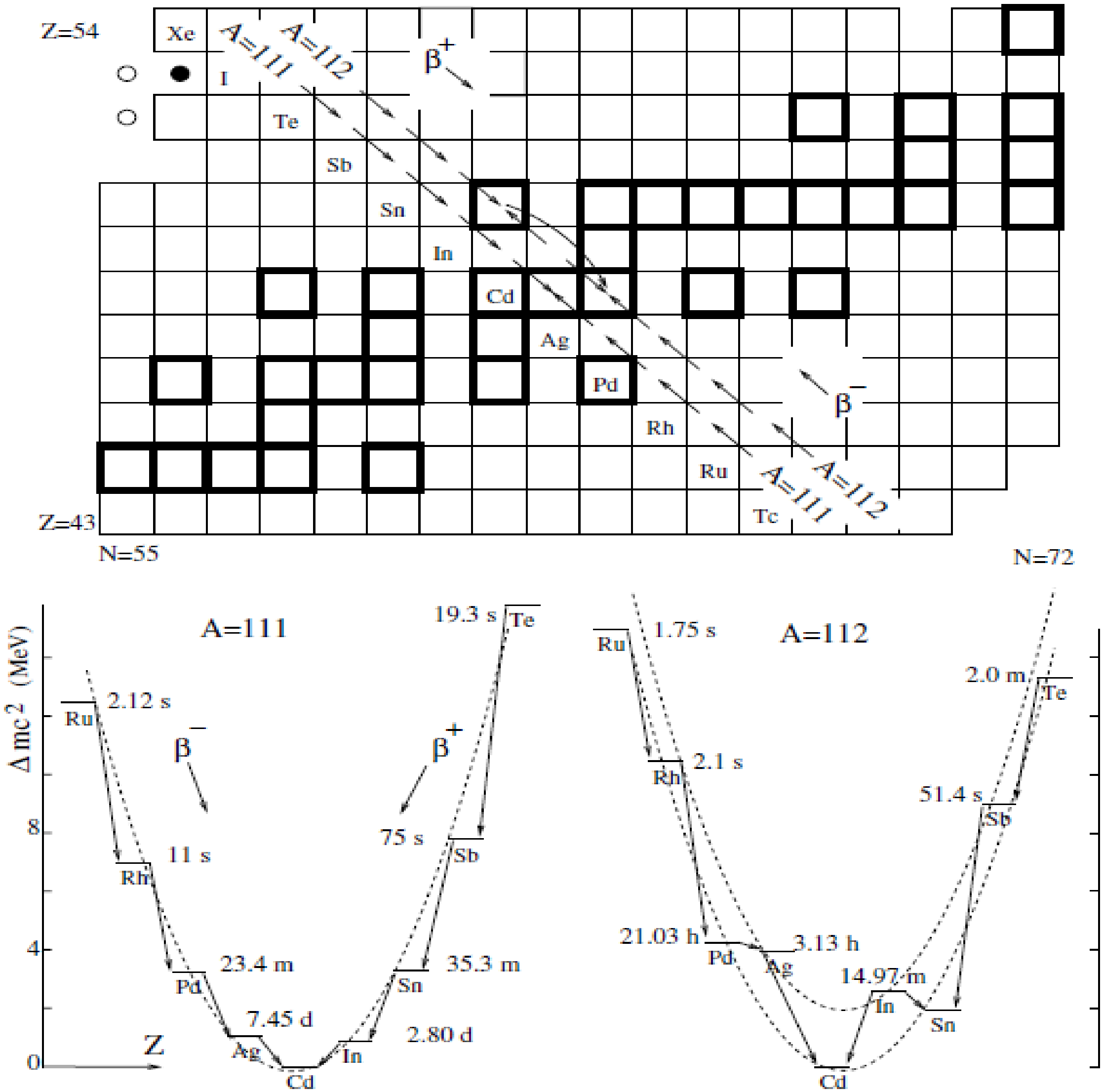

Fig. 2.6. The systematics of β-instability. The top panel shows a zoom of Fig. 2.1 with the β-stable nuclei shown with the heavy outlines. Nuclei with an excess of neutrons (below the β-stable nuclei) decay by β^- emission. Nuclei with an excess of protons (above the β-stable nuclei) decay by β^+ emission or electron capture. The bottom panel shows the atomic masses as a function of Z for $A = 111$ and $A = 112$. The quantity plotted is the difference between $m(Z)$ and the mass of the lightest isobar. The dashed lines show the predictions of the mass formula (2.13) after being offset so as to pass through the lowest mass isobars. Note that for even-A, there can be two β-stable isobars, e.g. ^{112}Sn and ^{112}Cd. The former decays by 2β-decay to the latter. The intermediate nucleus ^{112}In can decay to both.

Note that for even A one has two parabolas shifted by the value of pairing term.

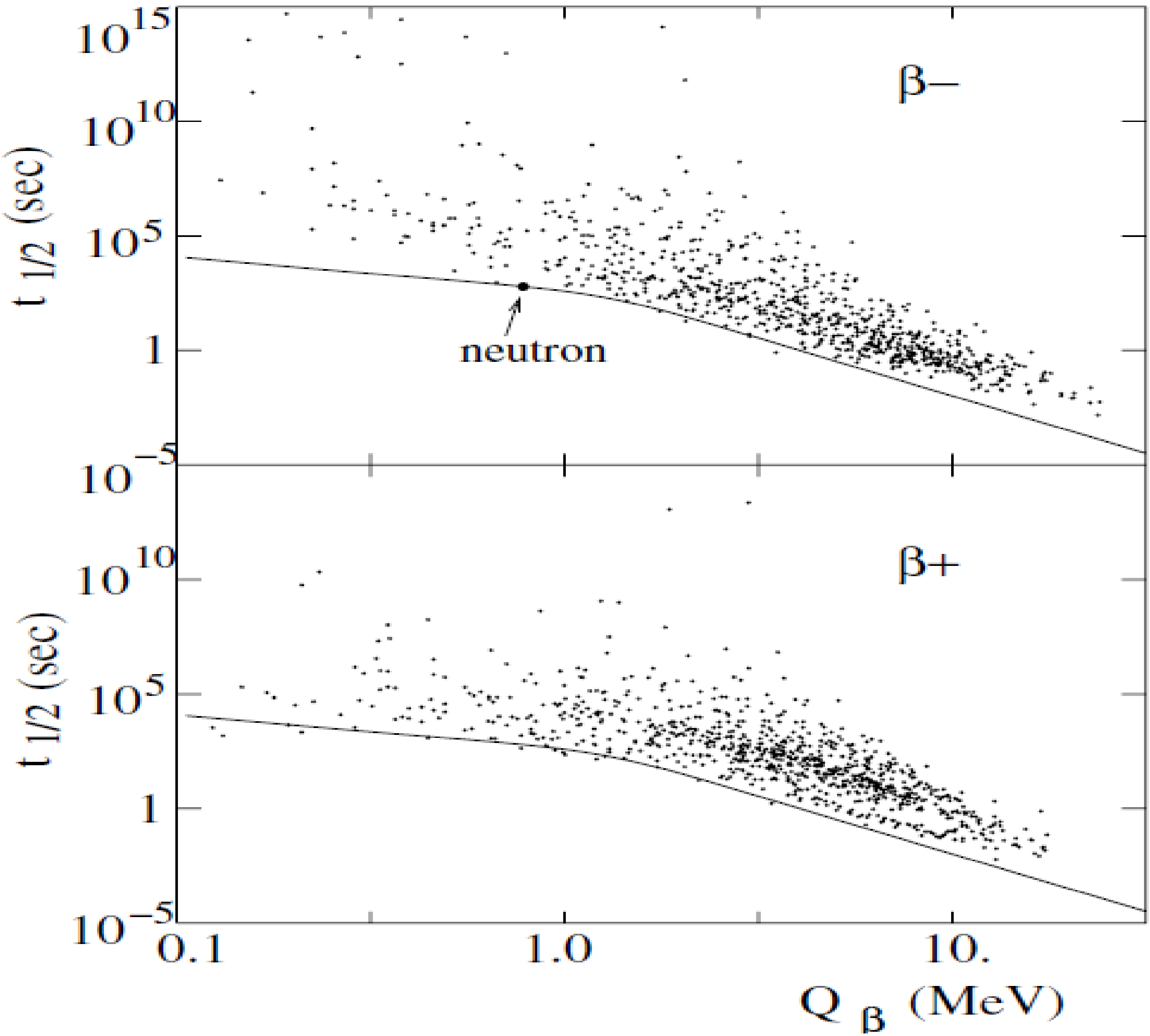

Fig. 2.13. The half-lives of β^- (top) and β^+ (bottom) emitters as a function of Q_β. The line corresponds to the maximum allowable β decay rate which, for $Q_\beta \gg m_e c^2$ is given by $t_{1/2}^{-1} \sim G_F^2 Q_\beta^2$. The complete Q_β dependence will be calculated in Chap. 4. For $Q_\beta < 1\,\mathrm{MeV}$, the lifetimes of β^+ emitters are shorter than those for β^- emitters because of the contribution of electron-capture.

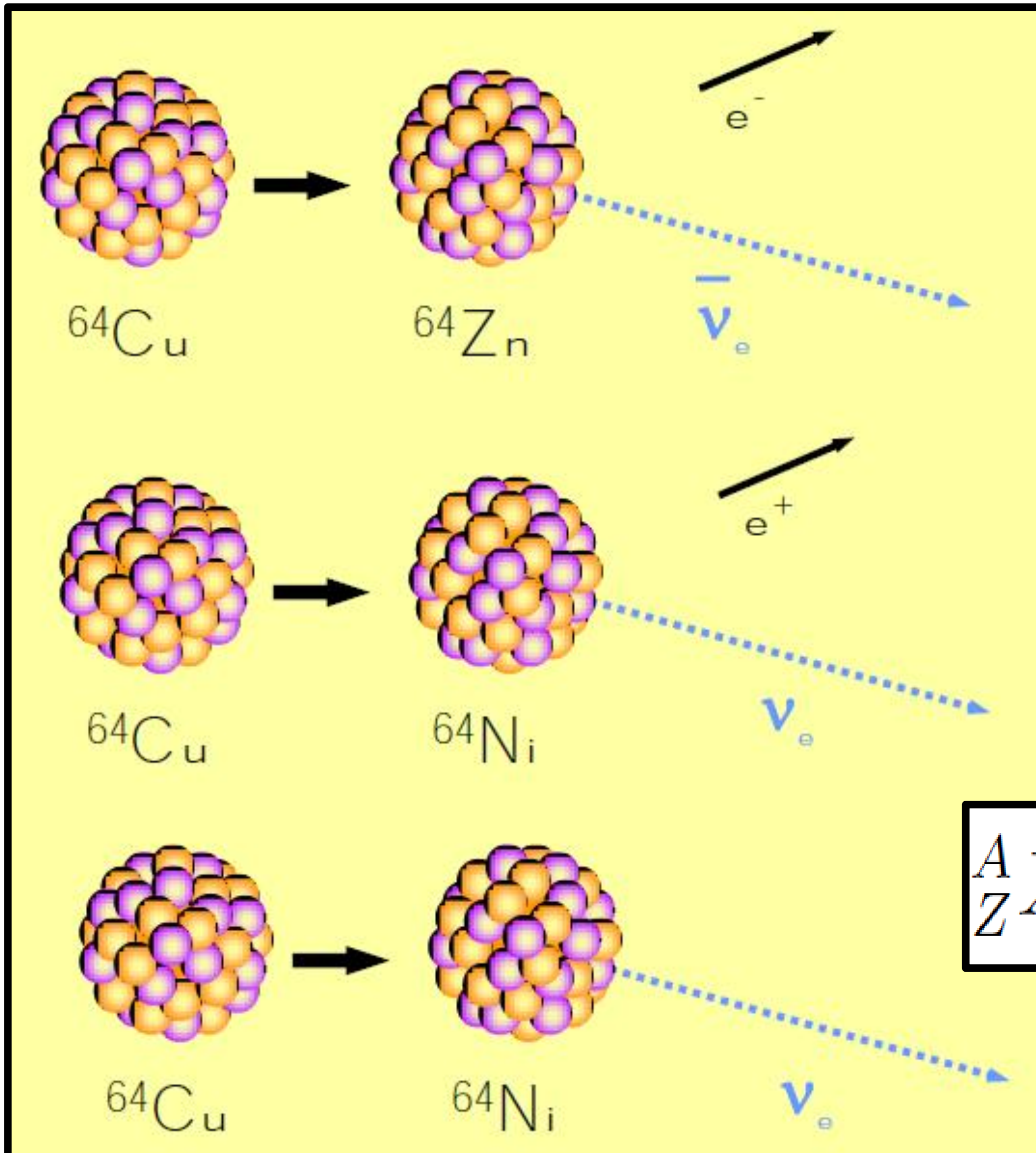

$$\boxed{{}^{A}_{Z}X \rightarrow {}_{Z+1}{}^{A}Y + e^{-} + \tilde{\nu}_e}$$

$$\boxed{{}^{A}_{Z}X \rightarrow {}_{Z-1}{}^{A}Y + e^{+} + \nu_e}$$

$$\boxed{{}^{A}_{Z}X + e^{-}_{\text{pow.at.}} \rightarrow {}_{Z-1}{}^{A}Y + \nu_e}$$

These reactions are governed by weak interaction

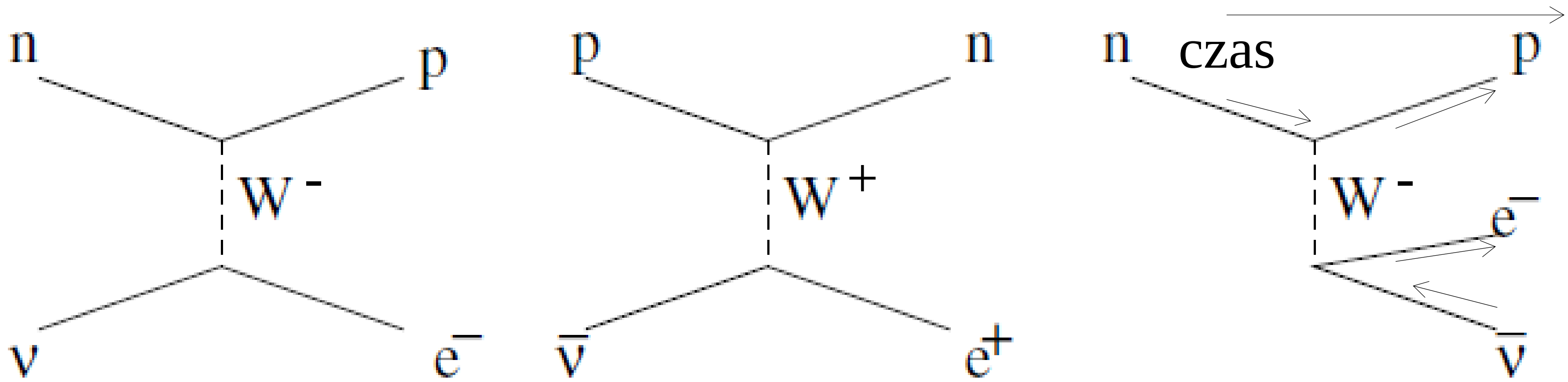

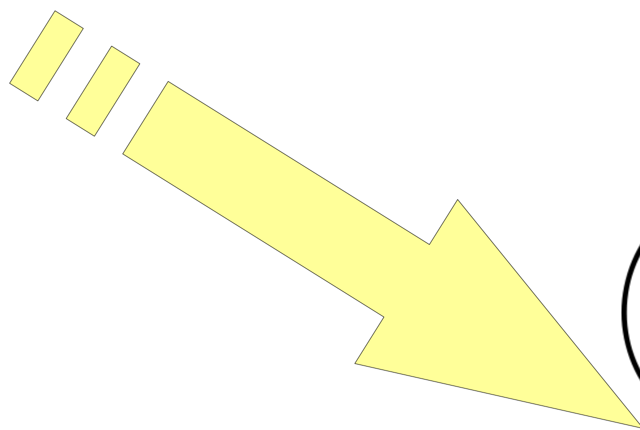

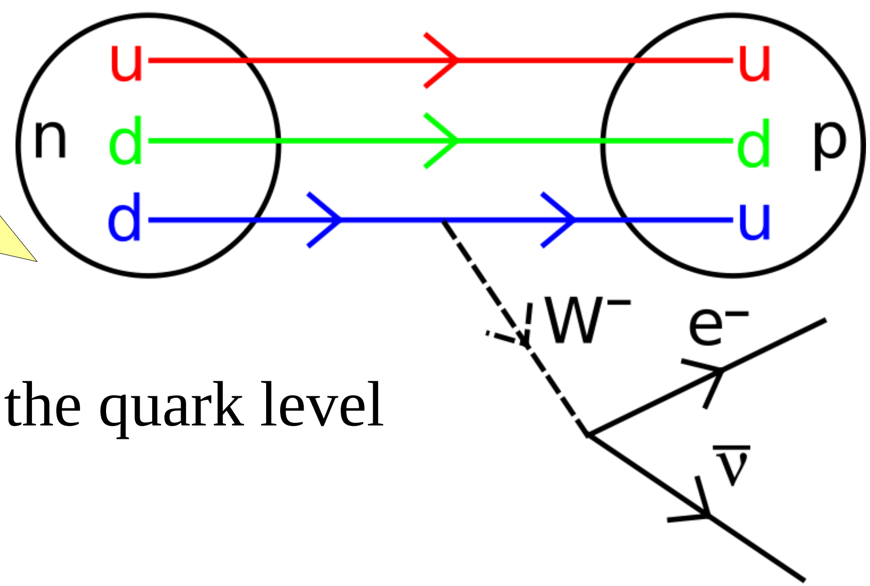

Beta decay on the quark level

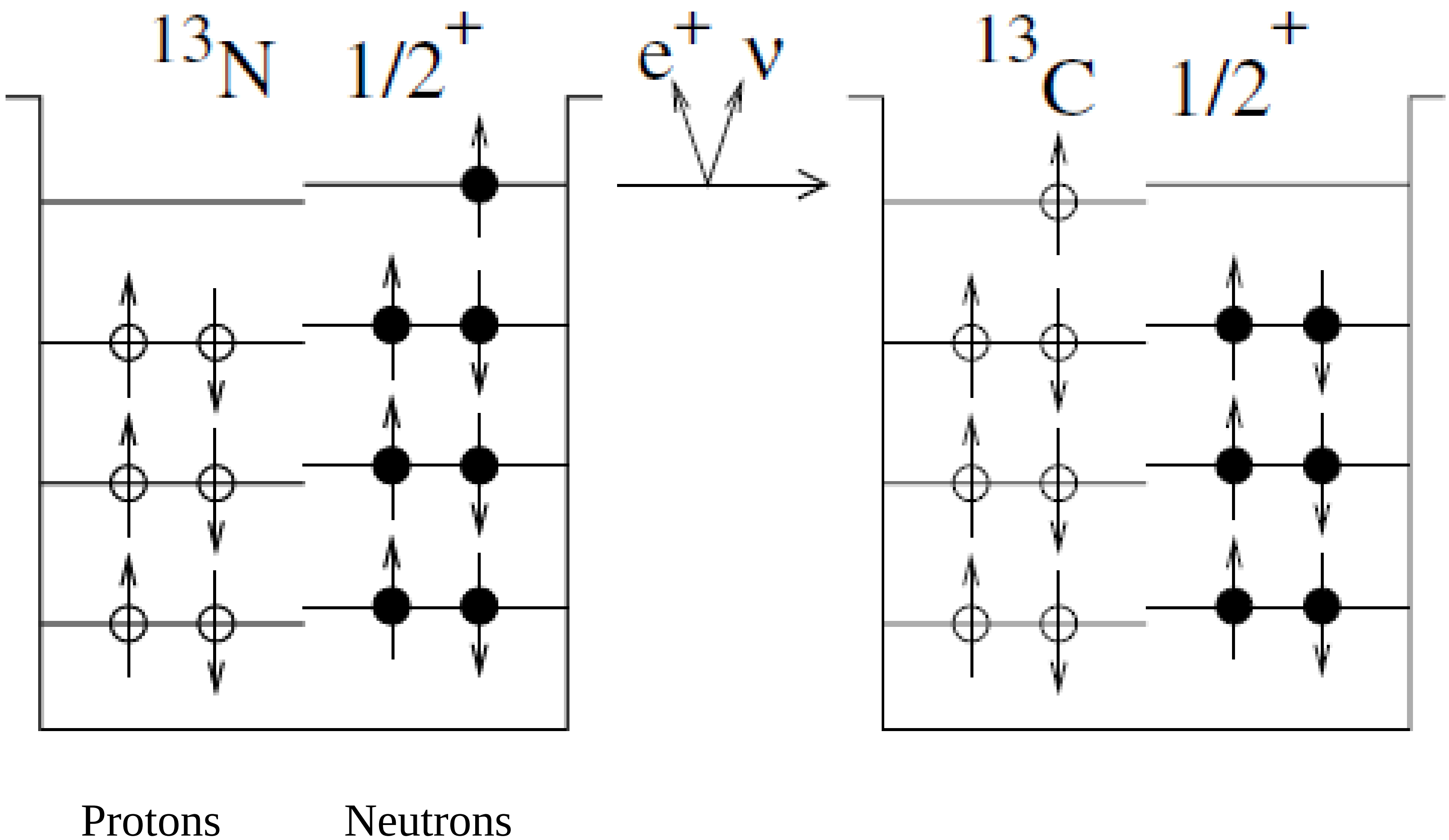

13N 1/2+
e+ ν
13C 1/2+
Protons
Neutrons

Beta decay usually leads to excited nuclear configuration

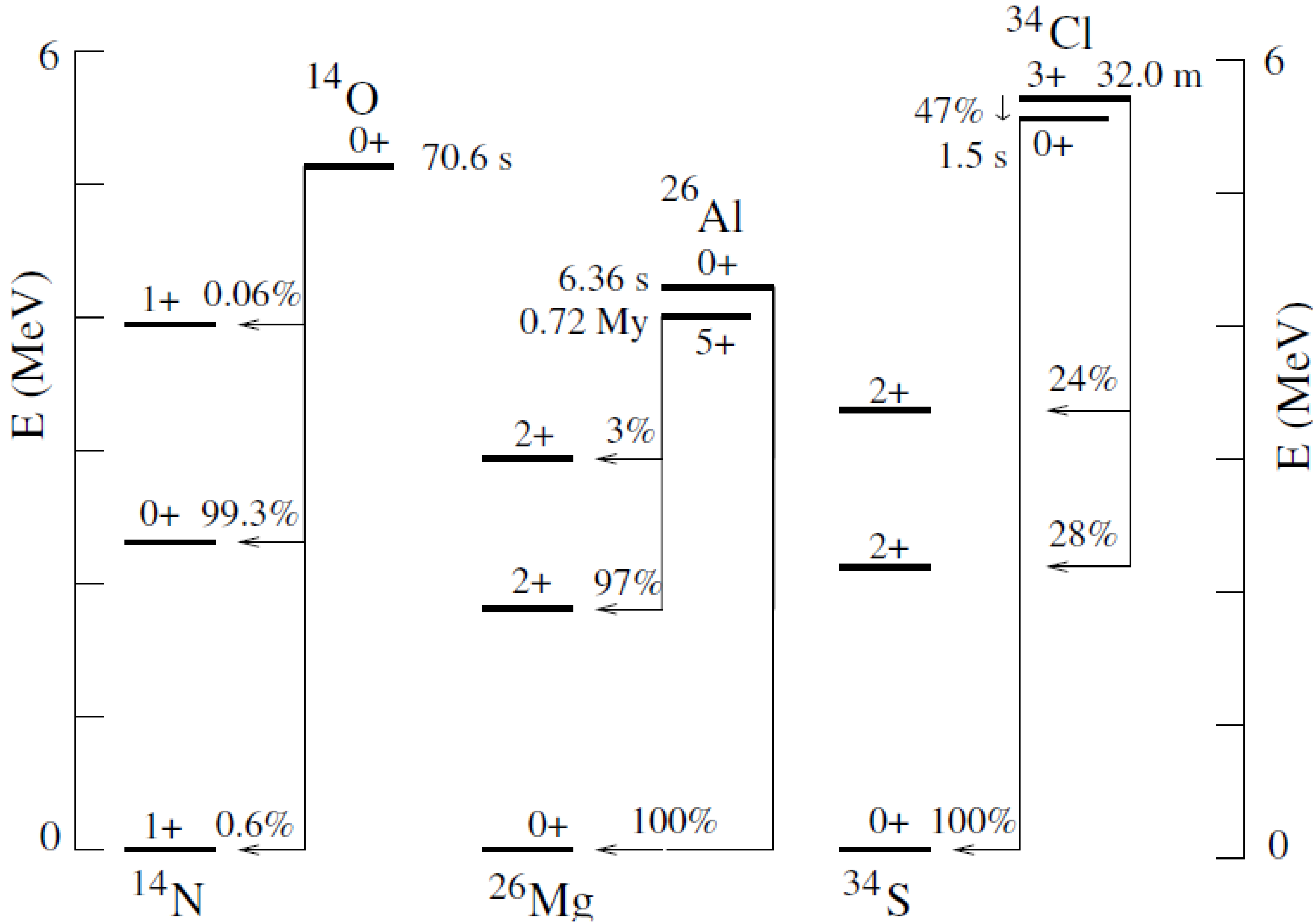

Parity nonconservation in beta decay

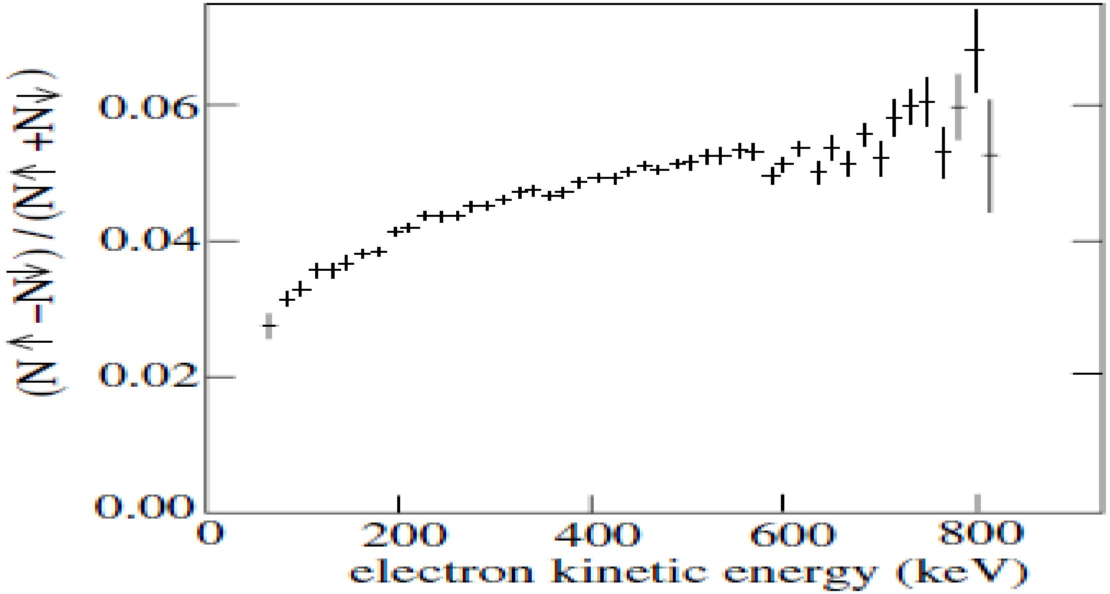

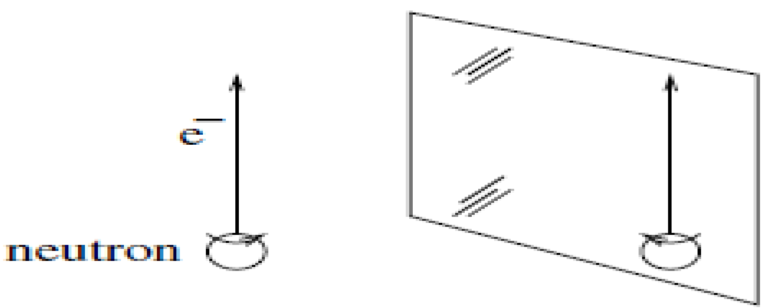

Fig. 4.10. The neutron β decay asymmetry for polarized neutrons. About 5% more neutrons are emitted in the direction of the neutron spin than opposite the direction of the neutron spin. This indicates that parity is violated in β-decay. This is demonstrated in the bottom figure where a spinning neutron decays with the electron emitted in the direction of the neutron (spin) angular momentum. Viewed in the mirror, the spin is reversed but the direction of the electron is not. The excess of electrons emitted in the direction of the neutron spin becomes, viewed in the mirror, an excess of electrons emitted opposite the direction of the neutron spin. What is viewed in the mirror does not correspond to the real world, indicating that physics in the real world does not respect parity symmetry.

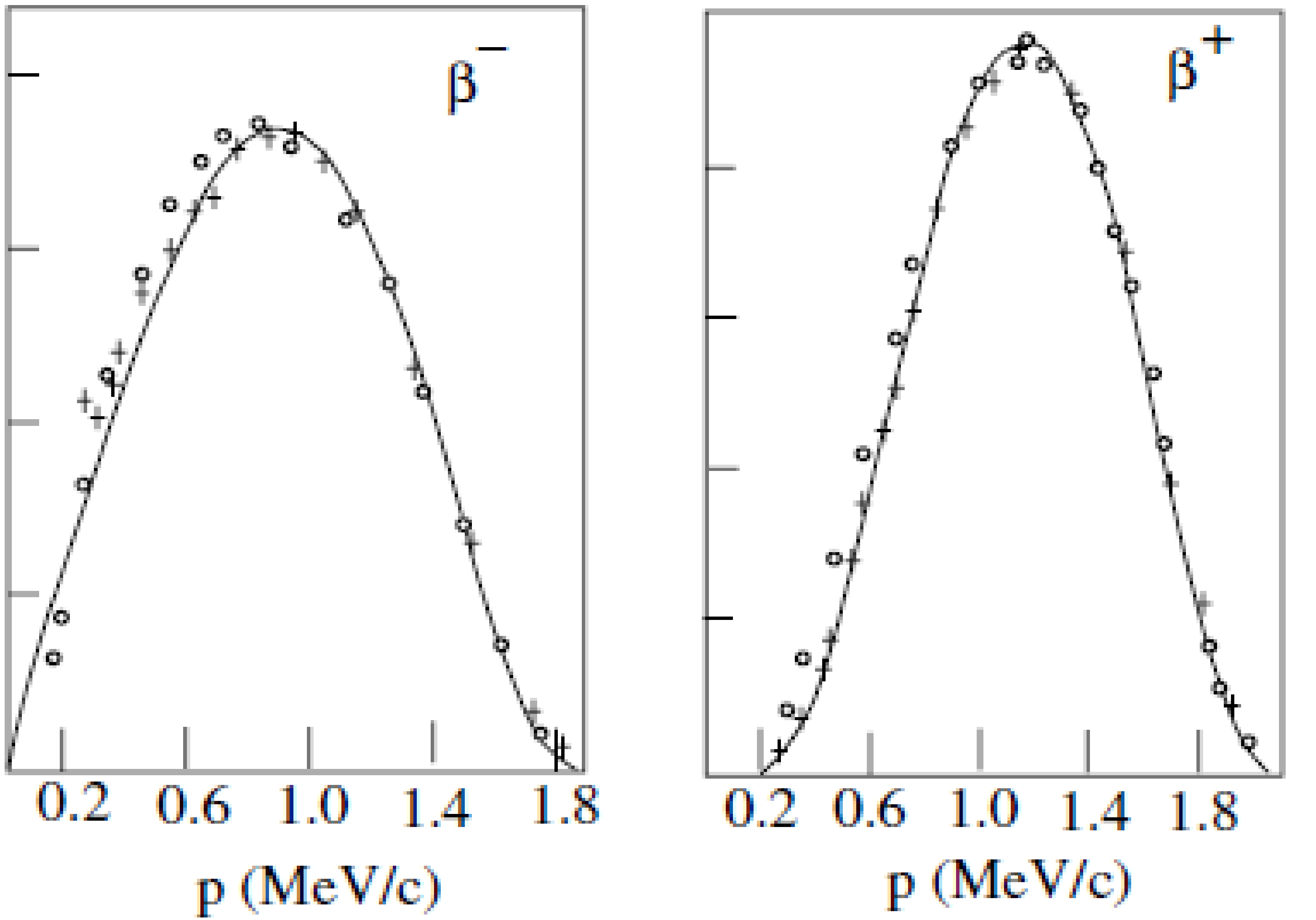

Fig. 4.14. The β^- and β^+ spectra of ^{64}Cu [44]. The suppression the of the β^+ spectrum and enhancement of the β^- at low energy due to the Coulomb effect is seen.

Neutrino detection

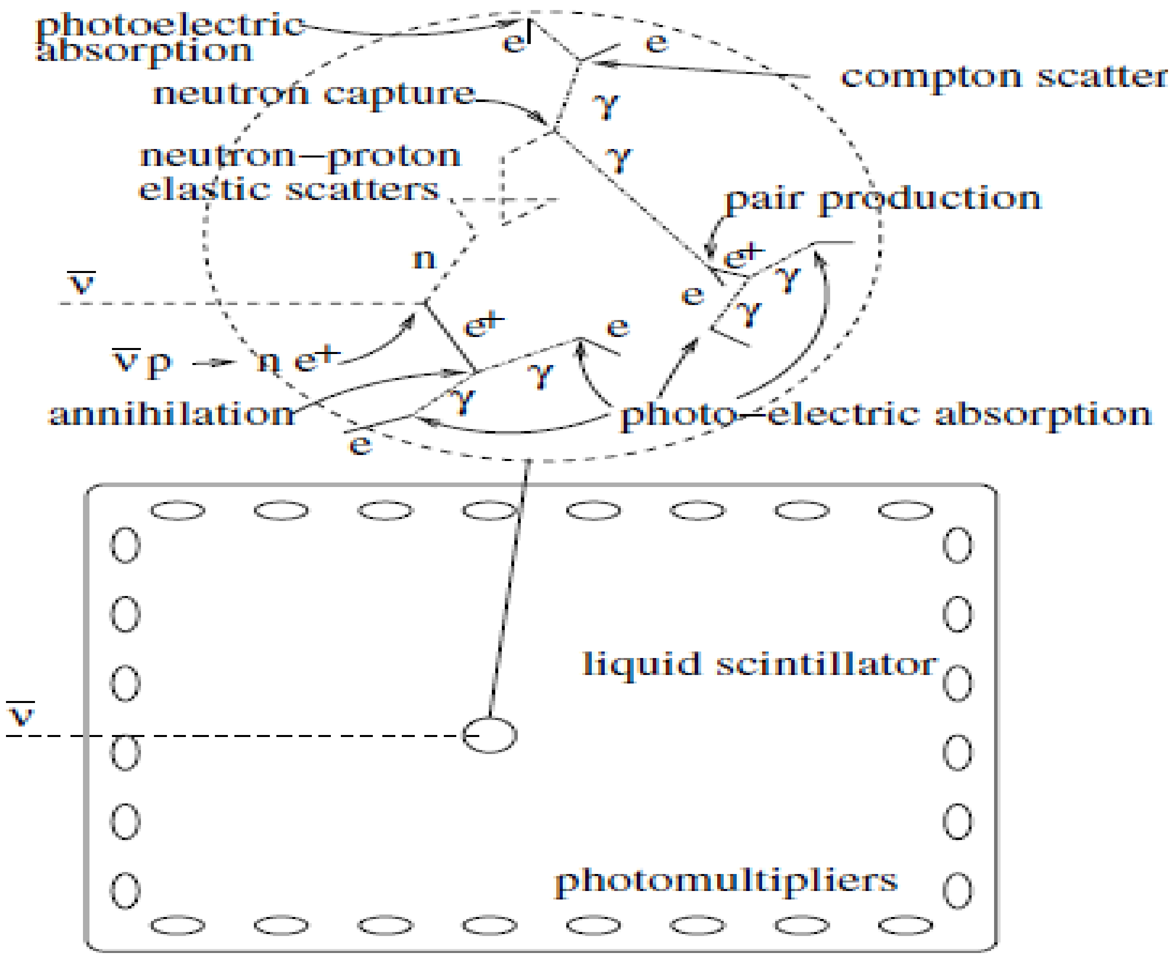

Fig. 4.20. A schematic of the standard method of detecting $\bar{\nu}_e$ through the reaction $\bar{\nu}_e$ p → e^+ n. The detector consists of liquid scintillator instrumented with photomultipliers. The $\bar{\nu}_e$ scatters on a proton contained in the scintillator, an organic compound. The positron stops through ionization loss (Sect. 5.3) and then annihilates, $e^+e^- \rightarrow \gamma\gamma$. The neutron thermalizes though elastic scatters on protons and is eventually captured on a nucleus, $n(A, Z) \rightarrow \gamma\gamma(A + 1, Z)$. The photons produced in the capture and in the annihilation either convert to e^+e^- pairs or lose energy through Compton scattering, eventually being absorbed photoelectrically. Scintillation light is produced by the electrons and positrons slowing down in the scintillator. The scintillation light is detected by the photomultipliers. The light comes in two flashes, the first from the positron produced in the original interaction, and the second from the Compton and photo-electrons after the thermalization and capture of the neutron.

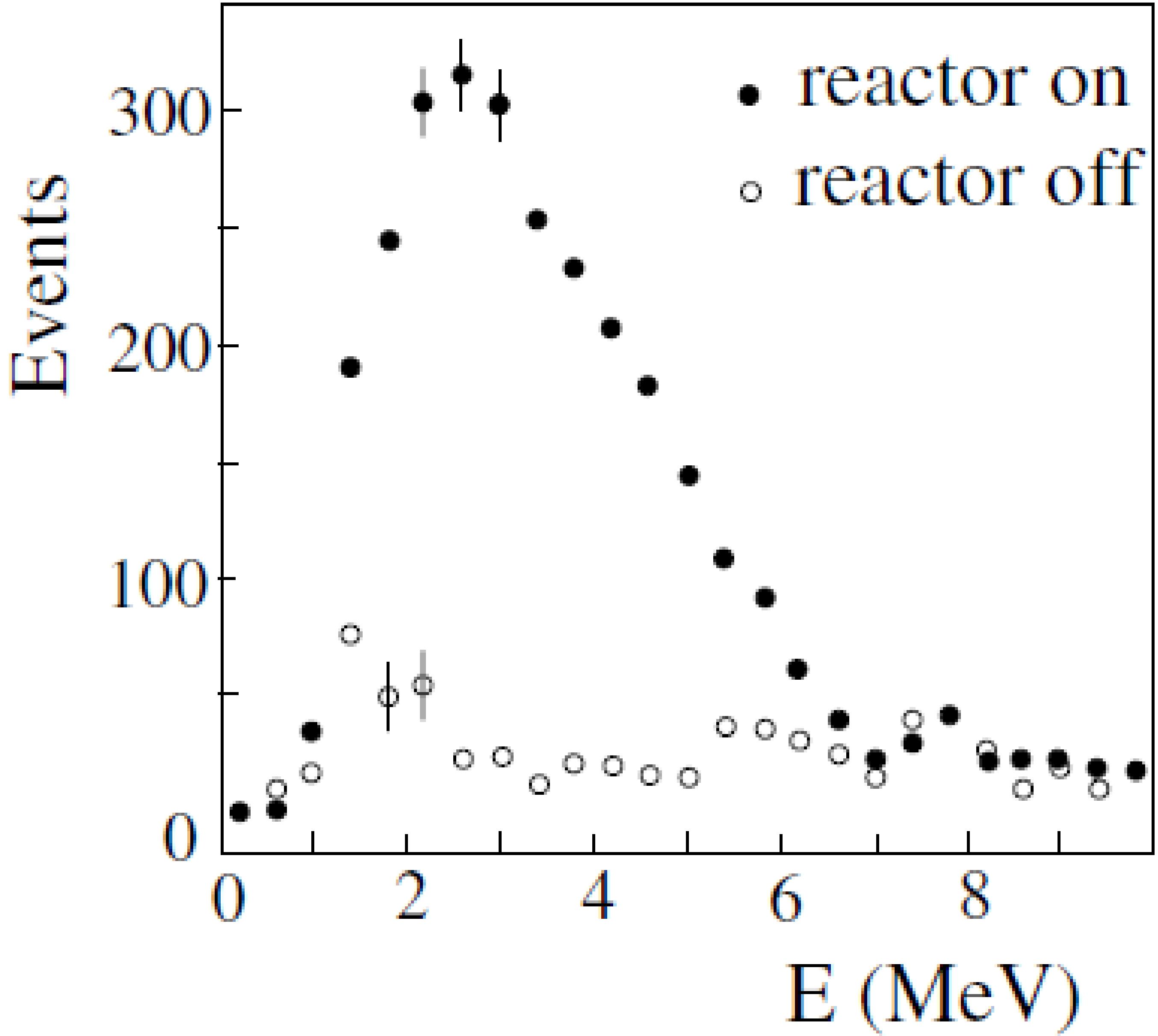

Fig. 4.21. Spectrum of positrons created by the reaction $\bar{\nu}_e\,p \rightarrow n\,e^+$ as observed by the Chooz neutrino experiment [47].

$$\boxed{{}^{A}_{Z}X \rightarrow {}^{A-4}_{Z-2}Y + {}^{4}_{2}\alpha\left({}^{4}_{2}He\right)}$$

2.6 α-instability

Because nuclear binding energies are maximized for $A \sim 60$, heavy nuclei that are β-stable (or unstable) can generally split into more strongly bound lighter nuclei. Such decays are called "spontaneous fission." The most common form of fission is α-decay:

$$(A, Z) \rightarrow (A-4, Z-2) + {}^4\mathrm{He} \quad , \tag{2.53}$$

for example

- ${}^{232}\mathrm{Th}_{90} \rightarrow {}^{228}\mathrm{Ra}_{88}\ \alpha + 4.08\mathrm{MeV} \quad ; \quad t_{1/2} = 1.4\ 10^{10}\,\mathrm{yr}$
- ${}^{224}\mathrm{Th}_{90} \rightarrow {}^{220}\mathrm{Ra}_{88}\ \alpha + 7.31\mathrm{MeV} \quad ; \quad t_{1/2} = 1.05\,\mathrm{s}$
- ${}^{142}\mathrm{Ce}_{58} \rightarrow {}^{138}\mathrm{Ba}_{56}\ \alpha + 1.45\mathrm{MeV} \quad ; \quad t_{1/2} \sim 5.10^{15}\,\mathrm{yr}$
- ${}^{212}\mathrm{Po}_{84} \rightarrow {}^{208}\mathrm{Pb}_{82}\ \alpha + 8.95\mathrm{MeV} \quad ; \quad t_{1/2} = 3.10^{-7}\mathrm{s}$

Figure 2.14 shows the energy release, Q_α in α-decay for β-stable nuclei. We see that most nuclei with $A > 140$ are potential α-emitters. However, naturally occurring nuclides with α-half-lives short enough to be observed have either $A > 208$ or $A \sim 145$ with ${}^{142}\mathrm{Ce}$ being lightest.

The most remarkable characteristic of α-decay is that the decay rate is an exponentially increasing function of Q_α. This important fact is spectacularly demonstrated by comparing the lifetimes of various uranium isotopes:

- ${}^{238}\mathrm{U} \rightarrow {}^{234}\mathrm{Th}\ \alpha + 4.19\,\mathrm{MeV} \quad ; \quad t_{1/2} = 1.4 \times 10^{17}\,\mathrm{s}$
- ${}^{236}\mathrm{U} \rightarrow {}^{232}\mathrm{Th}\ \alpha + 4.45\,\mathrm{MeV} \quad ; \quad t_{1/2} = 7.3 \times 10^{14}\,\mathrm{s}$
- ${}^{234}\mathrm{U} \rightarrow {}^{230}\mathrm{Th}\ \alpha + 4.70\,\mathrm{MeV} \quad ; \quad t_{1/2} = 7.8 \times 10^{12}\,\mathrm{s}$
- ${}^{232}\mathrm{U} \rightarrow {}^{228}\mathrm{Th}\ \alpha + 5.21\,\mathrm{MeV} \quad ; \quad t_{1/2} = 2.3 \times 10^{9}\,\mathrm{s}$
- ${}^{230}\mathrm{U} \rightarrow {}^{226}\mathrm{Th}\ \alpha + 5.60\,\mathrm{MeV} \quad ; \quad t_{1/2} = 1.8 \times 10^{6}\,\mathrm{s}$
- ${}^{228}\mathrm{U} \rightarrow {}^{224}\mathrm{Th}\ \alpha + 6.59\,\mathrm{MeV} \quad ; \quad t_{1/2} = 5.6 \times 10^{2}\,\mathrm{s}$

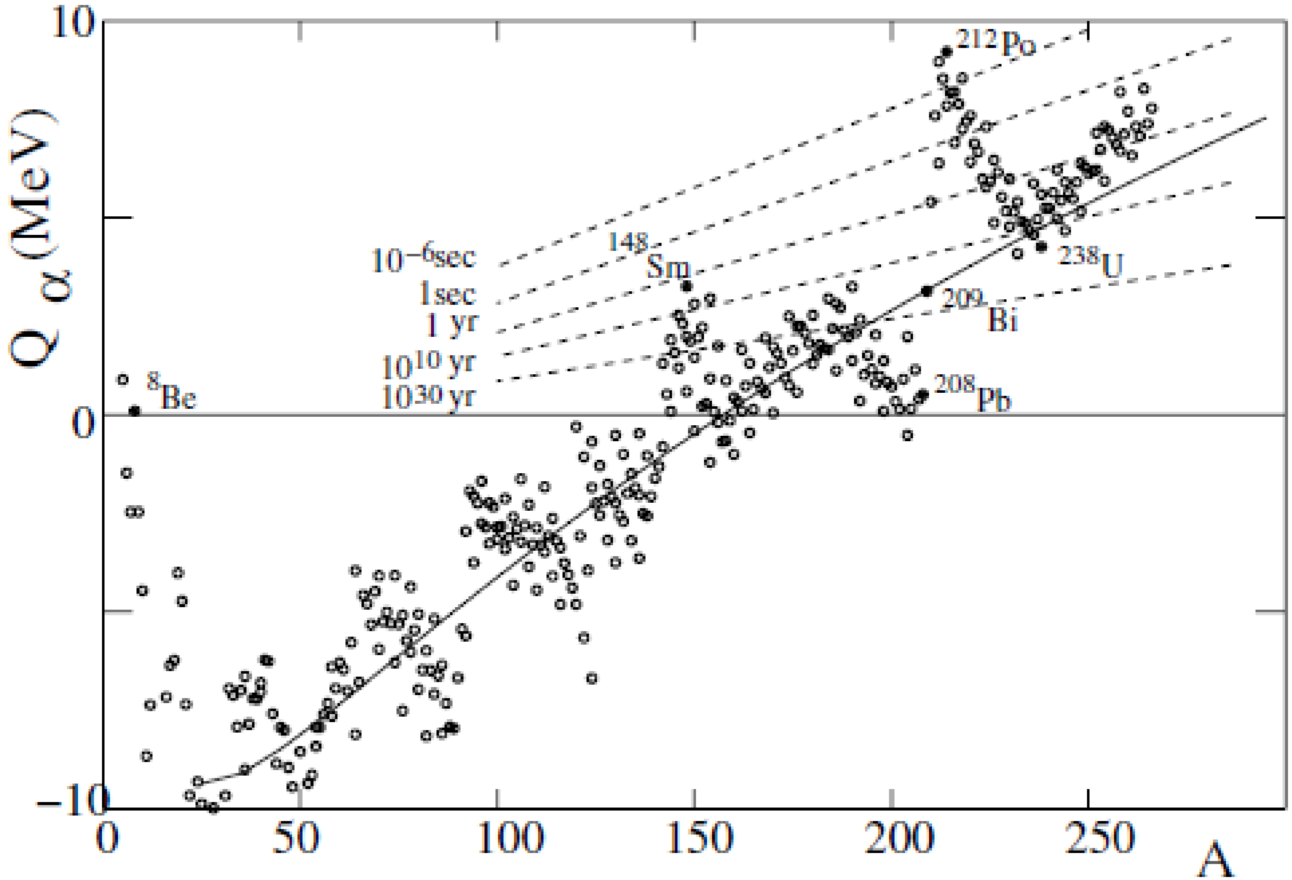

Fig. 2.14. Q_α vs. A for β-stable nuclei. The solid line shows the prediction of the semi-empirical mass formula. Because of the shell structure, nuclei just heavier than the doubly magic ^{208}Pb have large values of Q_α while nuclei just lighter have small values of Q_α. The dashed lines show half-lives calculated according to the Gamow formula (2.61). Most nuclei with $A > 140$ are potential α-emitters, though, because of the strong dependence of the lifetime on Q_α, the only nuclei with lifetimes short enough to be observed are those with $A > 209$ or $A \sim 148$, as well as the light nuclei ^{8}Be, ^{5}Li, and ^{5}He.

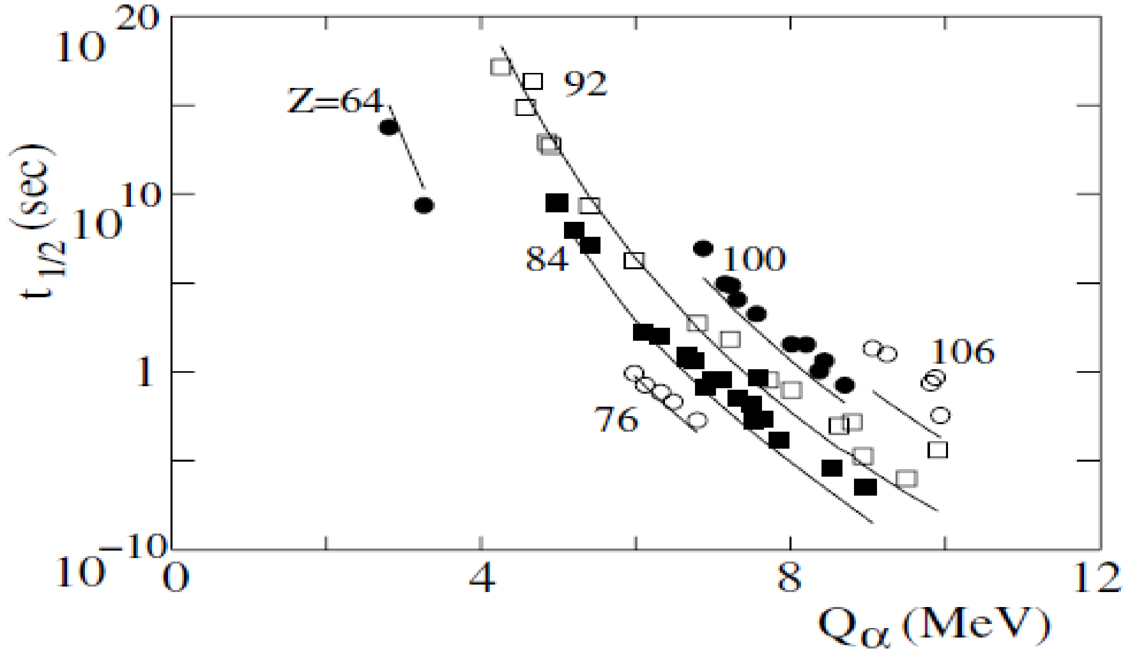

Fig. 2.15. The half-lives vs. Q_α for selected nuclei. The half-lives vary by 23 orders of magnitude while Q_α varies by only a factor of two. The lines shown the prediction of the Gamow formula (2.61).

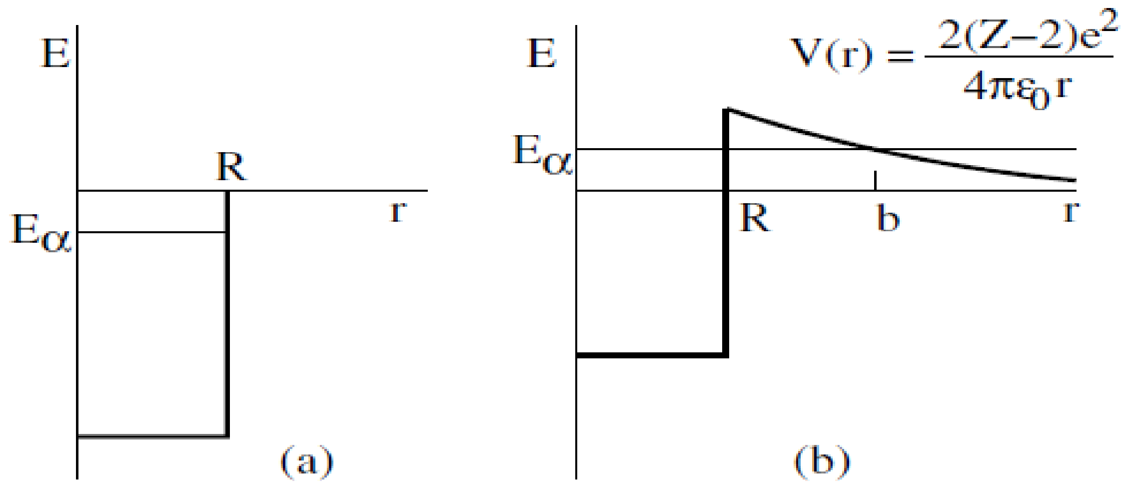

Fig. 2.16. Gamow's model of α-decay in which the nucleus contains a α-particle moving in a mean potential. If the electromagnetic interactions are "turned off", the α-particle is in the state shown on the left. When the electromagnetic interaction is turned on, the energy of the α-particle is raised to a position where it can tunnel out of the nucleus.

$$P \propto \mathrm{cte}\ e^{-2K\Delta}\ , \qquad K = \sqrt{\frac{2m(V - E_\alpha)}{\hbar^2}} \quad . \tag{2.54}$$

To calculate the tunneling probability for the potential of Fig. 2.16b, it is sufficient to replace the potential with a series of piece-wise constant potentials between $r = R$ and $r = b$ and then to sum:

$$P \ \propto \ \mathrm{e}^{-2\gamma} \qquad \gamma \ = \ \int_R^b \sqrt{\frac{2(V(r) - E_\alpha)mc^2}{\hbar^2 c^2}}\mathrm{d}r \tag{2.55}$$

where $V(r)$ is the potential in Fig. 2.16b. The rigorous justification of this formula comes from the WKB approximation studied in Exercise 2.9.

The integral in (2.55) can be simplified by defining the dimensionless variable

$$u \ = \ \frac{E}{V(r)} \ = \ r\,\frac{E}{2(Z-2)\alpha\hbar c}\ . \tag{2.56}$$

We then have

$$\gamma = \frac{2(Z-2)e^2}{4\pi\epsilon_0\hbar}\sqrt{\frac{2m_\alpha}{E}}\int_{u_{\min}}^{1}\sqrt{u^{-1}-1}\,\mathrm{d}u\ . \tag{2.57}$$

For large Z, (2.56) suggests that it is a reasonably good approximation to take $u_{\min}=0$ in which case the integral is $\pi/2$. This gives

$$\gamma = 2\pi(Z-2)\alpha\,\frac{c}{v} \tag{2.58}$$

where $v=\sqrt{2E/m_\alpha}$ is the velocity of the α-particle after leaving the nucleus. For ^{238}U we have $2\gamma \sim 172$ while for ^{228}U we have $2\gamma \sim 136$. We see how the small difference in energy leads to about 16 orders of magnitude difference in tunneling probability and, therefore, in lifetime.

To get a better estimate of the lifetime, we have to take into account the fact that $u_{\min}>0$. This increases the tunneling probability since the barrier width is decreased. It is simple to show (Exercise 2.8) that to good approximation

$$\gamma = \frac{2Z}{\sqrt{(E_\alpha(MeV))}} - \frac{3}{2}\sqrt{ZR(fm)}\quad . \tag{2.59}$$

The dependence of the lifetime of the nuclear radius provided one of the first methods to estimate nuclear radii.

The lifetime can be calculated by supposing that inside the nucleus the α bounces back and forth inside the potential. Each time it hits the barrier it has a probability P to penetrate. The mean lifetime is then just T/P where $T \sim R/v'$ is the oscillation frequency for the α of velocity $v' = \sqrt{2m_\alpha(E_\alpha + V_0)}$. This induces an additional Q_α dependence of the lifetime which is very weak compared to the exponential dependence on Q_α due to the tunneling probability. If we take the logarithm of the lifetime, we can safely ignore this dependence on Q_α, so, to good approximation, we have

$$\ln \tau(Q_\alpha, Z, A) \; = \; 2\gamma + \text{const} \, , \tag{2.60}$$

with γ given by (2.15). Numerically, one finds

$$\log(t_{1/2}/1\,\text{s}) \; \sim \; 2\gamma/\ln 10 + 25 \, , \tag{2.61}$$

which is the formula used for the lifetime contours in Figs. 2.14 and 2.15.

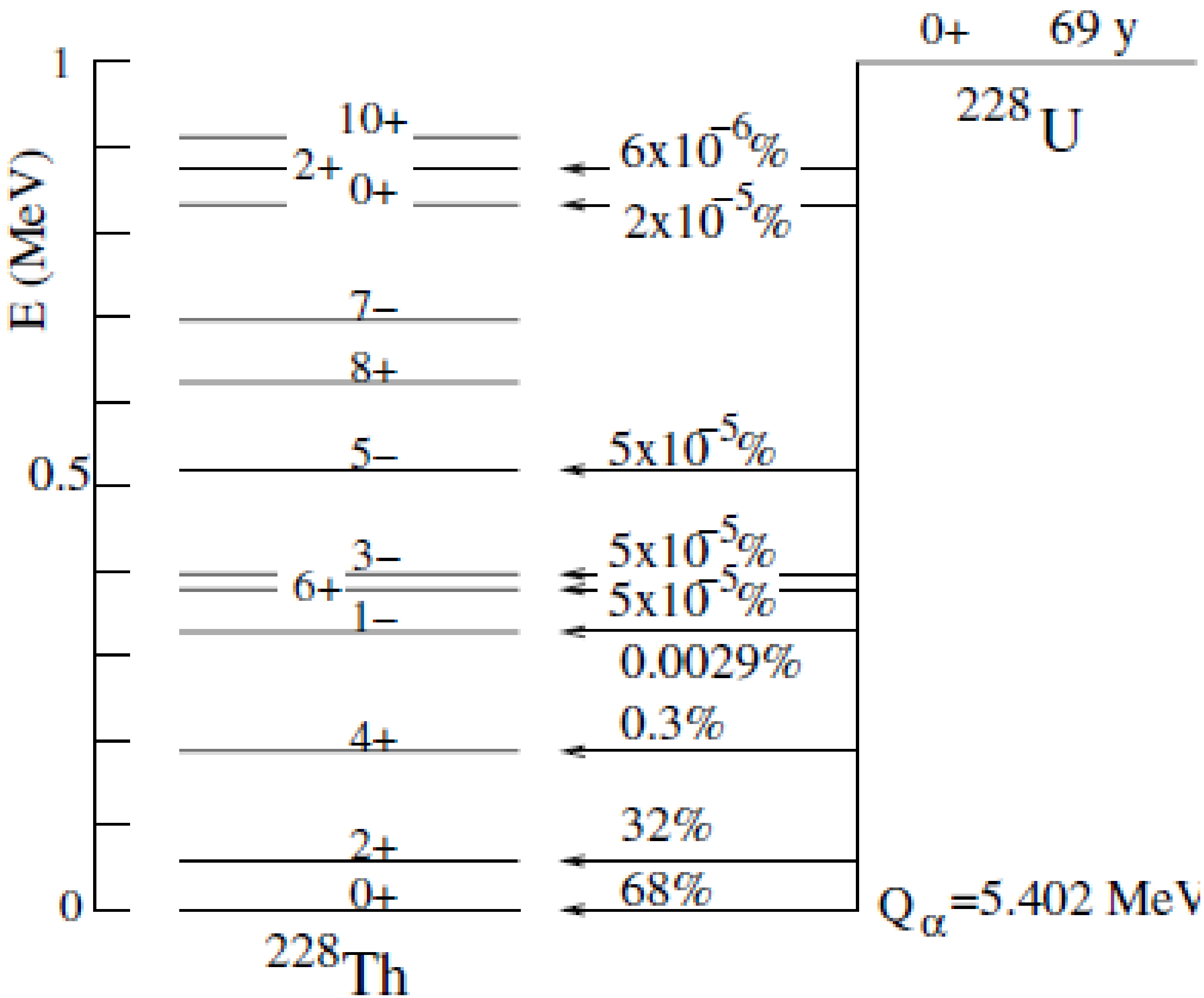

Fig. 2.17. The decay ^{228}U $\rightarrow$ α ^{228}Th showing the branching fractions to the various excited states of ^{228}Th. Because of the strong rate dependence on Q_α, the ground state his highly favored. There is also a slight favoring of spin-parities that are similar to that of the parent nucleus.

Fission

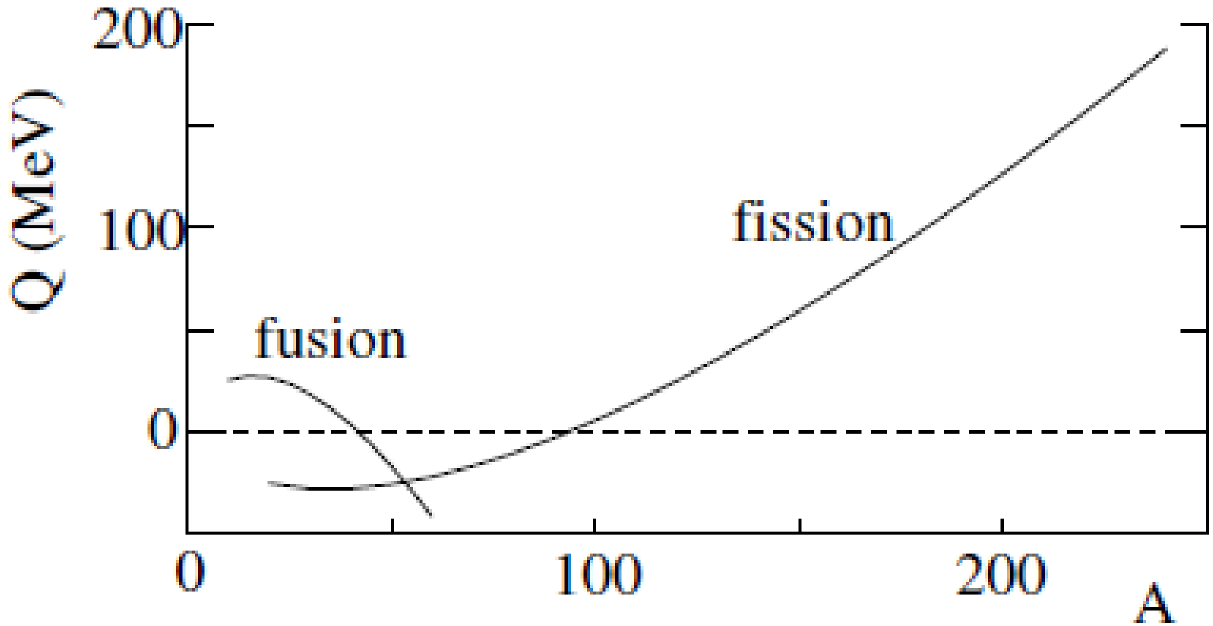

Fig. 6.1. The energy release in fission and self-fusion as predicted by the Bethe–Weizsäcker formula (2.13) for β-stable nuclei. Only nuclei with $40 < A < 95$ are stable against both fission and self-fusion. In this figure, $Q_{\mathrm{fis}}(A,Z)$ is calculated for symmetric fission, $A_1 = A_2 = A/2$ and $Z_1 = Z_2 = Z/2$. $Q_{\mathrm{fus}}(A,Z)$ is calculated for the production of a single nucleus of $A' = 2A$ and $Z' = 2Z$.

$${}^{(A_1+A_2)}_{(Z_1+Z_2)}X \;\rightarrow\; {}^{A_1}_{Z_1}X \;+\; {}^{A_2}_{Z_2}X \;+\; Q_{\mathrm{fis}}$$

-spontaneous fission

$$Q_{\mathrm{fis}} \;=\; m(A_1+A_2, Z_1+Z_2)c^2 - [m(A_1,Z_1) \;+\; m(A_2,Z_2)]c^2$$

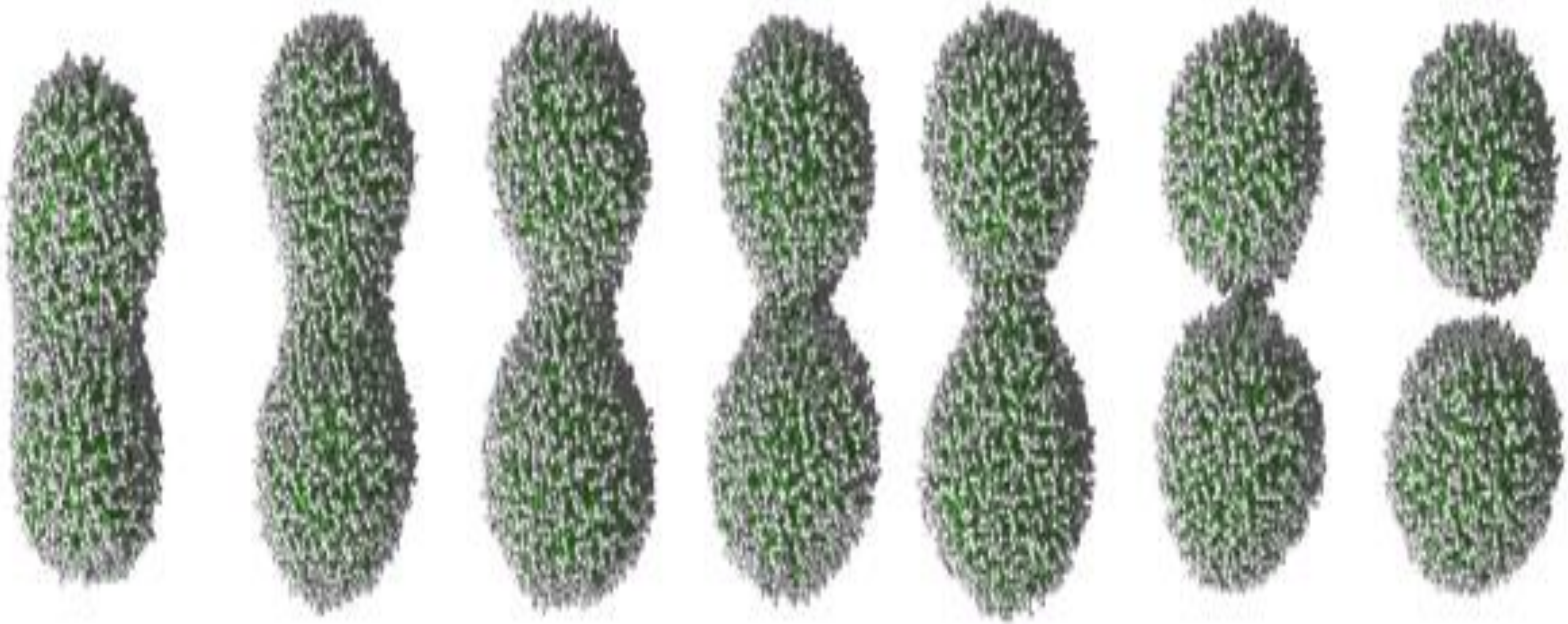

$$^{238}\mathrm{U} \ \rightarrow \ ^{234}\mathrm{Th}\,\alpha \qquad \mathrm{t}_{1/2} \ = \ 4.468 \times 10^{9}\mathrm{yr}\ , \qquad \mathrm{Q}_{\alpha} = 4.262\,\mathrm{MeV}\ ,$$

generates a power of

$$P \ = \ \frac{N_A}{238}\,\frac{Q_\alpha \ln 2}{t_{1/2}} \ = \ 8 \times 10^{-9}\,\mathrm{W\,g}^{-1}\ . \qquad (6.1$$

example

A given nucleus can fission in many ways. For ^{236}U, one possibility is

$$^{236}_{92}\mathrm{U} \rightarrow {}^{137}_{53}\mathrm{I} + {}^{96}_{39}\mathrm{Y} + 3\mathrm{n} \tag{6.8}$$

$$^{137}\mathrm{I} \rightarrow {}^{137}\mathrm{Xe}\,\mathrm{e}^{-}\,\bar{\nu}_{e} \quad t_{1/2} = 24.5\,\mathrm{s}$$

$$^{137}\mathrm{Xe} \rightarrow {}^{137}\mathrm{Cs}\,\mathrm{e}^{-}\,\bar{\nu}_{e} \quad t_{1/2} = 3.818\,\mathrm{m}$$

$$^{137}\mathrm{Cs} \rightarrow {}^{137}\mathrm{Ba}\,\mathrm{e}^{-}\,\bar{\nu}_{e} \quad t_{1/2} = 30.07\,\mathrm{yr}$$

$$^{96}\mathrm{Y} \rightarrow {}^{96}\mathrm{Zr}\,\mathrm{e}^{-}\,\bar{\nu}_{e} \quad t_{1/2} = 5.34\,\mathrm{s}\,,$$

or, globally

$$^{236}_{92}\mathrm{U} \rightarrow {}^{137}_{56}\mathrm{Ba} + {}^{96}_{40}\mathrm{Zr} + 3\mathrm{n} + 4\mathrm{e}^{-} + 4\bar{\nu}_{e}\,. \tag{6.9}$$

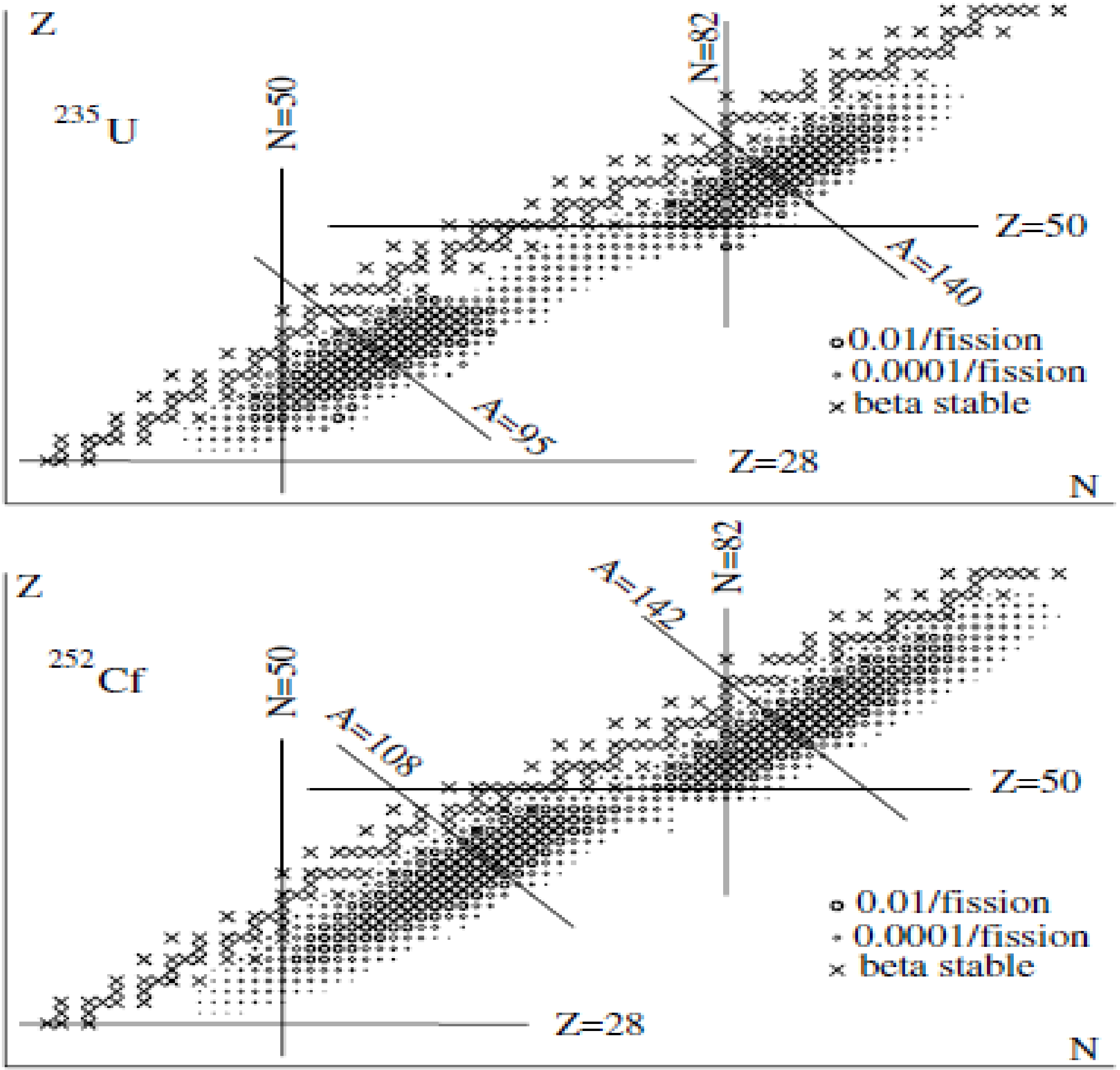

Fig. 6.2. The distribution of fission fragments for neutron induced fission of ^{235}U and for spontaneous fission of ^{252}Cf. The distribution for ^{235}U is dominated by asymmetric fission into a light nucleus ($A \sim 95$) and a heavier nucleus ($A \sim 140$), reasonably near the magic neutron numbers $N = 50$ and $N = 82$. The distribution for ^{252}Cf is broader but still dominated by asymmetric fission. Because of the large neutron excess in nuclei with $A > 230$, almost all fission fragments are below the line of β-stability and therefore decay by β^--emission.

We see that the fission process results in the production of a large variety of particles. They can be classified as

- Two fission fragments that are β^--unstable.
- Other "prompt" particles, mostly neutrons emitted in the fission process and photons emitted by the primary fission fragments produced in highly excited states.
- "Delayed" particles mostly e^-, $\bar{\nu}_e$, and γ emitted in the β^--decays of the primary fission fragments fragments and their daughters.

Most of the released energy is contained in the initial kinetic energies of the two fission fragments. The kinetic energy of each heavy fragment at the time of fragmentation is of the order of 75 MeV, with initial velocities of roughly 10^7 m s^{-1}. Given their large masses, their ranges are very small $\sim 10^{-6}$ m. The stopping process transforms the kinetic energy to thermal energy.

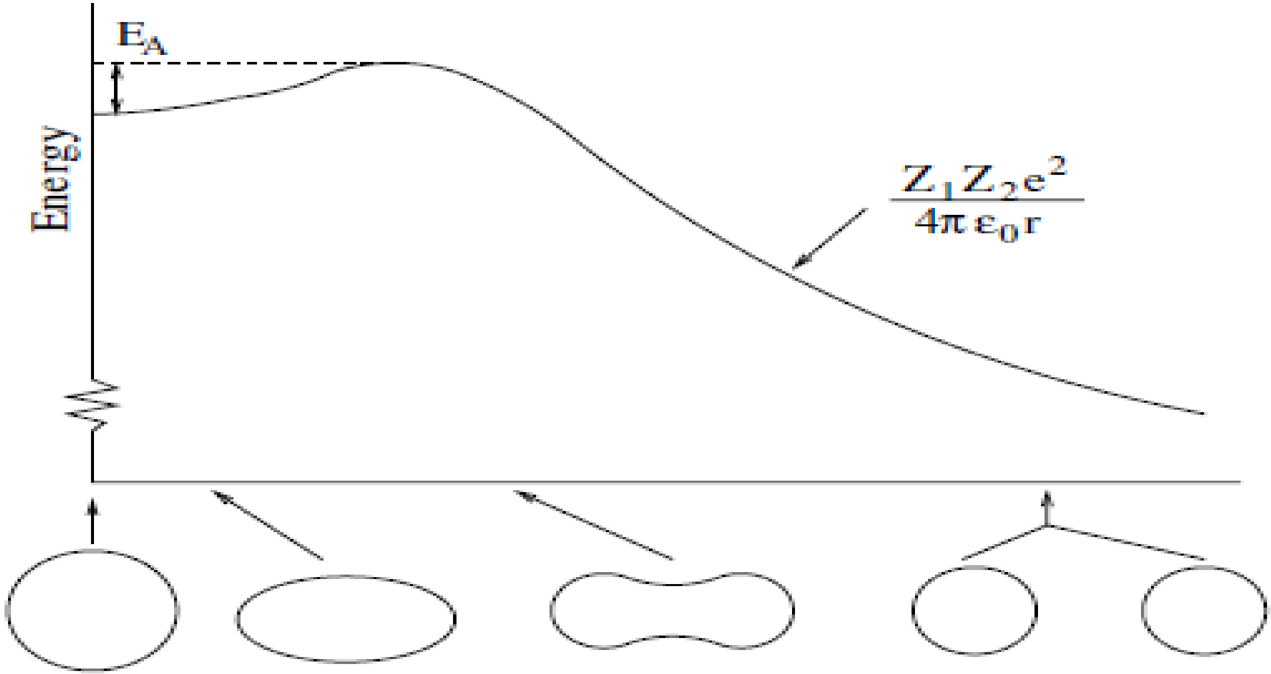

Fig. 6.3. Variation of the energy of a deformed nucleus as a function of the distortion as sketched. For small distortions, the energy increases with increasing distortion because of the increasing surface area. When the two fragments are separated, the energy falls with increasing separation because of the decreasing Coulomb energy. An energy barrier E_A must be crossed for fission to occur.

$$\frac{E_c}{E_s} = \frac{0.7103\,\mathrm{MeV}\ Z^2 A^{-1/3}}{17.804\,\mathrm{MeV}\ A^{2/3}} = \frac{Z^2/A}{25.06} . \tag{6.10}$$

Nuclei with $Z^2/A > 25$ would be expected to have small barriers because the Coulomb energy (decreasing function of separation) dominates the surface energy (increasing function of separation). In fact, by calculating the surface area and Coulomb energies of a nucleus in the shape of an ellipsoid, it can be shown that the surface area varies twice as fast as the Coulomb energy as the nucleus is deformed while keeping the volume constant. This means that we expect fission to be instantaneous for

$$E_c > 2E_s \quad \Rightarrow \frac{Z^2}{A} > 50 . \tag{6.11}$$

Super-heavy nuclei have $Z/A \sim 1/3$ implying $Z > 150$ for instantaneous fusion. This is an absolute upper limit on the size of nuclei.

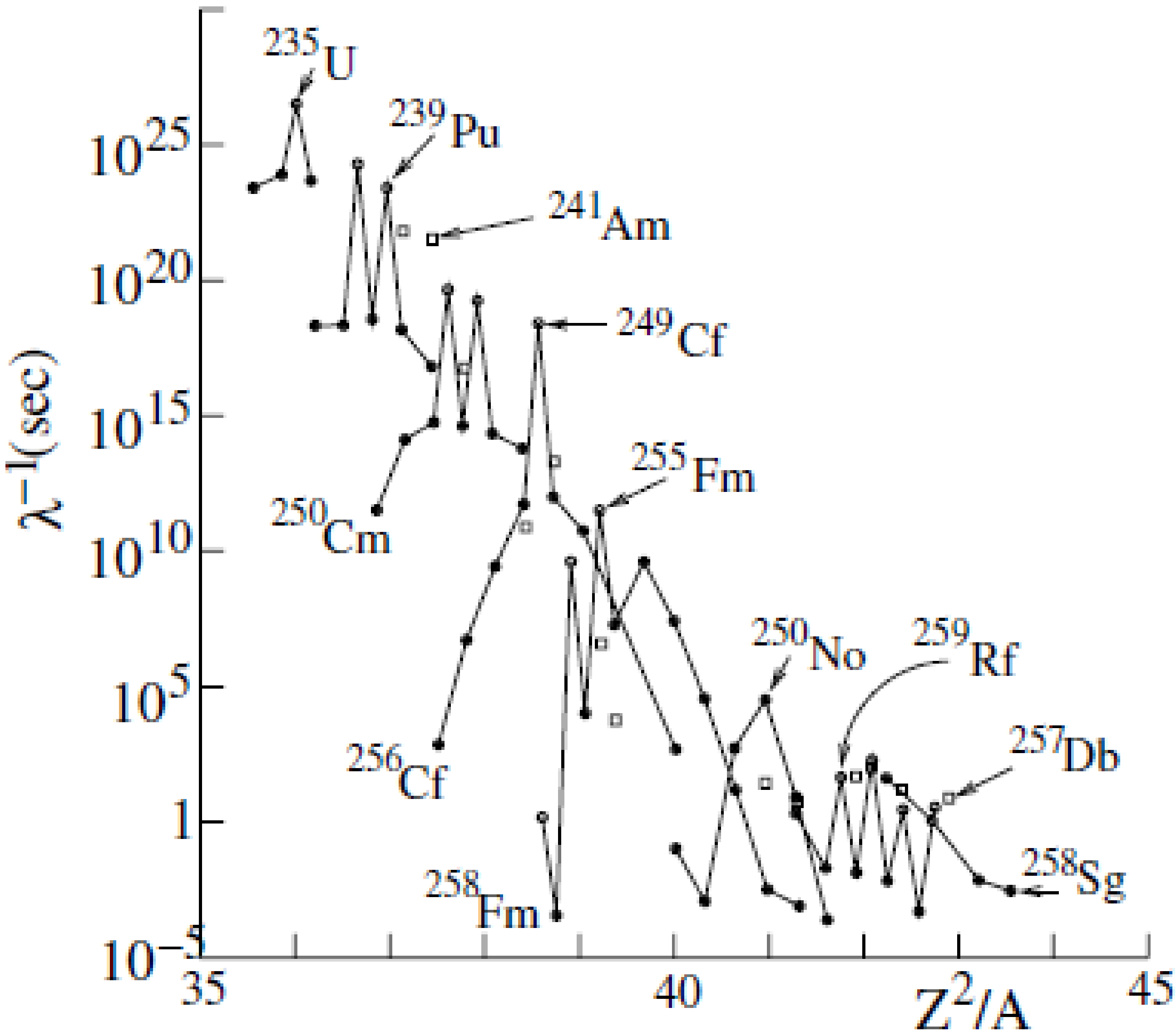

Fig. 6.4. Spontaneous fission lifetimes as a function of the fission parameter Z^2/A for selected nuclei. Circles are for even-Z nuclei, filled circles for even-even nuclei and open circles for even-odd nuclei. Squares are for odd-Z nuclei.

Induced fission

$$\gamma \, {}^{A}_{Z}X \rightarrow {}^{A}_{Z}X^{*} \rightarrow \text{fission}$$

Fission induced by photon (photo-fission)

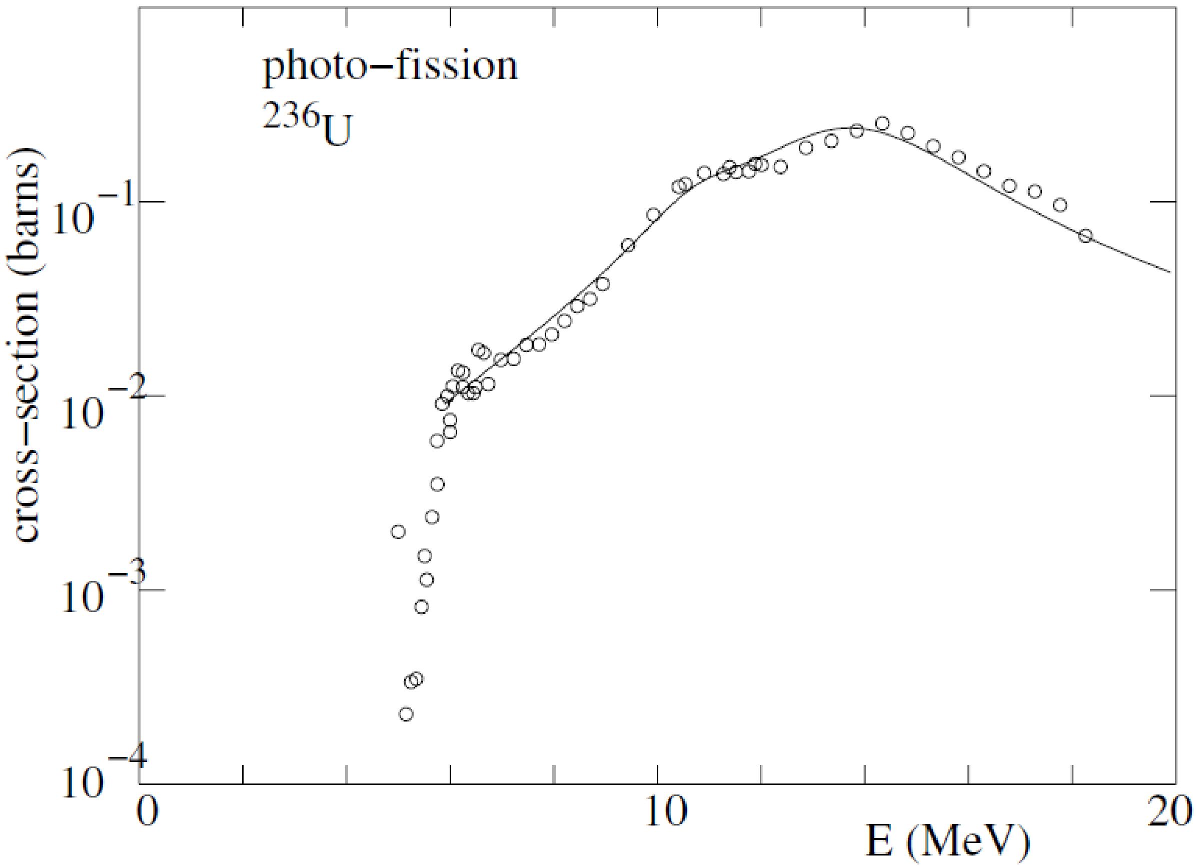

Fig. 6.5. Cross-section for $\gamma\,^{236}\mathrm{U} \rightarrow$ fission [30].

About 5.7MeV has to be added to 236U to increase significantly fission probability.
It is about 1 MeV less than the height of the Coulomb barrier but it is enough to make the tunneling process rapid.

Table 6.1. Fission threshold energy ΔE_S and neutron separation energy S_{n} for selected nuclei (A, Z). ΔE_S gives the effective threshold for photo fission. The effective threshold for neutron-induced fission of the nucleus $(A-1)$ is $T_{\mathrm{n}} = \Delta E_S - S_{\mathrm{n}}$. For the three odd-$(A-1)$ nuclei, $T_{\mathrm{n}} < 0$ so fission can be induced by thermal neutrons.

Fissioning nucleus (A, Z)	ΔE_S (MeV) (A, Z)	S_{n} (MeV) (A,Z)	T_{n}(threshold) (MeV) $(A-1, Z)$	neutron target $(A-1, Z)$
$^{234}_{92}$U	5.4	6.9		$^{233}_{92}$U
$^{236}_{92}$U	5.7	6.3		$^{235}_{92}$U
$^{240}_{94}$Pu	5.5	7.3		$^{239}_{94}$Pu
$^{233}_{90}$Th	6.4	5.1	1.3	$^{232}_{90}$Th
$^{235}_{92}$U	5.8	5.3	0.5	$^{234}_{92}$U
$^{239}_{92}$U	6.0	4.8	1.2	$^{238}_{92}$U

Neutron induced fission

$$\mathrm{n}\,{}^{\mathrm{A}-1}\mathrm{X}_{\mathrm{Z}} \rightarrow {}^{\mathrm{A}}\mathrm{X}_{\mathrm{Z}}^{*} \rightarrow \text{fission}\,.$$

The effective threshold for neutron-induced fission, i.e. the minimum neutron kinetic energy necessary to give a large probability for inducing fission, is

About 1 MeV less than the height of the fission barrier

$$T_{\mathrm{n}}(A-1) = \Delta E_S(A) - S_{\mathrm{n}}(A)\,,$$

Separation energy depends on A (pairing energy!)

Due to pairing energy it is easier to induce fission (by neutron capture) in even-even nucleus.

Above we assumed that neutrons are thermal: their kinetic energy is very small (small fraction of eV) and coming from thermal motion only.

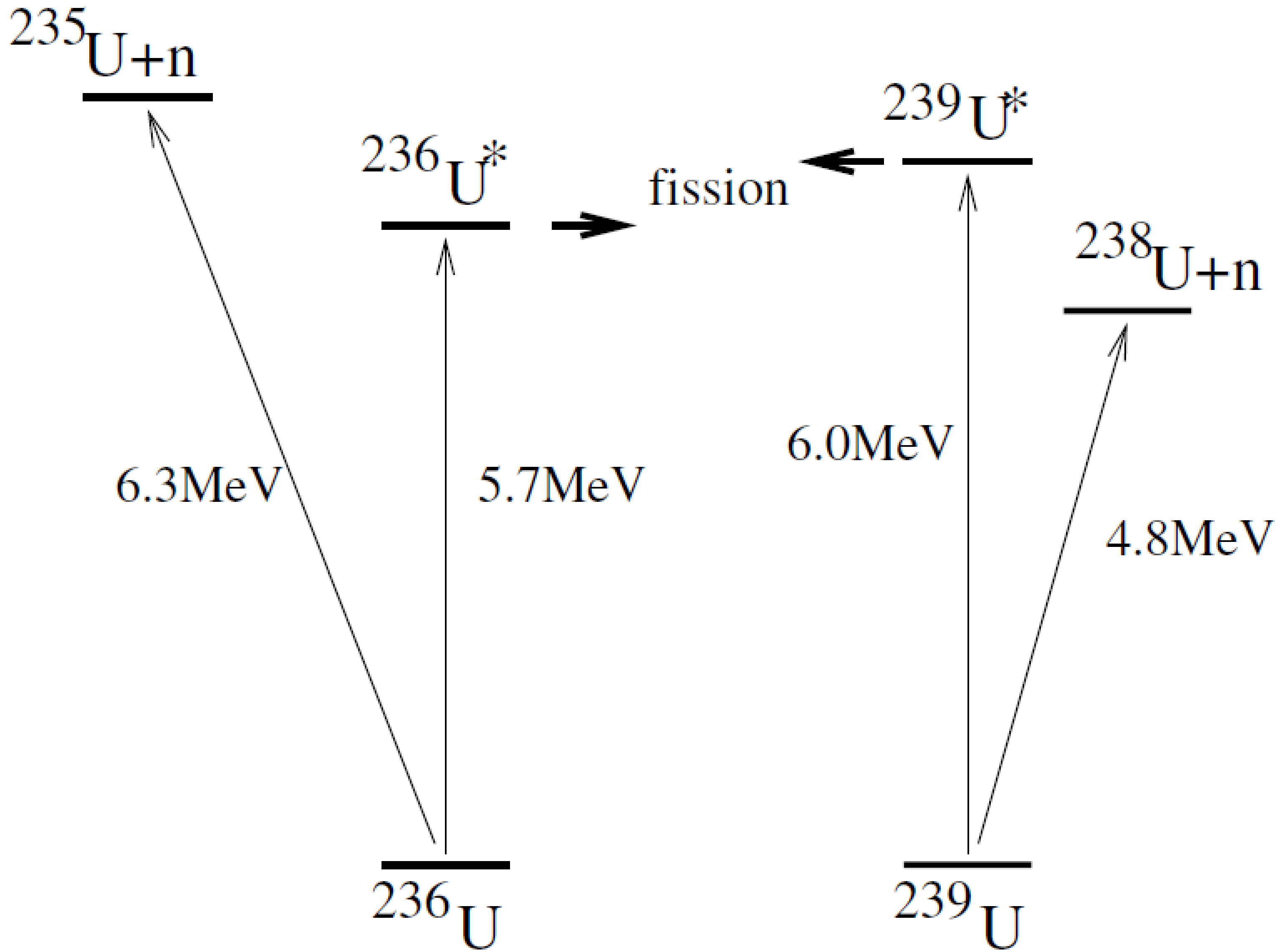

Fig. 6.6. Levels of the systems $A = 236$ and $A = 239$ involved in the fission of ^{236}U and ^{239}U. The addition of a motionless (or thermal) neutron to ^{235}U can lead to the fission of ^{236}U. On the other hand, fission of ^{239}U requires the addition of a neutron of kinetic energy $T_{\mathrm{n}} = 6.0 - 4.8 = 1.2\,\mathrm{MeV}$.

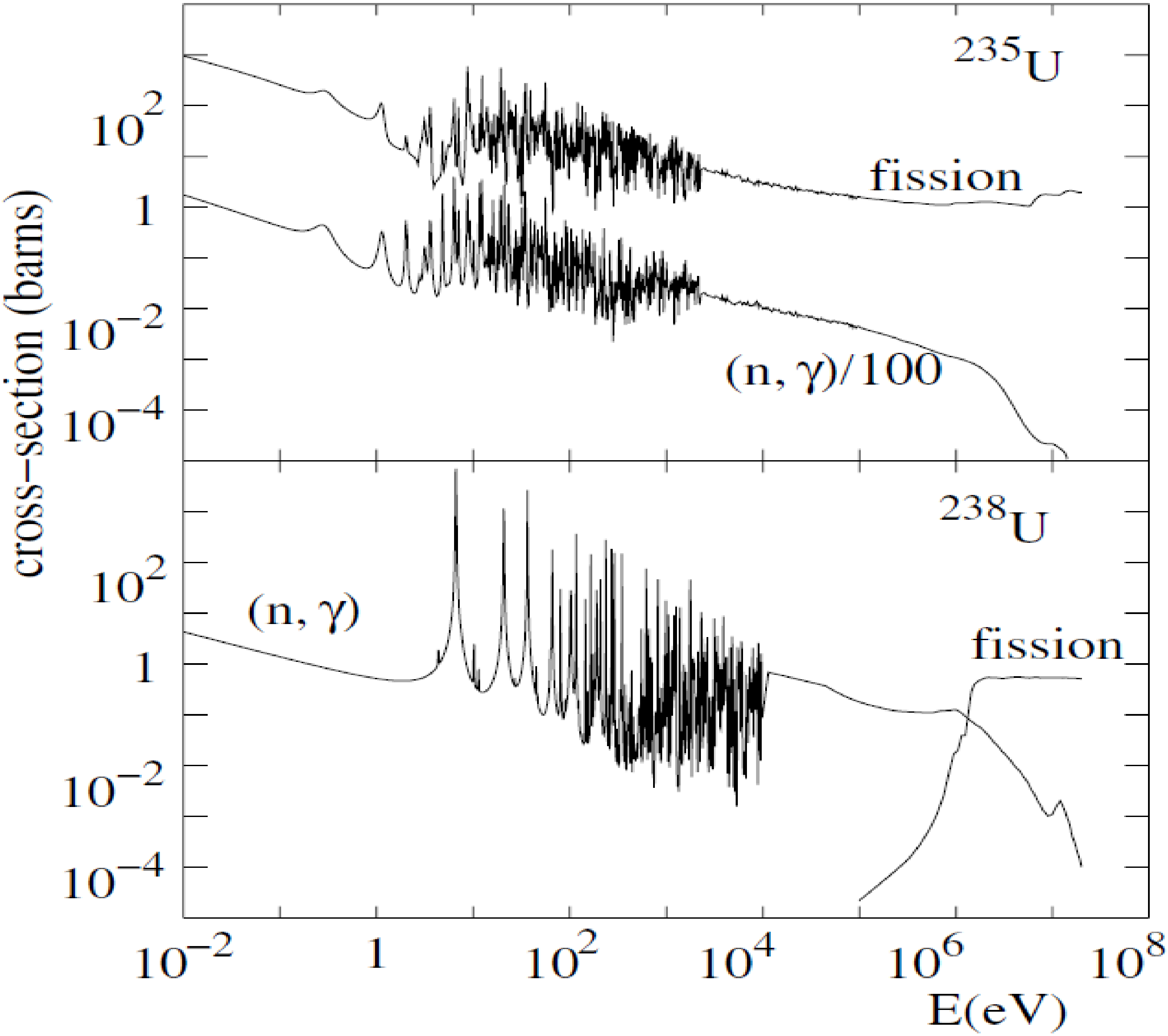

Fig. 6.7. Neutron-induced fission and radiative-capture cross-sections for ^{235}U and ^{238}U as a function of the incident neutron energy. The fission cross-section on ^{238}U has an effective threshold of $\sim 1.2\,$MeV while the cross-section on ^{235}U is proportional, at low energy, to the inverse neutron velocity, as expected for exothermic reactions. Both fission and absorption cross-sections have resonances in the range $1\,\mathrm{eV} < E < 10\,\mathrm{keV}$.

Three even-odd nuclei used most frequently as a fuel in reactors: $^{233}_{92}\mathrm{U}$, $^{235}_{92}\mathrm{U}$, $^{239}_{94}\mathrm{Pu}$, $^{241}_{94}\mathrm{Pu}$,
They rapidly fission after thermal neutron capture.

Of the three fissile nuclides, only ^{235}U exists in significant quantities on Earth, which explains its historical importance in the development of nuclear technology. Terrestrial uranium is (at present) a mixture of isotopes containing 0.72% ^{235}U and 99.3% ^{238}U.

On the other hand, ^{239}Pu and ^{233}U have α-decay lifetimes too short to be present in terrestrial ores. They are produced artificially by neutron capture starting from the *fertile materials* ^{238}U and ^{232}Th:

$$\mathrm{n}\,{}^{238}_{92}\mathrm{U} \;\rightarrow\; {}^{239}_{92}\mathrm{U}\,\gamma \tag{6.16}$$

$$ {}^{239}_{92}\mathrm{U} \;\rightarrow\; {}^{239}_{93}\mathrm{Np}\,\mathrm{e}^-\,\bar{\nu}_\mathrm{e} \qquad t_{1/2} \;=\; 23.45\,\mathrm{m}$$

$$ {}^{239}_{93}\mathrm{Np} \;\rightarrow\; {}^{239}_{94}\mathrm{Pu}\,\mathrm{e}^-\,\bar{\nu}_\mathrm{e} \qquad t_{1/2} \;=\; 2.3565\,\mathrm{day}$$

and

$$\mathrm{n}\,{}^{232}_{90}\mathrm{Th} \;\rightarrow\; {}^{233}_{90}\mathrm{Th}\,\gamma \tag{6.17}$$

$$ {}^{233}_{90}\mathrm{Th} \;\rightarrow\; {}^{233}_{91}\mathrm{Pa}\,\mathrm{e}^-\,\bar{\nu}_\mathrm{e} \qquad t_{1/2} \;=\; 22.3\,\mathrm{m}$$

$$ {}^{233}_{91}\mathrm{Pa} \;\rightarrow\; {}^{233}_{92}\mathrm{U}\,\mathrm{e}^-\,\bar{\nu}_\mathrm{e} \qquad t_{1/2} \;=\; 26.967\,\mathrm{day}$$

Chain reactions

The induced fission of ^{235}U:

$$\mathrm{n}\,^{235}\mathrm{U} \rightarrow \mathrm{A} + \mathrm{B} + \overline{\nu}\mathrm{n}\,, \qquad (6.18)$$

creates on average $\overline{\nu} \sim 2.5$ neutrons. These secondary neutrons can induce the fission of other ^{235}U nuclei. When they are emitted in a fission reaction, the neutrons have a large kinetic energy, 2 MeV on the average. They can be brought back to thermal energies by exchanging energy with nuclei in the medium via elastic scatters.

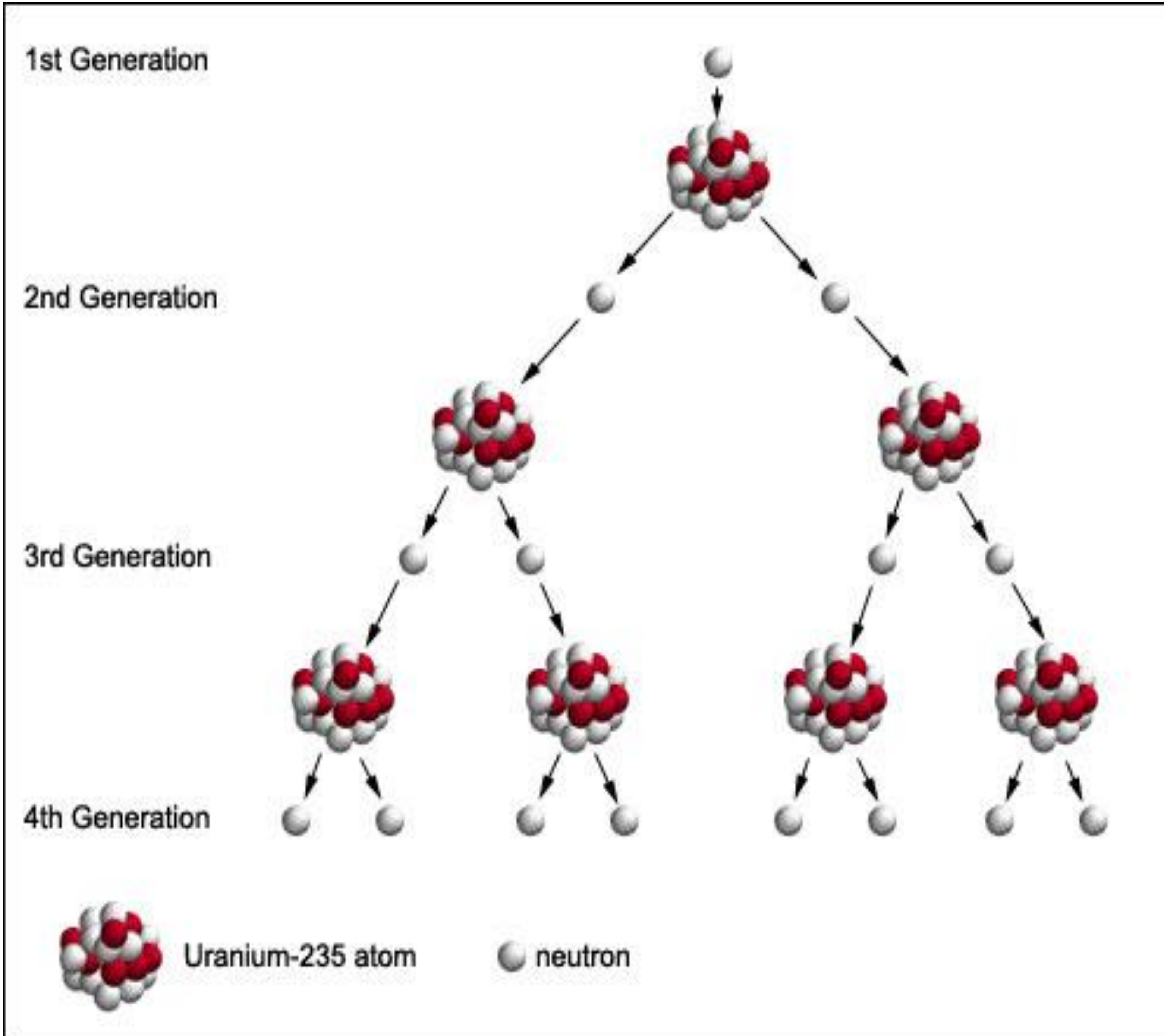
1st Generation
2nd Generation
3rd Generation
4th Generation
Uranium-235 atom
neutron

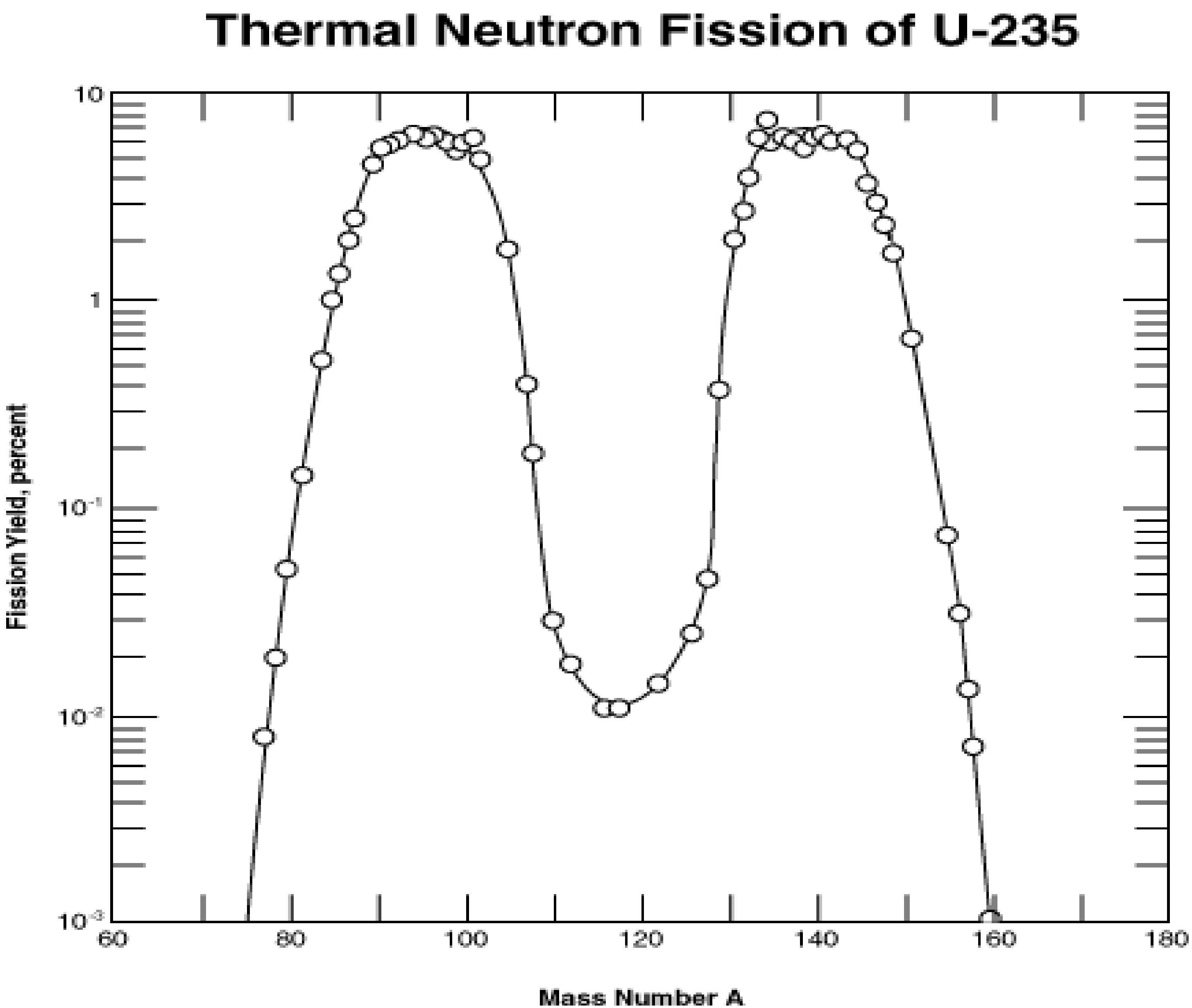

Thermal Neutron Fission of U-235
Fission Yield, percent
10
1
10⁻¹
10⁻²
10⁻³
60
80
100
120
140
160
180
Mass Number A

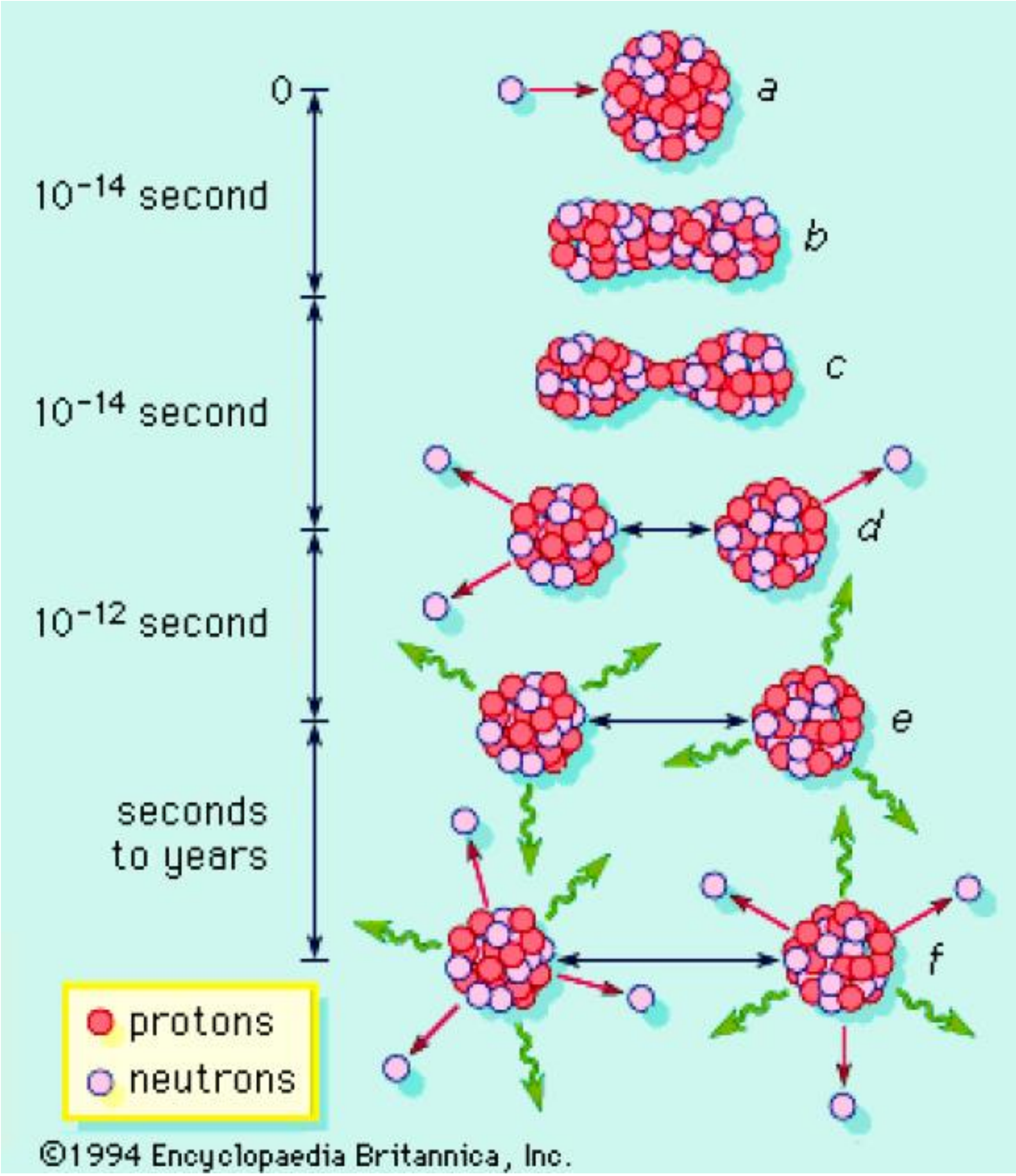

Time scales:
The fission process is much faster than the subsequent neutron emission.

The only inherent neutron-loss mechanism is radiative capture on the nucleus constituting the fuel

$$\mathrm{n}\,{}^{A}\mathrm{U} \;\rightarrow\; \gamma\,{}^{A+1}\mathrm{U} \qquad\qquad \sigma \equiv \sigma_{(\mathrm{n},\gamma)}\ . \tag{6.19}$$

If this is the only loss mechanism, then the number of neutrons that induce fission will be

$$\overline{\nu}' \;=\; \overline{\nu}\,\frac{\sigma_{\mathrm{fis}}}{\sigma_{\mathrm{fis}}+\sigma_{(\mathrm{n},\gamma)}}\ . \tag{6.20}$$

Reactors using uranium as fuel generally have mixtures of the two isotopes ^{238}U and ^{235}U. It is therefore necessary to take into account fission and absorption by both isotopes. For mixtures not to far from the natural terrestrial mixture, $f_{235} = 0.007$, fast neutron fission and absorption is dominated by the primary isotope ^{238}U. On the other hand, for thermal neutrons fission is due entirely to ^{235}U while absorption is due to both ^{235}U and ^{238}U so for thermal neutrons

$$\overline{\nu}' = \overline{\nu}_{235} \frac{f_{235}\sigma_{\mathrm{fis},235}}{f_{235}(\sigma_{\mathrm{fis},235} + \sigma_{(\mathrm{n},\gamma),235}) + (1 - f_{235})\sigma_{(\mathrm{n},\gamma),238}} \,. \tag{6.21}$$

As shown in Table 6.2, the natural mixture gives a number of available neutrons $\overline{\nu}' = 1.33$ while increasing f_{235} to 0.025 increases the number to $\overline{\nu}' = 1.8$.

Table 6.2. Comparison of selected configurations for nuclear reactors with the last column giving the number k of fission-produced neutrons available to induce further fissions. It is necessary to have $k \geq 1$ for a chain reaction to occur. The neutron energy $E_n \sim 2\,\mathrm{MeV}$ corresponds to "fast" neutron reactors while $E_n \sim 0.025\,\mathrm{eV}$ corresponds to "thermal" neutron reactors. The fuels shown are pure isotopes of uranium and plutonium as well as the natural terrestrial mixture of uranium ($0.7\%\,^{235}$U) and a commonly used enriched mixture ($2.5\%\,^{235}$U). σ_{fis} and $\sigma_{(n,\gamma)}$ are the cross-sections (in barns) for neutron induced fission and radiative neutron capture (appropriately weighted for the isotopic mixtures). $\overline{\nu}$ is the mean number of neutrons produced per fission and $\overline{\nu}'$ is the mean number after correction for radiative capture on the fuel mixture. Finally, for thermal neutrons we show, in the final column, the number of neutrons k after multiplying by δ (Table 6.3) to account for neutron losses from radiative capture on the thermalizing medium (moderator). The three thermalizers are normal water, heavy water, and carbon.

E_n	fuel	σ_{fis}	$\sigma_{(n,\gamma)}$	$\overline{\nu}$	$\overline{\nu}'$	k
$\sim 2\,\mathrm{MeV}$	^{235}U	1.27	0.10	2.46	2.28	$=\overline{\nu}'$
	^{238}U	0.52	2.36	2.88	0.52	$=\overline{\nu}'$
	^{239}Pu	2	0.10	2.88	2.74	$=\overline{\nu}'$
$\sim 0.025\,\mathrm{eV}$	^{233}U	524	69	2.51	2.29	1.72 (^1H_2O) 2.2 (^2H_2O) 2.0 (C)
	^{235}U	582	108	2.47	2.08	1.56 (^1H_2O) 2.0 (^2H_2O) 1.8 (C)
	^{238}U	0	2.7	0	0	0
	^{239}Pu	750	300	2.91	2.08	1.56 (^1H_2O) 2.0 (^2H_2O) 1.8 (C)
	$0.7\%\,^{235}$U	4.07	3.5	2.47	1.33	0.99 (^1H_2O) 1.3 (^2H_2O) 1.16 (C)
	$2.5\%\,^{235}$U	14.5	5.4	2.47	1.8	1.37 (^1H_2O) 1.8 (^2H_2O) 1.6 (C)

Moderators and neutron thermalization

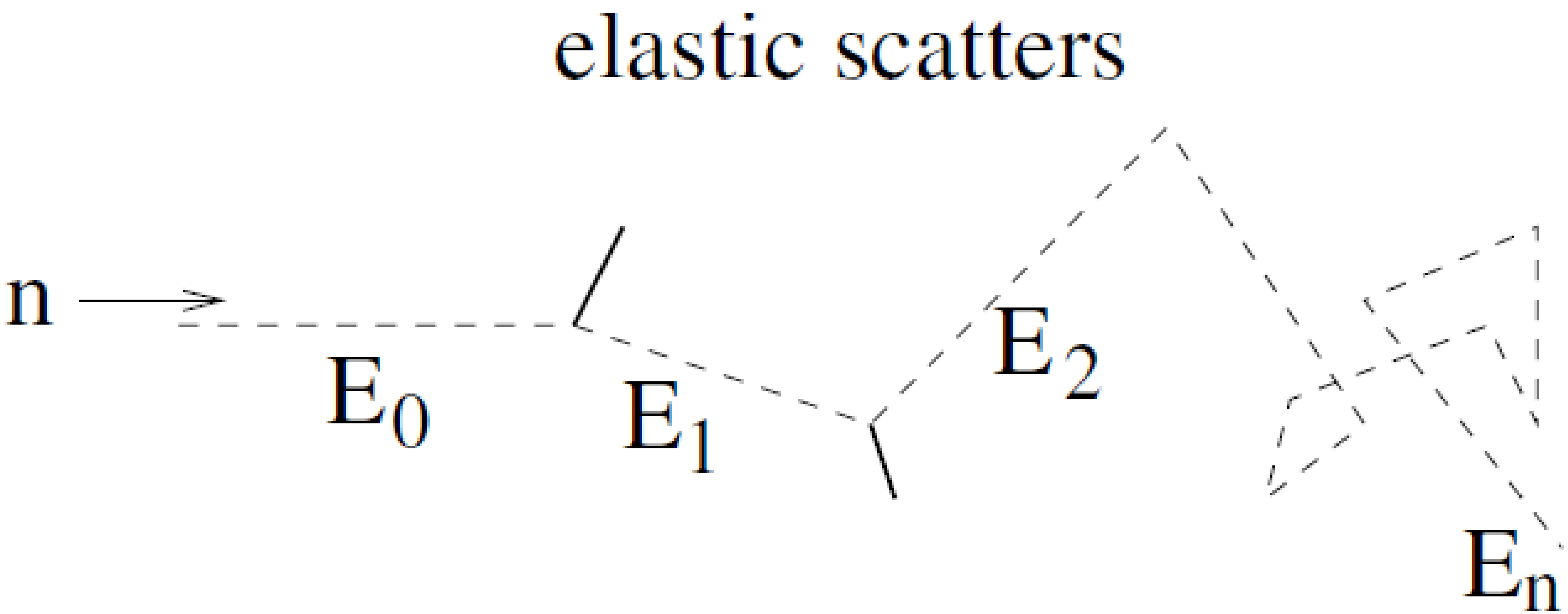

Fig. 6.8. A series of neutron–nucleus elastic scatters leading to the thermalization of the neutron.

The cooling of fission neutrons is achieved through elastic collisions with nuclei of mass $\sim Am_{\mathrm{n}}$ in a moderating medium, as represented in Fig. 6.8. In such a collision, the ratio of final to initial neutron energies as a function of center-of-mass scattering angle θ is

$$E'/E = (A^2 + 2A\cos\theta + 1)/(A+1)^2\,. \tag{6.22}$$

Assuming isotropic scattering in the center-of-mass, a good approximation for neutron energies less than $\sim 1\,\mathrm{MeV}$, one has on the average :

$$\langle E'/E \rangle = (A^2 + 1)/(A+1)^2 \quad . \tag{6.23}$$

$$\begin{aligned} \langle \log(E/E') \rangle &= -\frac{1}{2}\int_{-1}^{1} \log[E'/E]\mathrm{d}\cos\theta \\ &= 1 - \frac{(A-1)^2}{2A}\log\frac{(A+1)}{A-1}\,. \end{aligned}$$

(For $A = 1$ this expression reduces to $\langle \log(E/E') \rangle = 1$.)

Consider a series of collisions as represented in Fig. (6.8). The center-of-mass scattering angles are $\theta_1, \theta_2, \cdots \theta_n$. After n collisions, the mean neutron energy E_n is given by

$$E_n/E_0 = \prod_{i=1}^{n} E_i/E_{i-1} \Rightarrow \log E_n/E_0 = \sum_{i=1}^{n} \log(E_i/E_{i-1}) \,, \qquad (6.25)$$

and, in a series of random collisions, there will be after n collisions :

$$\langle \log(E_n/E_0) \rangle = n \langle \log(E'/E) \rangle \,. \qquad (6.26)$$

The average number of collisions N_{col} which are necessary in order to reduce the energy of fission neutrons from $E_{\text{fis}} \sim 2$ MeV to the thermal energy $E_{\text{th}} \sim 0.025$ eV, is given by :

$$N_{\text{col}} = \frac{\log \left(E_{\text{fis}}/E_{\text{th}} \right)}{\langle \log(E/E') \rangle} \quad , \qquad (6.27)$$

Probability of radiative capture of a neutron:

$$p = \frac{\sigma_{(\mathrm{n},\gamma)}}{\sigma_{\mathrm{el}} + \sigma_{(\mathrm{n},\gamma)}} ,$$

Probability of neutron survival in the thermalization process:

$$\delta = (1 - p)^{N_{\mathrm{col}}} ,$$

Table 6.3. Comparison of the three most commonly used neutron moderators in nuclear reactors, water, heavy water and graphite. The cross-sections per molecule for elastic scattering and radiative absorption are σ_{el} and $\sigma_{(\mathrm{n},\gamma)}$. The probability p for absorption per collision is given by the ratio of the elastic cross-section and the total cross-section. The number of elastic collisions N_{col} necessary to thermalize a neutron with $E_{\mathrm{n}} \sim 2\,\mathrm{MeV}$ is given by (6.27). The last column gives the probability of neutron survival during thermalization.

	σ_{el}	$\sigma_{(\mathrm{n},\gamma)}$	$p = \sigma_{(\mathrm{n},\gamma)}/\sigma_{\mathrm{tot}}$	N_{col}	$\delta = (1-p)^{N_{\mathrm{col}}}$
^1H_2O	44.8	0.664	1.5×10^{-2}	18	0.76
^2H_2O	10.4	10^{-3}	9.6×10^{-5}	25	0.998
C	4.7	4.5×10^{-3}	9.6×10^{-4}	115	0.895

From the last column of Table 6.2, we see that there are three main types of theoretically feasible reactors:

- Natural uranium reactors using heavy water or carbon as moderators.
- Enriched uranium reactors. A 2.5% enrichment in ^{235}U allows the use of light water as the moderator.
- Fast neutron reactors work without moderators. The most efficient fuel is ^{239}Pu with $k = 2.74$. The neutron flux is sufficiently high that one often adds a mixture of uranium (generally depleted in ^{235}U after previous use as nuclear fuel) that results in a production of ^{239}Pu through neutron capture on ^{238}U (6.16). Such *breeder* reactors can actually produce more fuel (^{239}Pu) than they consume. Breeder reactors are more complicated than those using thermal neutrons because, in order to avoid thermalizing the neutrons, a liquid containing only heavy nuclei (usually sodium) must be used to evacuate heat from the reactor core.

Neutron transport in matter and critical mass

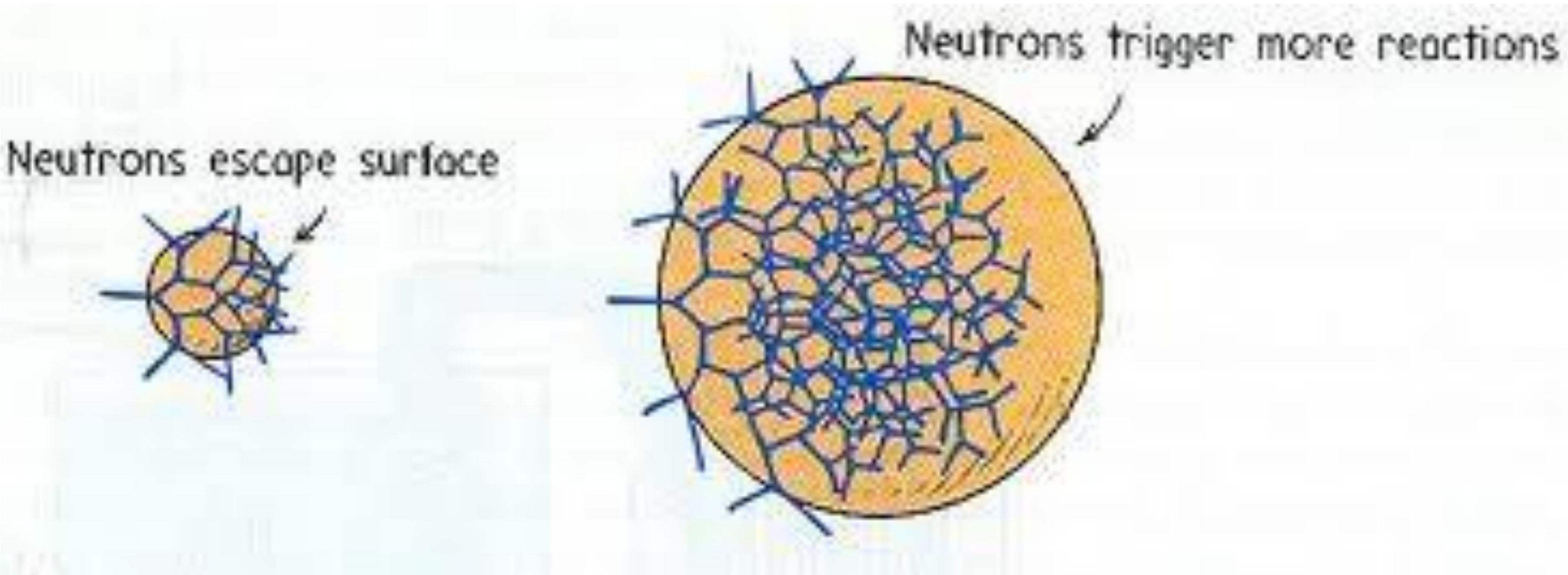

Simplified analysis neglecting inhomogeneities of a material, neutron-neutron scattering, finite neutron lifetime and assuming the neutron mean free path is much shorter than size of the system:

$$\frac{\partial n}{\partial t} + \nabla \cdot J = -\lambda_{\rm abs} n + 4\pi S(r) \ ,$$

n(r,t) – local density of neutrons
J(r,t) - neutron current density
S(r) - source term: increase of neutron number due to fission

$$\lambda_{\rm abs} = v n_{239} \sigma_{\rm abs} \ .$$

n_239 – density of scattering centers eg. 239Pu
v - mean neutron velocity.

$$\sigma_{\rm abs} = \sigma_{\rm (n,\gamma)} + \sigma_{\rm fis} \ .$$

In the local quasi-equilibrium state we may use the diffusion law (Fick's law):

$$J = -Dv\nabla n \,.$$

$$D = \frac{v}{3\lambda_{\rm el}} = \frac{l}{3} \quad .$$

- Diffusion coefficient

$$\frac{\partial n}{\partial t} - Dv\nabla^2 n = -\lambda_{\rm abs} n + 4\pi S(r) \,.$$

Assume that the mean neutron kinetic energy is about 2 MeV

The total cross-section is $\sigma_{\rm tot} = \sigma_{\rm abs} + \sigma_{\rm el}$, and the total reaction rate is

$$\lambda_{\rm tot} = n_{239}\sigma_{\rm tot} = v/l \quad , \tag{6.47}$$

where l is the mean free path of the neutrons in the medium.

The source term in (6.43) corresponds to the rate of neutron production by fission. If $\sigma_{\rm fis}$ is the fission cross-section ($\sigma_{\rm fis} < \sigma_{\rm abs}$), and $\overline{\nu}$ is the average number of neutrons produced in a fission, the rate of increase of the density $n(\boldsymbol{r})$ due to fissions is

$$4\pi S(\boldsymbol{r}) \;=\; \overline{\nu} n_{239}\, n(\boldsymbol{r})\, v\sigma_{\rm fis}\;. \tag{6.48}$$

If we insert the expression (6.44) for $\boldsymbol{J}$ and this source term into (6.43), we obtain the evolution equation for n^2

$$\nabla^2 n + \frac{(\overline{\nu}\lambda_{\rm fis} - \lambda_{\rm abs})}{vD} n \;=\; \frac{1}{vD}\frac{\partial n}{\partial t}\;. \tag{6.49}$$

If we set $k = \overline{\nu}\sigma_{\rm fis}/\sigma_{\rm abs}$, as done previously, we obtain

$$\nabla^2 n + B^2 n \;=\; \frac{1}{vD}\frac{\partial n}{\partial t}\;, \tag{6.50}$$

where we have defined

$$B^2 \;=\; (k-1)\frac{\lambda_{\rm abs}}{vD}\;. \tag{6.51}$$

(We assume that $k \geq 1$.)

Since we assume that the medium is finite, spherical, of radius R, vn depends only on the distance r from the center. The conditions we must impose on vn are the following : $vn \geq 0$ for $r \leq R$, and $vn(0,t)$ is finite.

However, equation (6.50) is only valid *inside* the medium. There are no *incoming* neutrons from the outside. In diffusion theory, a simple but accurate empirical way to simulate this condition is to impose that n vanishes at an "extrapolated distance " R_e :

$$n(R_e, t) = 0 \quad \text{with} \quad R_e = R + 0.71l \,, \tag{6.52}$$

where l is the mean free path $1/n\sigma_{\text{tot}}$.

Of particular interest is the *stationary solution* (critical regime) of (6.50), i.e. a solution for which $(\partial n/\partial t = 0)$. We then have to solve $\nabla^2 n + B^2 n = 0$ or, in spherical coordinates,

$$\frac{1}{r}\frac{\mathrm{d}^2}{dr^2} rn + B^2 n = 0 \quad . \tag{6.53}$$

Setting $u(r) = rn(r)$, this equation is readily solved:

$$u(r) = \alpha \sin Br + \beta \cos Br \quad , \tag{6.54}$$

and, since vn must be regular at the origin,

$$n(r) = \alpha \frac{\sin Br}{r} \quad . \tag{6.55}$$

The limiting condition (6.52) imposes

$$B\, R_e = \pi \quad . \tag{6.56}$$

In other words, there is only one value R_c of the radius R of the fissile sphere for which a critical regime exists (permanent or stationary regime) :

$$R_c = \pi/B - 0.71\ \lambda \,. \tag{6.57}$$

For plutonium

$$D = 1.14\ 10^{-2}\ \text{m} \quad ,$$

$$B = 39\ \text{m}^{-1} \quad .$$

Therefore, there is a *critical radius* R_c and a *critical mass* M_c:

$$R_c = 5.63\ 10^{-2}\text{m} \quad , \tag{6.58}$$

$$M_c = = \rho_{239}(4\pi/3)R_c^3 = 14.7\,\text{kg} \quad . \tag{6.59}$$

For $R \neq R_c$, a stationary regime cannot occur. One can readily check this by searching for solutions of the type :

$$n(r,t) \;=\; e^{\gamma t} f(r) \; , \tag{6.60}$$

that:

- for $R > R_c$, necessarily $\gamma > 0$, this corresponds to a *supercritical* regime, the system diverges and explodes;
- for $R < R_c$, necessarily $\gamma < 0$, this corresponds to a *sub-critical regime*; the leaks (finite medium) are not compensated and the chain reaction cannot take place. The neutron density decreases exponentially in time.

The calculation leading to the plutonium critical mass is oversimplified. The actual values for critical masses of spheres of pure metals are $M_c = 6\,\mathrm{kg}$ for ^{239}Pu and $M_c = 50\,\mathrm{kg}$ for ^{235}U. These values can be reduced if the material is surrounded by a non-fissile medium consisting of heavy nuclei so that neutrons have a high probability of scattering back into the fissile material.

Table 6.4. Characteristics of ^{239}Pu needed in the calculation of the critical radius and mass. All cross-sections are given for 2 MeV neutrons.

Elastic scattering cross-section	$\sigma_{\mathrm{el}} = 3.45\,\mathrm{b}$
Neutron-induced fission cross-section	$\sigma_{\mathrm{fis}} = 1.96\,\mathrm{b}$
Radiative capture cross-section	$\sigma_{\mathrm{n},\gamma} = 0.080\,\mathrm{b}$
Total absorption cross-section	$\sigma_{\mathrm{abs}} = \sigma_{\mathrm{n},\gamma} + \sigma_{\mathrm{fis}} = 2.04\,\mathrm{b}$
Total cross-section	$\sigma_{\mathrm{tot}} = \sigma_{\mathrm{el}} + \sigma_{\mathrm{abs}} = 5.87\,\mathrm{b}$
Neutrons produced per fission	$\overline{\nu} = 2.88$
Neutrons not radiatively absorbed	$k = \overline{\nu}' = 2.74$
Density	$\rho_{239} = 19.74 \times 10^3\,\mathrm{kg\,m^{-3}}$
neutron mean free path	$l = (\sigma_{\mathrm{tot}}\rho_{239}/m_{239})^{-1} = 0.0343\,\mathrm{m}$
Critical radius	$R_{\mathrm{c}} = 0.056\,\mathrm{m}$
Critical mass	$M_{\mathrm{c}} = (4/3)\pi R_{\mathrm{c}}^3 \rho_{239} = 14.7\,\mathrm{kg}$

Fusion

Some typical exothermic reactions:

$$\mathrm{d\,d} \rightarrow {}^{3}\mathrm{He\,n} + 3.25\,\mathrm{MeV}$$

$$\mathrm{d\,d} \rightarrow {}^{3}\mathrm{H\,p} + 4\,\mathrm{MeV}$$

$$\mathrm{d\,t} \rightarrow {}^{4}\mathrm{He\,n} + 17.5\,\mathrm{MeV}$$

$$\mathrm{n}\,{}^{6}\mathrm{Li} \rightarrow {}^{3}\mathrm{H}\,{}^{4}\mathrm{He} + 4.8\,\mathrm{MeV}$$

$$\mathrm{d}\,{}^{6}\mathrm{Li} \rightarrow 2\,{}^{4}\mathrm{He} + 22.4\,\mathrm{MeV}$$

$$\mathrm{p}\,{}^{11}\mathrm{B} \rightarrow 3\,{}^{4}\mathrm{He} + 8.8\,\mathrm{MeV}\,.$$

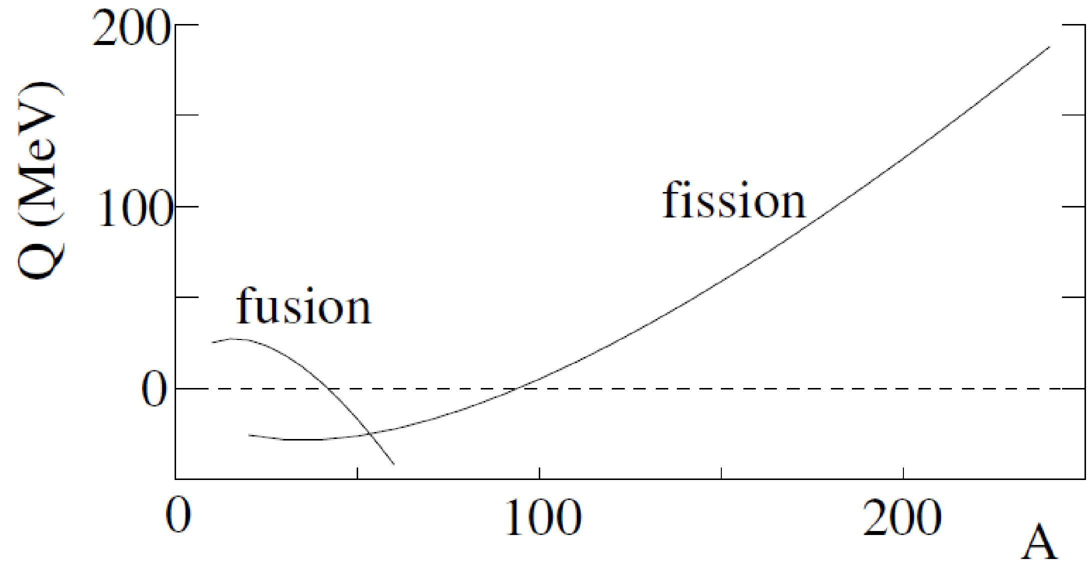

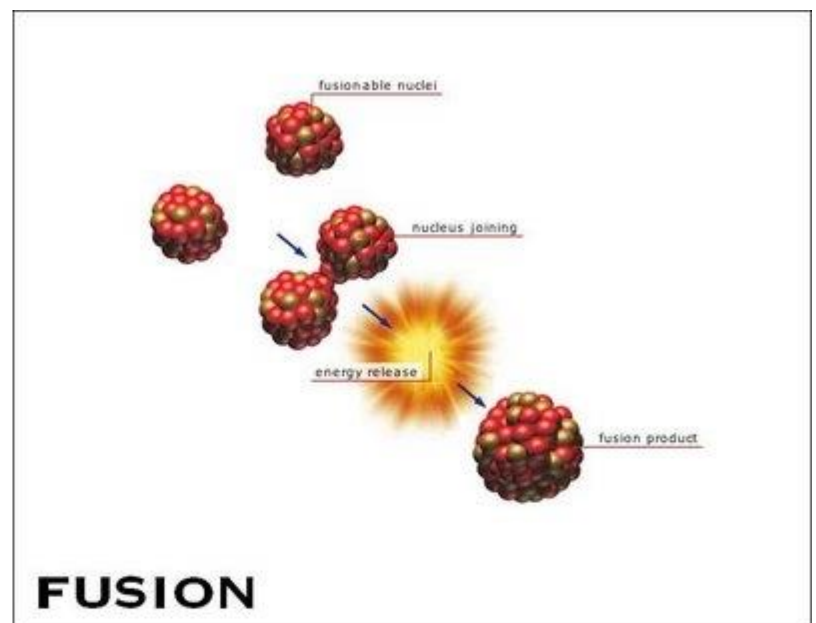

Coulomb barrier:

$$\frac{Z_1 Z_2 e^2}{4\pi\epsilon_0 a} = \frac{Z_1 Z_2 \alpha \hbar c}{a} = 1.4\,\mathrm{MeV} \times Z_1 Z_2 \frac{1\,\mathrm{fm}}{a}$$

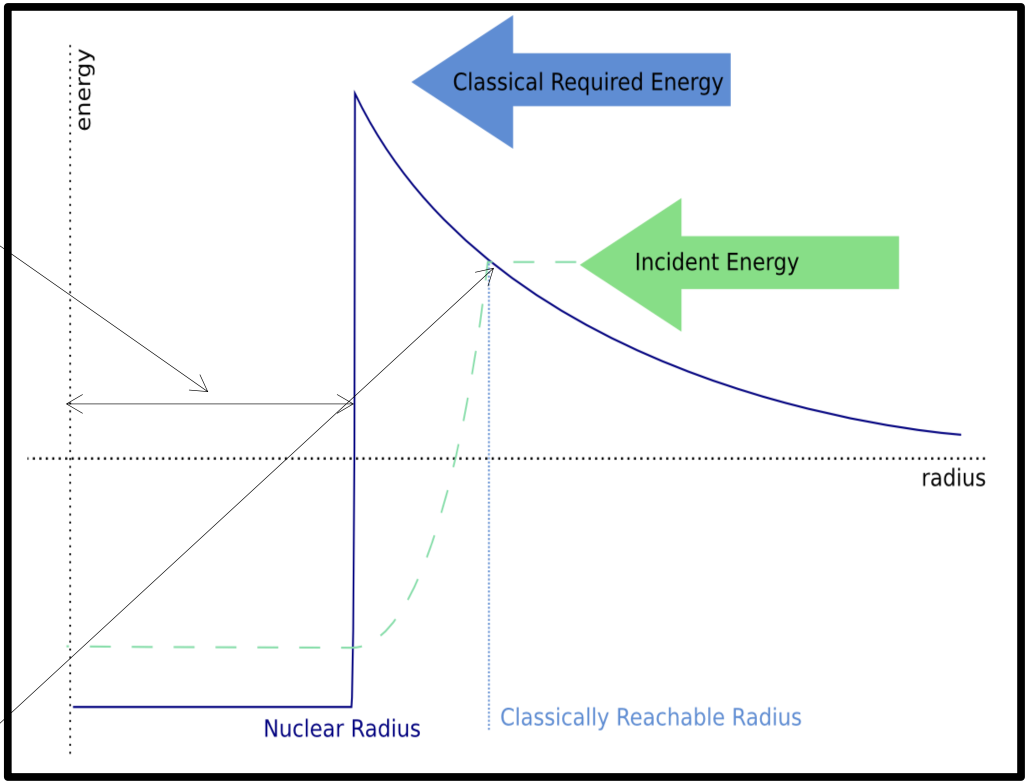

Fusion can occur even at energies below the Coulomb barrier due to the tunneling process.

Probability of tunneling:

$$P \sim \exp\left[-2\int_a^b \sqrt{\frac{2m(V(r)-E)}{\hbar^2}}\mathrm{d}r\right] \qquad (7.11)$$

where m is the reduced mass $m = m_1 m_2/(m_1 + m_2)$ of the two interacting nuclei and b is the classical turning point defined by $V(b) = E$ where $V(r)$ is the repulsive Coulomb potential.

The integral can be easily performed under condition:

$$a \ll b = \frac{Z_1 Z_2 e^2}{4\pi\epsilon_0 E} = \frac{Z_1 Z_2 \alpha\hbar c}{E} = 143\,\mathrm{fm} \times Z_1 Z_2 \frac{10\,\mathrm{keV}}{E}$$

Leading to:

$$P \sim \exp\left(\frac{-2\pi Z_1 Z_2 e^2}{4\pi\epsilon_0 \hbar v}\right) = \exp\left(\sqrt{-E_B/E}\right) . \tag{7.13}$$

where v is the relative velocity and $E = \mu v^2/2$ is the center-of-mass kinetic energy for a reduced mass μ. The barrier is characterized by the parameter

$$E_B = 2\pi^2 Z_1^2 Z_2^2 \alpha^2 \mu c^2 = 1052\,\mathrm{keV} \times Z_1^2 Z_2^2 \frac{\mu c^2}{1\,\mathrm{GeV}} . \tag{7.14}$$

It means that for nuclei of charge 1 (e.g. d+d) probability varies with the incident energy:

$$E = 1\mathrm{keV} \Rightarrow P \sim 10^{-13} \qquad E = 10\,\mathrm{keV} \Rightarrow P \sim 10^{-3}\,.$$

In stars the energy of fusing nuclei comes from the thermal motion.
1 eV corresponds to the temperature of about 10000 K

$$\sigma(E) = \frac{S(E)}{E} \exp\left(-\sqrt{E_B/E}\right)$$

Gamow formula for the cross section for fusion reaction.
S(E) is a smoothly varying function of energy in the center of mass frame.

Table 7.1. Some fusion reactions. The first three are used in terrestrial fusion reactors. The last three make up the "PPI" cycle responsible for most of the energy generation in the Sun. Note the tiny $S(E)$ for the weak-reaction $pp \to de^+\nu_e$. It can only be calculated using weak-interaction theory.

reaction	Q (MeV)	$S(10\,\mathrm{keV})$ (keV b)	E_B (keV)	$E_G(1\,\mathrm{keV})$ (keV)	$E_G(20\,\mathrm{keV})$ (keV)
$d\,d \to n\,^3\mathrm{He}$	3.25	58.3	987.	5.1	37.5
$d\,d \to p\,^3\mathrm{H}$	4.	57.3	987.	5.1	37.5
$d\,t \to n\,^4\mathrm{He}$	17.5	14000.	1185	6.8	50.1
$p\,p \to d\,e^+\,\nu_e$	1.442	3.8×10^{-22}	526	5.1	37.5
$p\,d \to \,^3\mathrm{He}\,\gamma$	5.493	2.5×10^{-4}	701	5.6	41.2
$2\,^3\mathrm{He} \to p\,p\,^4\mathrm{He}$	12.859	5×10^3	25200.	18.5	136

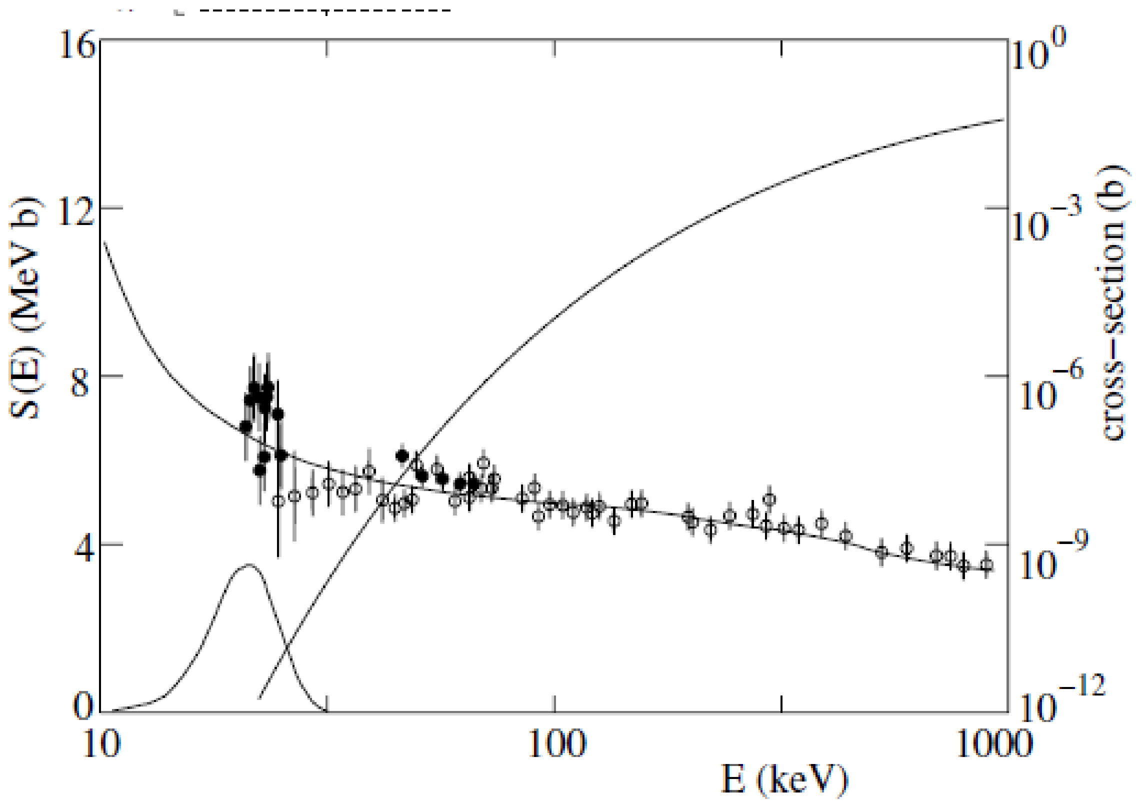

Fig. 7.1. Cross-section and $S(E)$ for $^3\mathrm{He}\,^3\mathrm{He} \to ^4\mathrm{He}\,\mathrm{p}\,\mathrm{p}$, as measured by the LUNA underground accelerator facility [69]. The top panel shows the small ($\sim 1\,\mathrm{m}^2$) experiment consisting of a ^{3}He ion source, a 50 kV electrostatic accelerator, an analyzing magnetic spectrometer, a gaseous (^{3}He) target chamber, and a beam calorimeter to measure the beam intensity. The sides of the target chamber are instrumented with silicon ionization counters that measure $\mathrm{d}E/\mathrm{d}x$ and E of protons produced by $^3\mathrm{He} +^3 \mathrm{He} \to^4 \mathrm{He} + \mathrm{p}\,\mathrm{p}$ in the chamber. Because of the very small cross-sections to be measured, the experiment is in the deep underground laboratory LNGS, Gran Sasso, Italy, where cosmic-ray background is eliminated. The bottom panel shows the LUNA measurements as well as higher energy measurements [70]. The lowest energy measurements cover the region of the solar Gamow peak for this reaction (Fig. 7.3). Note that while the cross-section varies by more than 10 orders of magnitude between $E = 20\,\mathrm{keV}$ and $1\,\mathrm{MeV}$, the factor $S(E)$ varies only by a factor ~ 2.

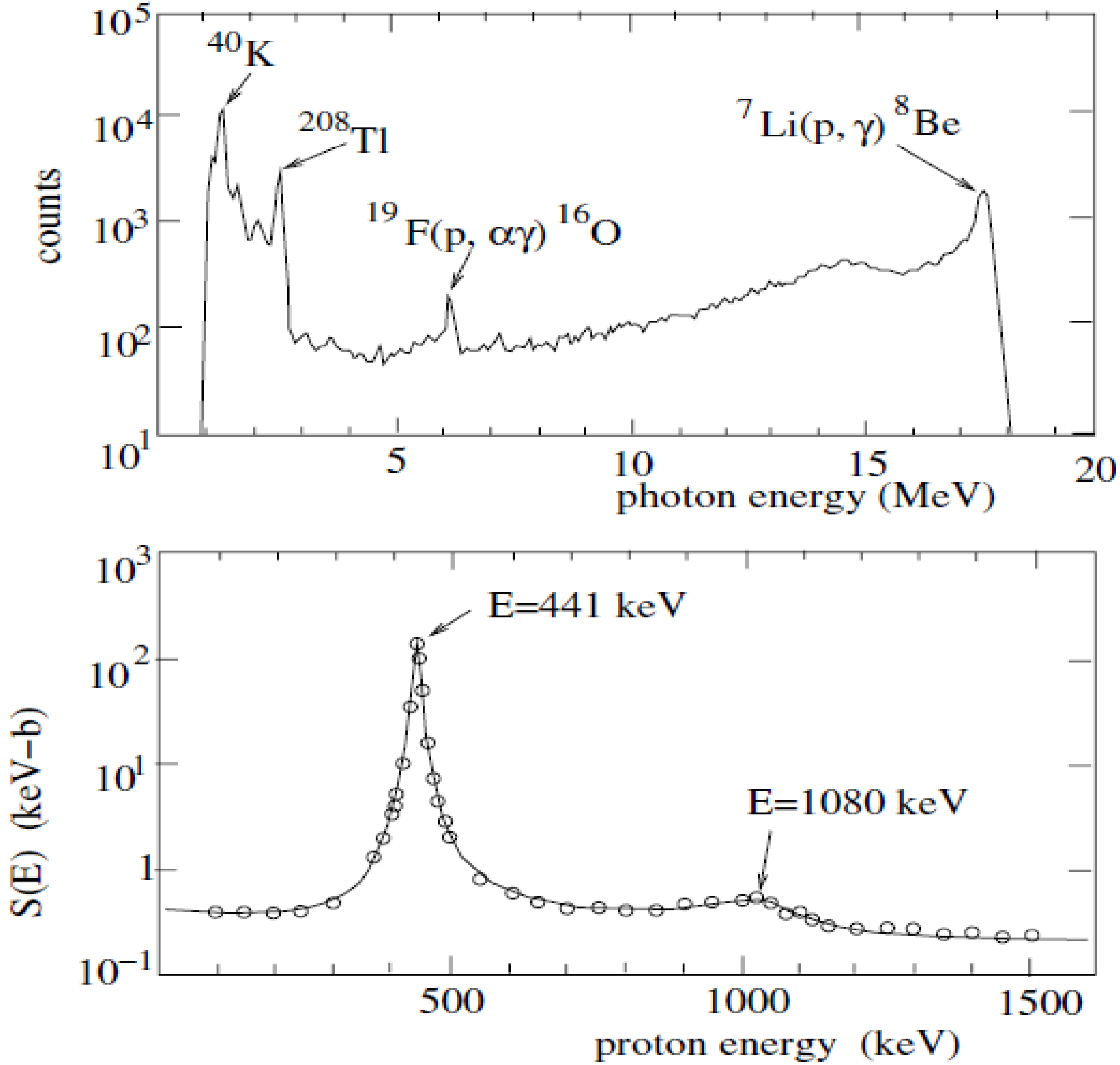

Fig. 7.2. $S(E)$ for $p\,^7\mathrm{Li} \to {}^8\,\mathrm{Be}\,\gamma$ as measured by [71]. The top panel shows how a proton beam impinges upon a target consisting of $10\,\mu\mathrm{g\,cm}^{-2}$ of LiF evaporated on a copper backing. The target is inside a large NaI scintillator that detects photons emerging from the target. The middle panel shows a typical photon energy spectrum showing peaks due to $^7\mathrm{Li}(\mathrm{p},\gamma)^8\mathrm{Be}$, in addition to peaks due to $^{19}\mathrm{F}(\mathrm{p},\alpha\gamma)^{16}\mathrm{O}$ and to natural radioactivity in the laboratory walls. The S-factor deduced from the photon counting rate is shown on the bottom panel as a function of proton energy. It shows the presence of two resonances due to excited states of ^{8}Be.

Reaction rate in a medium

Consider a mixture of two types of light elements where the fusion reaction can occur (e.g. deuterium and tritium)

Probability for fusion reaction when one element is moving with velocity v among elements of concentration n_2 reads:

$$\lambda = n_2 \sigma(v) v$$

Consequently reaction rate per unit volume can be estimated as:

$$R = n_1 n_2 \sigma(v) v$$

Taking into account that the system is at fixed temperature and therefore velocities have to be averaged, one gets:

$$R = n_1 n_2 \langle \sigma(v) v \rangle$$

$$\langle\sigma v\rangle \sim \int \mathrm{d}^3v\, \mathrm{e}^{-E/kT}\sigma(v)v \sim \int v^3 \mathrm{e}^{-mv^2/2kT}\sigma(v)\mathrm{d}v \quad . \tag{7.20}$$

In reality, both species are in motion so the integral is slightly more complicated. For nuclear of masses of m_1 and m_2, we have

$$\langle\sigma v\rangle = \left(\frac{m_1}{2\pi kT}\right)^{3/2}\left(\frac{m_2}{2\pi kT}\right)^{3/2}\int \mathrm{e}^{-(m_1v_1^2+m_2v_2^2)/2kT}\sigma(v)v\,\mathrm{d}^3v_1\mathrm{d}^3v_2\ ,$$

where $v = |\boldsymbol{v}_1 - \boldsymbol{v}_2|$ is the relative velocity. Turning to center-of-mass variables, $\mu = m_1m_2/(m_1+m_2)$ being the reduced mass, we can integrate over the total momentum (or the velocity of the center of gravity). This leads to

$$\langle\sigma v\rangle = \sqrt{\frac{8}{\pi\mu(kT)^3}}\int \mathrm{e}^{-E/kT}E\sigma(E)\mathrm{d}E \quad . \tag{7.21}$$

Using (7.15) this is

$$\langle\sigma v\rangle = \sqrt{\frac{8}{\pi\mu(kT)^3}}\int \mathrm{e}^{-\sqrt{E_B/E}}\mathrm{e}^{-E/kT}S(E)\mathrm{d}E \quad . \tag{7.22}$$

The integrand contains the product of two exponentials shown in Fig. 7.3. Their product peaks at the *Gamow energy*

$$E_G = E_B^{1/3}(kT/2)^{2/3}\ , \tag{7.23}$$

where E_B is given by (7.14). As long as $S(E)$ has no resonances (e.g. as in Fig. 7.2) only the narrow region around the Gamow energy (called the Gamow peak) contributes significantly to $\langle\sigma(v)v\rangle$. Its position determines the effective energy at which the reaction takes place.

In the absence of resonances, the nuclear factor $S(E)$ varies slowly and only the value $S(E_G)$ is relevant so it can be taken out of the integral (7.22). We can also make a Taylor expansion of the argument of the exponential in the region E_G:

$$\sqrt{E_B/E} + E/kT \sim \frac{3}{2}\left(\frac{E_B}{kT/2}\right)^{1/3} + \frac{1}{2}\frac{(E-E_G)^2}{\Delta_E^2} \ , \tag{7.24}$$

where the width of the Gamow peak is

$$\Delta_E = \frac{2}{\sqrt{3}}E_G\left(\frac{kT}{E_G}\right)^{1/2} = \frac{2}{\sqrt{3}}E_B^{1/6}\left(\frac{kT}{2}\right)^{5/6} \ . \tag{7.25}$$

[Note that the Gamow peak is relatively narrow: $\Delta_E/E_G \sim (kT/E_B)^{1/6}$.] We then have

$$\langle\sigma v\rangle = \frac{8\pi}{\sqrt{\mu}}(kT)^{-3/2}S(E_G)\exp\left[-(3/2)\left(\frac{E_B}{kT/2}\right)^{1/3}\right]$$
$$\times\int\exp\left(\frac{(E-E_G)^2}{2\Delta_E^2}\right)\mathrm{d}E \ . \tag{7.26}$$

The Gaussian integral just gives a factor Δ_E so we end up with

$$\langle \sigma v \rangle \; = \; \frac{8\pi}{\sqrt{\mu}}(kT)^{-2/3}E_B^{1/6}S(E_G)\exp\left[-(3/2)\left(\frac{E_B}{kT/2}\right)^{1/3}\right] \qquad (7.27)$$

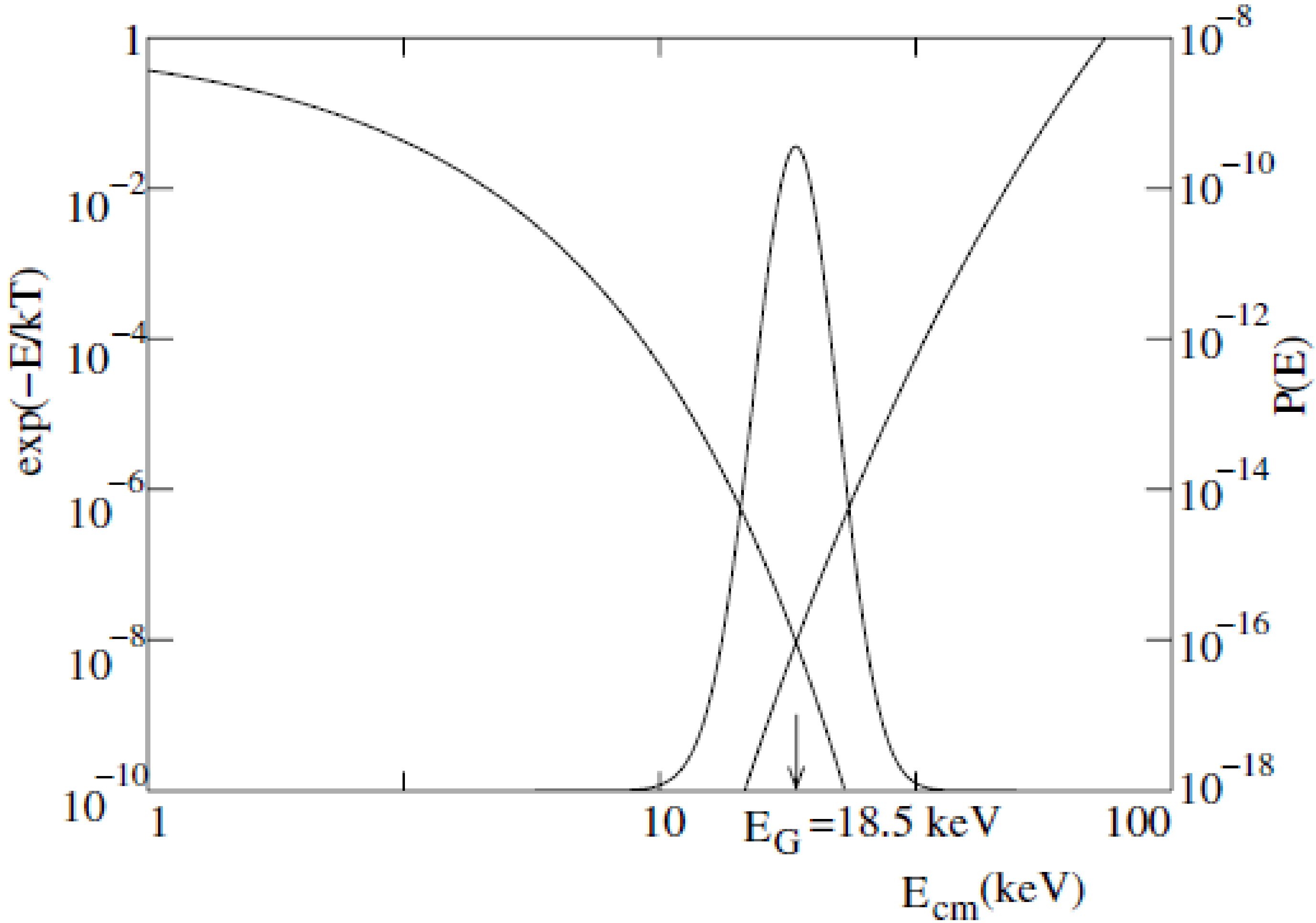

Fig. 7.3. Factors entering the calculation of the pair reaction rate (7.22). The Boltzmann factor $\exp(-E/kT)$ (logarithmic scale on the left) and the barrier penetration probability $P(E) = \exp(-\sqrt{E_B/E})$ (7.13) (logarithmic scale on the right) are calculated for $kT = 1\,\text{keV}$ (corresponding to the center of the Sun) and for the reaction $^3\text{He}\,^3\text{He} \rightarrow {}^4\text{He}\,\text{pp}$. The product is the Gaussian-like curve in the center (shown on a linear scale). It is maximized at $E_G = (\sqrt{E_B}kT/2)^{2/3} \sim 18.5\,keV$ and most reactions occur within $\sim 5\,\text{keV}$ of this value. Note the small values of $\exp(-E_{Gm}/kT) \sim 10^{-8}$ and $P(E_G) \sim 10^{-16}$.

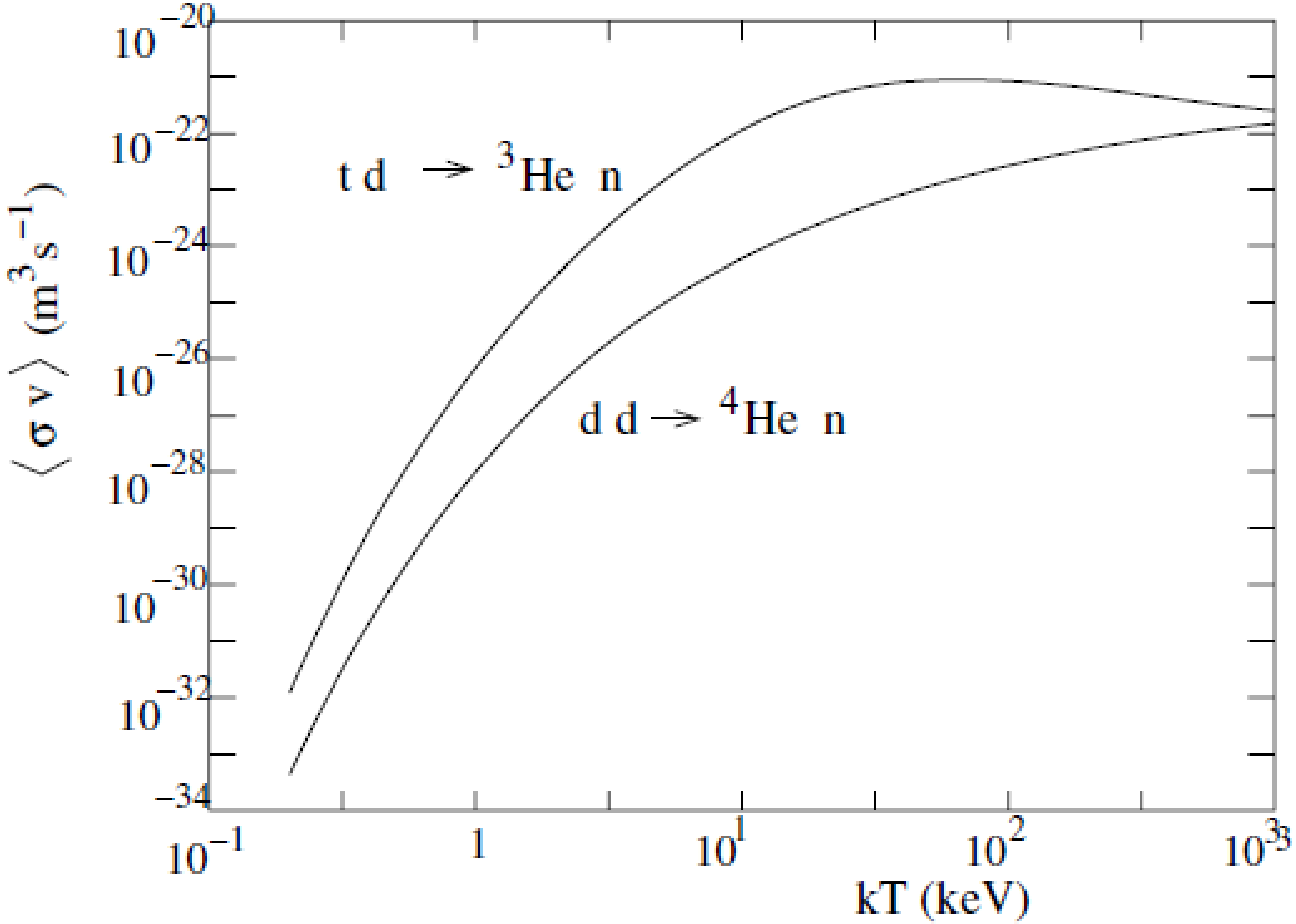

Fig. 7.4. Variation of the pair reaction rate $\langle v\sigma \rangle$ as a function of the temperature for d-d and d-t mixtures.

Resonant fusion

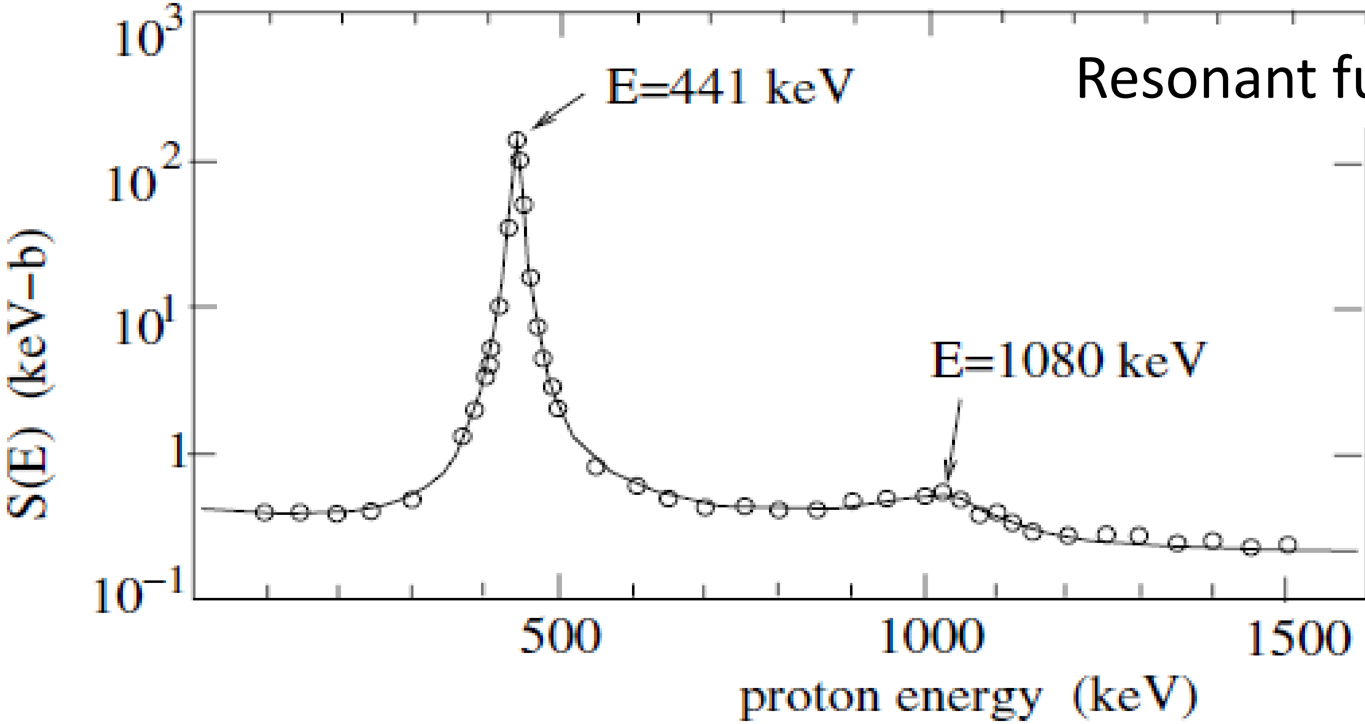

Fig. 7.2. $S(E)$ for $p^7Li \rightarrow {}^8Be\,\gamma$ as measured by [71]. The top panel shows how a proton beam impinges upon a target consisting of $10\,\mu g\,cm^{-2}$ of LiF evaporated on a copper backing. The target is inside a large NaI scintillator that detects photons emerging from the target. The middle panel shows a typical photon energy spectrum showing peaks due to ${}^7Li(p,\gamma){}^8Be$, in addition to peaks due to ${}^{19}F(p,\alpha\gamma){}^{16}O$ and to natural radioactivity in the laboratory walls. The S-factor deduced from the photon counting rate is shown on the bottom panel as a function of proton energy. It shows the presence of two resonances due to excited states of ${}^8Be$.

$$
\begin{aligned}
{}^8Be^* &\rightarrow p\,{}^7Li \qquad \Gamma_p = 6\,keV\,, \\
{}^8Be^* &\rightarrow \gamma\,{}^8Be \qquad \Gamma_\gamma = 12\,eV\,.
\end{aligned}
$$

Near the peak of the resonance, the cross-section for $\mathrm{p}\,{}^7\mathrm{Li} \to {}^8\mathrm{Be}\,\gamma$ is given by (3.183)

$$\sigma_{i\to f}(E) \sim 4\pi \frac{(\hbar c)^2}{2\mu E} \frac{(\Gamma_{\mathrm{p}}/2)(\Gamma_\gamma/2)}{(E-E_0)^2+\Gamma^2/4} \quad , \tag{7.30}$$

where we have neglected the spin factors and where $\Gamma = \Gamma_\gamma + \Gamma_{\mathrm{p}}$. The contribution to the integral in (7.21) coming from the resonance region is then just proportional to the cross-section on resonance, $4\pi(\Gamma_\gamma/\Gamma)(\hbar c)^2/(2\mu E)$ times the width Γ:

$$\int_{\mathrm{res}} \mathrm{e}^{-E/kT} E\sigma(E)\mathrm{d}E \sim \mathrm{e}^{-E_{\mathrm{res}}/kT} \frac{(\hbar c)^2}{\mu c^2} \Gamma_\gamma \,. \tag{7.31}$$

Comparing this with the non-resonant rate (7.22) we get the ratio of the contributions of the resonance and the Gamow peak

$$\frac{\langle \sigma v \rangle_{\mathrm{res}}}{\langle \sigma v \rangle_{\mathrm{Gamow}}} \sim \frac{\mathrm{e}^{-E_{\mathrm{res}}/kT}}{\mathrm{e}^{-E_{\mathrm{G}}/kT}} \frac{1}{\mathrm{e}^{-\sqrt{E_B/E_{\mathrm{G}}}}} \frac{(\hbar c)^2/\mu c^2}{S(E_{\mathrm{G}})} \frac{\Gamma_\gamma}{\Delta_E} \,. \tag{7.32}$$

Stability condition: pressure vs gravitation

$$\frac{\mathrm{d}P}{\mathrm{d}r} = -\rho(r)\,\frac{GM(r)}{r^2}\,, \qquad\qquad P = nkT \qquad\qquad (8.1)$$

where $M(r)$ is the mass contained within a sphere of radius r. Clearly, the pressure must decrease as r increases.

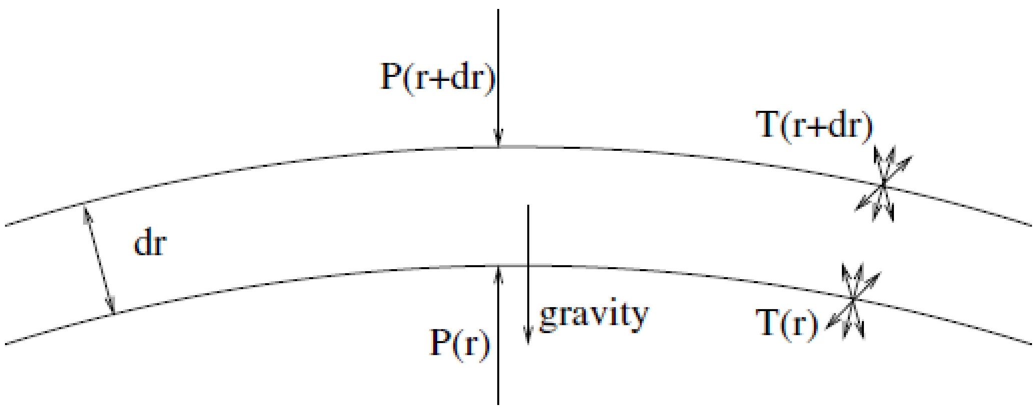

Fig. 8.1. The pressure and temperature gradients of a stable star can be qualitatively understood by considering a thin layer of material at a distance r from the center of a star. The material in the layer experiences downward forces from gravity and from the pressure $P(r+\mathrm{d}r)$. The upward force comes only from the pressure $P(r)$. If the pressure gradient satisfies (8.1) the upward and downward forces balance. Additionally, the surfaces at r and at $r+\mathrm{d}r$ radiate isotropically blackbody photons. If the temperature gradient satisfies (8.4), the difference between the energy radiated outward from the surface at r and the energy radiated inward from the surface $r+l_\gamma$ is equal to the net luminosity (l_γ=photon mean free path).

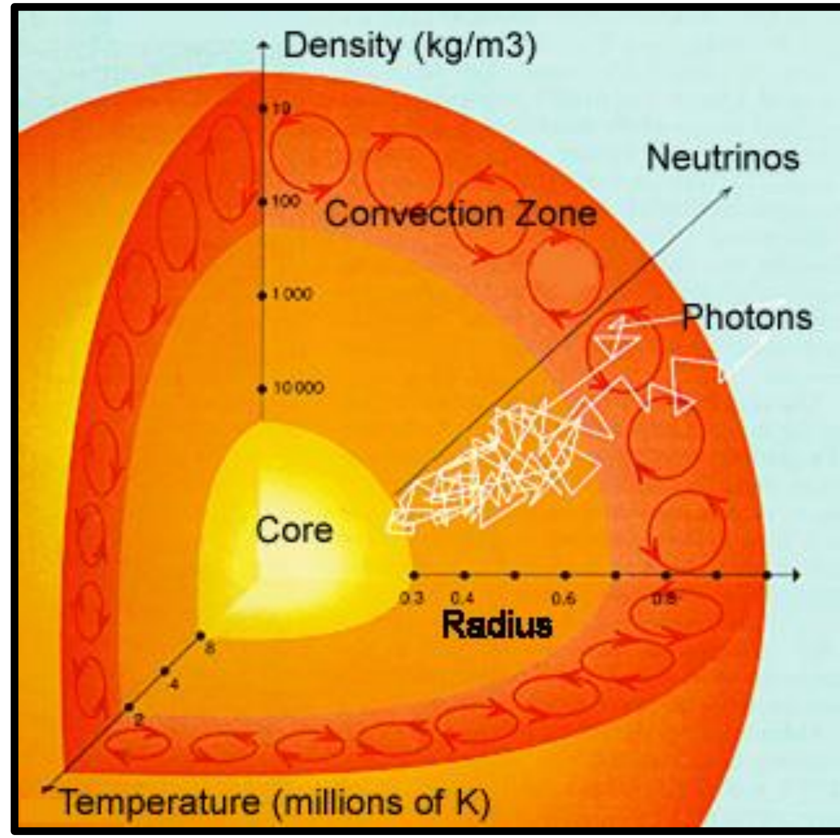

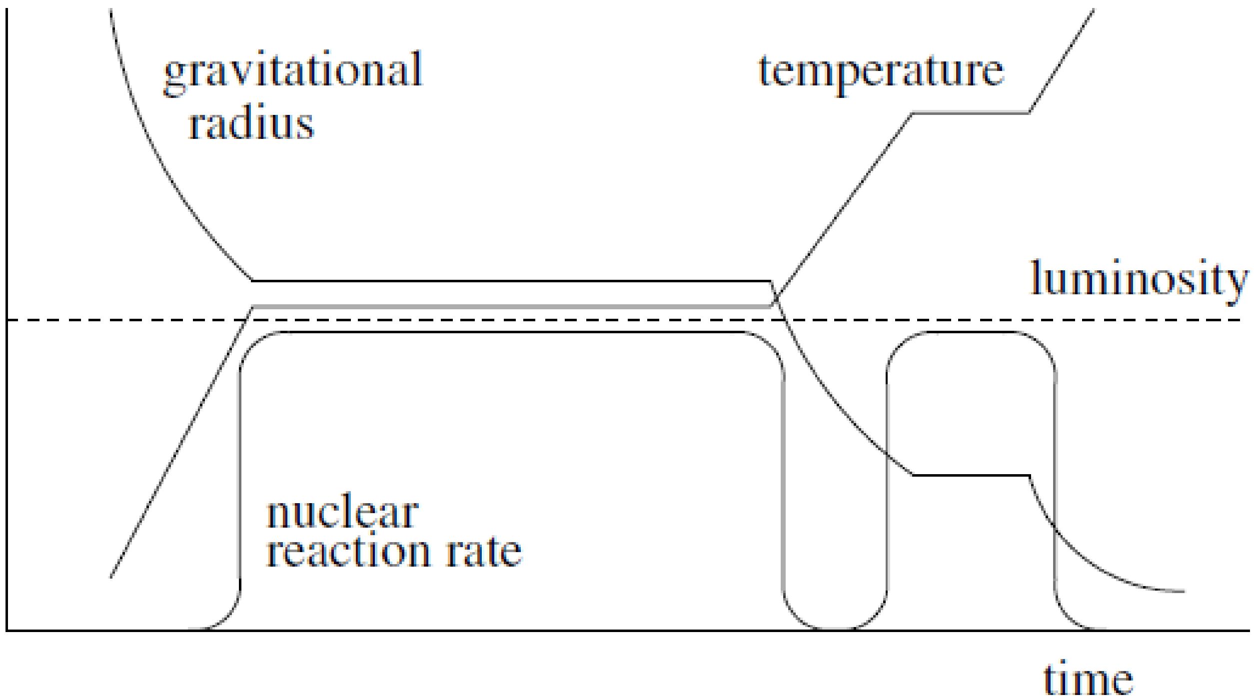

Fig. 8.3. The simplified evolution of a classical star. The star initially contracts and the temperature rises until hydrogen fusion is initiated. The radius and temperature then remain constant until the fuel is exhausted, at which point another contraction phase begins. The temperature rises until another fuel (helium) can be burned. During all this time, the luminosity is constant if the mean photon cross-section remains constant.

Table 8.1. The energy released in the (idealized) stages that transform 56 protons and 56 electrons to one ^{56}Fe nucleus and 26 electrons. Columns 2 and 3 give the available energy. We see that most of the energy comes in the first stage when hydrogen is fused to helium. The fourth column gives f_ν, the fraction of the energy released that goes to neutrinos and is therefore not available for heating the medium. (For hydrogen burning, this fraction depends on the precise reaction chain that dominates and we have taken those in the Sun.) The final two columns give the approximate stellar ignition temperatures. It should be emphasize that the five stages listed here do not represent distinct stages in real stars, in which many different reactions may take place simultaneously but at different depths.

reaction	$Q/56$ (MeV)	Q/m $10^{12}\,\mathrm{J\,kg^{-1}}$	f_ν	T (10^9K)	kT (keV)
$14[4\,^1\mathrm{H} \rightarrow\ ^4\mathrm{He}]$	6.683	640	0.02	0.015	1.3
$2[7\,^4\mathrm{He} \rightarrow\ ^{12}\mathrm{C}\,^{16}\mathrm{O}]$	0.775	75	0	0.15	15
$2[^{12}\mathrm{C}^{16}\mathrm{O} \rightarrow\ ^{28}\mathrm{Si}]$	0.598	57	0	0.8-2.0	100
$2\,^{28}\mathrm{Si} \rightarrow\ ^{56}\mathrm{Ni}$	0.195	19	0	3.5	300
$^{56}\mathrm{Ni} \rightarrow\ ^{56}\mathrm{Co} \rightarrow\ ^{56}\mathrm{Fe}$	0.120	12	0.2		
total	8.371	803	.02		

Hydrogen burning:

PPI:

$$
\begin{array}{ll}
{}^{1}\mathrm{H}\,{}^{1}\mathrm{H} \rightarrow {}^{2}\mathrm{H}\,e^{+}\,\nu_{e} & {}^{1}\mathrm{H}\,{}^{1}\mathrm{H} \rightarrow {}^{2}\mathrm{H}\,e^{+}\,\nu_{e} \\
{}^{1}\mathrm{H}\,{}^{2}\mathrm{H} \rightarrow {}^{3}\mathrm{He}\,\gamma & {}^{1}\mathrm{H}\,{}^{2}\mathrm{H} \rightarrow {}^{3}\mathrm{He}\,\gamma\,. \\
\multicolumn{2}{c}{{}^{3}\mathrm{He}\;{}^{3}\mathrm{He} \rightarrow {}^{4}\mathrm{He}\,2\,{}^{1}\mathrm{H} \qquad .}
\end{array}
$$

preferred by low mass stars

PPII and PPIII:

$$^{1}\mathrm{H}\ ^{1}\mathrm{H} \rightarrow\ ^{2}\mathrm{H}\ e^{+}\ \nu_{e}$$

$$^{1}\mathrm{H}\ ^{2}\mathrm{H} \rightarrow\ ^{3}\mathrm{He}\ \gamma$$

$$^{4}\mathrm{He}\ ^{3}\mathrm{He} \rightarrow\ ^{7}\mathrm{Be}\ \gamma$$

$$e^{-}\ ^{7}\mathrm{Be} \rightarrow\ ^{7}\mathrm{Li}\ \nu_{e}\ \ (\mathrm{PPII}) \qquad \mathrm{or} \qquad ^{1}\mathrm{H}\ ^{7}\mathrm{Be} \rightarrow\ ^{8}\mathrm{B}\ \gamma\ \ (\mathrm{PPIII})$$

$$^{1}\mathrm{H}\ ^{7}\mathrm{Li} \rightarrow\ ^{8}\mathrm{Be}\ \gamma \qquad\qquad ^{8}\mathrm{B} \rightarrow\ ^{8}\mathrm{Be}\ e^{+}\ \nu_{e}$$

$$^{8}\mathrm{Be} \rightarrow 2\,^{4}\mathrm{He}\,.$$

The luminosity of our Sun comes predominantly from PPI (about 90%) and PPI (about 10%)

CNO cycle :

$$^{1}H\ ^{12}C \rightarrow\ ^{13}N\ \gamma$$

$$^{13}N \rightarrow\ ^{13}C\ e^{+}\ \nu_e$$

$$^{1}H\ ^{13}C \rightarrow\ ^{14}N\ \gamma$$

$$^{1}H\ ^{14}N \rightarrow\ ^{15}O\ \gamma$$

$$^{15}O \rightarrow\ ^{15}N\ e^{+}\ \nu_e$$

$$^{1}H\ ^{15}N \rightarrow\ ^{12}C\ ^{4}He \qquad \text{or} \qquad ^{1}H\ ^{15}N \rightarrow\ ^{16}O\ \gamma$$

$$^{1}H\ ^{16}O \rightarrow\ ^{17}F\ \gamma$$

$$^{17}F \rightarrow\ ^{17}O\ e^{+}\ \nu_e$$

$$^{1}H\ ^{17}O \rightarrow\ ^{14}N\ ^{4}He$$

preferred by high mass stars (large temperatures required) and later generations of stars

Helium burning

There is no exothermic two-body reaction involving 4He

Endothermic reaction: $^4\mathrm{He}\,^4\mathrm{He} \leftrightarrow {}^8\mathrm{Be}$ $|\mathrm{Q}| = 92\,\mathrm{keV}$

In equilibrium the relative abundaces of 4He and 8Be is a function of temperature:

$$\frac{n_{8\mathrm{Be}}}{n_{4\mathrm{He}}} = \frac{n_{4\mathrm{He}}}{(mkT)^{3/2}/(4\pi^2\hbar^3)} \mathrm{e}^{-92\,\mathrm{keV}/kT}, \tag{8.58}$$

where m is the $^4\mathrm{He}-{}^4\mathrm{He}$ reduced mass. The typical density in a $^4\mathrm{He}$-burning core are $\rho \sim 10^5 \mathrm{g\,cm}^{-3}$ and $kT \sim 15\,\mathrm{keV}$, so (8.58) gives only a tiny $^8\mathrm{Be}$ abundance of $\sim 10^{-9}$ of the $^4\mathrm{He}$ abundance.

Using this small abundances of ^{8}Be, it is possible to produce ^{12}C through the reaction

$$^{4}\mathrm{He}\,^{8}\mathrm{Be} \rightarrow \,^{12}\mathrm{C}\,\gamma \qquad\qquad Q = 7.366\,\mathrm{MeV} \tag{8.59}$$

Because of the very small quantity of ^{8}Be, this would normally lead to a very small production rate of ^{12}C. However, as we noted in Sect. 7.1.3, the rate can be greatly increased if ^{12}C has an excited state near the Gamow energy for the reaction, $E_G \sim 200\,\mathrm{keV}$ for $kT \sim 15\,\mathrm{keV}$. This lead Hoyle [75] to predict the existence of such a state and subsequent measurements lead to its discovery (Fig. 8.5). This 0^+ excited state of ^{12}C is 7654 keV above the ^{12}C ground state and 283 keV above $^{4}\mathrm{He} -^{8}\mathrm{Be}$. It decays mostly via α decay, returning the original ^{8}Be, but also has a $\sim 10^{-3}$ branching ratio to the ground state of ^{12}C:

$$\begin{aligned}
^{4}\mathrm{He}\,^{8}\mathrm{Be} \rightarrow \,^{12}\mathrm{C}^{*} & \qquad Q = -283\,\mathrm{keV} \\
^{12}\mathrm{C}^{*} \rightarrow \,^{8}\mathrm{Be}\,^{4}\mathrm{He} & \qquad \Gamma = 8.3\,\mathrm{eV} \\
^{12}\mathrm{C}^{*} \rightarrow \,^{12}\mathrm{C}\,\gamma\gamma & \qquad \Gamma_\gamma = 3 \times 10^{-3}\,\mathrm{eV}
\end{aligned} \tag{8.60}$$

The irreversible production of ^{12}C thus proceeds through

$$3\,^{4}\mathrm{He} \rightarrow \,^{4}\mathrm{He}\,^{8}\mathrm{Be} \rightarrow \,^{12}\mathrm{C}^{*} \rightarrow ^{12}\mathrm{C}\,\gamma\gamma\,. \tag{8.61}$$

This sequence is called the "triple-α" process.

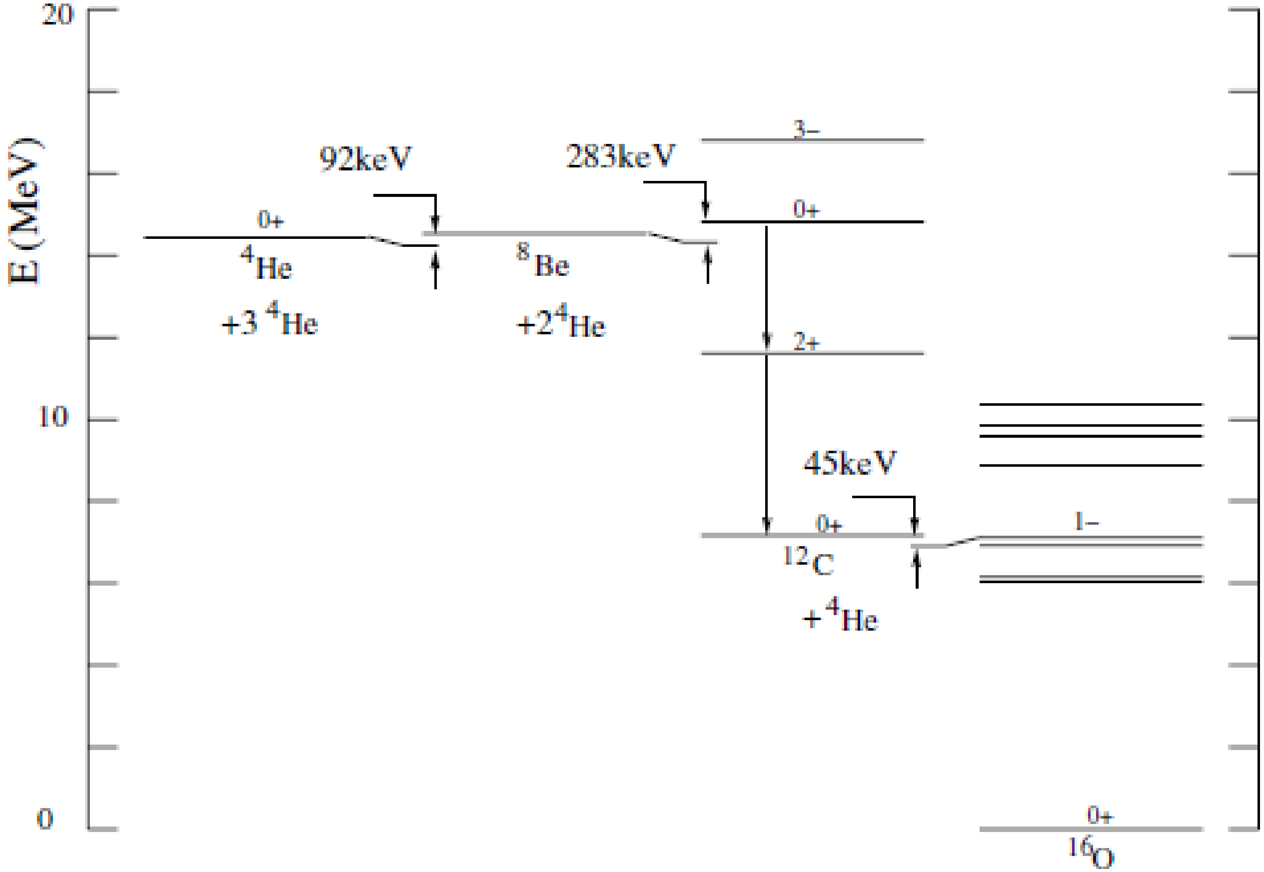

Fig. 8.5. The energy levels of four ^{4}He nuclei.

The energy liberated by the triple-α process can generate the star's luminosity when the central temperature reaches $kT \sim 10\,\mathrm{keV}$, i.e. $T \sim 10^8$K. As the ^{4}He in the core is depleted, ^{12}C burning is initiated via the non-resonant reaction

$$^4\mathrm{He}\,^{12}\mathrm{C} \;\to\; ^{16}\mathrm{O}\,\gamma \qquad \mathrm{Q} \;=\; 7.162\,\mathrm{MeV} \tag{8.62}$$

This reaction competes favorably with the triple-α process once the ^{4}He is depleted because its rate is linear in the concentration of ^{4}He while the rate of the triple-α process is proportional to the third power of the ^{4}He concentration. The helium-burning stage thus generates a mixture of ^{12}C and ^{16}O.

A peculiar characteristic of the triple-α process is that its end result depends critically on the details of the three remarkable energy alignments of the 0^+ states of ^{8}Be, ^{12}C and the 1^- state of ^{16}O (Fig. 8.5):

$$^4\mathrm{He}\,^4\mathrm{He} \;\to\; ^8\mathrm{Be} \qquad \mathrm{Q}_4 \;=\; -0.092\,\mathrm{MeV}\;, \tag{8.63}$$

$$^4\mathrm{He}\,^8\mathrm{Be} \;\to\; ^{12}\mathrm{C}^* \qquad \mathrm{Q}_8 \;=\; -0.283\,\mathrm{MeV}\;, \tag{8.64}$$

$$^4\mathrm{He}\,^{12}\mathrm{C} \;\to\; ^{16}\mathrm{O}^*\,\gamma \qquad \mathrm{Q}_{12} = +0.045\,\mathrm{MeV}\;. \tag{8.65}$$

Advanced stages of burning

The later stages of nuclear burning are rather complicated for reasons of both astrophysics and nuclear physics.

The nuclear reaction chains are rather complicated because of the multiple final states for reactions involving two nuclei. For example, in carbon burning, there are three possible exothermic reactions:

$$\begin{aligned} {}^{12}\mathrm{C}\,{}^{12}\mathrm{C} \;\rightarrow\; & {}^{24}\mathrm{Mn}\,\gamma & Q &= 13.93\,\mathrm{MeV} \\ \rightarrow\; & {}^{23}\mathrm{Na}\,\mathrm{p} & Q &= 2.24\,\mathrm{MeV} \\ \rightarrow\; & {}^{20}\mathrm{Ne}\,{}^{4}\mathrm{He} & Q &= 4.62\,\mathrm{MeV}\,. \end{aligned}$$

These three reactions can be considered to be a single reaction consisting of the formation of a "compound nucleus," i.e. an excited state of ^{24}Mn which then decays by photon, proton, or α emission

$$ {}^{12}\mathrm{C}\,{}^{12}\mathrm{C} \;\rightarrow\; {}^{24}\mathrm{Mn}^{*} \;\rightarrow\; \mathrm{x}\,\mathrm{y}\,. \tag{8.66}$$

Proton or α emission have larger probabilities than photon emission. The protons and α-particles produced in ^{24}Mn* decay is are then absorbed by ^{12}C to produce ^{13}N or ^{16}O.

Advanced stages of burning

After Fe is created in the star core nuclear reactions in the core cease and the star starts to implode.
The increase of the density leads to the production of neutrinos through the electron capture process.
This leads subsequently to neutronization of the star.

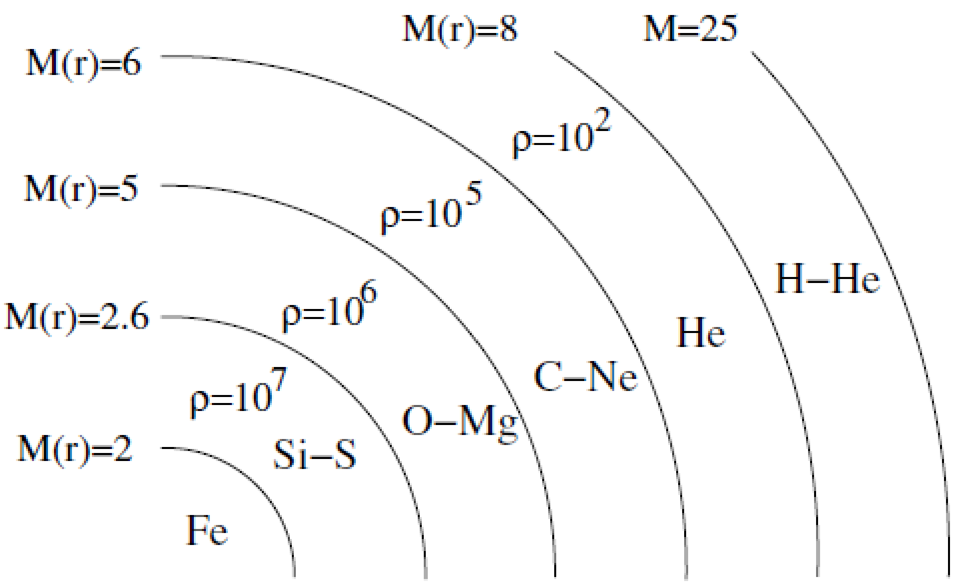

Fig. 8.7. The profile of a $25M_{\odot}$ star when its core has burned to ^{56}Fe. For each concentric shell, the characteristic density (in gm cm^{-3}) and dominant nuclear species are shown.

reaction	$Q/56$ (MeV)	Q/m $10^{12}\,\mathrm{J\,kg^{-1}}$	f_ν	T $(10^9\mathrm{K})$	kT (keV)
$14[4\,{}^1\mathrm{H} \to {}^4\mathrm{He}]$	6.683	640	0.02	0.015	1.3
$2[7\,{}^4\mathrm{He} \to {}^{12}\mathrm{C}\,{}^{16}\mathrm{O}]$	0.775	75	0	0.15	15
$2[{}^{12}\mathrm{C}\,{}^{16}\mathrm{O} \to {}^{28}\mathrm{Si}]$	0.598	57	0	0.8-2.0	100
$2\,{}^{28}\mathrm{Si} \to {}^{56}\mathrm{Ni}$	0.195	19	0	3.5	300
${}^{56}\mathrm{Ni} \to {}^{56}\mathrm{Co} \to {}^{56}\mathrm{Fe}$	0.120	12	0.2		
total	8.371	803	.02		

Latest stage of star evolution

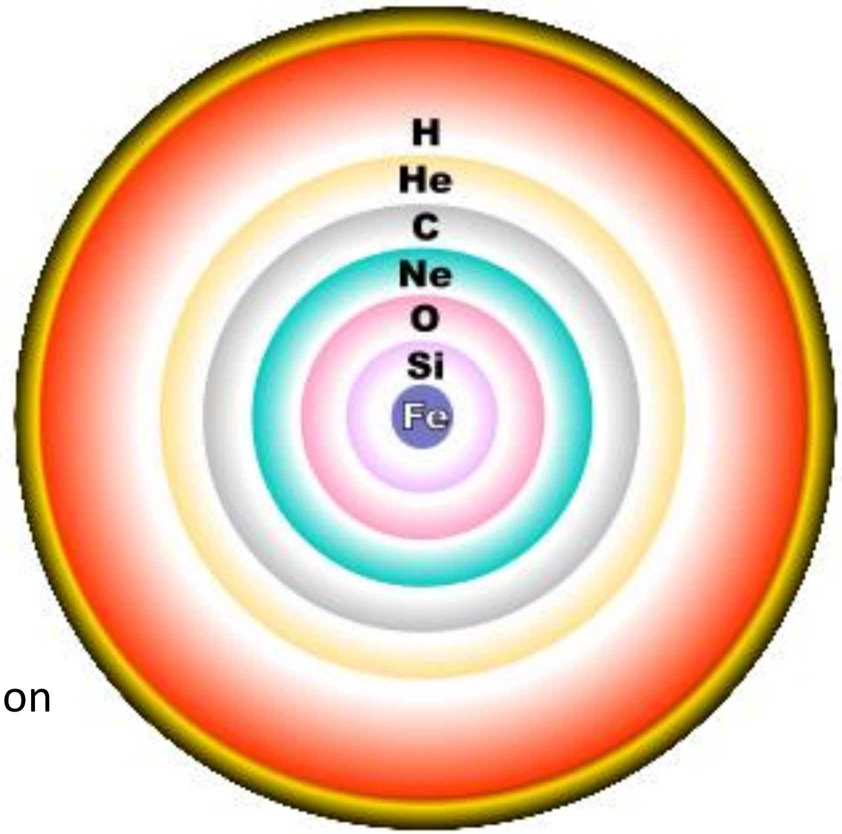

During the collapse the process of neutronization starts: $e^- p \rightarrow n\nu_e$.

It is energetically favourable to turn proton and electron into neutron when the density of matter is increasing.
It is the quantum effect: consequence of uncertainty and Pauli pirinciples.

Estimate: 10^8 supernova explosions in 10^10 years in our galaxy

Once the protons have been converted to neutrons, the collapse may be halted at the radius corresponding to a degenerate gas of neutrons. The energy change of the $1.4M_\odot$ core in the process of collapsing from $R \sim 1000\,\mathrm{km}$ to $R \sim 10\,\mathrm{km}$ is

$$\Delta E \sim (3/5)\frac{GM^2}{R} \sim 3 \times 10^{46}\,\mathrm{J} \quad \text{for } M = 1.5M_\odot\,. \tag{8.68}$$

This energy is mostly carried out by neutrinos which escape from the star (neutrinos weakly interact with matter).

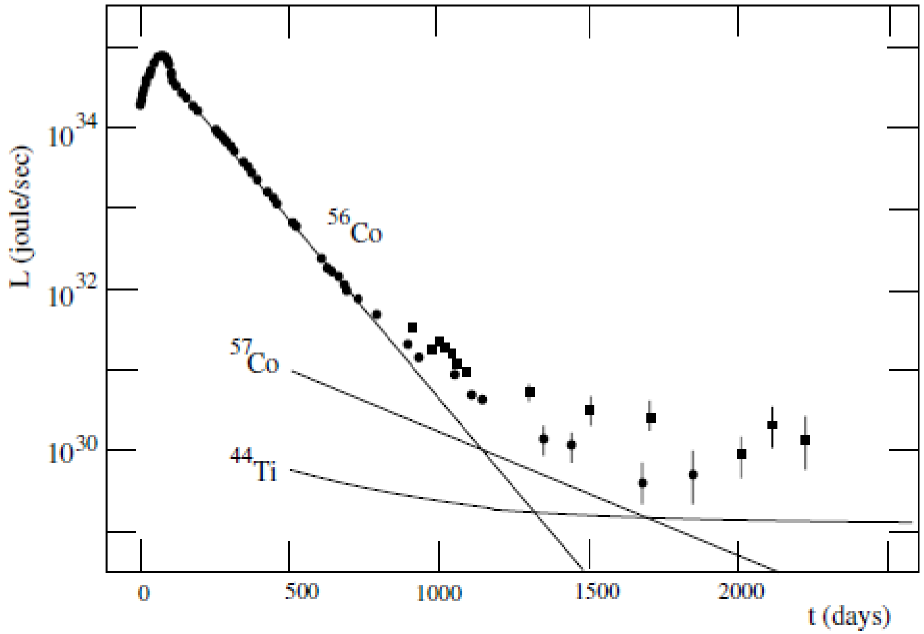

Fig. 8.8. The total luminosity of SN1987a as a function of time [78]. The labeled curves show the calculated contribution to the luminosity from the β-decay of ^{56}Co, ^{57}Co, and ^{44}Ti.

The outer layers of exploding star are blown off into the interstellar medium. They consist of light and medium nuclei 4<A<56 and are immersed in large neutrino and neutron fluxes.

Stellar nucleosynthesis

Alpha nuclei – consist of integer number of 4He

Light nuclei are created mostly in various stages of burning in stars .
Later they possibly were dispersed in the interstellar medium due to the process of supernova explosion.

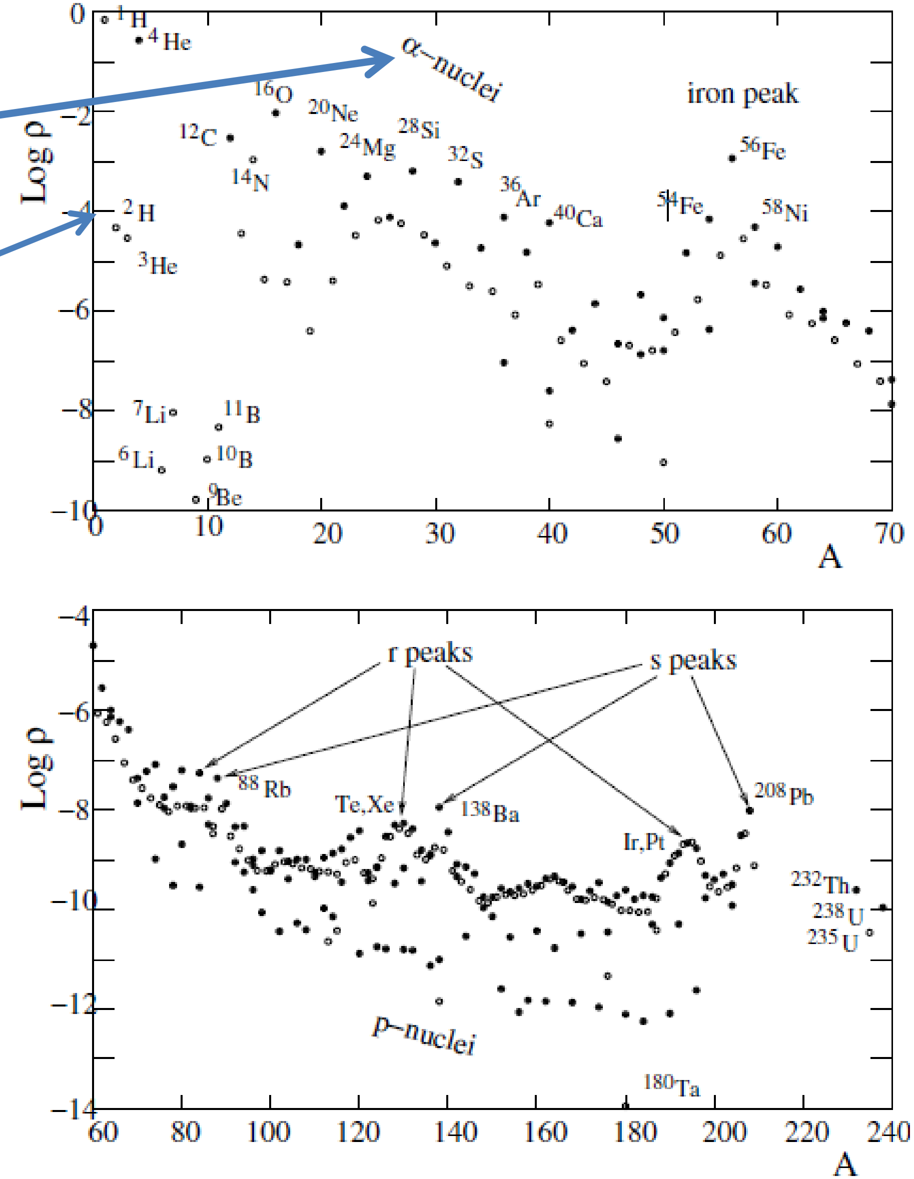

Fig. 8.9. The solar system abundances $\rho(A,Z)/\rho_{tot}$ [79]. The filled circles correspond to even-even nuclei. For $A < 70$, the distribution is visually dominated by cosmogenic ^{1}H and ^{4}He and by "iron-peak" elements near $A = 56$ Between these two features, the distribution is dominated by "α-nuclei" comprised of an integer number of ^{4}He nuclei. For $A > 60$, the distribution has peaks corresponding to neutron magic numbers that are produced by the s-process. The r-process produces peaks shifted to lower A after neutron-rich magic-N nuclei β-decay to the bottom of the valley of stability. Rare elements are produced by the p-process.

S- process

S – process is the process of creation of heavy elements in stars through the neutron capture.

This process is rather slow as there not too many free neutrons in the stars. Typical reaction being a source of free neutrons:

$$
\begin{aligned}
{}^{4}\mathrm{He}\,{}^{13}\mathrm{C} &\to \mathrm{n}\,{}^{16}\mathrm{O} \qquad Q = 3.00\,\mathrm{MeV} \\
{}^{4}\mathrm{He}\,{}^{22}\mathrm{Ne} &\to \mathrm{n}\,{}^{25}\mathrm{Mn} \qquad Q = 0.30\,\mathrm{MeV}\,.
\end{aligned}
$$

Ge_{32}		−1.0	1.8	1.5	3.9	3.1	7.4	5.1		6.0				3.7	
Ga_{31}	−0.8	−0.9	1.5	2.2	3.0	4.5	5.5	3.6		3.1		4.7	4.2	2.7	2.1
Zn_{30}	2.2	1.9	4.5	3.4		7.3				3.5		2.2	5.2	1.4	2.0
Cu_{29}	1.9	3.2	4.1	2.8		4.7		2.5	5.3	1.5	2.2	0.7	1.3	0.8	0.6
Ni_{28}		12.4				9.5		4.0	5.3	1.3	1.3	1.1		0.3	0.3
Co_{27}	7.4	6.8		8.2	3.8	2.0	1.4	−0.5	0.1	−0.6	−0.4	−0.7	−0.6	−0.8	−0.7
Fe_{26}				6.6	13.7	2.6	1.8	0.8	0.3	−0.4	−0.4	−0.3	−1.0	−0.8	
	N=30	31	32	33	34	35	36	37	38	39	40	41	42	43	44

Fig. 8.10. Nucleosynthesis by neutron capture starting at ${}^{56}\mathrm{Fe}$. The decimal logarithm of the half-life in seconds is shown for β-unstable nuclei. If the neutron flux is small, β-decay occurs "immediately" after neutron absorption and the path follows the nuclei at the bottom of the stability valley indicated by the arrows. This is the s-process. On the other hand, if the neutron flux is sufficiently high, the r-process is operative where nuclei can absorb many neutrons before β-decaying so the path may ascend the sides of the valley until the nuclei are either photo-dissociated or β decay. Along the Fe-line, this is shown as happening at ${}^{66}_{40}\mathrm{Fe}_{26}$. After the neutron flux is turned off, the nuclei on the slopes of the valley β-decay down to the bottom. Note that the neutron capture path in a nuclear reactor (Fig. 6.12) is intermediate between the astrophysical s- and r- processes since the time for neutron absorption is typically a month or so.

The s-process is slow in comparsion to beta decay. Consequently it produces nuclei along the stability valley.

s-process

r-process

R-process

R-process is the process of neutron capture which occurs during supernova explosion.
Nuclei are immersed in a large neutron flux at high temperature and consequently the process is fast (much faster than beta decay).
Consequently it produces very neutron-rich nuclei which subsequently decay towards stability valley.

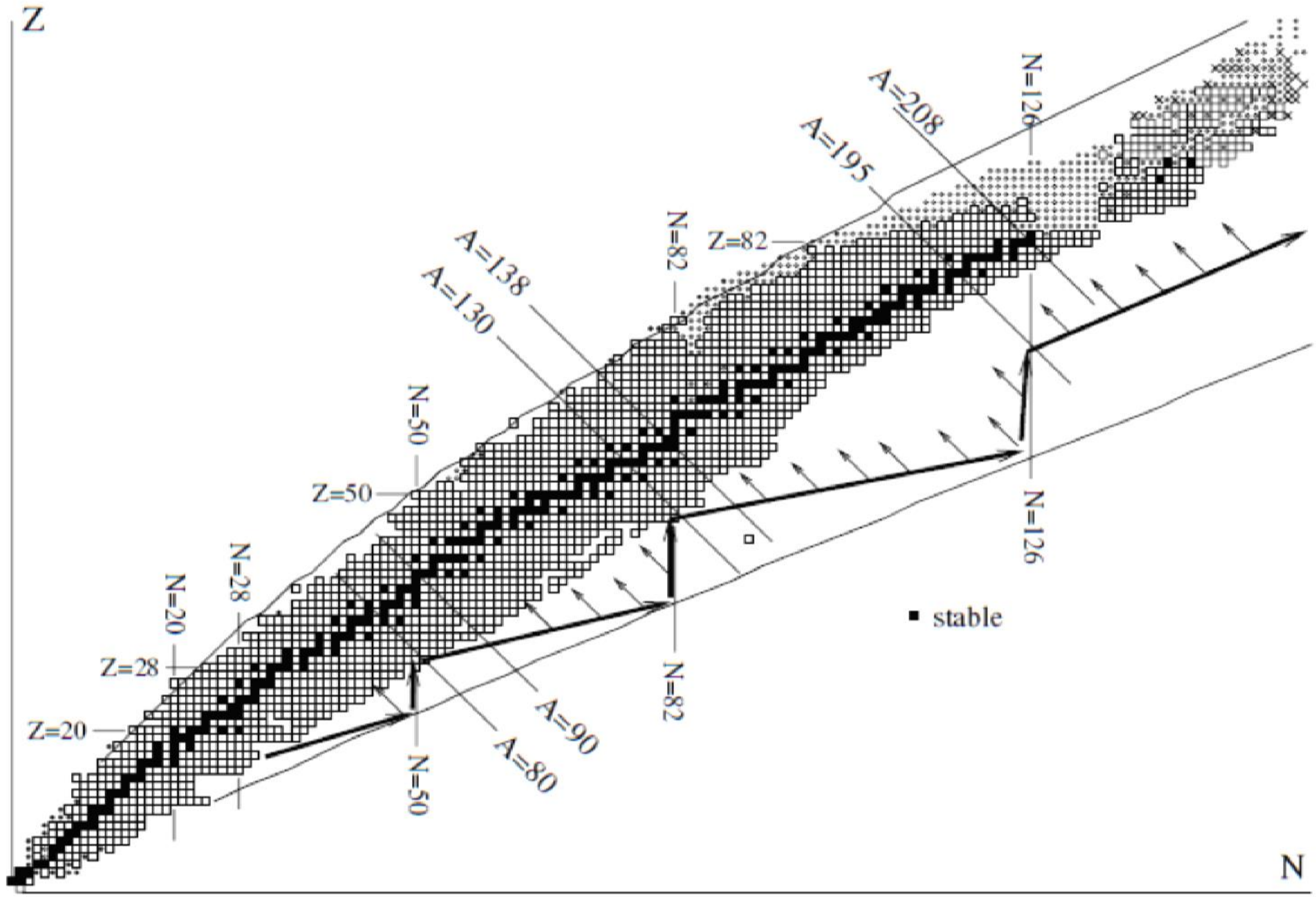

Fig. 8.11. The paths for nucleosynthesis by slow and fast neutron capture. In the s-process, the prompt β-decays insure that all produced nuclei are near the bottom the of the stability valley. In the r-process, rapid neutron absorption during an intense pulse of neutrons leads to nuclei distributed along the thick arrow on the southern slope of the valley. After the pulse is turned off, the nuclei β-decay down to the bottom of the valley, as indicated by the thin arrows.

Nucleosynthesis

S-process stops here since nuclei A=210, 211 have too short lifetime with respect to alpha emission.

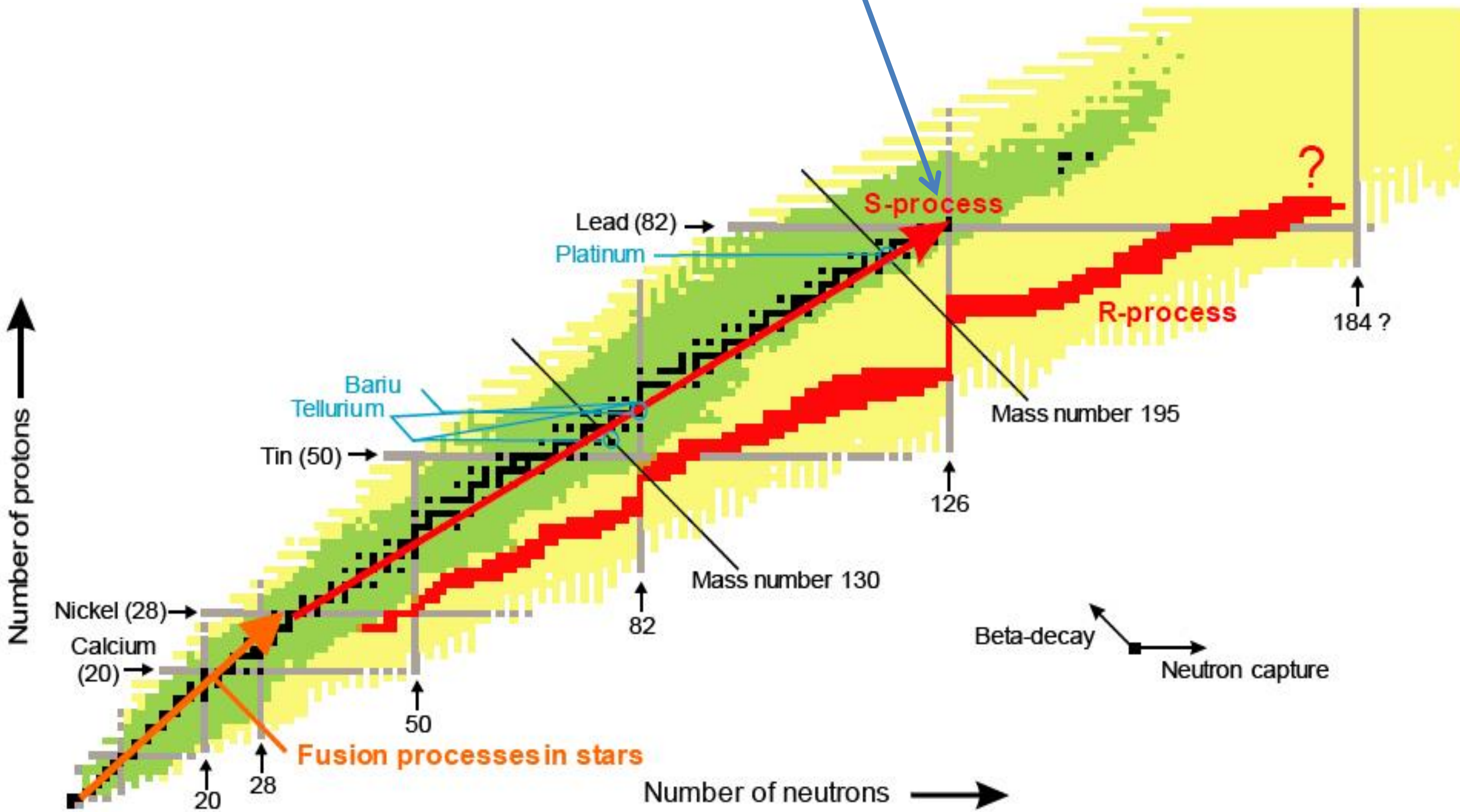

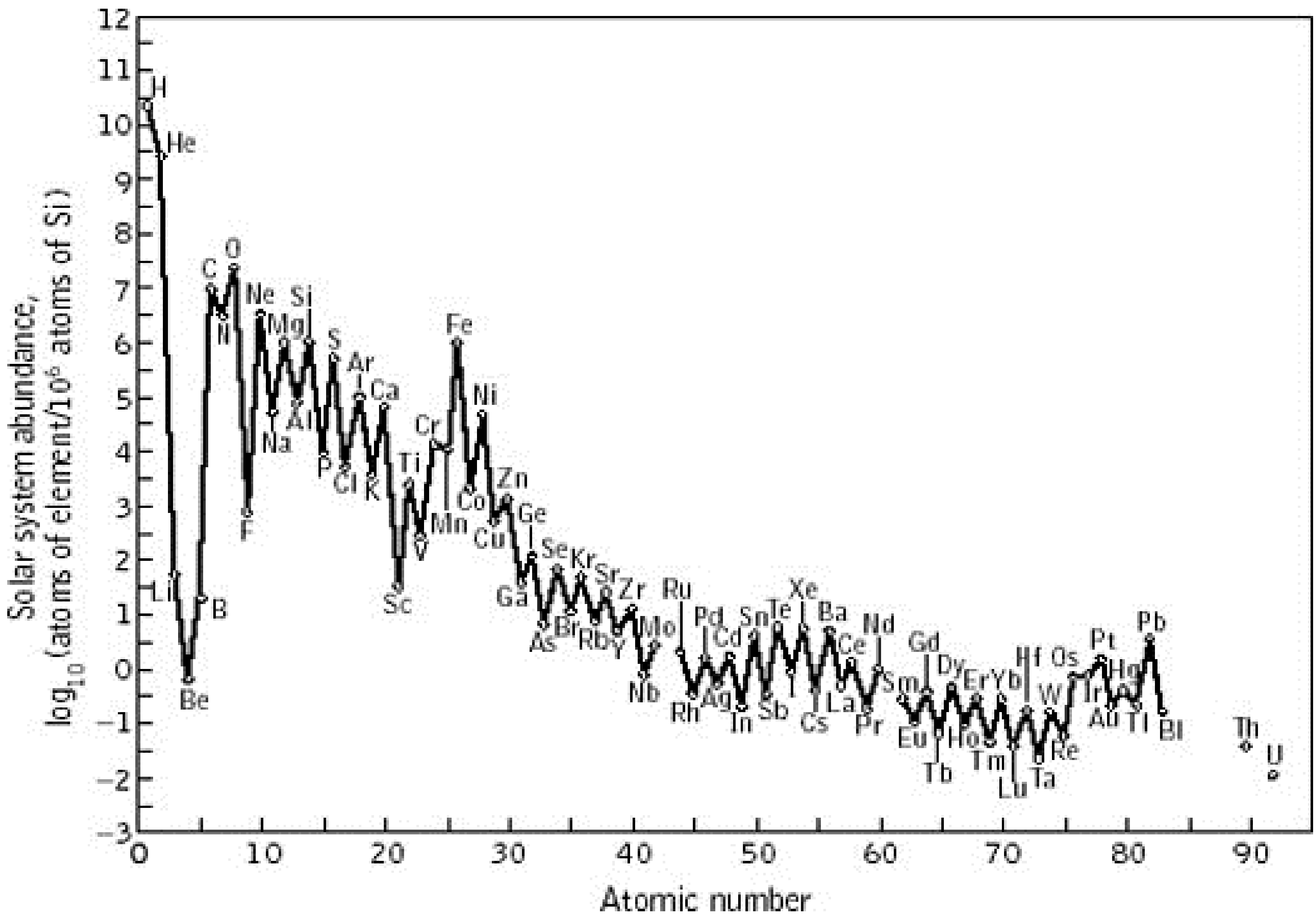

Solar system abundance,
$\log_{10}$ (atoms of element/10^6 atoms of Si)
Atomic number
H
He
Li
Be
B
C
N
O
F
Ne
Na
Mg
Al
Si
P
S
Cl
Ar
K
Ca
Sc
Ti
V
Cr
Mn
Fe
Co
Ni
Cu
Zn
Ga
Ge
As
Se
Br
Kr
Rb
Sr
Y
Zr
Nb
Mo
Ru
Rh
Pd
Ag
Cd
In
Sn
Sb
Te
Xe
Cs
Ba
La
Ce
Pr
Nd
Sm
Eu
Gd
Tb
Dy
Ho
Er
Tm
Yb
Lu
Hf
Ta
W
Re
Os
Ir
Pt
Au
Hg
Tl
Pb
Bi
Th
U

Bird’s view on nuclear physics

The Nuclear Many-Body Problem

Energy, Distance, Complexity
Different degrees-of-freedom

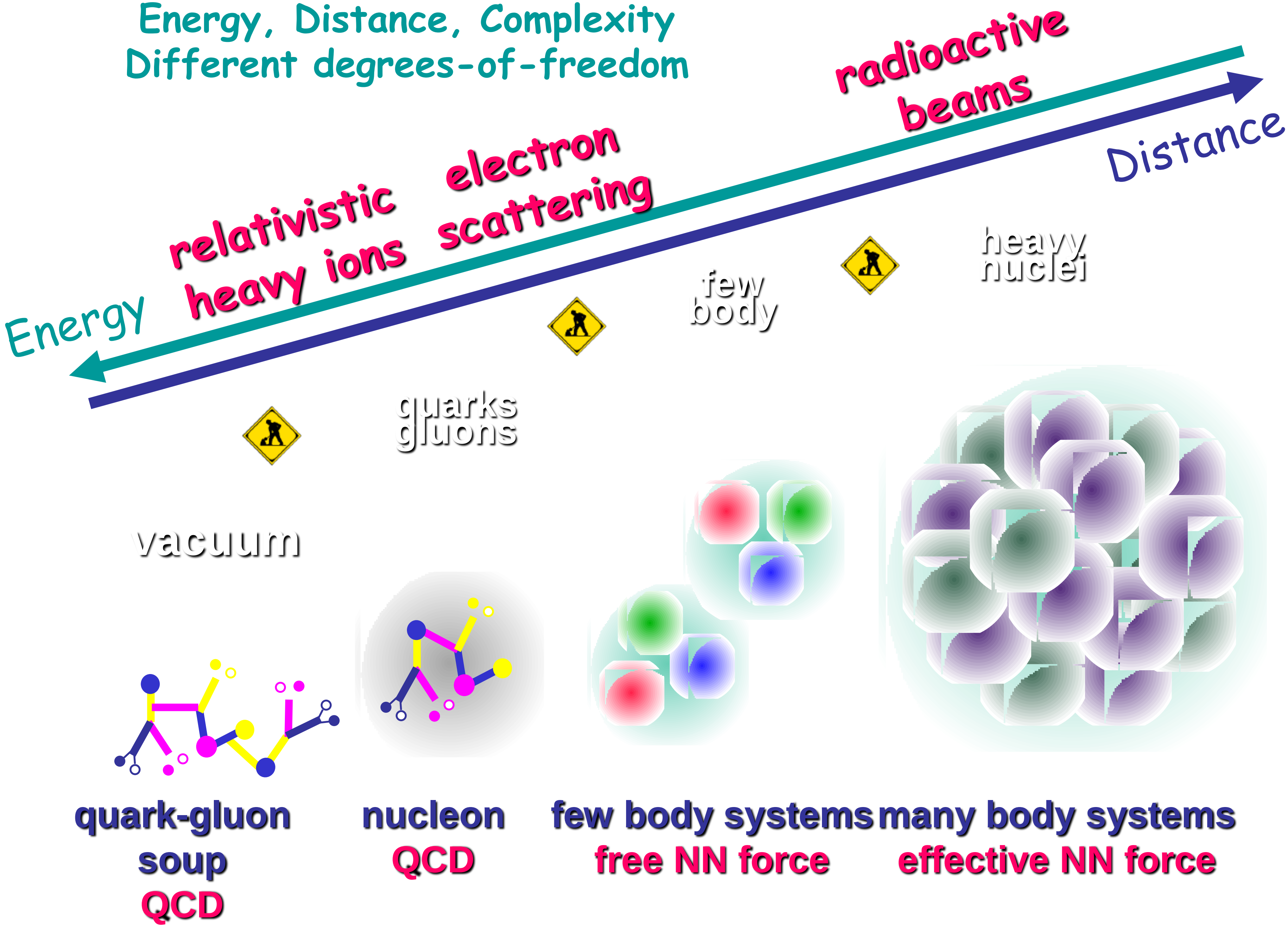

Questions that Drive the Field

- How do protons and neutrons make stable nuclei and rare isotopes?
- What is the origin of simple patterns in complex nuclei?
- What is the equation of state of matter made of nucleons?
- What are the heaviest nuclei that can exist?

Physics of nuclei

- When and how did the elements from iron to uranium originate?
- How do stars explode?
- What is the nature of neutron star matter?

Nuclear astrophysics

- How can our knowledge of nuclei and our ability to produce them benefit the humankind?
  - Life Sciences, Material Sciences, Nuclear Energy, Security

Applications of nuclei

And for something different:

- Nuclear system at the extreme:

  Giant nucleus – neutron star.

Neutron star discovery

-The existence of neutron stars was predicted by Landau (1932), Baade & Zwicky (1934) and Oppenheimer& Volkoff (1939).

- On November 28, 1967, Cambridge graduate student Jocelyn Bell (now Burnell) and her advisor, Anthony Hewish discovered a source with an exceptionally regular pattern of radio flashes. These radio flashes occurred every 1 1/3 seconds like clockwork. After a few weeks, however, three more rapidly pulsating sources were detected, all with different periods. They were dubbed "pulsars."

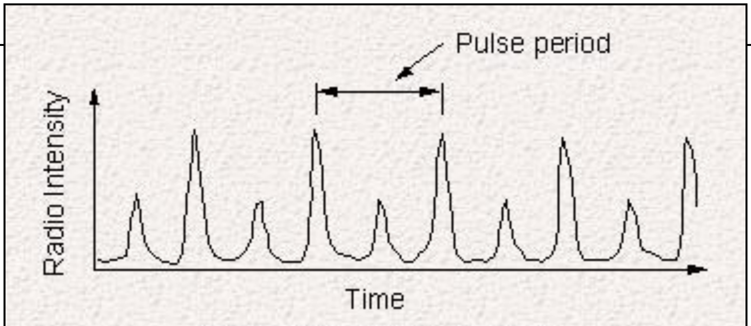

Radio pulses from a Pulsar

Nature of the pulsars

pulse rate = 30/second
slowing down rate = 38 nanoseconds/day

Pulsar in the Crab Nebula

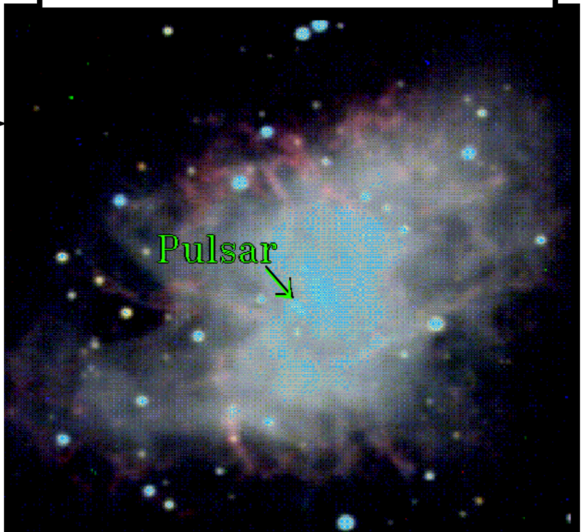

Calculated energy loss due to rotation of a possible neutron star $\approx$ Energy radiated

Conclusion: the pulses are produced by

Basic facts about neutron stars:

Radius: $\sim$ **10 km**
Mass: $\sim$ **1-2 solar masses**
Average density: $\sim 10^{14}\, g/cm^3$
Magnetic field: $\sim 10^{8} - 10^{12}$ **G**
Magnetars: $\sim 10^{15}$ **G**
Rotation period: 1.5 msec. – 5 sec.

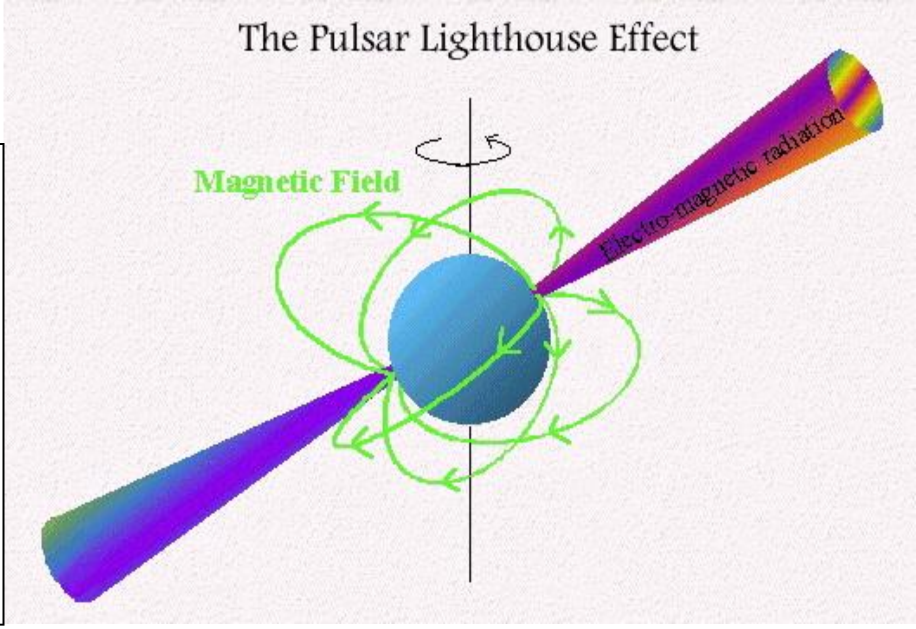

Number of known pulsars: > 1000
Number of pulsars in our Galaxy: $\sim 10^{8}$

Gravitational energy of a nucleon at the surface of neutron star $\sim$ **100 MeV**

Binding energy per nucleon in an atomic nucleus: $\sim$ **8 MeV**

Neutron star is bound by gravitational force

Birth of a neutron star

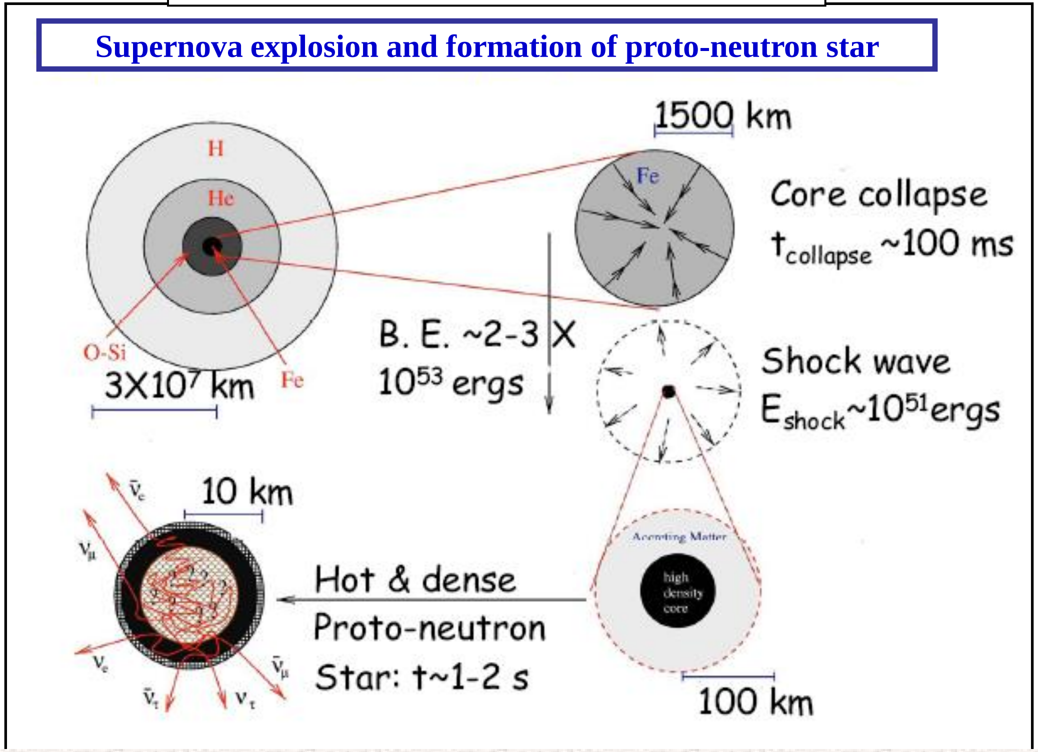

Summary: End Points of Stellar Evolution						
Remnant	**Progenitor Mass**	**Remnant Mass**	**Size**	**Density**	**Means of Support**	**Final Stage**
White Dwarf	$M_* < 8M_\odot$	$M_{WD} < 1.4M_\odot$	$R_{WD} \sim R_{earth}$	1 ton/cm^3	e^- degeneracy	Planetary Nebula
Neutron Star	$8M_\odot < M_* < 20M_\odot$	$M_{NS} < 3M_\odot$	$R_{NS} \sim 10$ km	200 million ton/cm^3	n degeneracy	Supernova
Black Hole	$M_* > 20M_\odot$	$M_{BH} > 3M_\odot$	0 $R_{grav} = 2GM/c^2$	∞	none	?

Pethick and Ravenhall, Annu. Rev. Nucl. Part. Sci. 45, 429 (1995)

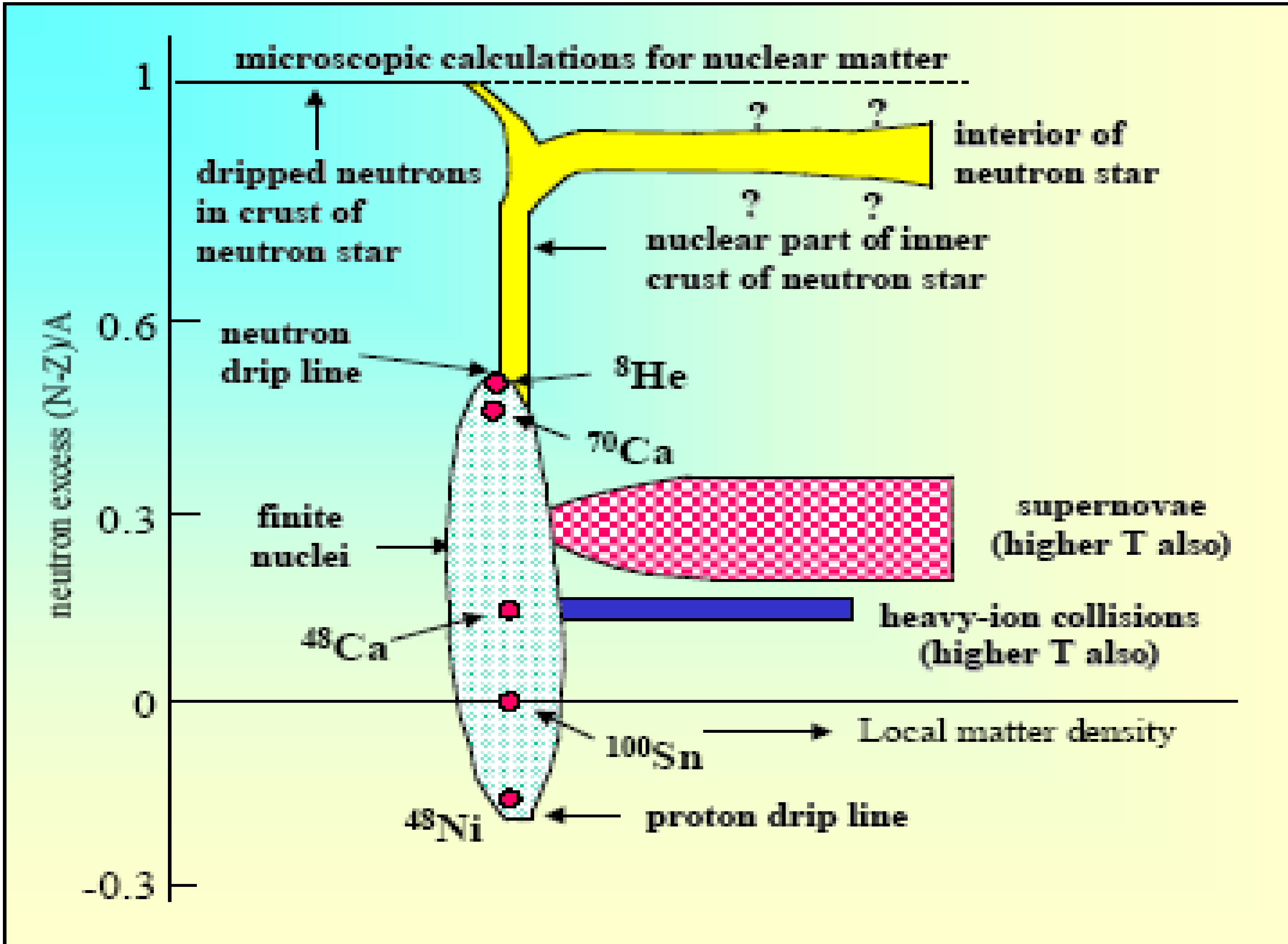

Thermal evolution of a neutron star:

Temperature: 50 MeV → 0.1 MeV $(t \sim \text{min.})$

URCA process:

$$p + e \rightarrow n + \nu_e$$
$$n \rightarrow p + e + \bar{\nu}_e$$

Temperature: 0.1 MeV → 100eV $(t \sim 10^5\, yr.)$

MURCA process:

$$p + p + e \rightarrow p + n + \nu_e$$
$$n + p + e \rightarrow n + n + \nu_e$$
$$p + n \rightarrow p + p + e + \bar{\nu}_e$$
$$n + n \rightarrow n + p + e + \bar{\nu}_e$$

Energy transfer between core and surface:

$$\frac{\partial T}{\partial t} = \nabla D \nabla T, \quad D = \frac{\kappa}{C_v}$$

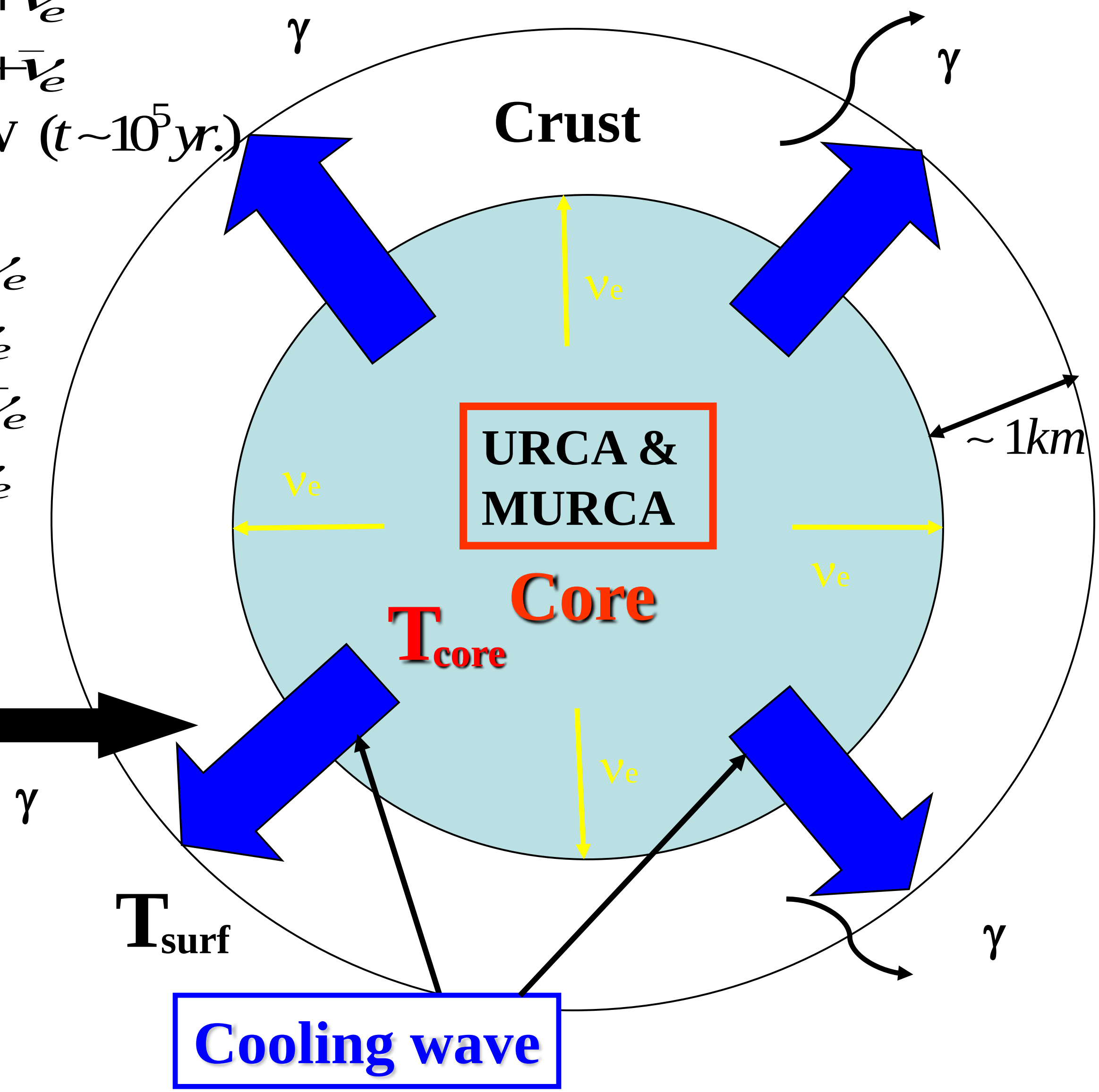

For τ < 100 years:

$\boxed{T_{core} < T_{surf}}$

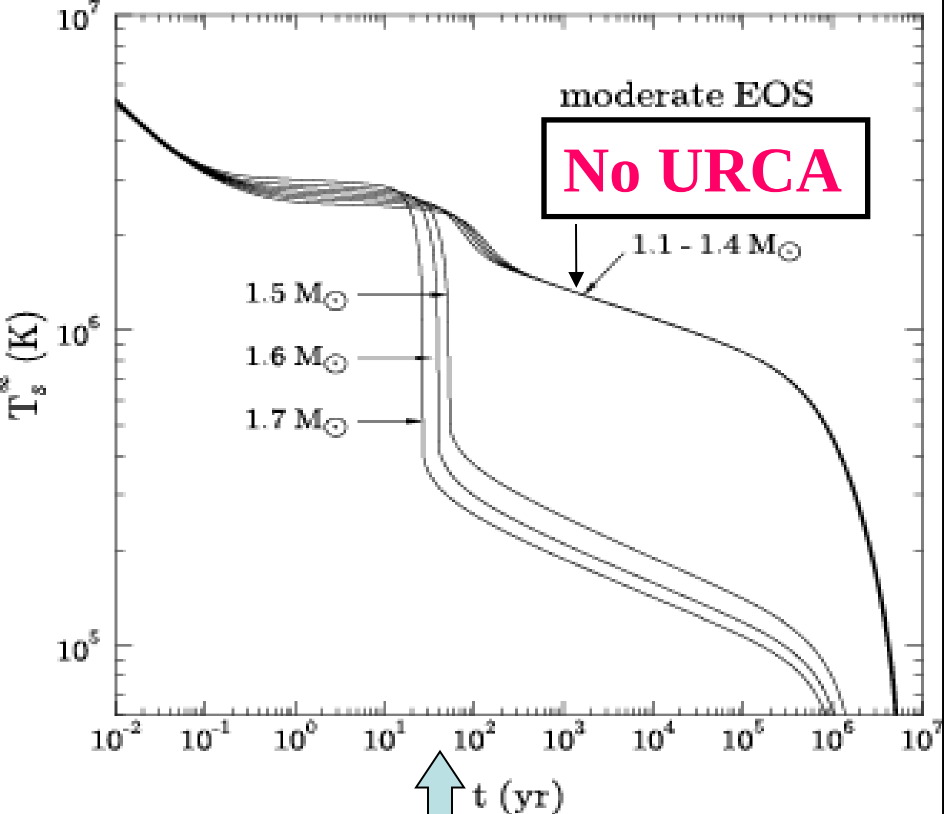

Relaxation time: a typical time for the cooling wave to reach the surface

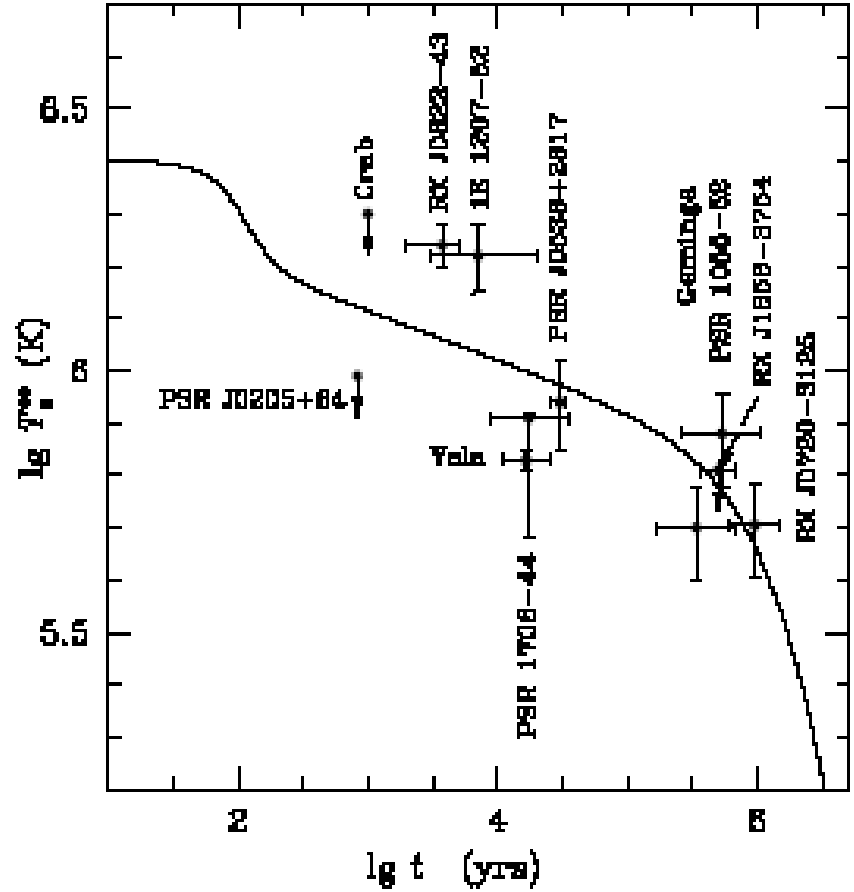

M.E. Gusakov, A.D. Kaminker, D.G. Yakovlev, and O.Y. Gnedin, Astron. Astrophys. 423 (2004) 1063.

Structure of a neutron star

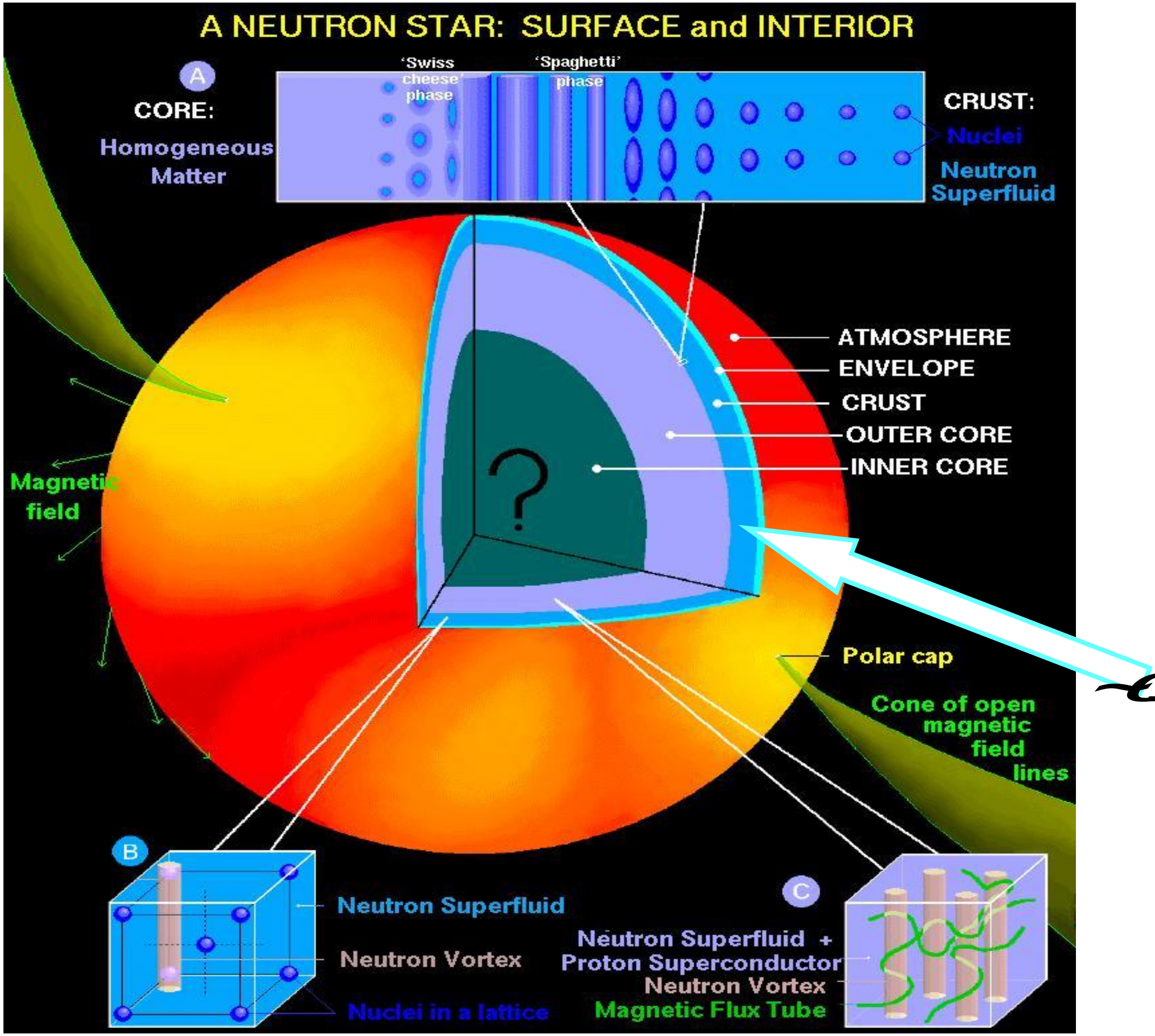

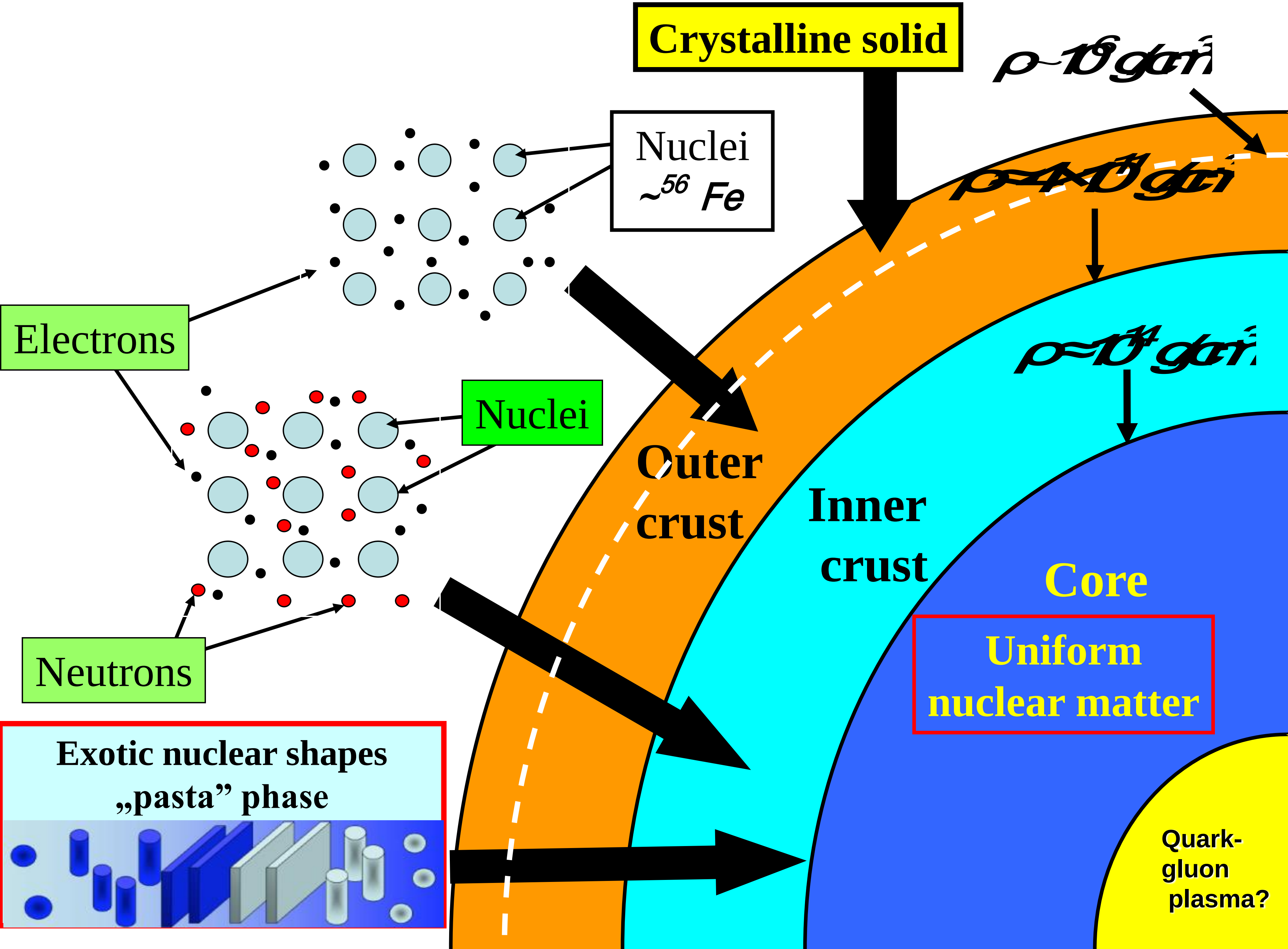

Crystalline solid
$\rho \sim 10^{6}\ g\ cm^{-3}$
Nuclei
$\sim^{56} Fe$
$\rho \approx 4\times10^{11}\ g\ cm^{-3}$
$\rho \approx 10^{14}\ g\ cm^{-3}$
Electrons
Nuclei
Neutrons
Outer crust
Inner crust
Core
Uniform nuclear matter
Quark-gluon plasma?
Exotic nuclear shapes
„pasta” phase

Crucial questions of high energy physics:
- nuclear phase diagram
- probing early stages of our UNIVERSE

Introduction: phase diagram

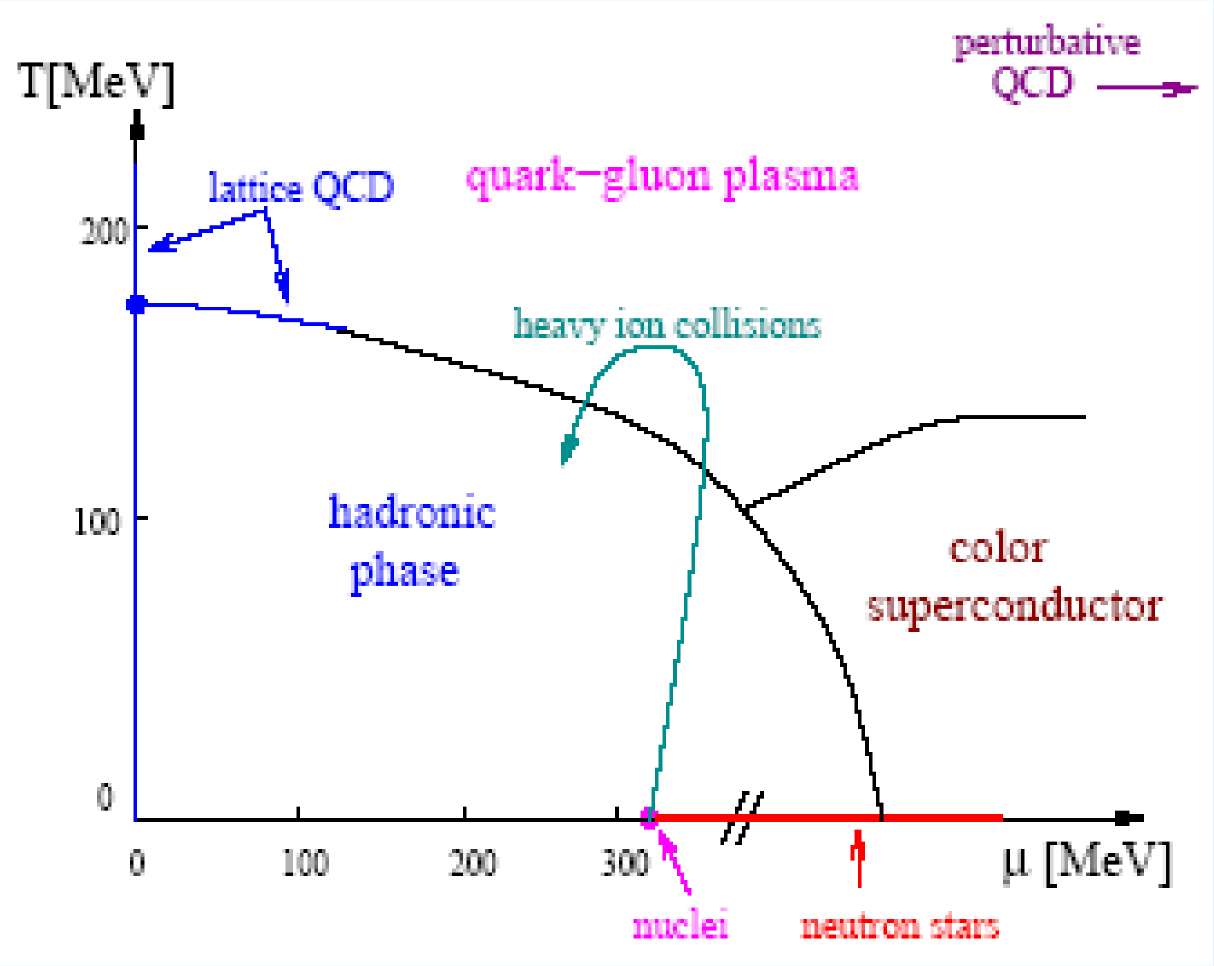

Hadronic phase:

confinement

chiral symmetry broken

Quark-gluon plasma:

no confinement

chiral symmetry restored

Color supeconductor:

diquark condensation

rich phase structure

Phase diagram of QCD: Chiral quark models

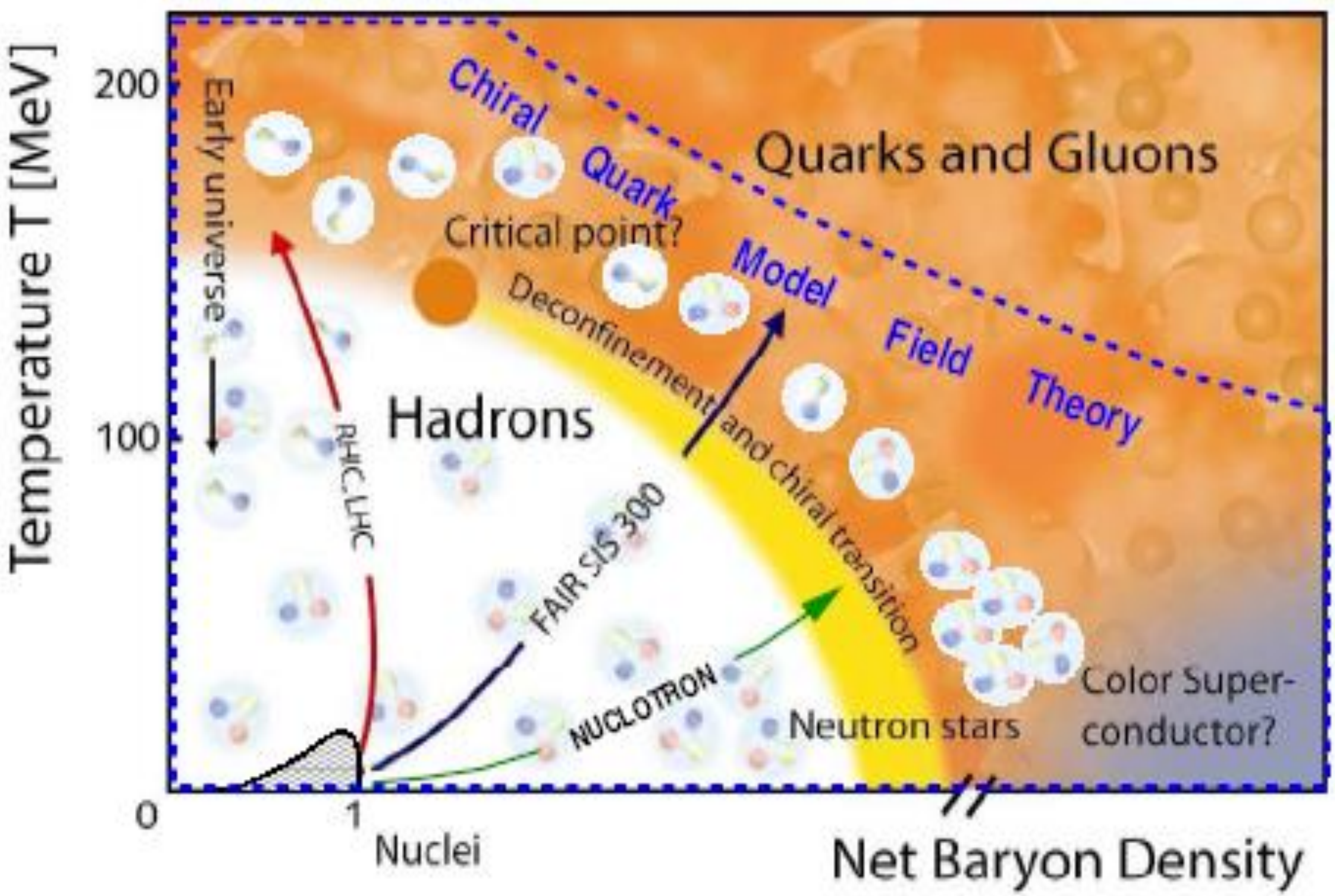

THE END